

Emerging Technologies in Traffic Safety Risk Evaluation, Prevention, and Control

Lead Guest Editor: Jian Lu

Guest Editors: Shan Bao, Feng Chen, Qing Cai, Jinghui Yuan, and Zeyang Cheng





Emerging Technologies in Traffic Safety Risk Evaluation, Prevention, and Control

Journal of Advanced Transportation

**Emerging Technologies in Traffic
Safety Risk Evaluation, Prevention, and
Control**

Lead Guest Editor: Jian Lu





Guest Editors: Shan Bao, Feng Chen, Qing Cai,
Jinghui Yuan, and Zeyang Cheng



Copyright © 2020 Hindawi Limited. All rights reserved.













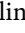









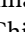
This is a special issue published in "Journal of Advanced Transportation." All articles are open access articles distributed under the Creative Commons Attribution License, which permits unrestricted use, distribution, and reproduction in any medium, provided the original work is properly cited.

Associate Editors

Juan C. Cano , Spain
Steven I. Chien , USA
Antonio Comi , Italy
Zhi-Chun Li, China
Jinjun Tang , China

Academic Editors

Kun An, China
Shriniwas Arkatkar, India
José M. Armingol , Spain
Socrates Basbas , Greece
Francesco Bella , Italy
Abdelaziz Bensrhair, France
Hui Bi, China
María Calderon, Spain
Tiziana Campisi , Italy
Giulio E. Cantarella , Italy
Maria Castro , Spain
Mei Chen , USA
Maria Vittoria Corazza , Italy
Andrea D'Ariano, Italy
Stefano De Luca , Italy
Rocío De Oña , Spain
Luigi Dell'Olio , Spain
Cédric Demonceaux , France
Sunder Lall Dhingra, India
Roberta Di Pace , Italy
Dilum Dissanayake , United Kingdom
Jing Dong , USA
Yuchuan Du , China
Juan-Antonio Escareno, France
Domokos Esztergár-Kiss , Hungary
Saber Fallah , United Kingdom
Gianfranco Fancello , Italy
Zhixiang Fang , China
Francesco Galante , Italy
Yuan Gao , China
Laura Garach, Spain
Indrajit Ghosh , India
Rosa G. González-Ramírez, Chile
Ren-Yong Guo , China

Yanyong Guo , China
Jérôme Ha#rri, France
Hocine Imine, France
Umar Iqbal , Canada
Rui Jiang , China
Peter J. Jin, USA
Sheng Jin , China
Victor L. Knoop , The Netherlands
Eduardo Lalla , The Netherlands
Michela Le Pira , Italy
Jaeyoung Lee , USA
Seungjae Lee, Republic of Korea
Ruimin Li , China
Zhenning Li , China
Christian Liebchen , Germany
Tao Liu, China
Chung-Cheng Lu , Taiwan
Filomena Mauriello , Italy
Luis Miranda-Moreno, Canada
Rakesh Mishra, United Kingdom
Tomio Miwa , Japan
Andrea Monteriù , Italy
Sara Moridpour , Australia
Giuseppe Musolino , Italy
Jose E. Naranjo , Spain
Mehdi Nourinejad , Canada
Eneko Osaba , Spain
Dongjoo Park , Republic of Korea
Luca Pugi , Italy
Alessandro Severino , Italy
Nirajan Shiwakoti , Australia
Michele D. Simoni, Sweden
Ziqi Song , USA
Amanda Stathopoulos , USA
Daxin Tian , China
Alejandro Tirachini, Chile
Long Truong , Australia
Avinash Unnikrishnan , USA
Pascal Vasseur , France
Antonino Vitetta , Italy
S. Travis Waller, Australia
Bohui Wang, China
Jianbin Xin , China



Hongtai Yang , China
Vincent F. Yu , Taiwan
Mustafa Zeybek, Turkey
Jing Zhao, China
Ming Zhong , China
Yajie Zou , China




Contents

A Mixed-Flow Cellular Automaton Model for Vehicle Nonstrict Priority Give-Way Behavior at Crosswalks

Yunxuan Li , Zeyang Cheng , Jian Lu , and Lin Zhang 

Research Article (11 pages), Article ID 5073023, Volume 2020 (2020)

An Alternative Method for Traffic Accident Severity Prediction: Using Deep Forests Algorithm

Jing Gan , Linheng Li , Dapeng Zhang , Ziwei Yi , and Qiaojun Xiang 

Research Article (13 pages), Article ID 1257627, Volume 2020 (2020)

Towards a Severity Assessment Method for Potential Cyber Attacks to Connected and Autonomous Vehicles

Qiyi He , Xiaolin Meng, and Rong Qu

Research Article (15 pages), Article ID 6873273, Volume 2020 (2020)

Study on a Right-Turning Intelligent Vehicle Collision Warning and Avoidance Algorithm Based on Monte Carlo Simulation

Chuanliang Shen, Shan Zhang , Zhenhai Gao , Binyu Zhou, Wei Su, and Hongyu Hu

Research Article (11 pages), Article ID 9405760, Volume 2020 (2020)

In Search of the Consequence Severity of Traffic Conflict

Ruoxi Jiang, Shunying Zhu , Pan Wang, QiuCheng Chen, He Zou, and Shiping Kuang



Research Article (15 pages), Article ID 9089817, Volume 2020 (2020)

Determinants of Bicyclist Injury Severity Resulting from Crashes at Roundabouts, Crossroads, and T-Junctions

Jinxing Shen, Tiantong Wang, Changjiang Zheng , and Miao Yu


Research Article (12 pages), Article ID 6513128, Volume 2020 (2020)

Traffic Incident Clearance Time Prediction and Influencing Factor Analysis Using Extreme Gradient Boosting Model

Jinjun Tang, Lanlan Zheng, Chunyang Han, Fang Liu , and Jianming Cai 

Research Article (12 pages), Article ID 6401082, Volume 2020 (2020)

A Study on Correlation of Traffic Accident Tendency with Driver Characters Using In-Depth Traffic Accident Data

Lin Hu, Xingqian Bao, Hequan Wu, and Wenguang Wu 


Research Article (7 pages), Article ID 9084245, Volume 2020 (2020)

Driving Fatigue Prediction Model considering Schedule and Circadian Rhythm

Qi Zhang , Chaozhong Wu , and Hui Zhang 

Research Article (10 pages), Article ID 9496259, Volume 2020 (2020)

Optimizing the Junction-Tree-Based Reinforcement Learning Algorithm for Network-Wide Signal Coordination

Yi Zhao , Jianxiao Ma, Linghong Shen, and Yong Qian



Research Article (11 pages), Article ID 6489027, Volume 2020 (2020)

Understanding Electric Bikers' Red-Light Running Behavior: Predictive Utility of Theory of Planned Behavior vs Prototype Willingness Model

Tianpei Tang , Hua Wang , Xizhao Zhou, and Hao Gong

Research Article (13 pages), Article ID 7097302, Volume 2020 (2020)

Developing a New Spatial Unit for Macroscopic Safety Evaluation Based on Traffic Density Homogeneity

Chen Wang , Lin Liu, and Chengcheng Xu 

Research Article (9 pages), Article ID 1718541, Volume 2020 (2020)

Research Article

A Mixed-Flow Cellular Automaton Model for Vehicle Nonstrict Priority Give-Way Behavior at Crosswalks

Yunxuan Li ^{1,2,3}, Zeyang Cheng ^{1,2,3}, Jian Lu ^{1,2,3} and Lin Zhang ⁴

¹School of Transportation, Southeast University, Nanjing, Jiangsu 211189, China

²Jiangsu Key Laboratory of Urban ITS, Southeast University, Nanjing, Jiangsu 211189, China

³Jiangsu Province Collaborative Innovation Center of Modern Urban Traffic Technologies, Southeast University, Nanjing, Jiangsu 211189, China

⁴School of Civil Engineering and Transportation, South China University of Technology, Guangzhou 510641, China

Correspondence should be addressed to Jian Lu; lujian_1972@seu.edu.cn

Received 9 November 2019; Revised 23 November 2020; Accepted 10 December 2020; Published 29 December 2020

Academic Editor: Meaad Saberi

Copyright © 2020 Yunxuan Li et al. This is an open access article distributed under the Creative Commons Attribution License, which permits unrestricted use, distribution, and reproduction in any medium, provided the original work is properly cited.

The vehicle nonstrict priority give-way behavior (VNPGWB) is a common part of traffic interaction between motorized and nonmotorized vehicles in many countries. This study proposes a mixed-flow cellular automaton model to simulate the passing of vehicles in front of bicycles at crosswalks. The mixed-flow model combines a vehicle model with a bicycle model, using nonstrict priority give-way and strict give-way two driving behaviors defined as relating to the decision point rule and the launching rule, respectively. Simulation results showed that as the vehicle and bicycle inflow rates increased, a critical inflow rate divided vehicle and bicycle traffic flow into free flow and saturated flow conditions. The values of vehicle saturation flow decreased from 0.34 to 0.05, and the values of bicycle saturation flow decreased from 0.54 to 0.44, indicating that the mixed traffic flow has a negative effect on vehicle and bicycle saturated flow. Results also showed that VNPGWB effectively improves vehicle saturation flow over that of the strict give way. The advantage of VNPGWB is more significant when vehicles and bicycles are in saturation traffic flow.

1. Introduction

In many countries in Europe and Asia, the bicycle is still an important mode of transportation. For example, in China, more than 38% of commuters choose bicycles as their main travel mode [1, 2]. It is noteworthy that electric bicycles have grown rapidly in recent years, with the number of e-bikes exceeding 250 million in China [3, 4]. In addition, shared bicycles also have gained tremendous popularity as a result of their convenience [5, 6]. However, due to their vulnerability in a collision, cyclists are subject to higher safety risks than drivers of vehicles [7, 8]. Collisions between bicycles (including e-bikes) and vehicles tend to cause very severe injuries and fatalities. Some studies show that 90% of all cyclist fatalities are caused by collision with vehicles [6, 9–11]. In fact, vehicles and bicycles competing for priority are a common reason for conflicts and crashes at crosswalks [12]. Most traffic managers believe that drivers

should strictly give way to bicycles passing through a crosswalk [3, 13, 14]. However, actual investigations have found that drivers in many countries and regions, such as Norway, Finland, Germany, and China, do not strictly adhere to this rule [8, 15–19]. That is, during the real traffic conditions, vehicle drivers may not always assume they must comply with the rule of giving way, and instead, they compete for priority [17, 18]. For example, the decision a driver makes to pass through the crosswalk or not depends on the bicycle's position and speed. Since it is based on the driver's subject assessment, the behavior is defined as vehicle nonstrict priority give-way behavior (VNPGWB).

In the process of vehicles passing in front of bicycles at crosswalks, drivers have only two choices: passing without stopping or stopping to give way [17]. Drivers should generally adapt their speeds to avoid endangering cyclists at crosswalks, and if necessary, drivers should stop to give way to cyclists [12]. This rule ensures the orderly passing of

vehicles and bicycles at the crosswalk. However, when the vehicle and bicycle are in a condition of saturated traffic flow, the vehicle flow is usually blocked by the bicycle flow, which has a significant impact on the traffic capacity of the vehicle flow, especially near unsignalized intersections [15, 17]. Specifically, there is a great impact on traffic flow when vehicles are waiting for bicycles at crosswalks. In this case, nonstrict priority allows vehicles to leave the conflict area earlier, mitigating their effects on subsequent vehicles and thereby improving the capacity of the road and intersection. Therefore, despite the negative impact on traffic safety, many countries acquiesce to nonstrict priority in the practical management of traffic, administering no punishment for violators as long as no crash occurs [17, 19].

This study uses a cellular automaton (CA) model to simulate a vehicle passing in front of bicycles at crosswalks engaged in VNPGWB. In order to understand VNPGWB, the key focus is to combine a mixed-flow model (i.e., integrating a vehicle model and a bicycle model) with driving behaviors. Driving behaviors in this study are primarily divided into the decision point rule and the launching rule. By adjusting the proportion of driving behaviors (strict give way and nonstrict priority give way) in these two rules, the real traffic conditions for VNPGWB can be simulated.

The rest of this paper is organized as follows: Section 2 reviews the literature; Section 3 describes the proposed mixed method in detail; Section 4 measures numerical simulation; and Section 5 concludes the paper.

2. Literature Review

Few previous studies explored VNPGWB, Räsänen [16] was the first to examine the behavior of road users changed based on their knowledge of priority regulations, such as whether a turning vehicle needs to give way to a cyclist from the same or opposite direction. Results showed that the effect of priority regulations on road user behavior depended on the characteristics of the bicycle crossings. Most subsequent studies found that drivers choose a give-way behavior depending on their understanding of priority order. For example, Lin et al. [17] developed a microdriving force model, which included safety driving force and efficiency driving force, for right-turning drivers, who constitute the dominant group confronted with the nonstrict priority passing situation. Silvano et al. [7] presented a modeling framework to describe driver-cyclist interactions when they were approaching a conflict zone. In the framework, driver yielding, or give-way, behavior is modeled as a function of several explanatory variables. Ma et al. [8] established a three-layered mathematical model, including a decision layer, operation layer, and constraint layer, to simulate the variation in trajectories of right-turn vehicles. Bai et al. [19] estimated the capacity of left-turn vehicles under nonstrict priority. Results showed that the model was valid for estimating the capacity of an exclusive left lane with a permitted phase under nonstrict priority. In summary, most studies have assumed that all drivers follow VNPGWB; however, drivers who choose to strictly give way coexist in mixed traffic flow with those who do not. Further, a given driver

may make different decisions under free flow and saturated flow conditions.

When passing bicycles at crosswalks, most drivers constantly adjust their vehicles' speed. In order to simulate this behavior, this study will establish a microscopic simulation model. The most popular microscopic simulation methods used in previous studies are car-following models and cellular automaton (CA) models [20–22]. Because the car-following model primarily simulates the interaction between a front and rear vehicle, the model is only applicable to one-dimensional movement and cannot represent the full mixed traffic flow. The CA traffic flow model, in contrast, can make full use of computer operations to flexibly change its rules according to various traffic conditions. In fact, the movements of vehicles and bicycles are discrete, and the CA model can use discrete space-time and state variables to regulate evolution rules and thus to describe nonlinear behavior. Additionally, the CA model can simulate the gradual change in vehicle and bicycle behavior as conditions change from free flow to saturated flow [23–25]. It can be found, through long-term simulation, whether there is a phase transformation from free flow to saturation flow. In recent years, a large number of studies have used CA models to simulate mixed traffic flow. For example, Meng et al. [26] proposed a single-lane CA model to simulate mixed traffic with motorcycles and investigated the relationship between motorcycle lane changing behavior and density of traffic flow. Zhao [24] established a mixed bicycle traffic model, comprised of two bicycle types of bicycles, that shows bicycle traffic characteristics on eight physically separated bicycle paths in China. Ren et al. [21] improved a cellular automaton model by incorporating social forces that can describe interactions between pedestrians, making it useful for modeling the bidirectional pedestrian flow at crosswalks. Lu et al. [25] proposed a simulation model to represent vehicles yielding to pedestrians at crosswalks and demonstrated the relationship between saturated flow and yield behavior. The CA model can demonstrably be applied to simulate the behavior of vehicle drivers passing bicycles at crosswalks.

3. Model

The crosswalk is one of the most serious conflict areas between vehicles and bicycles. Obviously, cyclists are vulnerable road users in this conflict area. In order to avoid a crash, a vehicle driver's decision process begins from upstream of the conflict area, where the driver confirms whether there is a potential conflict or not. The decision process of giving way behavior can be divided into two situations, as shown in Figure 1. Situation 1 (Figures 1(a)–1(c)): the white car (red box) has observed the bicycle (red box) at the crosswalk and chooses to pass without giving way at all; Situation 2 (Figures 1(d)–1(f)): the blue car (red box) has observed the bicycle (red box) at the crosswalk and stops to give way. Based on field observation, a vehicle's passing through bicycles at the crosswalk can be divided into the following steps: (1) the vehicle reaches the decision point; (2) the vehicle stops outside the conflict area; (3) the vehicle

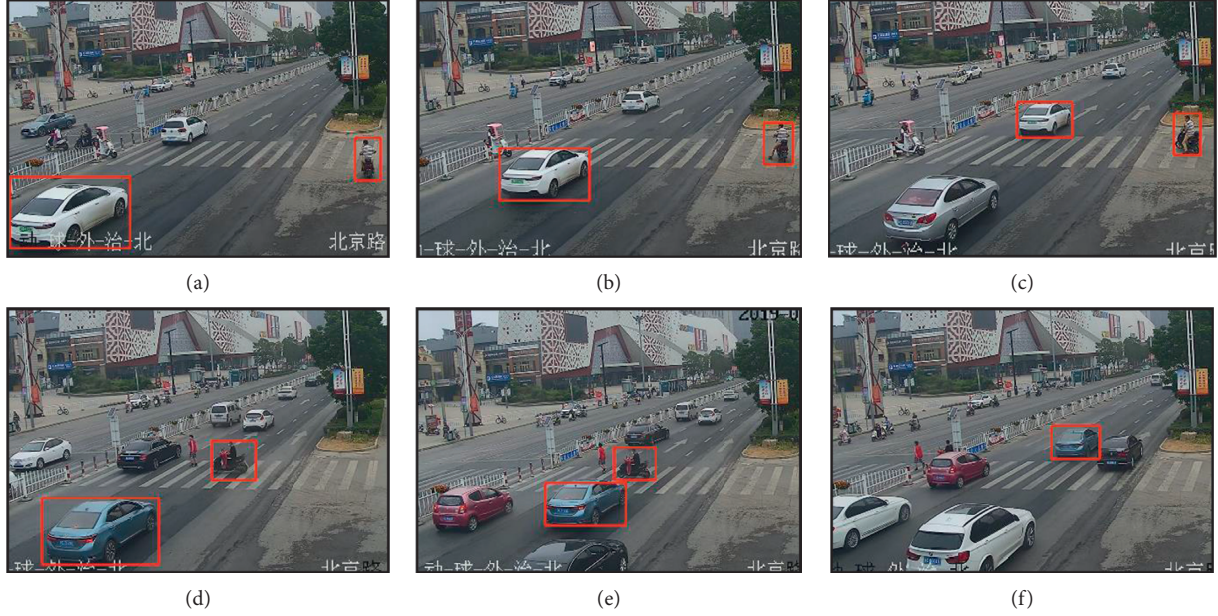


FIGURE 1: The process of vehicles passing bicycles at crosswalks in real traffic condition.

passes through the conflict area. It is worth noting that VNPGWB only occurs in Steps 1 and 2. The schematic diagram of these steps is depicted in (Figures 2(a)–2(c)). When a vehicle needs to pass through a crosswalk, the driver's decision process begins at a certain distance upstream of the conflict area, a distance defined as the decision point (Figure 2(a)). When a vehicle stops to give way to a bicycle, the driver usually adjusts speed and stops at the boundary of the conflict area. Once an acceptable gap exists, the driver will finish the traverse. The stop position in this study is defined as the launching point (Figure 2(b)). However, if the driver chooses to pass without giving way, Step 2 will not occur.

3.1. Definition and Delimitation of Cellular Space. A vehicle lane and a crosswalk were chosen as the research area for this study. First, the cellular space is defined as a two-dimensional matrix, and the n th cellular unit in the cellular space position is (x_n, y_n) . Then, because of the different sizes of vehicles and bicycles, a finer cellular unit size is defined in order to comply with the actual speed and minimum vehicle space for each. One bicycle occupies two cellular units (x_n^b, y_n^b) and one vehicle (x_n^v, y_n^v) occupies 6×4 cellular units. The vehicle lane widths are l^v m and the bicycle lane widths are l^b m; thus, the overlap area between the vehicle lane and the bicycle lane is $l^v \times l^b$ m². Finally, the conflict area in the cellular space position is shown in Figure 3.

3.2. Vehicle Model. According to the vehicle's position in its lane, the vehicle model can be divided into three rules: the driving rule, the decision point rule, and the launching rule. When following the driving rule, the driver selects an acceptable distance in understanding the interaction rules with consideration of safety and other factors. Then, the decision

point rule is used: when drivers observe the bicycle lanes, different drivers (strict give way and nonstrict priority give way) make different decisions about whether to give way. If the vehicle slows down and stops at the boundary of the conflict area, it will be launched through the area when there is an acceptable gap. The launching rule is used to determine the acceptable gap for the different types of drivers making different decisions.

3.2.1. Vehicle Rule 1: Driving Rule. This study assumes that the vehicle is not affected by lane changes and reverse lanes. All vehicles move at an expected maximum velocity, and they adjust their velocity in order to avoid collisions with vehicles in front of them. For a process of $t \rightarrow t + 1$, the driving rule evolution is as follows:

Step 1: acceleration; $v_n^v \rightarrow \min(v_n^v + a^v, v_{\max}^v)$

Step 2: slowing down; $v_n^v \rightarrow \min(v_n^v, d_n^v)$

Step 3: randomization with probability p_s ; if $\text{rand} > p_s$, then $v_n^v \rightarrow \max(v_n^v - a^v, 0)$

Step 4: movement; $x_n^v \rightarrow x_n^v + v_n^v$,

where x_n^v and v_n^v represent the position and velocity, respectively, of vehicle n ; a^v represents vehicle acceleration; $d_n^v = x_{n+1}^v - x_n^v - l^v$ is the number of cellular spaces between vehicle n and vehicle $n + 1$; l^v is the length of the vehicle; and rand is a random number between 0 and 1, where p_s is the randomization with probability.

This model adopts an open boundary: when vehicles' road position is updated, the positions of the head vehicle and the tail vehicle are monitored as x_{lead}^v and x_{last}^v at the moment of $t \rightarrow t + 1$. If $x_{\text{last}}^v > v_{\max}^v$, vehicles at the velocity of v_{\max}^v will enter the cellular $\min[x_{\text{last}}^v - v_{\max}^v, v_{\max}^v]$ with an inflow rate of a^v . At the point of exiting the road, if $x_{\text{lead}}^v > L_{\text{road}}^v$, vehicles will leave the road.

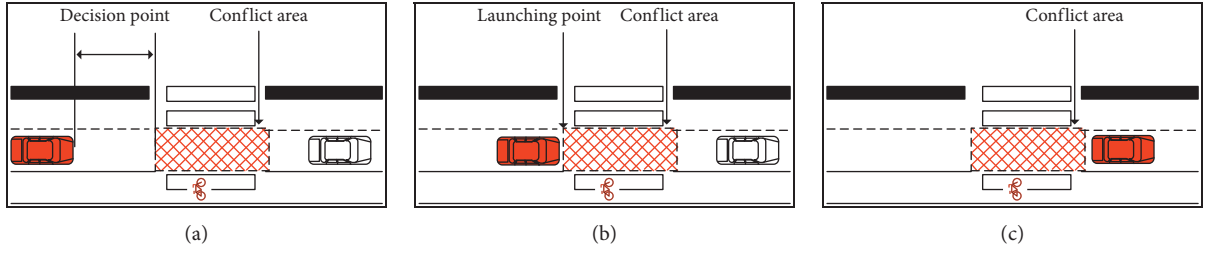


FIGURE 2: Schematic diagram of vehicles passing bicycles at crosswalks.

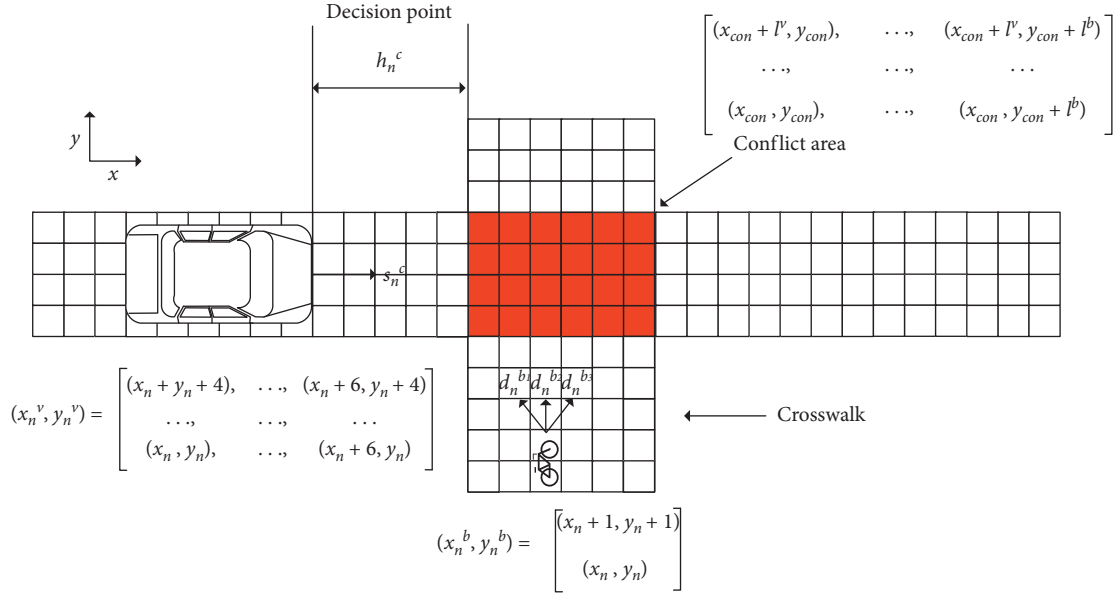


FIGURE 3: Schematic diagram of mixed-flow cellular space.

3.2.2. Vehicle Rule 2: Decision Point Rule. The decision point is defined as the place where the vehicle driver needs to decide whether or not to give way when encountering a bicycle. In order to mirror the process of a vehicle driver's decision, a deceleration restriction is introduced in the decision point rule and the decision time is a time step. a^v is the acceleration and D is the deceleration. It is important to note that the position of the decision point is not a fixed point, but varies with different drivers and is impacted by actual conditions. At the instant of t , the decision point is given by

$$h_n^v = v_n^v + \sum_{i=1}^{t_n^d} (v_n^v - D \times i) \geq x_v + l_b - x_n^v, \quad (1)$$

$$t_n^d = \frac{v_n^v}{D}, \quad (2)$$

where x_n^v and v_n^v represent the position and velocity of vehicle n , respectively; $x_v + l_b$ is the conflict area boundary; the

summation represents the distance from deceleration to stopping; and t_n^d means the time from deceleration to stop.

When a vehicle is at the decision point, the driver adjusts to a suitable velocity to make sure the cyclist safely traverses the conflict area. Suitable velocity is defined as a velocity that ensures the vehicle not only can pass through the conflict area safely but also can decelerate to a timely stop. In order to capture the stochasticity of different drivers at the decision point, a binary variable (γ_n^d) is presented as

$$\gamma_n^d = \begin{cases} 1, & \text{if rand}() > \beta_1^v, \\ 0, & \text{else,} \end{cases} \quad (3)$$

where $\gamma_n^d = 1$ represent the driver choosing to give way to the cyclist; $\gamma_n^d = 0$ represents the driver choosing not to give way, that is, selecting nonstrict priority give way; and β_1^v represents the proportion of nonstrict priority give-way drivers. Thus, the suitable velocity s_n^v is presented at the instant of t :

$$s_n^v = \begin{cases} \min(x_v - x_n^v, \max(v_n^v - D, D)), & \text{Case I,} \\ (1 - \gamma_n^d) \times \min(v_n^v + a^v, v_{\max}^v) + \gamma_n^d \times \max(v_n^v - D, D), & \text{Case II,} \end{cases} \quad (4)$$

where “Case I” is the vehicle’s maximum velocity that will avoid a crash with the bicycle; “Case II” represents the choices of different drivers to give way or not; and D is the deceleration of vehicles.

3.2.3. Vehicle Rule 3: Launching Rule. The vehicle stops at the launching point and waits for an acceptable gap. Once an acceptable gap exists, the driver will take the opportunity to finish the traverse. The acceptable gap is defined as the time interval in which a vehicle successfully traverses the conflict area. In order to capture the stochasticity of different drivers at the launching point, another binary variable (γ_n^l) is presented as

$$\gamma_n^l = \begin{cases} 1, & \text{if } \text{rand}() > \beta_2^v, \\ 0, & \text{else,} \end{cases} \quad (5)$$

where $\gamma_n^d = 1$ represents the driver who needs to give way and waits for bicycles to traverse the conflict area; $\gamma_n^d = 0$ represents the driver who chooses nonstrict priority to give way, for whom the acceptable gap is equal to the launching time of the vehicles; and β_2^v represents the proportion of VNPGWB drivers. Thus, the acceptable gap is given by

$$t_n^l = \gamma_n^l + (1 - \gamma_n^l) \sqrt{\frac{2 \times l^b}{a^v}}. \quad (6)$$

In order to prevent vehicles from remaining static for a long period of time, a threshold vehicle waiting time T is defined. If the waiting time of a vehicle is longer than T , the vehicle will launch into the conflict area, and bicycles will be forced to stop.

3.3. Bicycle Model. There is great flexibility in the movement of bicycles, including both lateral and vertical movement. This study chose a new cellular type of bicycle model to simulate one-way bicycle travel in order to explore the interference between bicycles and vehicles in conflict areas. This model consists of two steps, lateral movement and vertical movement, as shown in Figure 3. Both the two steps adopt parallel rules. A bicycle can move to the left, forward, and right: $d_n^{la_1}$, $d_n^{la_2}$, and $d_n^{la_3}$ describe the number of empty cellular units on the left front, front, and right front, respectively; and $d_n^{ve_1}$, $d_n^{ve_2}$ describe the number of empty cell on the perpendicular left and right, respectively. The bicycle cellular coordinate is represented by $b_n = (x_n^b, y_n^b)$, where $b_n = 0$ means that there is no bicycle occupying this cell; and $b_n = 1$ means that there is a bicycle occupying this cell; $v_n^{b_{la}}$ represents the lateral velocity of the bicycle; $v_n^{b_{ve}}$ represents the vertical velocity of the bicycle, and $v_n^{b_{ve}} = -v$ means the bicycle moves to the left; $v_n^{b_{ve}} = v$ means the bicycle moves to the right; $a^{b_{la}}$ is the lateral acceleration of the bicycle; and $a^{b_{ve}}$ is the vertical acceleration of the bicycle.

3.3.1. Bicycle Rule 1: Lateral Movement. For the process of $t \rightarrow t + 1$, the lateral movement rules are as follows:

$$\text{Step 1: acceleration; } v_n^{b_{la}} \rightarrow \min(v_n^{b_{la}} + a^{b_{la}}, v_{n_{\max}}^{b_{la}})$$

$$\text{Step 2: slow down; } d_n^b \rightarrow \max(d_n^{la_1}, d_n^{la_2}, d_n^{la_3}), \\ v_n^{b_{la}} \rightarrow \min(v_n^{b_{la}} + d_n^b)$$

$$\text{Step 3: randomization with probability } p_s; \text{ if } \text{rand}() > p_s, \\ \text{then } v_n^{b_{la}} \rightarrow \max(v_n^{b_{la}} + a^{b_{la}}, 0)$$

$$\text{Step 4: movement; } y_n^b \rightarrow y_n^b + v_n^{b_{la}}$$

This model adopts an open boundary: when the vehicles’ road position is updated, the positions of the head vehicle and the tail vehicle are monitored as y_{lead}^b and y_{last}^b at the moment of $t \rightarrow t + 1$. If $y_{\text{last}}^b > y_{\text{max}}^b$, bicycles at the speed of v_{max}^b will enter the cellular $\min[y_{\text{last}}^b - v_{\text{max}}^b, v_{\text{max}}^b]$ with an inflow rate of a^b . At the exit point of the road, if $y_{\text{lead}}^b > L_{\text{road}}^b$, the bicycles will exit the road.

3.3.2. Bicycle Rule 2: Vertical Movement. In this study, there are two main situations in which bicycles can move perpendicularly. First, if there is no space in the front, a cyclist can choose vertical movement. Second, if a bicycle moves laterally, vertical movement can be chosen if the number of empty cells on either side is more than or equal to the number in front. The two situations are illustrated in detail as follows:

Situation 1. If $d_n^{la_1} = d_n^{la_2} = d_n^{la_3} = 0$, the cyclist chooses vertical movement in order to pass the crosswalk as soon as possible, and $v_n^{b_{ve}} \rightarrow \max(d_n^{ve_1}, d_n^{ve_2})$. If $d_n^{ve_1} = d_n^{ve_2}$, then

$$\delta_{ve} = \begin{cases} -1 & \text{if } \text{rand}() \leq p_{ve}^1, \\ 1 & \text{if } \text{rand}() > p_{ve}^1, \end{cases} \text{ and } v_n^{b_{ve}} = \delta_{ve} \cdot d_n^{ve}.$$

Situation 2. If $d_n^{la_1}$, $d_n^{la_2}$, and $d_n^{la_3}$ are not all zero, then the cyclist chooses the largest space in front as far as possible,

$$\text{and } v_n^{b_{ve}} = \begin{cases} -1 & \text{if } d_n^{la_1} = d_n^{la_2} = d_n^{la_3} \\ 0 & \text{if } d_n^{la_1} = d_n^{la_2} = d_n^{la_3} \\ 1 & \text{if } d_n^{la_1} = d_n^{la_2} = d_n^{la_3} \end{cases}.$$

If there are two or more choices with the same maximum number of cells, then

$$\delta_{ve} = \begin{cases} -1 & \text{if } \text{rand}() < p_{ve}^2 \\ 0 & \text{if } p_{ve}^2 \leq \text{rand}() \leq p_{ve}^3, \\ 1 & \text{if } \text{rand}() > p_{ve}^3 \end{cases} \text{ and } v_n^{b_{ve}} = \delta_{ve} \cdot d_n^{ve}.$$

3.4. Algorithm for the Mixed-Flow CA Model. In order to simulate the mixed-flow CA model, the abovementioned methods are integrated into one executable algorithm, which is processed in a parallel computing setting using the Python programming environment. The algorithm (Algorithm 1) calculates the process of $t \rightarrow t + 1$. In each step, the following three rules are conducted in order from first to last, and all are applied to every vehicle. When the algorithm ends, the updates are applied to all vehicles and bicycles in parallel. The complete framework of this algorithm’s four steps is shown in Figure 4.

4. Numerical Simulation

4.1. Simulation Parameter Setting. The data inputs in the following simulations are set as follows. The cellular size is $1 \text{ m} \times 1 \text{ m}$; the vehicle lane length (L^v) is 100 cell units, which therefore corresponds to 100 m; vehicle lane width (L^v) is 4

Step 1: driving rule.

Step 1.1: input the current vehicle position (x_n^v, y_n^v) ; current vehicle velocity v_n^v ; a randomization with probability p_s .

Step 1.2: if the vehicle position is at decision point (equation (1)), then go to Step 2.

Step 1.3: if the vehicle position $x_n^v + v_n^v > L_{\text{road}}^v$ boundary, then vehicles will leave the road.

Step 1.4: the vehicle adjusts velocity v_n^v according to the distance d_n^v to the front vehicle; go to Step 4.

Step 2: decision point rule.

Step 2.1: input the current bicycle positions (x_n^b, y_n^b) and current bicycle velocities $v_n^{b_{ia}}$ and $v_n^{b_{ve}}$.

Step 2.2: assume that there exists a time $t_n^1, 1 \leq t_n \leq t_n^d + 1$. If $x_{\text{con}} \leq x_n^b + v_n^{b_{ia}} t_n^1 \leq x_{\text{con}} + l_v$ and $y_{\text{con}} \leq y_n^b + v_n^{b_{ve}} t_n^1 \leq y_{\text{con}} + l_b$, then the vehicle will crash with bicycles. This vehicle needs to stop at the conflict area boundary and go to Step 3.

Step 2.3: if the driver chooses to give way, then go to Step 2.2; if the driver chooses nonstrict priority give way, then go to Step 4. The vehicle velocity is given by equation (4).

Step 3: launching rule.

Step 3.1: input the current bicycle positions (x_n^b, y_n^b) , current bicycle velocities $v_n^{b_{ia}}$ and $v_n^{b_{ve}}$, and waiting time t^w .

Step 3.2: assume that there exists another time t_n^2 and the acceptable gap t_n^l is given by equation (6). If the driver chooses to give way and $x_{\text{con}} \leq x_n^b + v_n^{b_{ia}} (t_n^2 + t_n^l) \leq x_{\text{con}} + l_v, y_{\text{con}} \leq y_n^b + v_n^{b_{ve}} (t_n^2 + t_n^l) \leq y_{\text{con}} + l_b$, then the vehicle continues to wait; for waiting time, add 1; if the driver chooses nonstrict priority give way, then go to Step 4. The vehicle velocity $v_n^v = (1 - \gamma_n^l) a_n^v$.

Step 3.3: if the waiting time t^w is longer than T , the vehicle will launch into the conflict area, and bicycles will be forced to stop.

Step 4: movement.

Update the position of vehicles (x_n^v, y_n^v) and bicycles (x_n^b, y_n^b) based on their velocities v_n^v and $v_n^{b_{ia}}, v_n^{b_{ve}}$. For the vehicle, $x_n^v(t+1) = x_n^v(t) + v_n^v, y_n^v(t+1) = y_n^v(t)$. For the bicycle, $x_n^b(t+1) = x_n^b(t) + v_n^{b_{ia}}, y_n^b(t+1) = y_n^b(t) + v_n^{b_{ve}}$.

ALGORITHM 1: The algorithm of mixed-flow CA model.

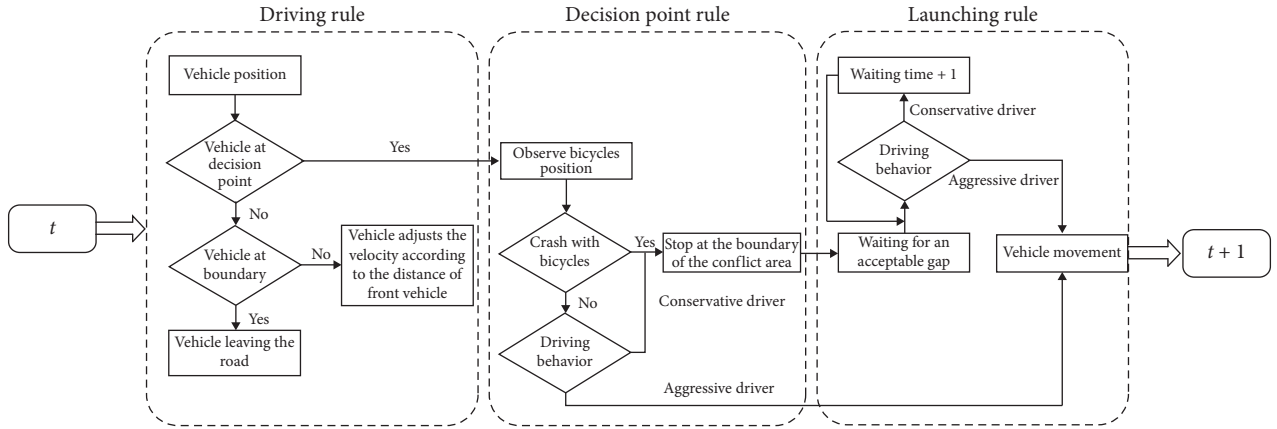


FIGURE 4: Complete mixed-flow CA model framework.

cells, which corresponds to 4 m; the crosswalk length (L^b) is 100 cell units, and it corresponds to 100 m; crosswalk width (l^b) is 6 cell units, and it corresponds to 6 m and the size of the conflict area is 6×4 cell, and it corresponds to $6 \times 4 \text{ m}^2$. The simulation parameters are shown in Table 1. In order to obtain vehicle and bicycle traffic flow data, the virtual detectors are set at the boundaries of the vehicle and crosswalk. When a vehicle or bicycle leaves the lane, the detector's counter adds one. Moreover, q^v and q^b are the vehicle and bicycle flow, respectively, and the unit is veh/(time \times lane). The simulation steps are 100,000 s, and the preceding 20,000 s are abandoned.

4.2. Model Validation. To verify the reliability of the mixed-flow CA model, the traffic flux-density relationship is the fundamental diagram that describes driver-cyclist interactions. With settings of $\beta_1^v = 0.1$, $\beta_2^v = 0.1$, and $T = 30 \text{ s}$,

TABLE 1: The simulation parameters in mixed-flow CA model.

Variable	Vehicle	Bicycle
Lane length (m)	$L^v = 100$	$L^b = 50$
Lane width (m)	$l^v = 4$	$l^b = 6$
Max velocity (m/s)	$v_{\text{max}}^v = 20$	$v_{\text{max}}^{b_{ia}} = 6$ $v_{\text{max}}^{b_{ve}} = 2$
Acceleration (m/s^2)	$a^c = 4$	$a^{b_{ia}} = 2$
Deceleration (m/s^2)	$D = 10$	—
Randomization with probability	$p_s = 0.5$	$p_{ve}^1 = 0.5$ $p_{ve}^2 = 0.1$ $p_{ve}^3 = 0.9$

Figures 5(a) and 6(a) show the microscopic fundamental relationships between flow and inflow rate for the vehicle and bicycle. When the bicycle's inflow rate $\alpha^b = 0$, there is no bicycle passing the crosswalk, and the vehicle flow q^v shows an upward trend and remains stable at 0.34 (Figure 5(b)). When bicycle's inflow rate $\alpha^b = 1$, the maximal point of

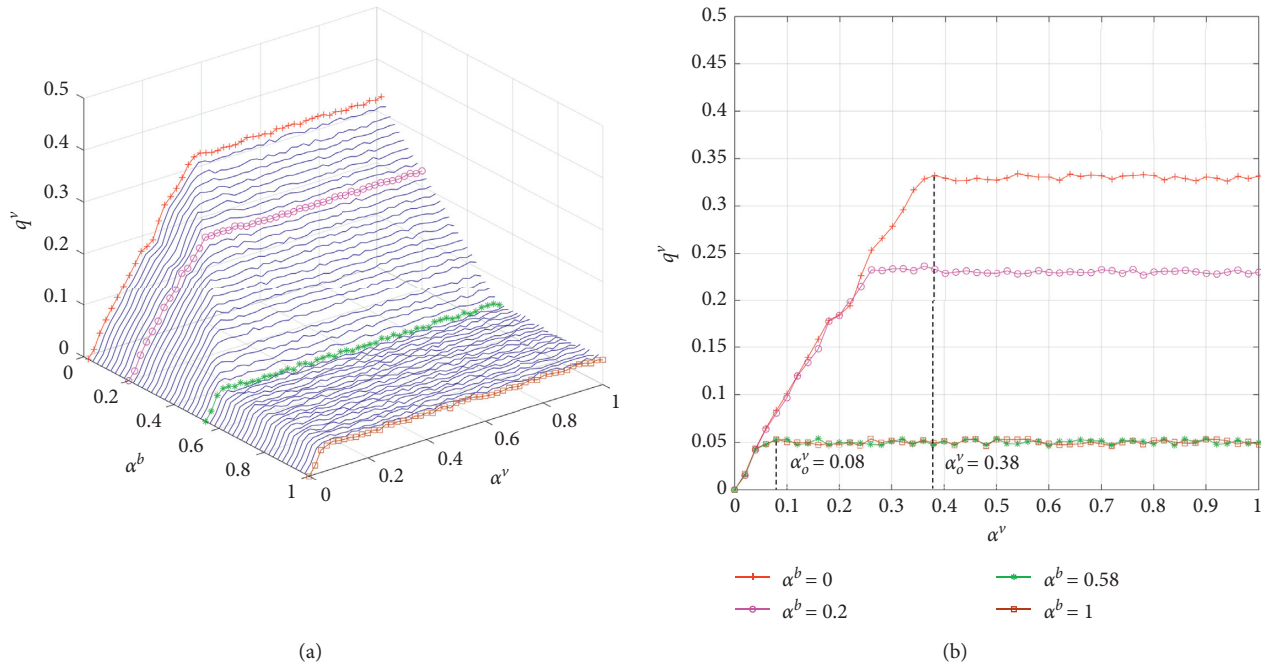


FIGURE 5: The relationship between the vehicle flow and the vehicle and bicycle inflow rate.

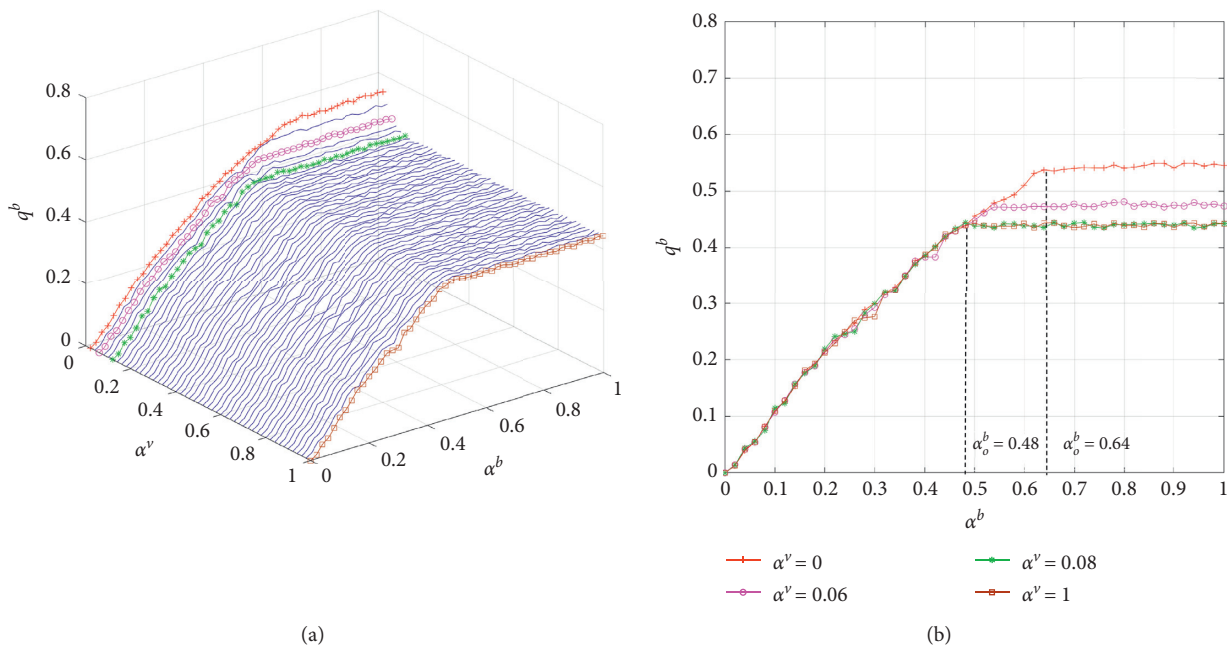


FIGURE 6: The relationship between the bicycle flow and the vehicle and bicycle inflow rate.

vehicle flow q_o^v is 0.05 (i.e., saturation flow), which is obviously lower than $\alpha^b = 0$. With more and more bicycles entering the mixed-flow cellular space, drivers must slow down and stop outside the conflict area to avoid crashes. Thus, only a few vehicles cross the conflict area. However, this situation does not occur for bicycle flow q^c , because bicycles have priority in passing over the crosswalk. The saturation flow rate of bicycles drops only slightly when bicycles are waiting for vehicles to cross the conflict area. Thus, in the proposed mixed-flow CA model, the transition phase from

the free flow to saturation is observed (Figure 7(a)). As shown in Figure 7(a), conflicts between vehicles and bicycles in the traffic system result in a drop in saturated flows, demonstrating that the model can reveal the interactions between vehicles and bicycles in the mixed traffic system.

4.3. Vehicle and Bicycle Flow Transition Phase. As can be seen in Figures 5(a) and 6(a), each curve has an obvious turning point (i.e., critical inflow rate) $\alpha_o^v(\alpha_o^b)$, which divides the flow

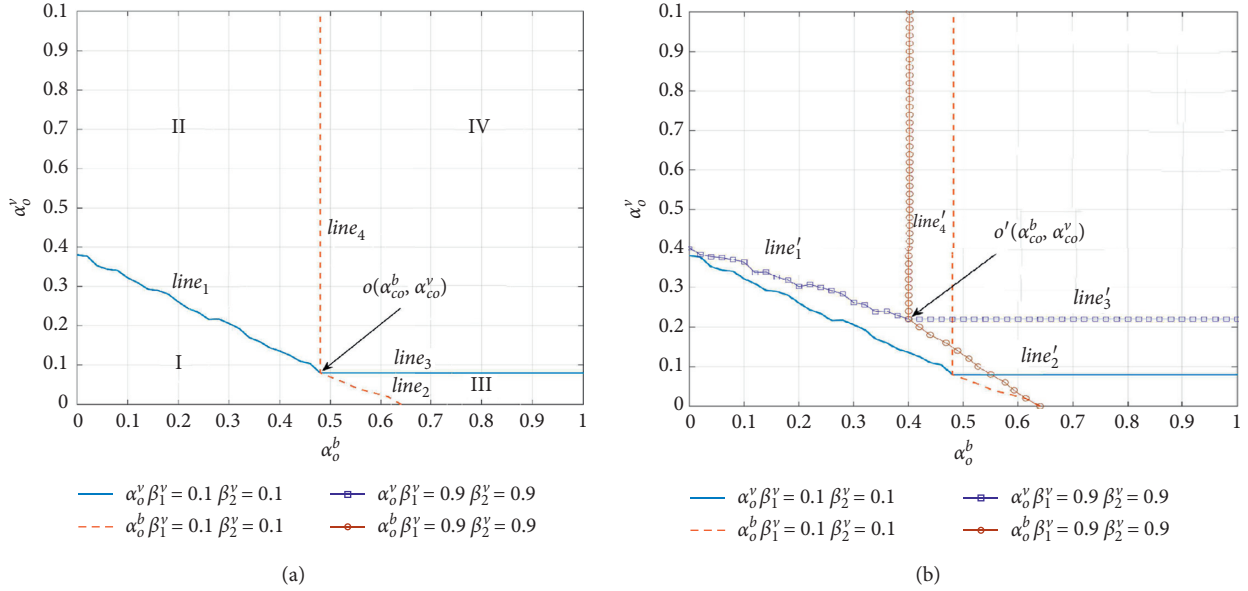


FIGURE 7: Phase diagram of vehicle and bicycle critical inflow rates.

into two regions: the free flow and saturated flow. This section mainly analyzes the transition phase between the vehicle flow q_o^v and bicycle flow q^c .

For $\alpha^v < \alpha_o^v$, the vehicle flow is free flow, and the vehicle flow only depends on its own inflow rate α^v . Conversely, for $\alpha^v > \alpha_o^v$, the vehicle flow is saturation flow, the vehicle flow q^v is independent of its own rate, and it reaches its saturation flow q_o^v , as shown in Figure 5(a). However, with an increase of bicycle inflow rate α^b , both the critical value of the inflow rate α_o^v and the saturation flow value q_o^v diminish until a minimum value is reached. To illustrate the relationship between the inflow rate α^v and the vehicle flow q^v , Figure 5(b) shows four curves of different bicycle inflow rates α^b . From this diagram, it is evident that the values of vehicle saturation flow q_o^v decrease from 0.34 to 0.05, and the critical values of inflow rate α_o^v decrease from 0.38 to 0.08. The drop ratio of q_o^v is about 85%. Similarly, for $\alpha^b < \alpha_o^b$, the bicycle flow is free flow, and for $\alpha^b > \alpha_o^b$, the bicycle flow is saturation flow. The bicycle flow q^b is independent of its own rate and reaches its saturation flow value q_o^b , as shown in Figure 6(b). The values of bicycle saturation flow q_o^b decrease from 0.54 to 0.44, and the critical values of inflow rate α_o^b decrease from 0.64 to 0.48. The drop ratio of q_o^b is about 19%.

It is noteworthy that the vehicle (bicycle) critical inflow rate α_o^v (α_o^b) gradually decreases with the bicycle (vehicle) inflow rate α^b (α^v). Moreover, the collective effect of vehicles and bicycles only appears when α^v and α^b surpass their critical value. The critical inflow rate α_o^v (α_o^b) is calculated and presented in the phase diagram in Figure 7. This transition phase can be classified into four zones; for example, $line_1$ and $line_3$ are the boundaries of Zone I (III) and Zone II (IV), which correspond to the critical value of the vehicle inflow rate α_o^v . In Zone I and Zone III, the vehicle is in free flow, whereas in Zone II and Zone IV, it is in saturation flow. As the bicycle inflow rate (α^b) increases, the vehicle critical inflow rate (α_o^v) first decreases and then remains stable. Similarly,

the bicycle critical inflow rate α_o^b shows the same trend ($line_2$ and $line_4$). With the gradual interaction between the two traffic flows, the vehicle's critical inflow rate α_o^v and bicycle's critical inflow rate α_o^b reach equilibrium at cross point $o(\alpha_{co}^b, \alpha_{co}^v)$.

In a word, the mixed-flow CA model effectively illustrates the transition phase from free flow to saturation for both vehicles and bicycles. It is interesting that the collective effect of the vehicle flow q^v and bicycle saturation flow q^b only appears when q_o^v and q_o^b surpass their critical inflow rate.

4.4. Comparison between Give-Way and Nonstrict Priority Give-Way Behavior. Demonstrating the effects of VNPGWB in mixed traffic flow, the proportion of VNPGWB drivers β_1^v and β_2^v has increased from 0.1 to 0.9, respectively. Figure 8(a) shows the relationships between flow and inflow rate for the vehicle and bicycle in the case of $\beta_1^v = 0.9$, $\beta_2^v = 0.9$, and $T = 30$ s. The vehicle saturation flow increases from 0.34 to 0.36 when $\alpha^b = 0$, while the vehicle saturation flow increases from 0.08 to 0.12 when $\alpha^b = 1$. When the bicycle inflow rate is low, the VNPGWB driver will quickly pass through the crosswalk, whereas the strict give-way driver will slow down to pass through the crosswalk due to caution. Thus, the vehicle saturation flow resulting from nonstrict priority behavior is slightly higher than from strict give-way behavior. With the further increase of the bicycle traffic flow rate, the VNPGWB driver can pass through the crosswalk more easily than can the strict give-way driver. In this way, VNPGWB can indeed improve the vehicle saturation flow, as the vehicle saturation flow of nonstrict priority is 1.5 times larger than that of strict give way. Figure 8(b) shows the effect of VNPGWB on vehicle saturation flow in the decision point rule and launching rule. The vehicle saturation flow decreases nonlinearly with an increasing proportion of VNPGWB drivers, with the

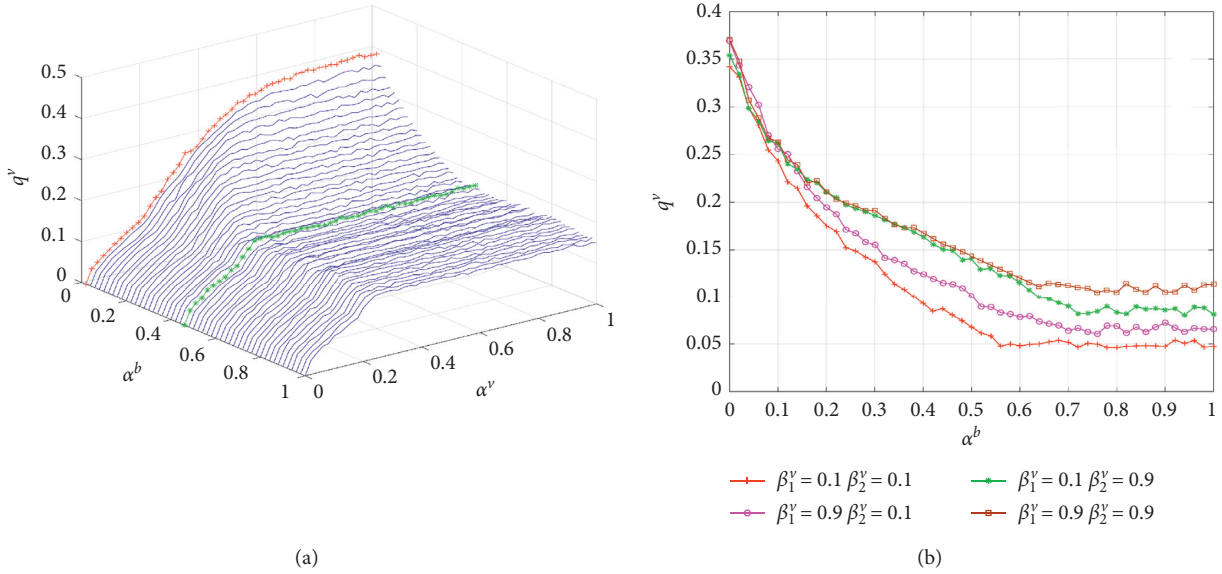


FIGURE 8: Relationship between vehicle flow and vehicle and bicycle inflow rate under different driving behaviors.

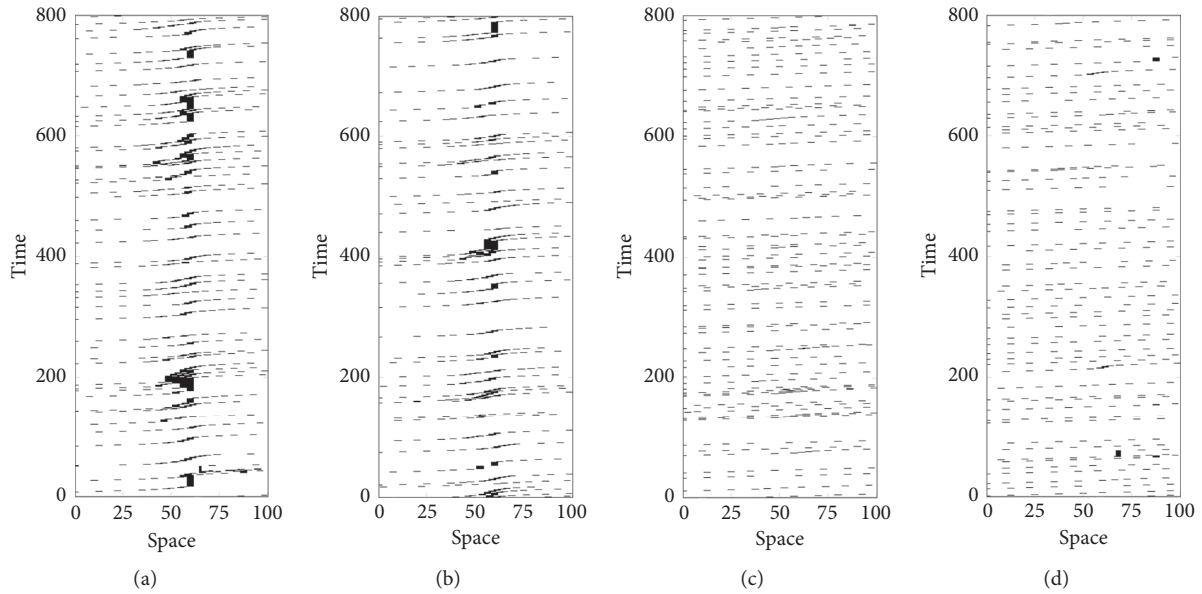


FIGURE 9: Space-time diagrams of free flow vehicles under different driving behaviors ($\alpha^v=0.1, \alpha^b=0.1$). (a) $\beta_1^v=0.1, \beta_2^v=0.1$. (b) $\beta_1^v=0.1, \beta_2^v=0.9$. (c) $\beta_1^v=0.9, \beta_2^v=0.1$. (d) $\beta_1^v=0.9, \beta_2^v=0.9$.

advantage of VNPGWB being more significant in the decision point rule than in launching rule. As shown in Figure 7(b), VNPGWB also affects the vehicle and bicycle critical inflow rates. For $\beta_1^v=0.9$ and $\beta_2^v=0.9$, the boundary of $line_1$ and $line_3$ moves up and boundary of $line_2$ and $line_4$ moves down. In other words, the proportion of free flow vehicle traffic increases with the increase of VNPGWB.

To further verify that the proposed model can simulate VNPGWB in the real world, the space-time trajectory diagrams for the vehicle lane are shown in Figures 9 and 10. Obviously, the microscopic model proposed in this study is primarily used to describe different microlevel driving behaviors. When the vehicle and bicycle are in free flow

(Figure 9), most vehicles pass through the crosswalk normally, while some drivers choose to slow down and temporarily stop to give way to bicycles at cellular spaces between 40 and 60. As mentioned in Section 3.2.2., the decision point is not a fixed point, which is also depicted in the space-time trajectory diagrams. When the vehicle and bicycle are in free flow, only $\beta_1^v=0.1$ produces congestion at cellular space 60, and it dissipates very quickly (Figures 9(a) and 9(b)). On the other hand, when vehicles and bicycles are in saturation flow, most vehicles need to slow down and stop outside the conflict area, as shown in Figure 10. In this case, the congestion cannot dissipate immediately. The β_2^c in the launching rule has a more significant effect on vehicle

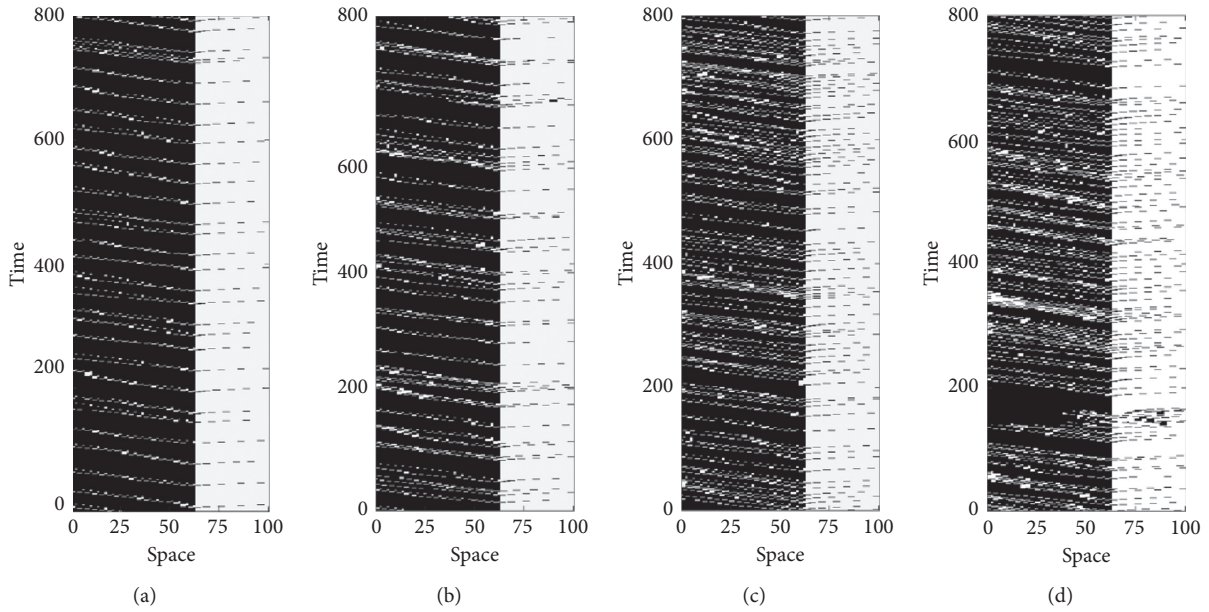


FIGURE 10: Space-time diagrams of saturation flow vehicles under different driving ($\alpha^v=0.5$, $\alpha^b=0.5$). (a) $\beta_1^c=0.1$, $\beta_2^v=0.1$. (b) $\beta_1^c=0.1$, $\beta_2^v=0.9$. (c) $\beta_1^c=0.9$, $\beta_2^v=0.1$. (d) $\beta_1^c=0.9$, $\beta_2^v=0.9$.

saturation flow than does β_1^c in the decision point rule. Due to bicycle saturation flow, the vehicles form a long queue and waiting for an acceptable gap. For $\beta_2^c=0.1$, the stopped vehicle can only be launched when its waiting time exceeds the waiting threshold (Figures 10(a) and 10(c)). For $\beta_1^c=0.9$, some of the space trajectories continue to pass into the conflict area, primarily due to nonstrict priority drivers sometimes choosing to follow the front vehicle through the crosswalk when the bicycle flow is high.

Overall, the space-time trajectory diagrams show that the proposed model in this study effectively simulates the interference between vehicles and bicycles. It is further demonstrated that VNPGWB can improve vehicle flow over strict give way. Especially, when the vehicle and bicycle are in saturation flow, this advantage of VNPGWB is significant. These conclusions can provide support for acquiescence to nonstrict priority behavior for practical management in those countries (e.g., China).

5. Conclusions

The crosswalk is one of the most serious conflict areas between vehicles and bicycles. With the aim of improving traffic flow without compromising safety, this study proposed a new mixed-flow cellular automaton model (CA) to simulate the vehicle nonstrict priority give-way behavior (VNPGWB) in the crosswalk conflict area. To consider the driving behaviors in the appropriate proportions, the proposed model simulates VNPGWB in real traffic conditions. This model was divided into three rules: the driving rule, the decision point rule, and the launching rule; VNPGWB occurs in the decision point rule and the launching point rule. The main results of the simulation model are as follows:

- (1) The mixed-flow CA model effectively illustrated the transition phase from free flow to saturation flow for

both vehicles and bicycles. As the vehicle and bicycle inflow rate increased, there is a critical inflow rate in each curve which divided the traffic flow between free flow and saturated flow. Moreover, the collective effect of vehicles and bicycles appeared only when the inflow rate surpassed its critical value.

- (2) Phase diagrams showed that the mixed traffic flow had a negative effect on the saturated flow of both vehicles and bicycles. When the bicycle inflow rate increased from 0 to 1, vehicle saturation flow values decreased from 0.34 to 0.05, and the critical values of inflow rate decreased from 0.38 to 0.08. When vehicle inflow rate increased from 0 to 1, bicycle saturation flow values decreased from 0.54 to 0.44, and the critical values of inflow rate decreased from 0.64 to 0.48.
- (3) The simulation results showed that the vehicle saturation flow of nonstrict priority behavior is 1.5 times larger than that of the strict give way, indicating that VNPGWB can improve the vehicle saturation flow. The space-time trajectory diagrams confirmed these results and thereby demonstrate the reliability of the simulation model. The advantage of VNPGWB over strict give way is most significant when the vehicle and bicycle are in saturation flow.

The simulation results, however, still require calibration of observed data to confirm the model's accuracy. Using field data to verify the model's association of parameters is recommended in the future study. In addition, the lack of variation in the size and speed of the simulated vehicles and bicycles in this study was a limitation that will be improved upon in future models. Moreover, the proposed model can also consider machine learning methods such as logistic regression and random forest to predict driving behavior.

Finally, similar studies can be conducted for the purpose of implementing traffic control at crosswalks with devices such as signal lights or stop signs. Nonetheless, this model provides insights that can be beneficial to traffic engineers and managers.

Data Availability

The simulation result data used to support the findings of this study are available from the corresponding author upon request.

Conflicts of Interest

The authors declare that they have no conflicts of interest.

Acknowledgments

This work was supported by Jiangsu Provincial Key Research and Development Program (Social Development) Project (BE2019713).

References

- [1] C. Yang, W. Wang, X. Shan, J. Jin, J. Lu, and Z. Li, "Effects of personal factors on bicycle commuting in developing countries," *Transportation Research Record: Journal of the Transportation Research Board*, vol. 2193, no. 1, pp. 96–104, 2010.
- [2] S. Cai, X. Long, L. Li, H. Liang, Q. Wang, and X. Ding, "Determinants of intention and behavior of low carbon commuting through bicycle-sharing in China," *Journal of Cleaner Production*, vol. 212, pp. 602–609, 2019.
- [3] C. Wang, C. Xu, J. Xia, and Z. Qian, "The effects of safety knowledge and psychological factors on self-reported risky driving behaviors including group violations for e-bike riders in China," *Transportation Research Part F: Traffic Psychology and Behaviour*, vol. 56, pp. 344–353, 2018.
- [4] L. Yang, Y. Wang, Q. Bai, and S. Han, "Urban form and travel patterns by commuters: comparative case study of wuhan and Xi'an, China," *Journal of Urban Planning and Development*, vol. 144, no. 1, 2018.
- [5] D. Zhao, G. P. Ong, W. Wang, and X. J. Hu, "Effect of built environment on shared bicycle reallocation: a case study on Nanjing, China," *Transportation Research Part A: Policy and Practice*, vol. 128, pp. 73–88, 2019.
- [6] X. Wu, W. Xiao, C. Deng, D. C. Schwebel, and G. Hu, "Unsafe riding behaviors of shared-bicycle riders in urban China: a retrospective survey," *Accident Analysis & Prevention*, vol. 131, pp. 1–7, 2019.
- [7] A. P. Silvano, H. N. Koutsopoulos, and X. Ma, "Analysis of vehicle-bicycle interactions at unsignalized crossings: a probabilistic approach and application," *Accident Analysis & Prevention*, vol. 97, pp. 38–48, 2016.
- [8] Z. Ma, J. Sun, and Y. Wang, "A two-dimensional simulation model for modelling turning vehicles at mixed-flow intersections," *Transportation Research Part C: Emerging Technologies*, vol. 75, pp. 103–119, 2017.
- [9] J. Pucher, R. Buehler, and M. Seinen, "Bicycling renaissance in North America? An update and re-appraisal of cycling trends and policies," *Transportation Research Part A: Policy and Practice*, vol. 45, no. 6, pp. 451–475, 2011.
- [10] L. Bai, P. Liu, Y. Chen, X. Zhang, and W. Wang, "Comparative analysis of the safety effects of electric bikes at signalized intersections," *Transportation Research Part D: Transport and Environment*, vol. 20, pp. 48–54, 2013.
- [11] P. Huertas-Leyva, M. Dozza, and N. Baldanzini, "Investigating cycling kinematics and braking maneuvers in the real world: e-bikes make cyclists move faster, brake harder, and experience new conflicts," *Transportation Research Part F: Traffic Psychology and Behaviour*, vol. 54, pp. 211–222, 2018.
- [12] A. Høyve and A. Laureshyn, "SeeMe at the crosswalk: before-after study of a pedestrian crosswalk warning system," *Transportation Research Part F: Traffic Psychology and Behaviour*, vol. 60, pp. 723–733, 2019.
- [13] H. C. Manual, *HCM2010. Transportation Research Board*, National Research Council, Washington, DC, USA, 2010.
- [14] N. Chaurand and P. Delhomme, "Cyclists and drivers in road interactions: a comparison of perceived crash risk," *Accident Analysis & Prevention*, vol. 50, pp. 1176–1184, 2013.
- [15] D. P. Allen, J. E. Hummer, N. M. Roupail, and J. S. Milazzo, "Effect of bicycles on capacity of signalized intersections," *Transportation Research Record: Journal of the Transportation Research Board*, vol. 1646, no. 1, pp. 87–95, 1998.
- [16] M. Räsänen, I. Koivisto, and H. Summala, "Car driver and bicyclist behavior at bicycle crossings under different priority regulations," *Journal of Safety Research*, vol. 30, no. 1, pp. 67–77, 1999.
- [17] D. Lin, W. Ma, L. Li, and Y. Wang, "A driving force model for non-strict priority crossing behaviors of right-turn drivers," *Transportation Research Part B: Methodological*, vol. 83, pp. 230–244, 2016.
- [18] Q. Bai, Y. Chen, Z. Qu, P. Tao, N. Cao, and Y. Shen, "Nonstrict priority left-turning maneuvers with a permitted phase at signalized: empirical study in China," *Journal of Transportation Engineering, Part A: Systems*, vol. 143, no. 3, 2017.
- [19] Q. Bai, Z. Qu, X. Song, S. Xiong, and N. Cao, "A method for determining the capacity of an exclusive left lane with a permitted phase under nonstrict priority," *Advances in Civil Engineering*, vol. 2019, Article ID 2357437, 8 pages, 2019.
- [20] K. Nagel and M. Schreckenberg, "A cellular automaton model for freeway traffic," *Journal De Physique I*, vol. 2, no. 12, pp. 2221–2229, 1992.
- [21] G. Ren, L. Lu, W. Wang, X. Gong, and Z. Huang, "Microscopic simulation model for pedestrian flow at signalized crosswalks," *Transportation Research Record: Journal of the Transportation Research Board*, vol. 2434, no. 1, pp. 113–122, 2014.
- [22] T.-Q. Tang, Y.-X. Rui, J. Zhang, and H.-Y. Shang, "A cellular automaton model accounting for bicycle's group behavior," *Physica A: Statistical Mechanics and Its Applications*, vol. 492, pp. 1782–1797, 2018.
- [23] S. Wolfram, *A New Kind of Science*, Wolfram Media, Champaign, IL, USA, 2002.
- [24] D. Zhao, W. Wang, C. Li, Z. Li, P. Fu, and X. Hu, "Modeling of passing events in mixed bicycle traffic with cellular automata," *Transportation Research Record: Journal of the Transportation Research Board*, vol. 2387, no. 1, pp. 26–34, 2013.
- [25] L. Lu, G. Ren, W. Wang, C.-Y. Chan, and J. Wang, "A cellular automaton simulation model for pedestrian and vehicle interaction behaviors at unsignalized mid-block crosswalks," *Accident Analysis & Prevention*, vol. 95, pp. 425–437, 2016.
- [26] J.-P. Meng, S.-Q. Dai, L.-Y. Dong, and J.-F. Zhang, "Cellular automaton model for mixed traffic flow with motorcycles," *Physica A: Statistical Mechanics and Its Applications*, vol. 380, pp. 470–480, 2007.

Research Article

An Alternative Method for Traffic Accident Severity Prediction: Using Deep Forests Algorithm

Jing Gan ¹, Linheng Li ¹, Dapeng Zhang ², Ziwei Yi ¹ and Qiaojun Xiang ¹

¹Jiangsu Key Laboratory of Urban ITS, School of Transportation, Southeast University, Nanjing 211189, China

²Big Data Research Center, Southwestern University of Finance and Economics, Chengdu 611130, China

Correspondence should be addressed to Qiaojun Xiang; xqj@seu.edu.cn

Received 10 February 2020; Revised 12 April 2020; Accepted 1 May 2020; Published 21 December 2020

Academic Editor: Qing Cai

Copyright © 2020 Jing Gan et al. This is an open access article distributed under the Creative Commons Attribution License, which permits unrestricted use, distribution, and reproduction in any medium, provided the original work is properly cited.

Traffic safety has always been an important issue in sustainable transportation development, and the prediction of traffic accident severity remains a crucial challenging issue in the domain of traffic safety. A huge variety of forecasting models have been proposed to meet this challenge. These models gradually evolved from linear to nonlinear forms and from traditional statistical regression models to current popular machine learning models. Recently, a machine learning algorithm called Deep Forests based on the decision tree ensemble has aroused widespread concern, which was proposed for the first time by a research team of Nanjing University. This algorithm was proved to be more accurate and robust in comparison with other machine learning algorithms. Motivated by this benefit, this study employs the UK road safety dataset to propose a novel method for predicting the severity of traffic accidents based on the Deep Forests algorithm. To verify the superiority of our proposed method, several other machine learning algorithm-based prediction models were implemented to predict traffic accident severity with the same dataset, and the prediction results show that the Deep Forests algorithm present good stability, fewer hyper-parameters, and the highest accuracy under different level of training data volume. It is expected that the findings from this study would be helpful for the establishment or improvement of effective traffic safety system within a sustainable transportation system, which is of great significance for helping government managers to establish timely proactive strategies in traffic accident prevention and effectively improve road traffic safety.

1. Introduction

Traffic safety has always been an important issue in sustainable transportation development. Traffic accidents will have some negative impacts on society, including casualties, traffic jams, and environmental pollution, which are not conducive to the sustainable and healthy development of the transportation system. With the gradual improvement of the level of automated information systems, in recent years, some government agencies and transportation industry companies have been committed to the development of intelligent transportation systems to help the sustainable development of transportation. Traffic accident prediction is a crucial and challenging issue in the domain of intelligent traffic safety management system; it is of great significance for analyzing the future development trend of traffic

accidents and implementing proactive prevention measures under existing road traffic conditions. To improve traffic safety management and control, it is necessary to seek timely and accurate methods for predicting traffic accident severity. In recent years, with the rapid development of science and technology, the advanced technology used in transportation has been strengthened at an unprecedented level. Unfortunately, these advanced technologies have no obvious advantages for the reduction of traffic accidents. Save LIVES-A road safety technical package 2017, issued by World Health Organization (WHO), indicated that road traffic accidents lead to the loss of over 1.2 million lives and cause nonfatal injuries to as many as 50 million people around the world each year, which are estimated to be the ninth leading cause of death across all age groups globally [1]. Road traffic crashes may be an everyday occurrence, but

they are predictable and preventable. Therefore, every traffic researcher has the responsibility to think over the causes of traffic accidents and help the administration in solving the problem of reducing the probability of traffic accidents. Over the years, researchers have tried various traffic accident severity analysis models from different perspectives. These modeling analyses are to explore the relationship between accident severity and its influencing factors, among which the most widely used is the discrete selection model based on the Logit or Probit model (e.g., [2–6]). These studies have shown that accurate traffic accident severity prediction plays an important role in improving traffic safety management, because, based on accurate prediction, the prominent influencing factors in high-risk road sections could be found out to provide beneficial suggestions for improving road safety.

Latterly, with the advancement of computer science, the era of big data has come. Many scholars began to try to apply some intelligent classification models based on knowledge discovery for accident degree analysis modeling, such as the Bayesian model, neural network model, decision tree model, and random forest model [7–11]. All of these models have one common characteristic that they do not require any assumptions on the relationship between the independent variables and dependent ones. Mujalli et al. [7] used Bayesian networks to improve classifying the traffic accident, which results in a reduction in the misclassification of deaths and serious injuries. García de Soto et al. [8] found that Artificial Neural Networks (ANNs) can be used as a feasible method to predict the frequency of road traffic accidents. Zhang and Fan [9] presented a data mining model using ID3 and C4.5 decision tree algorithms to analyze the traffic collision data. Pu et al. [10] conducted Full Bayesian before-after analysis of safety effects (crash severity levels, crash types, and crash causes) of variable speed limit system based on crashes data. Dadashova et al. [5] estimated the impact of the influencing factors on road traffic accident severity through random forests. It is worth noting that, in the above methods, random forest is an integrated learning method for classification, regression, and other tasks, which is more accurate and robust than other existing algorithms and effective for large databases. Therefore, in recent years, this method has been widely applied to various traffic problems [12–16]. Liu and Wu [12] established a traffic congestion prediction model using the machine learning classification algorithm, random forest. Mudali [13] analyzed the traffic big data using two comparative parallel algorithms M5P rules and random forest regression from the regression model for determining the nature of traffic big data. Nadarajan et al. [14] predicted a probabilistic space-time representation of complex traffic scenarios by using random forest algorithms. Kwon and Park [16] analyzed the impact of weather factors on traffic safety levels using k -means clustering and random forest techniques, and the result showed that the proposed model outperforms the conventional traffic safety prediction models.

There are certainly some shortcomings in the random forest model. Some researchers try to continuously improve the RFs (random forests) even though it already has many

advantages. Gao and Ke [17] employed a random survival forests model to analyze the incident duration analysis model and make a comparison with the traditional random forests model. The result shows that the random survival forests models are more accurate. Several researchers have proposed to incorporate RFs into the deep neural system [18–22]. The most representative of which is Deep Forests proposed by Zhou and Feng [18] in 2017. This algorithm with much fewer hyper-parameters was proved to achieve excellent performance in various domains by using the same parameter setting. Since this algorithm was recently proposed, there are almost no applications in the transportation field.

Road traffic accidents are the process of simultaneous damage to people or things caused by the miscoupling of dynamic and static factors (e.g., people, vehicles, roads, and the environment) [23–27]. The historical data of road traffic accidents can directly reflect the relationship between these factors during the accident. Benefitting from the excellent performance of Deep Forests, in this paper, we propose a traffic accident severity prediction method based on the Deep Forests algorithm, including data preprocessing, data feature selection, and accident severity prediction. After the data preprocessing is completed, we use the method of Random Forests to select the data features, which will be finally trained in Deep Forests algorithm. To the best of the authors' knowledge, this is the first time that the Deep Forests algorithm is used to predict the severity of traffic accidents. The correlations between each feature are inherently considered in the modeling. In addition, the final prediction results demonstrate that the proposed method for accident severity prediction has superior performance comparing with other machine learning algorithms.

The rest of this paper is organized as follows. Section 2 describes the dataset and the verification of its reliability. Section 3 presents the traffic accident severity prediction method based on the Deep Forests algorithm in this work, including the data preprocessing, which is of great importance for eliminating redundancies in the data and reorganizing the data efficiently. And the basic theory of feature selection and Deep Forests algorithm are introduced in this section as well. The experimental results are presented and discussed in Section 4, the application of this method is presented in Section 5, and conclusion and some future scopes are given in Section 6.

2. Data Description and Its Reliability Verification

This section firstly presents the data source adopted in this study. As this dataset has never been applied to severity prediction of a traffic accident, the reliability verification of this dataset is also conducted in this section.

2.1. Data Description. The analyses in this study are based on the road safety dataset of the United Kingdom in 2016. The data was obtained from the Kaggle website, a data prediction competition platform that allows data analysts to compete

with each other to solve real and complex data science problems. The local characteristics of traffic accident data include 18 items in total, for example, longitude and latitude of the accident point, time characters of accident, type of the vehicle, gender of the driver, age of the driver, age of the vehicle, speed limit, light conditions, weather conditions, road surface conditions, and the other data characteristics. We use simple statistical analysis to perform a simple descriptive statistical analysis of the entire dataset. The age of driver ranges from 1 to 97 with an average of 36; the vehicle age is on average 5 ranging from 1 to 84 years. 70% of the drivers are male and others are female. The most vehicle type is car, accounting for 71%, followed by pedal cycle, occupying about 7%. As for the accident severity, about 85% are slight accident; fatal accidents account for only about 1%. Figure 1 shows the structure of this dataset.

2.2. Data Reliability Verification. As this dataset has never been applied to severity prediction of a traffic accident, the reliability verification of this dataset should be conducted before preprocessing of the data. Reasonable data distribution is an important manifestation of reliable data. Therefore, three dimensions (latitude and longitude distribution, date, and time) of data distribution are considered in this paper to verify the data reliability.

According to the latitude and longitude information of the original dataset, we use the visual plotting tools for intuitive analysis. Figure 2 shows the latitude and longitude distribution of the data, in which Figure 2(a) is a scatter plot based only on the longitude and latitude information of the dataset, while Figure 2(b) is obtained by matching the scatter plot with the real-world map. Through the visualization of data, we can obtain a general macroscopic understanding of the distribution of the entire accident data. Furthermore, we can easily find that the latitude and longitude information of the traffic accident is consistent with the map information, and there is no deviation beyond the range of the map, which indicates that the dataset is reliable in accident position distribution dimension.

Besides the location dimension, the “date” dimension and the “time” dimension are also two important dimensions for analyzing the dataset reliability. As for the measure index, we choose the month for the “date” dimension and week for the “time” dimension in this study. As is shown in Figure 3(a), the data is equally distributed through all months. From Figure 3(b), it is not difficult to find that the accidents occurred mostly on Friday, and the accidents on Saturday and Sunday were relatively mild, which is fully compatible with the actual situation. Additionally, in order to explore the law of traffic accident occurrence at a different time of the day, we separate the day’s hours from the “time” dimension and combine with the week index. The heat map of the accident occurring in different hours of one day is shown in Figure 4, from which we can find that most of the accidents occurred in the morning and evening peak hours of the working day. This is completely consistent with people’s travel characteristics during the weekday, which indicates that the data is therefore reliable.

3. Methodology

This section discusses the method used for our prediction study. To ensure and improve the prediction accuracy, data preprocessing including data cleansing and data normalization is carried out before the feature selection and severity prediction. Random Forests algorithm is applied to extract the significant features of traffic accidents based on the preprocessed data. Finally, the Deep Forests algorithm is applied to predict the severity of a traffic accident. The flow diagram of traffic accident severity prediction in this paper is depicted in Figure 5.

3.1. Data Correlation Verification. Before we use machine learning to predict the severity of an accident, we must confirm the necessity to choose the machine learning method to deal with such a problem. If the data is highly correlated, we can directly use the simpler linear model to directly predict, and then there is no need to use machine learning to solve the problem. Thus, we conduct the data correlation relationship verification in this section.

As well as giving details of date, time, and location, the dataset gives a summary of all reported vehicles and pedestrians involved in road accidents and other related accident features. 18 variables are taken into account in this paper, including accident severity, month of year, hour of day, vehicle reference, vehicle type, vehicle manoeuvre, journey purpose of driver, sex of driver, age band of driver, engine capacity, propulsion code, age of vehicle, driver home area type, day of week, speed limit, light conditions, weather conditions, and road surface conditions. The correlation relationship between all the features in the data is analyzed. As a consequence, a Pearson correlation matrix was plotted to identify the amount of linear relationship between variables and to determine whether linear-based algorithms are suitable through gaining insight into data. The matrix is color-coded, the numerical value one expressed in dark blue represents a completely positive linear correlation between two features, while turquoise represents a zero, suggesting no linear correlation. As is shown in Figure 6, the accident severity is independent of any of the other 17 features, which means that we cannot directly predict the accident severity with a simple linear model. Therefore, this paper considers a smarter machine learning approach to deal with this problem.

Additionally, it is worth noting that, in Figure 6, most of the characteristic variables are linearly independent, except for weather conditions, road surface, and light condition, the light condition and hour of day, vehicle type, and engine capacity. It can be easily and reasonably explained for these results. When it rained, the road conditions will become wet and the light condition will change to some extent. Similarly, with the advent of the night, light and environment will change according to the characteristics of time. Besides, different types of vehicles have different engine capacities. Therefore, the interactive relationship between these variables also proves the reliability of this dataset on the other hand.

Information of driver			Information of road and environment			
Age_of_driver	Sex_of_driver	Journey_purpose_of_driver	Speed_limit	Light_conditions	Road_surface_conditions	Weather conditions
45	1 (male)	2 (commuting to/from work)	30	1 (daylight)	2 (wet/damp)	1 (fine without high winds)
21	2 (female)	1 (journey as part of work)	40	4 (darkness-lights lit)	1 (dry)	2 (raining without high winds)
36	1 (male)	3 (taking pupil to/from school)	20	6 (darkness-no lighting)	3 (snow)	3 (snowing without high winds)
15	2 (female)	4 (pupil riding to/from school)	50	5 (darkness-lights unlit)	4 (frost/ice)	7 (fog or mist)
.....

Information of vehicle				Accident information				
Vehicle_type	Age_of_vehicle	Engine_capacity	Vehicle_manoeuvre	Accident_index	Date	Time	Day of week	Accident_severity
8 (taxi)	1	1896	9 (turning right)	201506E098757	2015-03-09	12:56	2	3 (slight)
4 (motorcycle)	15	689	2 (parked)	201506F006668	2015-07-04	21:33	7	1 (fatal)
11 (bus or coach)	6	5883	11 (changing lane)	201506F003976	2015-07-22	8:40	4	2 (serious)
9 (car)	10	1995	18 (going ahead other)
.....

FIGURE 1: Structure of the road safety dataset of the United Kingdom.

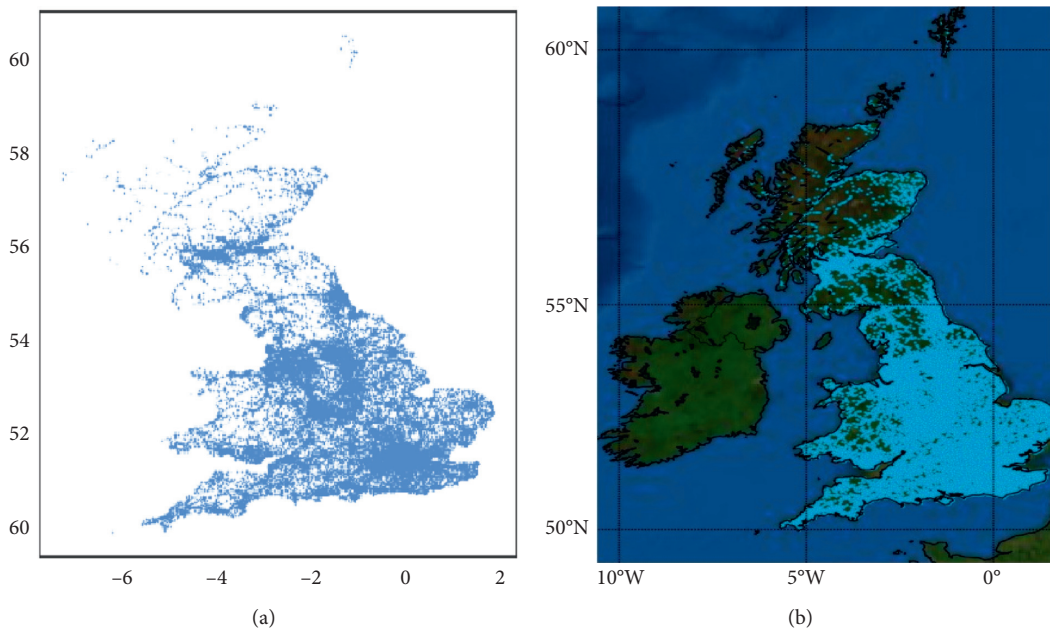


FIGURE 2: (a) The longitude and latitude map of the accident point and (b) the map-matching graph.

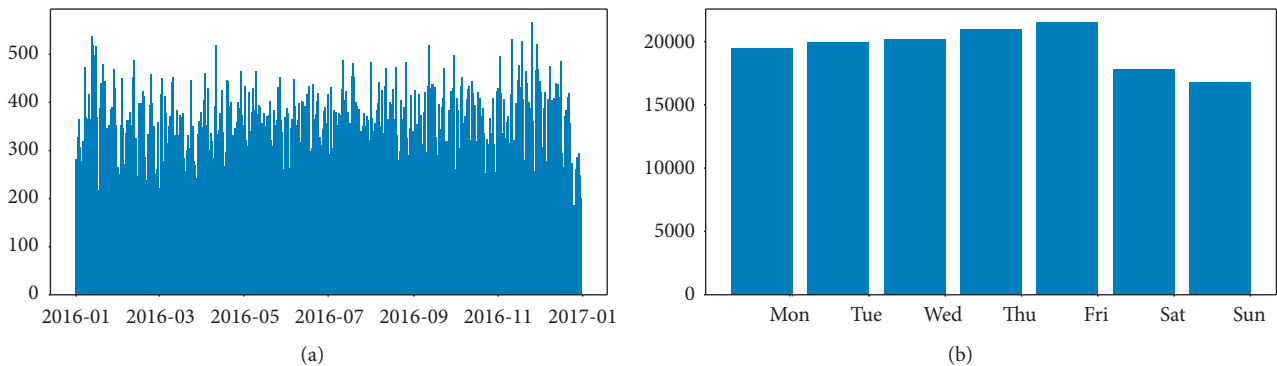


FIGURE 3: Date dimension and time dimension of the accident bar chart.

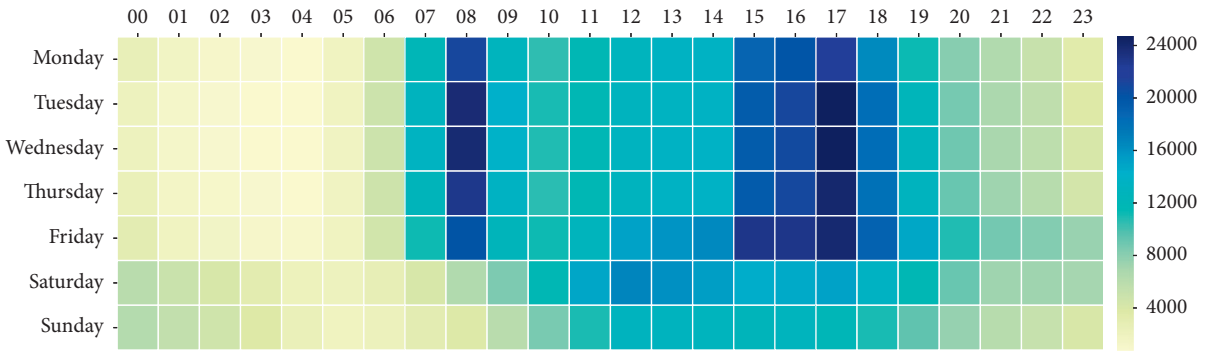


FIGURE 4: Traffic accident distribution per day and hour.

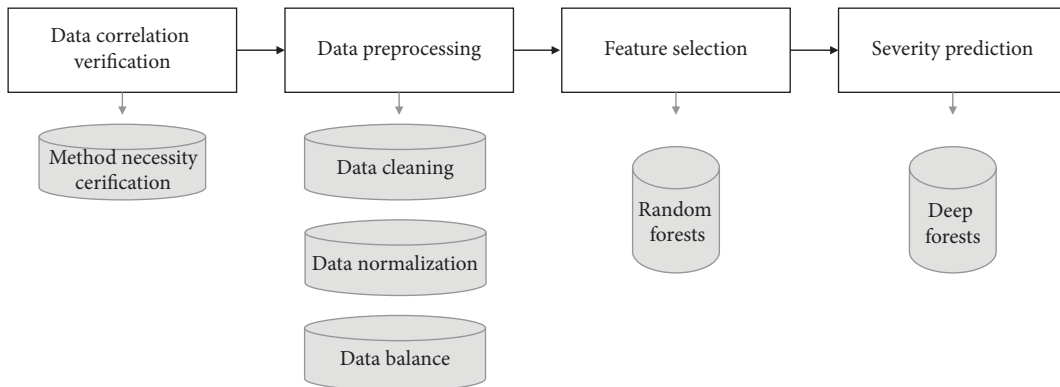


FIGURE 5: The flow diagram of traffic accident severity prediction method in this paper.

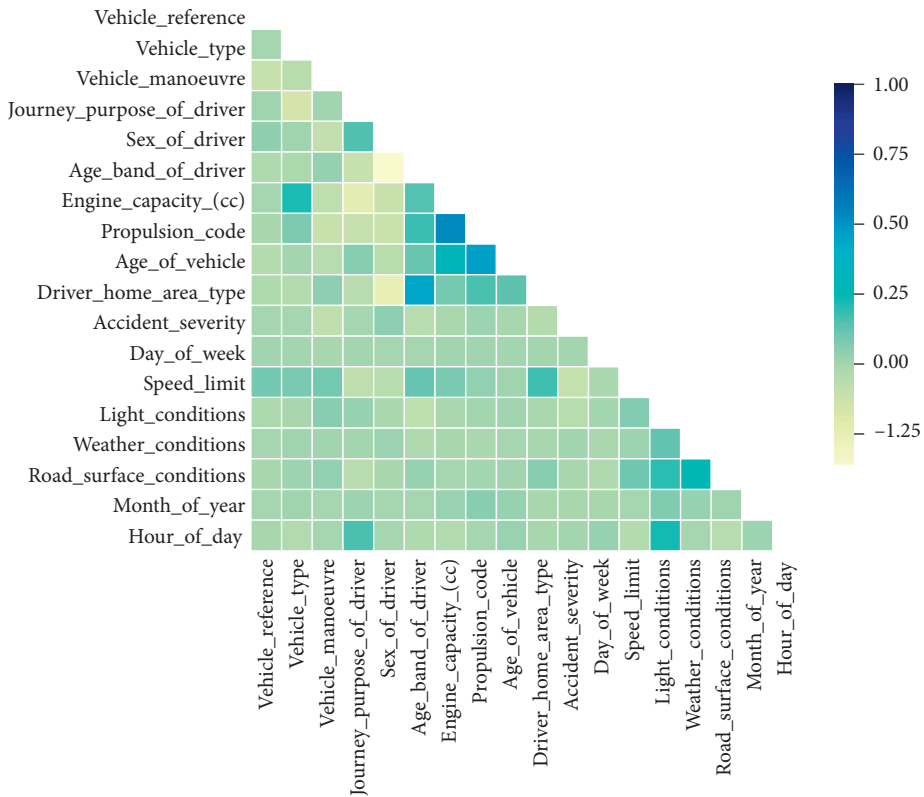


FIGURE 6: The Pearson correlation matrix of all features.

3.2. Preprocessing. It is of great importance to understand the nature of the available data and try to perform in-depth data analysis. Data preprocessing is very useful for meaningful data analysis; what we need to do is data cleaning, data normalization, and data selection in different class before our prediction analysis.

3.2.1. Data Cleaning. Data cleaning is the process of identifying incomplete, incorrect, inaccurate, or irrelevant parts of the data and then replacing, modifying, or deleting the dirty or coarse data from a record set, table, or database. The categorization criteria of all features in the dataset are listed, and the categorization criteria are defined by actual statistical results. So first, we need to observe the categorization criteria of each feature. However, due to the limited space, only a part of the categorization criteria of features is listed below. The categorization criteria of light conditions, weather conditions, and road surface conditions are shown in Table 1.

Through the statistical analysis of each feature of the original dataset, we found some obvious outliers and also some missing data that is labeled as “unknown” or “-1” needs to be cleaned up.

For some dimensions, the proportion of missing data exceeds 10%, and the average value replacement method was adopted. For example, in the dimension of *Age_of_Vehicle*, there are approximately 20% missing data labeled as “-1”; we adopted an average vehicle age of 5 to replace these missing values. For those dimensions with few missing data, we take a direct deletion method to clean them up, such as *Road_Surface_Condition*, where the missing data accounts for only 0.5%.

As for the obvious outliers, the same principle is adopted for the missing data processing method. For example, the *Age_of_Driver* is ranging from 1 to 97 with an average of 36; this age distribution is obviously unreasonable, because driving in the UK is only allowed for those over 17 years old. Because only 1% of the tags are under 17 years old, we thus directly delete them for the following processing.

3.2.2. Data Normalization. In the multi-index evaluation system, each evaluation index usually has different dimensions and orders of magnitude due to its different nature. When the levels between the indicators differ greatly if the analysis is performed directly with the original index values, the role of the higher-value indicators in the comprehensive analysis will be highlighted, and the effect of the low-level indicators will be relatively weakened. Therefore, in order to ensure the reliability of the results and to improve the convergence speed and accuracy of the model, the original indicator data needs to be normalized. Logarithm function conversion is adopted in this paper to conduct the normalization of all the given features to make sure features are on a similar scale. For example, for the feature *Age of Vehicle*, the age of the vehicle is between 1 and 84; the logarithmic method is used to standardize the distribution of the variable values so as to make the distribution of the variable values more “normal.” Figure 7(a) depicts the

distribution of *Age_of_Vehicle* before normalization, from which it can be easily found that the data shows obvious long tail characteristics. Normalization involves taking the logarithm of the given features. This is done because high values for certain variables computationally skew results more in favor of that variable than their actual contribution. In this case, age of the vehicle, for example, has values ranging from 1 to 84, when the majority of other categorical variables are binary or limited within 1–8 categories. After taking the log, one can notice that the values range from approximately 1 to 4, shown in Figure 7(b). This increases the performance of machine learning algorithms, as the numerical values do not have disproportionate amounts of computing value compared to all the other categorical variables.

3.2.3. Class Balance Verification. In the dataset, accident severity is listed as a classified label for prediction. Table 2 shows the criteria for categorizing accident severity and its distribution.

As can be seen from the distribution of data, the number of slight accidents is far greater than the number of fatal accidents, showing a long-tailed data distribution. In terms of model evaluation, accuracy was employed in this paper to compare the prediction performance. However, the accident severity level is unbalanced among three levels; therefore, the traditional classification algorithm with the overall classification accuracy as the learning goal will pay too much attention to the majority class, which will cause the accuracy paradox and deteriorate the classification performance of the minority class samples. This is why the data balance work should be conducted. The random sampling method was adopted in this paper. Both oversampling and undersampling have their own disadvantages, but this is the common problem of the imbalance of the dataset, which cannot be completely avoided.

After weighing the amount of data and enhancing the robustness of the model itself, we finally decided to take a combination of oversampling and undersampling to deal with this problem. Oversampling was adopted for training set to ensure as much training data as possible, trying repeated sampling to generate new rare samples to alleviate data imbalance. In addition, undersampling was adopted for test set to ensure that there are no duplicate samples in the test set, thereby improving the validity of the results.

After all this work was completed, 120,000 pieces of data for each category were obtained as the whole dataset. With the consideration of limited computational resources, 40,000 pieces of data for each category were randomly selected as the training set and 2,000 pieces of data for each category were screened out from the dataset as the test data for evaluating the performance of the model.

3.3. Feature Selection. An object usually has multiple properties, including related features, irrelevant features, and redundant features. Only these related features will improve the effectiveness of our learning algorithm. Since we are not aware which feature is effective for our prediction, dimensional disasters often occur in algorithmic

TABLE 1: Categorization criteria of several features.

Light conditions	Description	Weather conditions	Description	Road surface conditions	Description
1	Daylight: street lights present	1	Fine without high winds	1	Dry
2	Daylight: no street lighting	2	Raining without high winds	2	Wet/damp
3	Daylight: street lighting unknown	3	Snowing without high winds	3	Snow
4	Darkness: street lights present and lit	4	Fine with high winds	4	Frost/ice
5	Darkness: street lights present but unlit	5	Raining with high winds	5	Unknown
6	Darkness: no street lighting	6	Snowing with high winds		
7	Darkness: street lighting unknown	7	Fog or mist		
		8	Other		
		9	Unknown		

TABLE 2: Categorization criteria for traffic accident severity.

Accident severity code	Label	Distribution of the data
1	Fatal	2899 (1.12%)
2	Serious	34205 (13.27%)
3	Slight	220741 (85.61%)

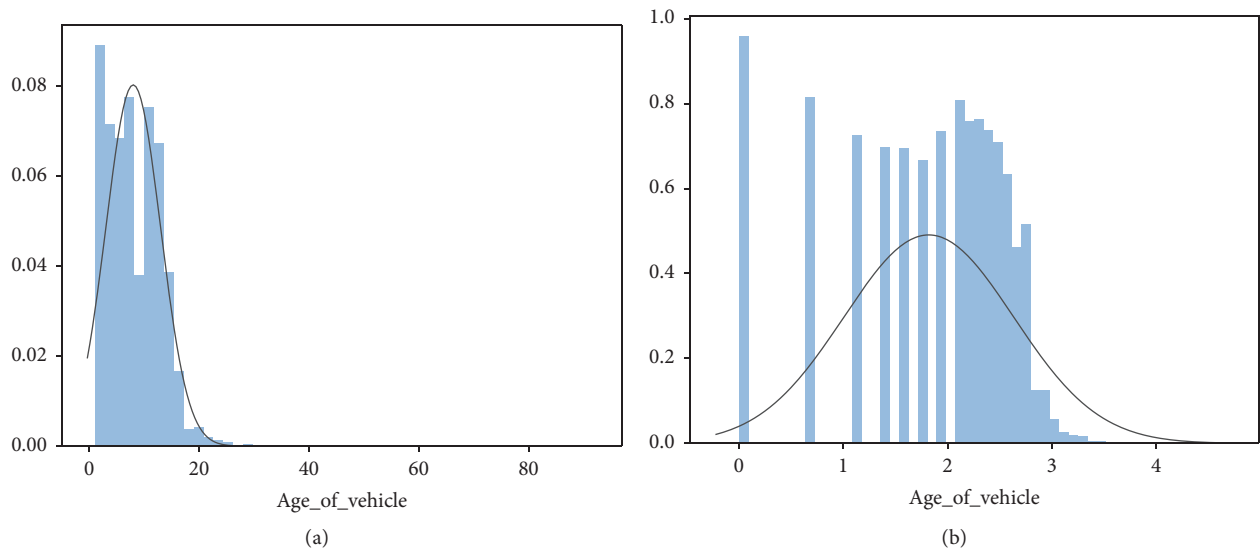


FIGURE 7: Data distribution (a) before normalization and (b) after normalization.

applications. So, it is of great significance to select relevant features from all features to improve the efficiency of the learning algorithm, especially for the analysis of complex data. A vast number of feature selection strategies have been proposed for applications in different fields [28–31]. In this paper, Random Forests (RFs) method is adopted to carry out feature selection according to the importance index of each feature, not only because of its ability to calculate the importance of a single feature variable, but also due to its good performance on most datasets.

RFs model is developed from decision-making regression trees, which will often generate hundreds of trees. The data of each tree is extracted from the bag of set B by

bootstrap sampling method, while the remaining out-of-bag (OOB) samples are defined as set \bar{B} , which will not appear in the training samples. Let C define a set of B and \bar{C} as a set of \bar{B} . Assuming $X_n \times p$ matrix is an n -dimensional test dataset with p characteristics, y is an n -dimensional label vector, and each value represents the corresponding category to which the test belongs. The random forest algorithm calculates the importance of the features by rearranging the errors before and after classification. Each feature X_j in the algorithm corresponds to a set of feature replacement tests with rearranged values. The importance of features is measured by comparing the classification error rates of the original features and the replaced randomly rearranged

features in the OOB test set, which is the extent to which the change of original feature affects the result. When the important features are replaced by the randomly rearranged features, their discrimination will decrease; that is, the OOB classification error rate will increase. When N trees are established, there are N OOB sets as test sets. Therefore, the characteristic importance index J_a is defined as follows:

$$J_a(x_j) = \frac{1}{N} \sum_{B_k \in \mathcal{C}} \frac{1}{|B_k|} \left(\sum_{i \in B_k} I(h_k^{\bar{x}_j}(i) \neq y_i) - I(h_k(i) \neq y_i) \right), \quad (1)$$

where y_i is a classification label in the i -th OOB, I denotes a characteristic function, $h_k(i)$ represents a classification label of sample i predicted by dataset B_k , and $h_k^{\bar{x}_j}(i)$ is a classification label after replacing characteristic x_j .

3.4. Severity Prediction. The representation learning in deep neural networks mainly depends on the processing of the original features by layer. Inspired by this, Zhou and Feng [18] obtained the cascade structure of Deep Forests as illustrated by the left schematic diagram in Figure 8. In a traditional deep neural network, each node denotes a neuron. In their research, the RFs were treated as a “forest neuron” and were stacked into multiple layers in deep learning. The cascade structure of deep neural networks is also presented by the right schematic diagram in Figure 8. Comparing with deep neural networks, the design concept of using Deep Forests resembles deep neural networks, and the “concatenate” and “vote” in Deep Forests resemble the nonlinear transformation procedures in deep learning. More significantly, the Deep Forests algorithm has much fewer hyper-parameters, each grade can be regarded as an ensemble of ensembles, and excellent performance is achieved in various domains by using the same parameter setting.

Each level of cascade receives feature information processed by its preceding level and outputs its processing result to the next level. Each level is an ensemble of decision trees forests, which means it can be regarded as an ensemble of ensembles. When a sample is given, each forest is calculated by calculating the percentage of different classes of training samples at the leaf nodes falling into the related instances, and then the average value of all the trees in the forest to generate the estimation of the distribution of the class. As shown in Figure 9, the red part highlights the path of each sample traversing leaf nodes. Different markings in leaf nodes represent different classes.

In order to reduce the risk of overfitting, the class vectors generated by each forest are generated by k -fold cross-validation. In particular, each instance will be used as the $K-1$ training data, producing a $K-1$ class vector, and then taking the average value to produce the final class vector as the enhancement feature at the lower level in the cascade. It is important to note that after a new level is extended, the performance of the entire cascade will be estimated on the validation set, and the training process will be terminated without significant performance gain. Therefore, the number of cascading cascades is automatically determined. Contrary

to most deep neural networks with fixed complexity of the model, Deep Forests can determine the complexity of its model (early stop) properly through termination training, which enables Deep Forests to be applied to training data of different scales, not limited to large-scale training data.

4. Experimental Work and Results

This section introduces our experimental work and results with the methodology proposed in Section 3. To verify the superiority of our proposed method, several other machine learning algorithm-based prediction models were implemented to predict traffic accident severity with the same dataset, and the prediction results show that the Deep Forests algorithm with fewer hyper-parameters presents good stability and the highest accuracy under different level of training data volume.

4.1. Feature Selection. As described in 3.1, our dataset includes 18 features, and these features are almost independent of each other, which means that the complexity of this dataset is relatively high, and not all features are useful for improving forecasting accuracy since there may be some irrelevant or redundant features in those features. Therefore, before using the Deep Forests algorithm to predict the dataset, the feature selection work first is of great importance.

A combination of the Randomized Search and Grid Search method was adopted in this paper for parameter optimization. The Randomized Search method is applied firstly to quickly help us determine the approximate range of a parameter, and then we use the Grid Search method to cross-validate the selected candidate parameters of the model iteration and determine the optimal value of a parameter. The output of the best parameters is 5 for Max_depth, 2 for Min_samples_leaf, 10 for Min_samples_split, and 1000 for n_estimators. Therefore, a total of 1000 trees were used to grow the forest, and this number was deemed sufficient to yield reliable results. The feature importance ranking from the RFs is shown in Figure 10. Using the node purity measure, the explored variables were ranked in rising order from the least to the most important. Our principle for choosing the importance threshold is the $\emptyset 80$ value of the cumulative value curve of importance. According to the importance value of each features, the $\emptyset 80$ value is around 0.04; we thus adopted 0.04 as the critical value for the important features. Finally, eight features were chosen to conduct the accident severity prediction, including engine capacity, hour of day, age of vehicle, month of year, day of week, age band of driver, vehicle manoeuvre, and speed limit.

4.2. Severity Prediction Results. In this section, the eight features selected by the feature selection are used as the main data features. And then the Deep Forests algorithm is adopted to predict the severity of traffic accidents and produce the predicted accuracy. In our experiment, the cascade structure used in Deep Forests is as follows: each level consists of 4 completely random tree forests and 4

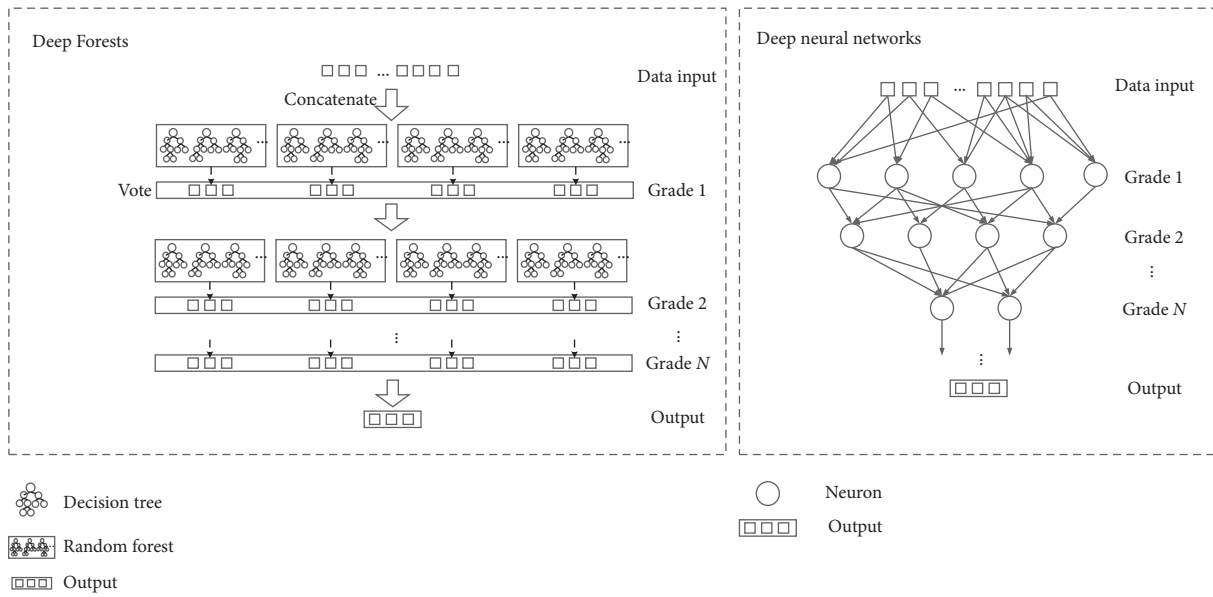


FIGURE 8: The cascade structure of Deep Forests and deep neural networks.

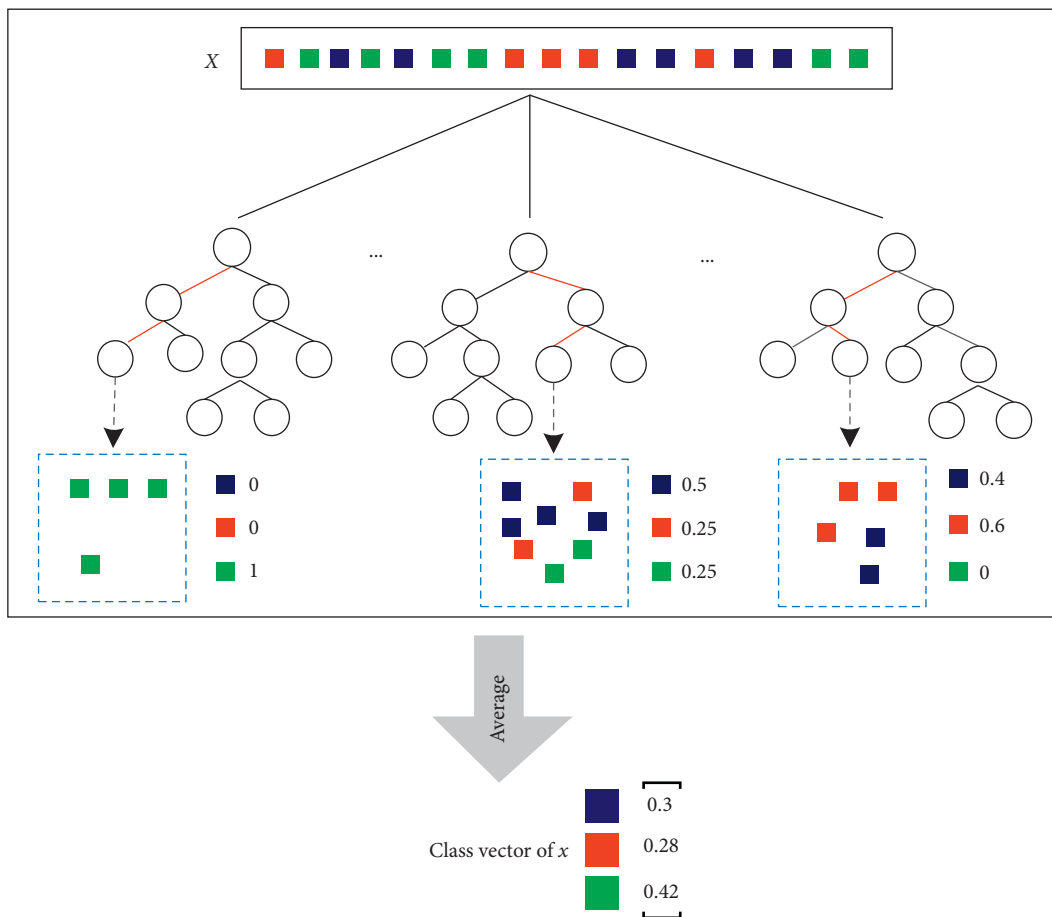


FIGURE 9: The classification process of training samples.

random forests, each with 500 trees, and three-fold CV is used for class vector generation. These settings of cascade structure are consistent with that proposed by Zhou and

Feng [18], because it has been proven that this cascade structure is able to achieve excellent performance by using the same default setting in their paper. Hence, it is supposed

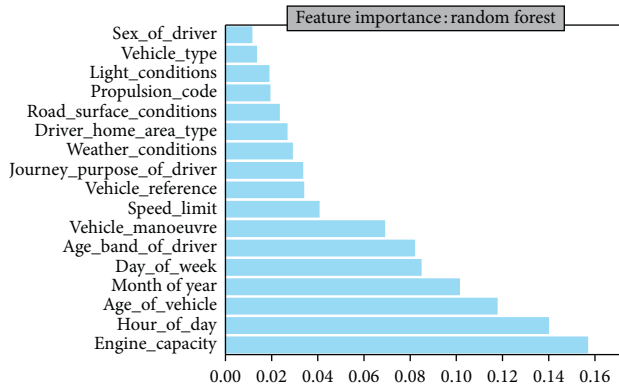


FIGURE 10: Feature importance results by Random Forests algorithm.

that this cascade structure is good enough with some consideration of performance and time consumption.

In order to verify that Deep Forests can achieve significant performance gains for traffic accident severity prediction, we compare Deep Forests with DNN and several other popular machine learning algorithms which are widely used in traffic accident prediction algorithms, such as Random Forests, LightGBM, XGboost, k-Nearest Neighbor (KNN), and decision trees. The computation progress for each algorithm is calculated and recorded by the same computer, which is equipped with a 2.8 GHz Intel Core i7 CPU and a 16 GB RAM. All of the forecasting models are implemented in Python language.

Table 3 illustrates the performance of Deep Forests, DNN, RFs, LightGBM, XGboost, KNN, and decision trees algorithms for traffic accident severity prediction. From the evaluation index results, Deep Forests algorithm performs better than other models. Recall is higher than other models; false alarm rate is lower than other models, so the overall F1 score is also higher. It shows that the model controls well the influence of data imbalance and learns the characteristics of different types of data. The ROC reached 90%, indicating that the model has learned the difference between different categories of data, and the prediction results are more reliable and stable.

In addition, the experimental results show that the direct use of DNN cannot achieve the desired effect on the problems studied in this paper. This is expected, because there are significant differences in the number of samples in different categories; it is difficult for the DNN model to learn the differences between categories. Without adding new data, we believe that constructing a more suitable deep learning model structure with carefully tuned hyper-parameters can achieve better results to a certain extent, but this is beyond the scope of this paper. This is also the reason why this paper chooses the Deep Forests algorithm based on the characteristics of the dataset and the problem itself.

Due to the classification tasks of many data imbalance problems, we tend to pay more attention to the performance of the model on the minority class, the predictive performance of different accident categories is presented, as shown in Table 4. It can be easily found that the model performs

TABLE 3: Average predictive performance of different models.

	Accuracy (%)	Recall	False alarm rates	F1 score	Roc
Deep forests	90.69	0.92	0.09	0.91	0.93
RFs	88.98	0.90	0.10	0.90	0.92
XGboost	83.49	0.83	0.16	0.83	0.87
LightGBM	83.01	0.83	0.17	0.83	0.87
Decision tree	81.04	0.81	0.19	0.81	0.85
KNN	77.26	0.77	0.23	0.77	0.82
DNN	53.52	0.54	0.47	0.47	0.52

worse in categories with fewer samples, compared with the predictive performance for the majority category. But the decline is less compared to other models, so the model adopted in this paper is more robust overall. In addition, in the performance of this imbalanced dataset, the tree-based models perform better than the neural network model; this is also the reason why we adopt Deep Forests model instead of the neural network model.

In order to better observe the performance of Deep Forests under different training data volumes, we divide the data into multiple orders of magnitude, and the accuracy of different magnitudes with different models are plotted in Figure 11, from which we can see that, with the increase of the sample size of the training set, the performance of each model has improved to a certain extent. However, the Deep Forests model is significantly better than other models at a small sample size, which also proves that the advantage of the model when dealing with small-scale sample size. In addition, the advantage of Deep Forests model is gradually weakened with the increase of sample size. When the sample size reaches 100,000, we can find that although the performance of Deep Forests is a little better than the random forest, it is not much different.

Additionally, compared with many traditional machine learning methods, the Deep Forests algorithm used in this paper has its own advantages. Deep Forests model has much fewer hyper-parameters than deep neural networks, although their iterative structure is similar. We usually do not know the optimal value of the model hyper-parameter for a given problem. Researchers generally rely on experience or use replicated values on other issues or search for the best values through trial and error. The increase in hyper-parameters will bring additional randomness to the model performance, which is too dependent on the regulation of hyper-parameters. For instance, there are many hyper-parameters in random forests that need to be constantly adjusted to optimize model prediction accuracy and speed up model calculations, including number of decision trees in the forest, the maximum number of features a random forest can have in a single tree, number of leaves, OOB sampling, and random state. However, the hyper-parameters in Deep Forests algorithm is less than random forests, and a set of hyper-parameters can be applied to different datasets as mentioned in literature [18], which is another big point of the deep forest algorithm used in this paper.

TABLE 4: The predictive performance of different accident categories.

	Recall			False alarm rates			F1 score			ROC		
	1	2	3	1	2	3	1	2	3	1	2	3
Deep Forests	0.93	0.82	1.00	0.17	0.09	0.01	0.88	0.86	1.00	0.91	0.88	1.00
RFs	0.91	0.77	1.00	0.19	0.10	0.01	0.86	0.83	1.00	0.90	0.86	1.00
XGboost	0.83	0.66	1.00	0.27	0.20	0.02	0.78	0.72	0.99	0.84	0.79	0.99
LightGBM	0.84	0.63	1.00	0.29	0.20	0.02	0.77	0.71	0.99	0.84	0.78	1.00
Decision tree	0.68	0.76	1.00	0.23	0.28	0.05	0.77	0.72	0.95	0.78	0.80	0.98
KNN	0.66	0.64	1.00	0.32	0.33	0.07	0.67	0.66	0.97	0.75	0.75	0.98
DNN	0.80	0.07	0.70	0.52	0.51	0.38	0.60	0.13	0.66	0.56	0.43	0.56

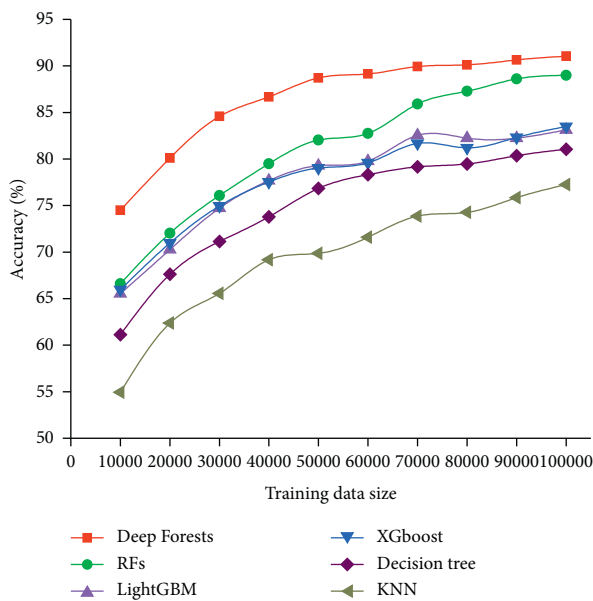


FIGURE 11: Accuracy rate comparison under different training data size.

5. Discussion

The higher prediction accuracy of our proposed method reveals that it can be used as a very useful tool for accident severity prediction. Fewer hyper-parameters in the deep forest will be more conducive to the transplantation of models; that is, a set of hyper-parameters can be applied to different datasets. Thus, it can be easily adapted to solve lots of different traffic problems as well, for instance, short-term forecast of travel time on expressway sections and traffic flow situation estimation. This is of great significance for the perfect improvement of the current traffic safety system within a sustainable transportation system, such as an intelligent transportation decision system and intelligent traffic safety management system.

From the perspective of traffic safety management implications, the more accurate severity prediction of traffic accidents has long been the research direction we are pursuing for sustainable transportation development. In most cases, many traffic safety control measures are still dominated by the limited experience of traffic managers, which may lead to a deviation from the actual

situation. On the contrary, the use of many excellent deep learning algorithms can learn from the historical accident data record effectively and efficiently. The application of Deep Forests algorithms proposed in this paper has been proved to have good performance in predicting the severity of an accident. The prediction results can be used as an important and effective reference for the subjective judgment of safety managers. For instance, if a traffic safety management want to identify the important influencing factors of traffic accident and the severity level of traffic accidents caused by these factors, the general method we proposed in this paper can be easily carried out for different dataset by these managers to achieve their goals. In addition, the prediction outcomes of severity level can also provide an effective reference for the implementation of traffic accident management and control measures, such as the improvement of transportation infrastructure, the improvement of lighting conditions, the implementation of road variable speed limit, and driving safety warning.

6. Conclusions

With the recognition of the importance of machine learning in solving some problems in the transportation field, in this paper we innovatively apply the Deep Forests algorithm to the prediction of traffic accident severity. The excellent forecasting performance of our proposed method reveals that it can be used as a very useful tool for accident severity prediction. Fewer hyper-parameters in the deep forest will be more conducive to the transplantation of models; that is, a set of hyper-parameters can be applied to different datasets. Thus, it can be easily adapted to solve lots of different traffic problems as well, for instance, short-term forecast of travel time on expressway sections and traffic flow situation estimation, although from the analysis results there is still room for improvement in prediction accuracy. This is because we have not done enough in the mining of raw data. For future research of this study, in order to improve prediction accuracy, we will try to summarize and construct some features that do not exist in the features of raw data based on the information of the data features. In addition, it should be noted that this paper does not focus on optimizing the model parameters, which is also a research direction in the future. Nevertheless, the method proposed in this paper has certain contributions to both theory and practice.

Data Availability

The data used in this article is from the open-source database Kaggle, which can be downloaded freely at <https://www.kaggle.com/>.

Conflicts of Interest

The authors declare that they have no conflicts of interest.

Acknowledgments

This research was funded by the National Key R&D Program of China (Grant no. 2018YFC0704704).

References

- [1] World Health Organization (WHO), *A Road Safety Technical Package*, World Health Organization, Geneva, Switzerland, 2017.
- [2] X. Meng, L. Zheng, and G. Qin, "Traffic accidents prediction and prominent influencing factors analysis based on fuzzy logic," *Journal of Transportation Systems Engineering and Information Technology*, vol. 2, p. 15, 2009.
- [3] P. T. Savolainen, F. L. Mannering, D. Lord, and M. A. Quddus, "The statistical analysis of highway crash-injury severities: a review and assessment of methodological alternatives," *Accident Analysis & Prevention*, vol. 43, no. 5, pp. 1666–1676, 2011.
- [4] K. Li, D. Qian, S. Huang, and X. Liang, "Analysis of traffic accidents on highways using latent class clustering," in *Proceedings of the 19th COTA International Conference of Transportation Professionals-CICTP*, pp. 1800–1810, Nanjing, China, July 2016.
- [5] B. Dadashova, B. A. Ramirez, J. M. McWilliams, and F. A. Izquierdo, "The identification of patterns of interurban road accident frequency and severity using road geometry and traffic indicators," *Transportation Research Procedia*, vol. 14, pp. 4122–4129, 2016.
- [6] Z. Yan, X. Lu, and W. Hu, "Analysis of factors affecting traffic accident severity based on heteroskedasticity ordinal Logit," in *Proceedings of the Sixth International Conference on Transportation Engineering ICTE 2019*, American Society of Civil Engineers Reston, pp. 422–435, Chengdu, China, September 2020.
- [7] R. O. Mujalli, G. López, and L. Garach, "Bayes classifiers for imbalanced traffic accidents datasets," *Accident Analysis & Prevention*, vol. 88, pp. 37–51, 2016.
- [8] B. Garcia de Soto, A. Bumbacher, M. Deublein, and B. T. Adey, "Predicting road traffic accidents using artificial neural network models," *Infrastructure Asset Management*, vol. 5, no. 4, pp. 132–144, 2018.
- [9] X.-F. Zhang and L. Fan, "A decision tree approach for traffic accident analysis of saskatchewan highways," in *Proceedings of the 2013 26th IEEE Canadian Conference on Electrical and Computer Engineering (CCECE)*, Toronto, Canada, May 2013.
- [10] Z. Pu, Z. Li, Y. Jiang, and Y. Wang, "Full bayesian before-after analysis of safety effects of variable speed limit system," *IEEE Transactions on Intelligent Transportation Systems*, vol. 99, pp. 1–13, 2020.
- [11] J. Zhang, Z. Li, Z. Pu, and C. Xu, "Comparing prediction performance for crash injury severity among various machine learning and statistical methods," *IEEE Access*, vol. 6, pp. 60079–60087, 2018.
- [12] Y. Liu and H. Wu, "Prediction of road traffic congestion based on random forest," in *Proceedings of the 2017 10th International Symposium on Computational Intelligence and Design (ISCID)*, vol. 2, pp. 361–364, Hangzhou, China, December 2017.
- [13] P. Mudali, J. Roopa, M. G. Raju, and A. Yadav, "Analysis of Parallel M5P and Random Forest Regression for Visualization of Traffic Behavior," in *Proceedings of the Computational Intelligence in Pattern Recognition*, pp. 231–241, Springer, Hangzhou, China, December 2020.
- [14] P. Nadarajan, M. Botsch, and S. Sardina, "Predicted-occupancy grids for vehicle safety applications based on autoencoders and the random forest algorithm," in *Proceedings of the 2017 International Joint Conference on Neural Networks (IJCNN)*, pp. 1244–1251, IEEE, Anchorage, AK, USA, January 2017.
- [15] J. Li, "Bus arrival time prediction based on random forest," in *Proceedings of the 2017 5th International Conference on Frontiers of Manufacturing Science and Measuring Technology (FMSMT 2017)*, Taiyuan, China, June 2017.
- [16] O. H. Kwon and S. H. Park, "Identification of influential weather factors on traffic safety using K-means clustering and random forest," *Advanced Multimedia and Ubiquitous Engineering*, vol. 393, pp. 593–599, 2016.
- [17] Y. R. W. Gao Z and A. Ke, "Urban expressway traffic incident duration prediction based on random survival forests," *Journal of Tongji University*, vol. 45, no. 9, pp. 1304–1310, 2017.
- [18] Z. Zhou and J. Feng, "Deep forest: towards an alternative to deep neural networks," in *Proceedings of the Twenty-Sixth International Joint Conference on Artificial Intelligence*, Melbourne, Australia, August 2017.
- [19] S. Rota Bulo and P. Kotschieder, "Neural decision forests for semantic image labelling," in *Proceedings of the IEEE Conference on Computer Vision and Pattern Recognition*, pp. 81–88, Columbus, OH, USA, June 2014.
- [20] P. Kotschieder, M. Fiterau, A. Criminisi, and S. Rota Bulo, "Deep neural decision forests," in *Proceedings of the IEEE International Conference on Computer Vision*, pp. 1467–1475, Santiago, Chile, December 2015.
- [21] G. Biau, E. Scornet, and J. Welbl, "Neural random forests," *Sankhya A*, vol. 81, no. 2, pp. 347–386, 2019.
- [22] Y. Wang, S.-T. Xia, Q. Tang, J. Wu, and X. Zhu, "A novel consistent random forest framework: bernoulli random forests," *IEEE Transactions on Neural Networks and Learning Systems*, vol. 29, no. 8, pp. 3510–3523, 2017.
- [23] M. S. Horswill and S. Helman, "A behavioral comparison between motorcyclists and a matched group of non-motorcycling car drivers: factors influencing accident risk," *Accident Analysis & Prevention*, vol. 35, no. 4, pp. 589–597, 2003.
- [24] E. K. Adanu, S. Jones, and K. Odero, "Identification of factors associated with road crashes among functionally classified transport modes in namibia," *Scientific African*, vol. 7, Article ID e00312, 2020.
- [25] Z. Pu, S. Wang, C. Liu, Z. Cui, and Y. Wang, "Road surface friction prediction using long short-term memory neural network based on historical data," *Electrical Engineering and Systems Science*, <https://arxiv.org/abs/1911.02372>, 2020.
- [26] M. Touahmia, "Identification of risk factors influencing road traffic accidents," *Engineering, Technology & Applied Science Research*, vol. 8, no. 1, pp. 2417–2421, 2018.
- [27] Z. Pu, Z. Cui, S. Wang, Q. Li, and Y. Wang, "Time-aware gated recurrent unit networks for forecasting road surface friction

- using historical data with missing values,” *IET Intelligent Transport Systems*, vol. 14, no. 4, pp. 213–219, 2020.
- [28] G. Chandrashekar and F. Sahin, “A survey on feature selection methods,” *Computers & Electrical Engineering*, vol. 40, no. 1, pp. 16–28, 2014.
- [29] R. Genuer, J.-M. Poggi, and C. Tuleau-Malot, “Variable selection using random forests,” *Pattern Recognition Letters*, vol. 31, no. 14, pp. 2225–2236, 2010.
- [30] J. Ou, J. Xia, Y.-J. Wu, and W. Rao, “Short-term traffic flow forecasting for urban roads using data-driven feature selection strategy and bias-corrected random forests,” *Transportation Research Record: Journal of the Transportation Research Board*, vol. 2645, no. 1, pp. 157–167, 2017.
- [31] L. Breiman, “Random forests,” *Machine Learning*, vol. 45, no. 1, pp. 5–32, 2001.

Research Article

Towards a Severity Assessment Method for Potential Cyber Attacks to Connected and Autonomous Vehicles

Qiyi He ¹, Xiaolin Meng,¹ and Rong Qu²

¹Nottingham Geospatial Institute, University of Nottingham, Nottingham, UK

²School of Computer Science, University of Nottingham, Nottingham, UK

Correspondence should be addressed to Qiyi He; qiyi.he@nottingham.ac.uk

Received 12 January 2020; Revised 29 May 2020; Accepted 21 August 2020; Published 3 September 2020

Academic Editor: Zeyang Cheng

Copyright © 2020 Qiyi He et al. This is an open access article distributed under the Creative Commons Attribution License, which permits unrestricted use, distribution, and reproduction in any medium, provided the original work is properly cited.

CAV (connected and autonomous vehicle) is a crucial part of intelligent transportation systems. CAVs utilize both sensors and communication components to make driving decisions. A large number of companies, research organizations, and governments have researched extensively on the development of CAVs. The increasing number of autonomous and connected functions however means that CAVs are exposed to more cyber security vulnerabilities. Unlike computer cyber security attacks, cyber attacks to CAVs could lead to not only information leakage but also physical damage. According to the UK CAV Cyber Security Principles, preventing CAVs from cyber security attacks need to be considered at the beginning of CAV development. In this paper, a large set of potential cyber attacks are collected and investigated from the aspects of target assets, risks, and consequences. Severity of each type of attacks is then analysed based on clearly defined new set of criteria. The levels of severity for the attacks can be categorized as critical, important, moderate, and minor. Mitigation methods including prevention, reduction, transference, acceptance, and contingency are then suggested. It is found that remote control, fake vision on cameras, hidden objects to LiDAR and Radar, spoofing attack to GNSS, and fake identity in cloud authority are the most dangerous and of the highest vulnerabilities in CAV cyber security.

1. Introduction

Connected and autonomous vehicle (CAV), as a subset of the Intelligent Transportation System, makes use of different hardware, e.g., electronic control units (ECUs) and sensors, software, e.g., entertainment system and decision-making units, and data fused from multiple sources to conduct driving tasks with different levels of automation. With these components, CAVs could not only drive without human involvement but also communicate with surroundings to navigate and take appropriate reactions. The automation of CAVs is supported by the sensors installed around the vehicle body which gather information of surrounding environments to make decisions. The connectivity is achieved by the communication with other vehicles, infrastructures, and pedestrians on the road to navigate and take relevant reactions.

Currently, a large number of companies investigate and focus on the research and development of CAVs. In China, one of the biggest IT companies Baidu released an open source autonomous driving platform named Apollo, aiming to address the challenging issues of precise sensing and decision-making [1]. In USA, Tesla released their Autopilot for assistant driving and Summon system for assistant parking in 2015 and 2016, respectively [2]. The latest news on Tesla official website [3] introduces the enhanced Autopilot system, which supports autonomous driving in certain scenarios such as highways. Google is also a leading player in connected and autonomous driving. Its subcompany Waymo, set up in 2009, has been focusing on the research and development of CAVs and finished more than 2 million miles road test [4]. Taxi-hailing company Uber also tests their own CAVs on public roads in Arizona [5]. In Europe, traditional vehicle manufactures including Audi and

Mercedes Benz also announce their initiatives on CAVs. Audi already conducted 550 km on-road test, based on their own autonomous vehicle “Jack” [6]. Mercedes Benz started to develop CAVs in 1980s; now, their latest S-class Benz vehicles completed 100 km road trials in Germany [7].

To accelerate the CAV development, governments also publish relevant regulations and principles. In USA, regulations and laws on CAV are built at the state level [8]. Chinese government also released a ten-year plan “Made in China 2025” plan, which aims to master the key CAV technologies by 2025 [9]. In addition, Chinese government launched an abundance of CAV demonstration projects and set up Jiading district in Shanghai as the first public test field for CAVs [10]. Moreover, CAV competitions among academic organizations have been held successfully several times around the world. These include the US DARPA Urban Challenge in 2007 and DARPA Grand challenge in 2004 [11]. In China, the Future Challenges of Intelligent Vehicles competition has been held since 2008, sponsored by the National Natural Science Foundation of China [12]. With the participation of an increasing number of research organizations, these competitions not only provide platforms for researchers to communicate but also raise public interests on CAV developments. According to a survey conducted by Boston Consulting Group, 55% of public would like to try an autonomous vehicle or even buy one [13].

However, all the CAV research works mentioned above focus on the functions of either automation or connectivity. The cyber security of CAVs is not being sufficiently addressed. As a fundamental part of the CAV development, cyber security plays a crucial role on the function safety of CAVs, which will influence public trust and CAV commercialization directly. According to the newly released UK CAV Cyber Security Principles [14], CAV cyber security should be considered at the early stage of CAV development from the design phase, based on which the whole supply chain could then prevent CAVs from cyber security risks and issues in the following phases.

Comparing to traditional networks, mobile network or traditional automobile network, CAV cyber security has specific characteristics including large amount of data, complex functions, and fatal consequences, as shown in Table 1. These differences indicate that the cyber security of CAVs should be considered specifically and in different ways compared to the cyber security strategies in traditional networks or automobile networks.

The main aim of this paper is to investigate different potential cyber attack points of CAV. The specific characteristics of CAV are analysed and potential attack points of CAV are listed. The authors also present new criteria to evaluate the potential attacks to CAVs. The severity of each attack is then analysed and mitigation methods are then suggested.

The main contributions of this paper are listed as below:

- (1) Definitions and categorization of all the potential attacks for CAVs: the attack categories cover both the autonomous elements such as the in-vehicle system

and sensors on the vehicles, and the connected parts or functions such as V2X communication in CAVs. The paper also identifies the gaps and the limitations of current studies. For example, there is a lack of research and developments on cyber security for the connectivity elements of CAVs. In addition, those papers in the literature discussing the attacks to CAVs focus on only some specific attack types. The missing types of attacks require further research. By defining the initial set of all potential attacks to CAVs within a structured category and of different severities, additional unexpected new attacks to CAVs could be added in the future research. That is, the categories of the potential attacks and criteria apply to new attacks; thus, the set of attacks is extendable to include new attacks.

- (2) A new severity assessment on potential attacks to CAVs: the assessment criteria used in engineering and information technology are adopted to define the criteria suitable for assessing CAVs attacks. This is a new adoption of such criteria assessing the severity of different CAV attacks.
- (3) A new categorization of mitigation methods to CAV attacks: the recovery and protection mechanisms are key issues in cyber security of CAVs. Defining mitigation methods presents guidance to future research, including intrusion detection or encryption to protect the overall CAV systems. The mitigation category method categorizes the mitigation methods into prevention, production, acceptance, transference, and contingency. With the establishment of test environments, this categorization could be adopted to respond to different attacks.

The paper is structured as follows. Section 2 introduces the related works on cyber security in CAVs and also the related subject of Vehicular Ad hoc Network. Section 3 then describes the methodology to define different criteria to assess the risk of different attacks. In Section 4, the potential cyber attacks are listed to analyse each of their severity with the criteria listed in Section 3. Mitigation methods of cyber security attacks on CAVs are then recommended in Section 5. Section 6 summarizes the paper and discusses the future challenges faced by CAV cyber security research.

2. Related Work

The SAE International defined “driving automation” as that the system could conduct part of or all DDT (Dynamic Driving Tasks) continuously [20]. DDT are defined as three different levels by the SAE J3061 standard, namely, operational functions, tactical functions, and strategic functions. The relations of these three functions are illustrated in Figure 1. Operational functions include basic motion control such as lateral and longitudinal motion controls. Tactical functions include all the operational functions plus OEDR (Object and Event Detection and Response). In the current DDT performance, the strategic functions such as destination and waypoint planning are not included.

TABLE 1: Comparison of CAVs/traditional vehicles/mobile networks.

Compared to traditional vehicles	Compared to computer network/mobile network
1. There are more ECUs and more codes in CAVs [15], which means more data to be processed	1. In addition to information leakage, cyberattacks to CAVs could cause physical damage or even fatal injuries
2. There are multiple communication protocols in CAVs, such as CAN [16], 5G, and DSRC [17]; different communication protocols lead to multiple data formats, which require more preprocessing time	2. CAVs require higher detection accuracy as well as shorter data processing time; in the Europe Metis project, the latency is expected to be less than 5 ms and the accuracy is expected to be 99.999% when transmitting a 1600 bytes data package [18]
3. There are more connected functions, meaning the number of potential attack points is also increasing [19]	3. The application scenarios are more complicated; CAVs are more likely to drive in unregulated areas such as parking lots, highways, and rural areas

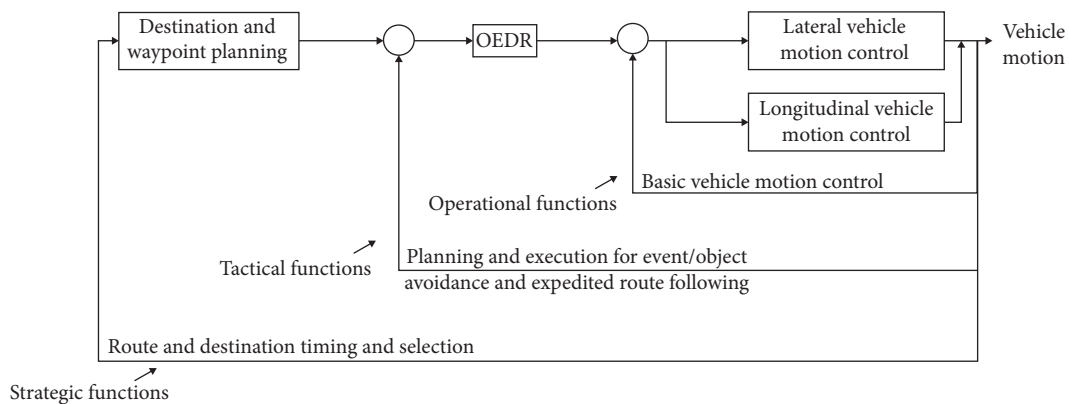


FIGURE 1: Schematic view of driving tasks [20].

The response by either users or the system to perform DDT when a system failure happens is defined as DDT fallback by SAE International. ODD (Operational Design Domain) is considered as the driving system which requires a specific running environment including environmental, geographical, or time restrictions. For example, some autonomous driving vehicles only operate in a closed environment [21], which indicates that the vehicle is still designed under a limited ODD. Based on the DDT performance, DDT fallback, and ODD, SAE International then defines the vehicle automation into 6 different levels, as shown in Table 2.

Besides the automation taxonomy, there are attempts to discuss CAV cyber security. In [22], the authors discussed the possible cyber security attacks on autonomous vehicles. After listing all the possible attacks, the authors then provided mitigation solutions to each attack. It is recommended that it is important to keep sufficient redundancy in autonomous vehicles. Sufficient sensor data could help vehicles to know the surroundings and positions. Among all these attacks, they believed that GNSS spoofing and fake message injection are the most threatening risks, both of which will threaten passengers' lives. It is believed that antispooing hardware and authentication methods are needed in autonomous vehicles.

In [23], the authors discussed cyber security in connected vehicles and believed that the vehicles would be more vulnerable with the increasing connectivity. This paper described the possible attack scenarios including USB

update attacks, communication attacks, and malicious application installation. A system using machine learning methods is then built to detect the anomaly behaviours in CAN-Bus (Controller Area Network) and the operating system.

In [24], the authors attempted to use the categories of cyber security in computer science to describe the possible attacks in CAVs. The possible attacks are divided into passive attacks and active attacks. The passive attacks are easy to prevent but difficult to detect, while the active attacks are easy to detect but difficult to prevent. Feasible mitigation methods including authentication and encryption were recommended.

In [25], the authors assumed that connected vehicles are similar to all the Internet devices and cyber security should be considered as a fundamental part of their development. The authors then discussed the potential cyber attacks on V2I (Vehicle-to-Infrastructure) Communication and proposed a novel cyber security architecture called CVGuard to detect the attacks in V2I. The CVGuard reduced 60% DDoS (Distributed Denial of Service) attacks which might cause vehicle conflicts.

In [19], it is pointed out that modern cars are already new targets for hackers. Engines, doors, and brakes could all be possible vulnerable points. In addition, nowadays, the attackers do not need to approach the target vehicle physically. All the vehicles in the communication range could be hacked. The authors also listed OBD (On-Board Diagnostics) threat, DSRC communication, Malware, and

TABLE 2: SAE automation levels [20].

Level	Name	DDT		DDT fallback	ODD
		Sustained motion control	OEDR		
0	No driving automation	Driver	Driver	Driver	N/A
1	Driver assistance	Driver and system	Driver	Driver	Limited
2	Partial driving automation	System	Driver	Driver	Limited
3	Conditional driving automation	System	System	Fallback-ready user (becomes the driver during fallback)	Limited
4	High driving automation	System	System	System	Limited
5	Full driving automation	System	System	System	Unlimited

automobile apps as the most vulnerable parts on vehicles. The authors then offered the solutions to address the cyber security issues including OTA solution, cloud based solution, and layer-based solution.

There are also research attempts in simulation environments to examine the influence of cyber attacks to CAVs. In [26], simulated slight attacks were made to study longitudinal safety of CAVs, i.e., on the positions and speed via GPS communications. An empirical model named PATH CAV from a field test [27, 28] and a RCRI (Rear-end Collision Risk Index) based on stopping distance was used to evaluate the safety. The authors found that the slight attacks to the CAV positions are severer than they are to the speed. The slight cyber attacks will also make severer impacts on decelerating than accelerating. In addition, the slight attacks to multiple CAVs are more dangerous than attacks of higher severity to fewer number of vehicles. This research will help to find a more efficient mitigation method to the attacks to V2V communications.

In [29], four possible attack points of the vehicle have been discussed, including signal controllers, vehicle detectors, roadside units, and onboard units. The focus was on the attacks to infrastructures. The authors attacked the traffic signal control systems by sending spoofed data, which showed to increase the delay. Some attacks in the experiments also showed to cause severe congestion. Based on the attacks, an approach was devised to identify this kind of attacks by analysing the attack locations, which helps to design a more stable transportation network.

As a fast emerging research topic, CAV cyber security has just started attracting increasing research attention. In addition to the limited research on cyber security in CAVs, research on VANET (Vehicular Ad hoc Networks) may contribute to the research on the connected functions of CAVs. VANET uses V2V communication and V2I communication to help vehicles gathering traffic information [30], while CAVs extend the boundaries to the wider V2X (Vehicle-to-Everything) communications.

VANET is a mobile ad hoc network, where the vehicles are the mobile nodes [31]. In [31], the authors listed the possible privacy and security challenges to the safety of VANET including the attacks on confidentiality, integrity, or data trust. They claimed that encryption is important to VANET.

In [32], the authors concluded that VANET has three specific characteristics, which are frequent vehicle movement, time critical response, and hybrid architecture. Other

attacks listed include bogus information, DoS attacks, Masquerade, and GPS spoofing. The authors also propose several mitigation methods including public key, certificate revocation approaches, and ID-based cryptography.

Research in [33] focused on threats and attacks to vehicular communication. The authors built a three-layer framework and pointed out the potential threats and attacks to V2X communication such as remote communication protocols including DSRC or Bluetooth. It also suggested machine learning and block chain as countermeasures to detect attacks.

In the literature listed above, the majority of the researchers believe that cyber security is a fundamental part in CAV developments, which demands urgently more research and investigations. The majority of researchers agreed that the increasing connected and autonomous functions will increase the possibilities of cyber attacks. However, existing research mainly focused on the cyber security of autonomous functions. The potential attacks should be considered from both the autonomous and connected aspects. There are attempts to discuss the most severe attacks, but there is a lack of systematic evaluation criteria in the literature. Some research discussed the mitigation methods including encryption or authentication, but there are still the needs of further investigations to identify comprehensive and systematic mitigation methods to categorized cyber attacks. Overall, the literature on CAV cyber security is limited and requires more investigation and research efforts. Awareness of cyber security in CAV should be raised as well.

This paper significantly extends the existing research by defining potential attacks to both connectivity and autonomy, as well as both in-vehicle and intervehicle potential cyber attacks. Moreover, severity evaluation criteria for cyber attacks are defined and the severity level of each attack is also evaluated based on the criteria defined in this paper. Corresponding mitigation methods are then suggested at the end. This research aims to raise cyber security awareness of consumers, OEMs, researchers, and manufactures and also present a starting point to develop the detection and prevention methods towards CAV cyber attacks.

3. Potential CAV Cyber Attack Criteria

The potential attack points or attack ports are analysed firstly. For each potential attack, the following criteria will then be adopted to assess its severity.

The new CAV assessment criteria are defined based on the widely used formula in engineering risk assessment in different areas including transportation and infrastructure [34], information technology system [35], and civil aviation [36]:

$$\text{Risk} = \text{Asset} * \text{Vulnerability} * \text{Threat}. \quad (1)$$

The new assessment criteria evaluate three aspects of cyber attacks, namely, the asset of the possible attack targets, vulnerability of the possible risks to the attack targets, and threat of the possible consequences. As mentioned in Section 1, due to several key differences between traditional automobile network cyber security and CAV cyber security, some extra criteria are adapted to our new CAV cyber security assessment. For example, to evaluate the severity of the risk, the assessment criteria of CAVs should consider not only the level of information leakage but also the level of physical damage.

3.1. Asset of the Attacked Targets

- (1) Asset name: in computer security, ISO/IEC 13335-1: 2004 defines that assets include all the hardware or software components on computers which are exposed to an attack target, e.g., a dataset and one piece of hardware or software code [37]. CAVs are equipped with a large number ECUs and sensors and are thus vulnerable to an abundance of possible attacks. More detailed assets will be explained in Section 4.
- (2) Asset importance: the importance of each asset is categorized into three levels:
 - (a) Low: the breakdown of this asset will not affect the operational and tactical functions of the whole CAV system. In the SAE J3016 standard [20], operational functions include lateral and longitudinal vehicle motion control, including the most basic functions of starting, stopping, driving, and controlling [38]. The tactical functions include the OEDR as introduced in Section 2.
 - (b) Medium: the breakdown of this asset might influence tactical functions of the vehicle, however would not have direct impacts on the operational functions. In addition, the asset function could be replaced or covered by other assets on the vehicle. For example, if cameras on CAV breakdown, the vehicle could still use other sensors to detect the surroundings.
 - (c) High: the breakdown of this asset may cause damage to operational functions of the vehicle directly. For example, the in-vehicle system, which sends instructions to ECUs to maintain the vehicle speed or stop the vehicle in certain situations, is of high importance.

3.2. Vulnerability of the Attacked Targets

- (1) Risk name: each asset may be exposed to more than one risk. This criterion assesses specific risks to each asset; more details are presented in Section 4.

(2) Difficulty of conduction: the difficulty of conducting an attack varies depends on its characteristics. Some attacks may require sufficient expertise from the attackers in specific areas such as GPS spoofing or fake identification. Some devices, such as GNSS satellites, are securely protected by the governments. Hacking into these devices needs not only knowledge but also sufficient time and money. The difficulty of conduction is considered based on the knowledge, time, and budget needed and can be graded into three levels listed as below:

- (a) Low: attackers do not need to acquire relevant knowledge to conduct the attack or the target asset is easy to be obtained/bought on the market. The attack is not time consuming.
 - (b) Medium: attackers only need to spend a short time (weeks/months) to learn the required knowledge. Hacking into the target asset needs to be purchased at a high price, or the hacking process is time consuming.
 - (c) High: attackers need to have extensive knowledge on the target asset or need to spend years to learn relevant knowledge. The target asset is difficult to find in the market or costs an astronomical figure.
- (3) Detection possibilities: this criterion defines the level of possibilities detecting attacks by the users or the CAV system. In computer science, the attacks are divided into two main categories, namely, passive attacks and active attacks [39]. Passive attacks do not interrupt the system but will monitor or eavesdrop it to access information. Active attacks will interrupt the system functions directly by methods such as injecting fake message. In general, passive attacks are difficult to detect but easy to defend, while active attacks are difficult to defend but easy to detect [24]. Although passive attacks may not cause harms on system functions, the information loss could also be a severe risk because CAVs will be the ultimate personal mobile device in the future [40], storing sensitive data including personal home address, contact numbers, and financial information. It is essential to evaluate the detection possibilities of different attacks. The levels of detection possibilities are categorized into three levels as listed below.
- (a) Low: the attacks will not affect any function (whether operational or tactical functions) of the CAV system. It is difficult to detect the attack in normal use. The best solution is to prevent the attacks from happening in advance with encryption or authentication.
 - (b) Medium: the attacks will not affect the operational functions of the CAV system so the users would not notice the attacks immediately. However, the attacks would affect some parts of the tactical or strategic functions. The system will detect the abnormal behaviour afterwards and warn users.

- (c) High: the attacks will influence the operational function immediately so the users could notice them immediately. For example, if the vehicle suddenly stopped on the road, the users would notice the abnormal situation immediately. In addition, if the cameras around the vehicle breakdown, the system will notice this abnormal situation promptly.

3.3. Consequences of the Attacks

- (1) Consequence name: to each possible risk, there may be more than one consequence. The consequences will be listed and then be analysed; more details are presented in Section 4.
- (2) Severity of information leakage: information leakage has been a major cyber security issue in computer science. Information leakage attacks usually damage the confidentiality, integrity, and availability of the system [37]. The severity is based on the scale and importance of the leaked information.
 - (a) Low: the attack will not leak any private information.
 - (b) Medium: the attack will leak nonconfidential personal information or unimportant information at a small scale. For example, the attacker may know the preference of the passenger on choosing routes or on the entertainment system. This type of information leakage will not cause further harm directly.
 - (c) High: the attack will leak highly important confidential information such as the financial information, the home address, or the personal ID. With this information, the attackers could conduct further harmful actions to the victims. In other situations, this information leakage would cause larger scale information leakage such as personal data stored in the cloud.
- (3) Severity of physical damage: compared with traditional networks, cyber attacks to CAVs could lead to physical damage or even fatalities directly. Tesla vehicle has already caused fatalities on a straight road with good visibility and in a good weather [41]. On March 2018, an Uber autonomous vehicle struck and killed a pedestrian crossing the road in Arizona, USA [42]. The Uber test vehicle failed to detect the pedestrian in the environment of low visibility and failed to conduct any corresponding actions. As a large machine, CAV could cause hazards or even be exploited as a weapon. With the possible consequences, the severity of physical damage can be categorized as below.
 - (a) Low: the attacks are not likely to cause physical damage to human or other vehicles, and infrastructures
 - (b) Medium: the attacks are likely to cause small hazards and damage to infrastructures or vehicles, but would not cause fatal injuries to people
 - (c) High: the attacks have a high possibility to cause fatal injuries
- (4) Combined severity level: a method evaluating the combined severity is adapted from risk management in the information system [35]. In the information system, the risks are determined by the likelihood and impact. To determine the combined severity levels to CAVs, a new severity matrix is built based on the severity of information leakage and physical damage, as shown in Table 3. If the severity of information leakage and physical damage are at the same level, then the combined severity will be at the same level as well. However, considering its importance, if the severity of physical damage is high, the combined severity level will be high as well.
- (5) Recovery time: this criterion evaluates the time needed to recover to normal situation after the attack has been detected.
 - (a) Low: after the detection, the damage caused by the attack can be fixed in a timescale of seconds
 - (b) Medium: after the detection, the damage caused by the attack can be fixed in a timescale of minutes to hours
 - (c) High: after the detection, the damage caused by the attack can be fixed in a timescale of hours to days

Based on these criteria, possible attacks in different scenarios are analysed in Section 4. It should also be noticed that this paper aims to discuss the possible cyber security attacks to a full CAV (Level 5), where all the possible attacks could be conducted via wireless communication remotely. The physical access of attacks is not considered when evaluating the severity. These criteria may not be comprehensive and exclusive, however could be further refined and extended. This research presents the initial attempt to define and rank the severity of possible attacks in CAV scenarios. This also aims to encourage further research developments to raise public and CAV practitioners' awareness towards CAV cyber security.

4. Possible Attacks

In this section, possible attacks of CAVs are listed and categorized, as shown in Table 4. Following the criteria defined in Section 3, severity of each attack will be analysed. CAV developments concern mainly two streams of research, which are connectivity and automation, covering in-vehicle and intervehicle components. Detailed potential attacks will be analysed within these two streams.

Different autonomous levels may be exposed to different attacks of different possibilities. This paper focuses on the attacks to a fully automated vehicle (i.e., level 5) according to the SAE automation level [20]. Level 5 CAV is capable of all the DDT under all circumstances. It is also assumed that all the vehicles on the road are CAVs. In real-world situations, there will be a mix of CAVs of different automation and traditional vehicles for a certain period of time. In addition,

TABLE 3: Combined severity level matrix (adapted from [35]).

Information leakage/physical damage	Low	Medium	High
Low	Low	Low	High
Medium	Low	Medium	High
High	Medium	High	High

it is known that CAVs will keep evolving and adapting more technologies. This paper only discusses attacks with existing CAV technologies. However, as the attacks are categorized on automation and connectivity in-vehicle and intervehicle, the list of possible attacks could be extended if new technologies are adapted to CAVs.

4.1. Automation in CAVs. In the current CAV development, all the vehicles from different companies have installed multiple sensors. The mainstream sensors include LiDAR, Radar, and camera [43, 44]. For example, Google Waymo vehicles are installed with a 360 degree camera on the roof as the vision system and several LiDAR sensors and Radar sensors around the vehicle body [45]. There are also supplemental sensors such as the sound detection sensors.

The possible attack target assets are analysed as below.

- (1) Audio/entertainment devices: audio devices have already been widely used in modern automobiles. It evolved to a colorful touchable screen showing more information in vehicles [46]. In CAVs, the audio/video system could be used to warn users about anomaly or abnormal behaviours detected in the system or surrounding environments.
 - (a) Loud volume: the first possible attack is to suddenly increase the volume of the voice such as background music on board. This attack could distract the passengers' attention or even cause panic in certain situations. The severity of information of leakage is low but the severity of physical damage is medium, which means that the overall severity is low.
 - (b) Fake sound: the attacker could use the audio system to make fake noise such as a crash sound. This attack might cause passengers' panic as well, although is not likely to cause information leakage.
 - (c) Remote control: this attack already happened in real world. Two white hackers in the USA hacked into a Jeep Great Cherokee from 10 miles away and then stopped the vehicle on a highway road through the entertainment system [47]. This is because the vehicle CAN and the entertainment system are combined together. If an attacker could control the vehicle remotely through the audio/entertainment system, the severity of physical damage could be high. In addition, the risk of information leakage will also be severe because the attackers could send remote instructions to gather private information. Moreover, in CAVs, the remote-control attacks might happen on other components leading to severe risks.
- (2) Cameras: cameras provide the vision data, an indispensable part in CAV. To detect the surrounding objects and position the vehicle, camera is a fundamental sensor on CAVs. However, the camera's function could be replaced by other sensors when they break down; thus, camera is of medium importance. There are already successful attacks to cameras to fool vehicles already [48].
 - (a) Blind vision: blind vision attack could be easily achieved by physical access. However, with the connectivity of the vehicle, it is even easier for the attackers. The attackers could disable the camera by controlling a strong light resource remotely. The attack would not leak the private information of the vehicle. However, this attack would not cause fatal injuries as well because it is easy to be detected, and CAV contains multisensors' data. If the cameras break down, other sensors could still help to 'see' the environment. Based on this, the overall severity level of the attack is low.
 - (b) Mislead camera (fake images): by controlling the cameras remotely, the attackers could inject fake image information to mislead the cameras. This attack is more dangerous than the blind vision attack because the detection possibility is lower. For blind vision attack, the system or the user could easily detect the abnormal situation. While in the mislead camera attack, it may take longer time to detect. In addition, the system might make decisions based on the fake images, the severity of physical attack is thus higher, and the overall severity is high.
- (3) Battery system: currently, the number of electric vehicles on road is increasing. As an environment-friendly transportation method, it is believed that the future CAVs would be electric vehicles. The vehicles' battery system would also then be an attack target.

The most possible attack to the battery system is the DoS (Denial of Services) attack. In computer science, the aim of DoS attack is to exhaust all the resources of the target to make the computer, server, or communication channel unavailable. In CAVs, the DoS attack could target the energy sources to exhaust the power sources including heating the seats on the vehicle. DoS attacks could be really dangerous to the battery system. It could trigger different parts to consume battery power in a short time. Sudden battery loss could cause damage to the basic functions of the vehicle. The severity of physical damage is medium, and the combined severity level is medium as well.

TABLE 4: Possible attacks in CAV.

Asset name	Importance	Risk name	Difficulty of conduction	Detection possibilities	Consequences	Severity of information leakage	Physical damage	Severity level	Recovery time
Audio/video devices	Low	Loud volume	Medium	High	Distract passenger's attention	Low	Medium	Low	Low
		Fake sound	Medium	High	Cause passenger's panic	Low	Low	Low	Low
		Remote control	High	Medium	Take control of the vehicle	High	High	High	High
Cameras	Medium	Blind vision	Low	High	Block the vision of vehicles	Low	Medium	Low	Low
		Mislead cameras (fake vision)	Low	Medium	Wrong reactions of vehicles	Low	Medium-high	High	High
Battery system	High	DoS	High	Medium	Consuming battery energy	Low	Medium	Medium	High
		Jamming	Medium	Medium	Decreasing the performance of LiDAR	Low	Medium	Low	Medium
Lidar	Medium	Hidden objects	Medium	Medium	Wrong reactions of vehicles	Low	Medium-high	High	Medium
		Fake objects	Medium	Medium	Wrong reactions of vehicles	Low	Medium	Medium	Medium
Radar	Medium	Jamming	Medium	Medium	Decreasing the performance of radar	Low	Medium	Low	Medium
		Hidden objects	Medium	Medium	Wrong reactions of vehicles	Low	Medium-high	High	Medium
		Fake objects	Medium	Medium	Wrong reactions of vehicles	Low	Medium	Medium	Medium
GNSS	Medium	Spoofing	High	Low	Wrong position	Medium	High	High	High
		Jamming	Medium	Low	Signal lose	Low	Medium	Low	Medium
		Injection	Medium	Medium	Information leakage and wrong reaction	Medium	Medium	Medium	Medium
In-vehicle system	High	Eavesdropping	Medium	Low	Leakage of personal information	High	Low	Medium	Low
		Traffic analysis	Low	Low	Leakage of daily usage	High	Low	Medium	Low
		Modification	High	Medium	Wrong message received	Medium	Medium	Medium	Medium

Automation

TABLE 4: Continued.

Asset name	Importance	Risk name	Difficulty of conduction	Detection possibilities	Consequences	Severity of information leakage	Physical damage	Severity level	Recovery time
		DoS	Low	High	Block vehicle communication channel	Low	Medium	Low	High
With other vehicles	Medium	Modification message Fake/ghost message	Medium	Medium	Wrong reactions of vehicles	Medium	Medium	Medium	Medium
		Change infrastructure sign	Medium	Medium	Wrong reactions of vehicles	Medium	Medium	Medium	Medium
	Low-medium	Block/remove sign	Low-medium	Medium	Wrong reactions of vehicles	Low	Medium	Medium	Low
Connectivity		Road line/infrastructure changing	Low	Medium	No reaction in specific position	Low	High	Medium	Low
	Low-medium	Fake identity	Low	High	Wrong reactions of vehicles	Low	Medium	Low	Low
	Medium	Injection	High	Medium	Identity leakage	High	Medium	High	Medium
Cloud system	Medium	Modification	High	Medium	Wrong message received	Medium	Medium	Medium	Medium-high
					Wrong information from cloud	Medium	Medium	Medium	Medium-high

- (4) LiDAR (light detection and ranging): LiDAR is the most fundamental sensor in CAVs to support localization and parking assistance [49]. It uses light point cloud to detect the distance and boundaries of surrounding obstacles and environments [50]. The importance of LiDAR is medium. There are successful attempts to attack the LiDAR by using strong lights in a simulation environment [48].
- (a) Jamming: this attack jams the LiDAR by using strong lights to reflect the origin light. The attackers could not gather any information through this attack. However, it may lead to physical damage because the detection performance of LiDAR will decrease.
 - (b) Hidden objects: because LiDAR uses the reflection of light to detect the surrounding environments, the attackers may use special materials to absorb the light to avoid detection. This attack would not cause any information leakage directly. However, in some situations, for example, if the object is covered by special reflection materials, the vehicle would not observe it. This could cause physical damage or even fatal injuries to the target vehicle. The combined severity of this attack is high as it may lead to fatal accident.
 - (c) Fake objects: the attackers could use light reflection to simulate a fake object, e.g., a barrier in front of the vehicle. The target vehicles would stop or change direction based on the false detection. If multiple vehicles detect this fake object, it could cause severe traffic congestion. Moreover, if there are multiple fake objects on the roads, this attack could cause physical damage when CAVs try to avoid those fake objects. With the other detection methods on the vehicle, however, the possibility of fatal injuries of this attack exists but is low. The severity of physical damage is medium and the combined severity is medium as well.
- (5) Radar: unlike LiDAR in CAVs, radar uses radio waves instead of light to detect the surroundings. Currently, there are two types of Radar on CAVs, millimeter Radar [51], and Ultrasonic Radar [52]. The millimeter radar is used on object detection [53], and the ultrasonic radar is used in short distance scenarios such as parking assistance system [54]. This is because the speed of ultrasonic radar is slow, which would lead to poor detection rate in high speed movements. Radar is also of medium importance.
- (a) Jamming: this attack is similar to the LiDAR jamming attack. In radar jamming attack, the attackers would use noise to degrade the signal of radar. The attacked radar system might not work properly and the vehicle could not detect the surrounding environments. If the noise source influences multiple CAVs, the traffic flow would be disturbed or it could even cause traffic collisions. This attack would not cause information leakage directly but might cause physical damage. The combined severity of this attack is medium.
 - (b) Hidden objects: currently, existing technologies are able to hide objects from radar detection and have been already adapted in the area of military aerospace [55]. The planes or the objects hide themselves by changing the regular reflection shape or using radar absorbing materials. In military, the mitigation method is already developed, which is called Radar Antistealth Technology [55]. This technology will strengthen the radar signal. This attack would not cause information leakage but might cause physical damage, or even hurt people directly. The combined severity level of this attack is high.
 - (c) Fake objects: the attackers broadcast fake radar signals to conduct the attack. Other vehicles would then detect the false signal and take corresponding reactions. This attack would not cause information leakage, however, might cause physical damage to infrastructures, e.g., collisions when vehicles are trying to avoid fake objects. The combined severity of this attack is medium.
- (6) GNSS (Global Navigation Satellite System): the most widely used GNSS system is GPS (Global Positioning System) from the USA [56]. Currently, other countries are developing their own GNSS such as Beidou from China, Galileo from Europe Union, and Glonass from Russia [57]. The GNSS system could help to locate and navigate the vehicle. Hacking into this system requires high-level knowledge. The GNSS system is a major resource for positioning and navigation, but as the positioning and navigation are cooperated via V2V communication, the importance of GNSS system is thus medium.
- (a) Spoofing: GNSS spoofing attack sends similar GNSS signals to mislead the receivers of the target CAVs. The attackers could use these devices to lead the vehicle to false location or wrong route. In 2013, researchers from the University of Texas at Austin successfully fooled an 80 million dollar super-yacht by their GPS spoofing devices [58]. Compared to the GNSS jamming attack, GNSS spoofing attack would be more dangerous. Without the GNSS signals, CAVs would use other methods such as V2V communication or SLAM (Simultaneous Localization and Mapping) to navigate and avoid the possible hazards such as collisions. However, if the information is wrong and not detected, CAVs would trust the wrong GNSS information and take wrong reactions, which may lead to collisions and fatal injuries. In addition, a vehicle that has been spoofed successfully could respond with private

information such as the location information and historic route information to the attackers, which would also cause information leakage. In that case, the severity of information leakage is medium and the severity of physical damage is high.

- (b) Jamming: in the GNSS jamming attack, the attackers will send stronger power signal to the CAV receiver. The GNSS signal is normally weak when they approach the receivers, and it could be easily covered by the jamming signal. The real GNSS signal will then be ignored. In addition, it is also difficult to detect the jamming attack because the GNSS signal is likely to decrease due to interference or limited number of satellites [59]. CAVs could not navigate and locate without the GNSS signal. However, V2V communication could help to navigate coordinately as a backup method. The severity levels of both information leakage and physical damage are medium.
- (7) In-vehicle system: in-vehicle system contains the microcontrollers and communication instructions in the vehicle sent by CAN (Controller Area Network) or other communication methods such as WiFi and Bluetooth. The in-vehicle system is related to all the operational functions, thus is of high importance.
- (a) Injection: the attackers would inject nonexistent information or even malware to the system through ports such as USB ports. With the fake information, CAVs might make wrong decisions leading to physical damage. As an active attack, injection could also cause leakage of sensitive data. The combined severity of this attack is medium.
 - (b) Eavesdropping: eavesdropping is a passive attack and is difficult to be noticed. The main objective of this attack is not to cause physical damage but to gain access to valuable data. Thus, the severity of information leakage is high and the severity of physical damage is low.
 - (c) Traffic analysis: traffic analysis is also a passive attack. The attackers will monitor and observe the data and then try to identify the pattern in the data flow. As a passive attack, the traffic analysis attack would not cause physical damage directly and the scale of information leakage is limited. The combined severity of this attack is low.
 - (d) Modification: this attack modifies the messages sent between different components and units. The wrong messages could lead to the wrong decision and action of the vehicle. The severity of this attack is medium.

4.2. *Connectivity in CAVs.* There are three main types of vehicle communication in CAV network. V2V (Vehicle-to-Vehicle) communication is between vehicles via wireless network. V2I (Vehicle-to-Infrastructure) communication is between vehicles and infrastructures via wireless network

and V2X (Vehicle-to-Everything) includes V2V, V2I, and communications between vehicles and other entities such as cloud database or pedestrians [60]. Compared with traditional automobiles, these communication methods could help to improve the accuracy of location in rural area and prevent accidents efficiently. Meanwhile, some computer cyber attacks might also happen in CAV environment. For example, in a network cyber attack benchmark KDD99 [61], cyber attacks such as DoS attack could be adapted into V2V communication. Nowadays, many communication technologies are being used in CAV network, e.g., DSRC (Dedicated Short Range Communication), LTE (Local Thermal Equilibrium), and 5G [62].

The possible attack target assets of connectivity are analysed as below.

- (8) V2V Communication (with other vehicles): V2V communication is a crucial part in future CAVs. However, there are no general adapted communication standards for V2V communication. Currently, the V2V communication standard in the USA is DSRC, which is based on IEEE 802.11p standard [63]. In Europe, there is ITS-G5 for V2V communication [64]. V2V communication could help to navigate or warn vehicles of potential hazards.
 - (a) DoS: in addition to the battery system, DoS attack could also happen in the V2V communication. The attackers could send huge amount of data to block the communication channel of the target vehicle from receiving external information. This attack would not cause information leakage but might cause physical damage especially in the rural area, where the V2V communication is the main data source for vehicle planning.
 - (b) Modification on message/fake message: the communication between vehicles would send different types of information including position coordinates, speed, and head angle. If the attackers send fake messages, the target vehicle would take wrong reactions. In addition, if the target vehicle trusts the fake message, it may respond to the attacker with private information. Based on this, the overall severity is medium.
 - (c) Hidden vehicle: this attack is also a type of passive attack. The attackers would disable their own message sender to hide their activities. This would not cause information leakage directly, but might cause physical damage if the vehicle hide its activities and approach the target vehicle silently.
- (9) V2I communication (with infrastructure): nowadays, there are some initial uses of V2I communication. For example, the ETC (Electronic Toll Collection) on roads and bridges use RFID (Radio Frequency Identification) to charge vehicles [65].

TABLE 5: Categories of severity of attacks.

Level	Description	Attack types
1	Critical	Remote control (audio/video devices); mislead cameras/fake vision (cameras); hidden objects (LiDAR); hidden objects (radar); spoofing (GNSS); fake identity (cloud authority)
2	Important	Fake objects (LiDAR); fake objects (radar); DoS attack (battery system); injection (in-vehicle system); modification (in-vehicle system); modification (V2V communication); fake/ghost message (V2V communication); change infrastructure sign (V2I communication); injection (cloud dataset); modification (cloud dataset)
3	Moderate	Blind vision (cameras); jamming (LiDAR); jamming (radar); jamming (GNSS); eavesdropping (in-vehicle system); traffic analysis (in-vehicle system); DoS attack (V2V communication); block/remove sign (infrastructure sign); road line changing (road)
4	Minor	Loud volume (audio/video devices); fake sound (audio/video devices)

Apart from the communication channel, which is similar to the V2V communication, there are other attack types in V2I communication.

- (a) Change infrastructure sign: the infrastructure signs in transportation help vehicles to navigate, locate, or control speed. CAVs could ‘read’ the sign and take corresponding actions. If the attackers change infrastructure signs such as the road direction sign, it will lead the vehicle to wrong route. In addition, if multiple traffic lights are changed intentionally, it could cause severe traffic congestion or even traffic collisions.
 - (b) Block/remove sign: the infrastructure signs could also be blocked or removed physically or remotely. If an emergency alert sign is removed intentionally, this could cause traffic congestion and accidents. However, this attack will not cause information leakage. The combined severity of this attack is medium.
- (10) V2X communication (mainly on cloud).
- (a) Cloud ID dataset: authority is important in CAV network. Each CAV would be assigned a unique ID such as an electronic plate. In order to confirm the reliability of the communication, only the information from the trusted CAVs in the dataset could be accepted. All the communication and information exchange are based on the authority from the CAV cloud.
 - (b) Cloud real-time traffic database: cloud database collects the traffic data to provide transportation guidance. It includes the real-time traffic congestion data and accident data to inform all the CAVs to avoid certain areas. If the attackers inject fake messages or modify messages, all the vehicles in the cloud database would receive wrong information. In addition, the attackers could also access valuable information in the dataset.

With the severity criteria, all the attacks are then grouped into four categories, as shown in Table 5. It can be seen that the critical attacks contain remote control, fake vision on cameras, hidden objects to LiDAR and Radar, spoofing

attack to GNSS, and fake identity in cloud authority. It could be summarized that all the critical attacks are related to spoofing and falsify messages. These attacks are difficult to realize and they could all lead to wrong reaction or even fatal injuries.

5. Mitigation Methods

For each of the attacks analysed in Section 4, the mitigation methods will be different. By adapting the mitigation methods in information security [35], the main types of mitigation methods could be grouped into five categories. To CAVs, the mitigation methods could be similar but need to be considered based on specific CAV characteristics.

- (1) Prevention: these methods prevent the attack from influencing the whole vehicle system negatively. In potential attacks to CAVs, the prevention is for passive attacks such as eavesdropping by encrypting the communication channel and messages. In addition, all the CAV users could be authorized with the credibility of the messages. For example, to the eavesdropping attacks in in-vehicle system, if the communication channel and messages are encrypted, it is much more difficult for attackers to make use of the information.
- (2) Reduction: reduction methods reduce the possibility or feasibility of the attack. It could also reduce the possible impacts of the attacks to a controllable level. In CAVs, the reduction methods include the redundant sensors. If one sensor breaks down, the vehicle could still rely on the data from other sensors to reduce the impact of each sensor. For example, to reduce the impact of the blind vision attack to the camera, the vehicle could use other sensors after detecting abnormal attacks.
- (3) Transference: transference shares the possible risks with others, such as a reliable third-party organization including governments and insurance companies. For example, in the Cloud of V2X communication, the authority of each CAV’s identity should be assigned by the government or relevant legitimate organizations. All the CAVs information should also be stored safely and monitored by the trusted third-party. Not all the

attacks could be resolved by transference. In CAVs, this mitigation method could only be used when a single vehicle manufacturer or a supplier could not handle all the information safely.

- (4) Acceptance: acceptance is to retain the risks caused by those attacks with limited negative impacts on CAVs. The attack might not have a proper countermeasure and the impact is at an acceptable level. For example, to the traffic analysis attack in in-vehicle communication, the leaked information could only be the size and timing of the communication package, which is not likely to cause physical damage. In addition, the traffic analysis attack, which is a passive attack, could not be prevented by message and communication channel encryption. In that case, the traffic analysis attack could be tolerated.
- (5) Contingency: contingency considers the possible reactions if the attacks happen. A contingency plan needs to be prepared to recover the system once attacked. If the CAV system detects an abnormal battery loss due to the DoS attack, it could pull up the CAV to a safe place.

6. Conclusion

CAV is a fundamental part of intelligent transportation systems and has started attracting increasing research attention in the last few years. Given the importance of CAVs in relation to personal information, physical damages, and passengers' lives, cyber security of CAVs are thus becoming highly important in research developments.

This paper has identified some of the most important cyber attacks to CAVs. For each identified cyber attack, the target asset, the possible risks, and the consequences have been analysed. The severity level of information leakage and physical damage are then estimated and considered based on a new criteria adapted from engineering and software developments. Possible mitigation methods are then categorized and suggested to resolve these attacks.

Among the attacks identified in this paper, the spoofing and falsify messages attacks including remote control, fake vision on cameras, hidden objects to LiDAR and Radar, spoofing attack to GNSS, and fake identity in cloud authority have been identified as the most dangerous attacks to CAVs. All of these attacks would cause severe consequences to information leakage and physical damage.

However, it should also be noticed that CAV technologies are fast evolving. This paper discusses the potential cyber attacks in the existing CAVs technologies and derives the potential attacks based on the traditional cyber attacks. Within the scope of CAV hardware, software, and data, the possible attacks listed in Table 4 will be further extended to reflect the latest developments in CAVs. Meanwhile, the overall severity of each attack is only judged by the listed criteria. It could be further discussed based on other criteria. Due to the emerging infrastructures under construction at different countries, and the unique characteristics of real-

world environments required, there is a lack of readily complete testing environments compliant to generally adopted standards available in research and practice. Apart from defining and categorizing the potential cyber attacks, it should also be stressed that the evaluations of the severity of each type of attacks also need to be defined and justified carefully based on real-world field tests. Furthermore, the severity assessment of the listed potential attacks only considers single sensor. For example, in real-world tests, if the cameras fail to recognize an obstacle on the road, the LiDAR and Radar might complement and help to recognize and avoid the obstacle. In some extreme situations, all the sensors or backup elements/functions might be ineffective or fail. The assessment of the severity for different attacks should consider and evaluated the integration of multiple sensors and would also be an interesting topic for future research. In addition, the advantage, disadvantage, and application scenarios of each mitigation method are not the focus in this paper. The presented mitigation methods will be extended and refined further in future research on CAVs cyber security.

Data Availability

The data used to support the findings of this study are available from the corresponding author upon request.

Conflicts of Interest

The authors declare no conflicts of interest.

Acknowledgments

The authors would like to thank Nottingham Geospatial Institute and the School of Computer Science University of Nottingham.

References

- [1] H. Fan, Z. Fan, C. Liu et al., *Baidu Apollo Em Motion Planner*, arXiv preprint arXiv:1807.08048, 2018.
- [2] M. Dikmen and C. M. Burns, "Autonomous driving in the real world: experiences with tesla autopilot and summon," in *Proceedings of the 8th International Conference on Automotive User Interfaces and Interactive Vehicular Applications Automotive'UI 16*, pp. 225–228, New York, NY, USA, 2016.
- [3] Tesla, *Future of Driving*, Tesla, Inc., San Carlos, CA, USA, 2018, <http://www.tesla.com/model3>.
- [4] L. Jones, "Driverless cars: when and where?" *Engineering & Technology*, vol. 12, no. 2, pp. 36–40, 2017.
- [5] B. J. Cottam, "Transportation planning for connected autonomous vehicles: how it all fits together," *Transportation Research Record*, vol. 2672, no. 51, pp. 12–19, Article ID 0361198118756632, 2018.
- [6] B. Schoettle and M. Sivak, *A Preliminary Analysis of Real-World Crashes Involving Self-Driving Vehicles*, University of Michigan Transportation Research Institute, Ann Arbor, MI, USA, 2015.
- [7] K. Bimbrow, "Autonomous cars: past, present and future a review of the developments in the last century, the present scenario and the expected future of autonomous vehicle technology," in *Proceedings of the 12th International*

- Conference on Informatics in Control, Automation and Robotics-Volume 1 (ICINCO)*, pp. 191–198, Colmar, France, 2015.
- [8] D. J. Fagnant and K. Kockelman, "Preparing a nation for autonomous vehicles: opportunities, barriers and policy recommendations," *Transportation Research Part A: Policy and Practice*, vol. 77, pp. 167–181, 2015.
 - [9] X. Xu and C.-K. Fan, "Autonomous vehicles, risk perceptions and insurance demand: an individual survey in China," *Transportation Research Part A: Policy and Practice*, vol. 124, pp. 549–556, 2019.
 - [10] X. Kuang, F. Zhao, H. Hao, and Z. Liu, "Intelligent connected vehicles: the industrial practices and impacts on automotive value-chains in China," *Asia Pacific Business Review*, vol. 24, no. 1, pp. 1–21, 2018.
 - [11] J. Guanetti, Y. Kim, and F. Borrelli, "Control of connected and automated vehicles: state of the art and future challenges," *Annual Reviews in Control*, vol. 45, pp. 18–40, 2018.
 - [12] D. Li and H. Gao, "A hardware platform framework for an intelligent vehicle based on a driving brain," *Engineering*, vol. 4, no. 4, pp. 464–470, 2018.
 - [13] World Economic Forum, *Self Driving Vehicles in an Urban Context*, World Economic Forum, Cologny, Switzerland, 2015.
 - [14] GOV UK, *The Key Principles of Vehicle Cyber Security for Connected and Automated Vehicles*, 2018, <https://www.gov.uk/government/publications/principles-of-cyber-security-for-connected-and-automated-vehicles/the-key-principles-of-vehicle-cyber-security-for-connected-and-automated-vehicles#contents>The access date is 06/08/2019.
 - [15] J. Cui, L. Shen Liew, G. Sabaliauskaite, and F. Zhou, *A Review on Safety Failures, Security Attacks, and Available Countermeasures for Autonomous Vehicles*, Ad Hoc Networks, Jaipur, India, 2018.
 - [16] H. M. Song, R. K. Ha, and H. K. Kim, "Intrusion detection system based on the analysis of time intervals of can messages for in-vehicle network," in *Proceedings of the 2016 International Conference on Information Networking (ICOIN)*, pp. 63–68, Kota Kinabalu, Malaysia, January 2016.
 - [17] H. Zhou, W. Xu, Y. Bi, J. Chen, Q. Yu, and X. S. Shen, "Toward 5G spectrum sharing for immersive-experience-driven vehicular communications," *IEEE Wireless Communications*, vol. 24, no. 6, pp. 30–37, 2017.
 - [18] L. Liang, H. Ye, and G. Y. Li, "Toward intelligent vehicular networks: a machine learning framework," *IEEE Internet of Things Journal*, vol. 6, no. 1, pp. 124–135, 2019.
 - [19] M. H. Hashem Eiza and Q. Ni, "Driving with sharks: rethinking connected vehicles with vehicle cybersecurity," *IEEE Vehicular Technology Magazine*, vol. 12, no. 2, pp. 45–51, 2017.
 - [20] SAE, *Taxonomy and Definitions for Terms Related to Driving Automation Systems for On-Road Motor Vehicles*, SAE, Warrendale, PA, USA, 2018.
 - [21] J. Levinson, J. Askeland, J. Becker et al., "Towards fully autonomous driving: systems and algorithms," in *Proceedings of the 2011 IEEE Intelligent Vehicles Symposium (IV)*, pp. 163–168, Baden-Baden, Germany, June 2011.
 - [22] J. Petit and S. E. Shladover, "Potential cyberattacks on automated vehicles," *IEEE Transactions on Intelligent Transportation Systems*, vol. 16, no. 2, pp. 546–556, 2015.
 - [23] M. Levi, A. Yair, and A. Kontorovich, "Advanced analytics for connected car cybersecurity," in *Proceedings of the 2018 IEEE 87th Vehicular Technology Conference (VTC Spring)*, pp. 1–7, Porto, Portugal, June 2018.
 - [24] Q. He, X. Meng, and R. Qu, "Survey on cyber security of cav," in *Proceedings of the 2017 Forum on Cooperative Positioning and Service (CPGP)*, pp. 351–354, Harbin, China, May 2017.
 - [25] M. Islam, M. Chowdhury, H. Li, and H. Hu, "Cybersecurity attacks in vehicle-to-infrastructure applications and their prevention," *Transportation Research Record: Journal of the Transportation Research Board*, vol. 2672, no. 19, pp. 66–78, 2017.
 - [26] Y. Li, Y. Tu, Q. Fan, C. Dong, and W. Wang, "Influence of cyber-attacks on longitudinal safety of connected and automated vehicles," *Accident Analysis & Prevention*, vol. 121, pp. 148–156, 2018.
 - [27] V. Milanés, S. E. Shladover, J. Spring, S. E. Shladover, H. Kawazoe, and M. Nakamura, "Cooperative adaptive cruise control in real traffic situations," *IEEE Transactions on Intelligent Transportation Systems*, vol. 15, no. 1, pp. 296–305, 2014.
 - [28] V. Milanés and S. E. Shladover, "Modeling cooperative and autonomous adaptive cruise control dynamic responses using experimental data," *Transportation Research Part C: Emerging Technologies*, vol. 48, pp. 285–300, 2014.
 - [29] Y. Feng, S. Huang, Q. A. Chen, H. Liu, and Z. Mao, "Vulnerability of traffic control system under cyberattacks with falsified data," *Transportation Research Record: The Journal of the Transportation Research Board*, vol. 2672, no. 1, pp. 1–11, Article ID 036119811875688, 2018.
 - [30] D. Satyajeet, A. R. Deshmukh, and S. S. Dorle, "Heterogeneous approaches for cluster based routing protocol in vehicular ad hoc network (vanet)," *International Journal of Computer Applications*, vol. 134, no. 12, pp. 1–8, 2016.
 - [31] M. N. Mejri, J. Ben-Othman, and M. Hamdi, "Survey on vanet security challenges and possible cryptographic solutions," *Vehicular Communications*, vol. 1, no. 2, pp. 53–66, 2014.
 - [32] M. S. Al-Kahtani, "Survey on security attacks in vehicular ad hoc networks (vanets)," in *Proceedings of the 2012 6th International Conference on Signal Processing and Communication Systems (ICSPCS)*, pp. 1–9, Gold Coast, Australia, December 2012.
 - [33] Z. El-Rewini, K. Sadatsharan, D. F. Selvaraj, S. J. Plathottam, and P. Ranganathan, "Cybersecurity challenges in vehicular communications," *Vehicular Communications*, vol. 23, Article ID 100214, 2020.
 - [34] J. Moteff, *Risk Management and Critical Infrastructure Protection: Assessing, Integrating, and Managing Threats, Vulnerabilities and Consequences*, Library of Congress Washington DC Congressional Research Service, Washington DC, USA, 2005.
 - [35] G. Stoneburner, Y. Alice, and A. Feringa, "Risk management guide for information technology systems," Technical Report, National Institute of Standards and Technology, Gaithersburg, MD, USA, 2002.
 - [36] G. Tamasi and M. Demichela, "Risk assessment techniques for civil aviation security," *Reliability Engineering & System Safety*, vol. 96, no. 8, pp. 892–899, 2011.
 - [37] R. Von Solms and J. Van Niekerk, "From information security to cyber security," *Computers & Security*, vol. 38, pp. 97–102, 2013.
 - [38] W. F. Powers and P. R. Nicastrì, "Automotive vehicle control challenges in the 21st century," *Control Engineering Practice*, vol. 8, no. 6, pp. 605–618, 2000.
 - [39] W. Stallings, *Cryptography and Network Security: Principles and Practice*, Pearson Education Ltd., London, UK, 6th edition, 2014.

- [40] C. Garling, *Why Cars Will Become the Ultimate Mobile Device*, 2017, <https://builttoadapt.io/why-cars-will-become-the-ultimate-mobile-device-33dbaad40118>The access date is 10/08/2019.
- [41] H. C. Barbosa, D. A. Lima, A. M. Neto et al., "The new generation of standard data recording device for intelligent vehicles," in *Proceedings of the 2016 IEEE 19th International Conference on Intelligent Transportation Systems (ITSC)*, pp. 2669–2674, Rio de Janeiro, Brazil, November 2016.
- [42] P. Kohli and A. Chadha, *Enabling Pedestrian Safety Using Computer Vision Techniques: A Case Study of the 2018 Uber Inc. Self-Driving Car Crash*, arXiv preprint arXiv:1805.11815, Texas A&M University, College Station, TX, USA, 2018.
- [43] C. J. Jacobus and H. Douglas, "All weather autonomously driven vehicles," US Patent 9,989,967, 2018.
- [44] M. Konrad and M. Schramm, "Validation of ADAS by sensor fusion," *ATZ Worldwide*, vol. 120, no. 6, pp. 56–59, 2018.
- [45] Waymo, *Waymo Safety Report: On the Road to Fully Self-Driving*, Waymo, Mountain View, CA, USA, 2017.
- [46] C. Wang, L. Yu, and H. Yanan, *Automotive Usability: Human Computer Interaction in the Vehicle*, Rensselaer Polytechnic Institute, Troy, NY, USA, 2012.
- [47] T. Ring, "Connected cars—the next target for hackers," *Network Security*, vol. 2015, no. 11, pp. 11–16, 2015.
- [48] J. Petit, B. Stottelaar, M. Feiri, and K. Frank, "Remote attacks on automated vehicles sensors: experiments on camera and lidar," *Black Hat Europe*, vol. 11, 2015.
- [49] R. Kummerle, D. Hahnel, D. Dolgov, S. Thrun, and W. Burgard, "Autonomous driving in a multi-level parking structure," in *Proceedings of the 2009 IEEE International Conference on Robotics and Automation ICRA'09*, pp. 3395–3400, Kobe, Japan, May 2009.
- [50] André Ibsch, S. Stümper, H. Altinger et al., "Towards autonomous driving in a parking garage: vehicle localization and tracking using environment-embedded lidar sensors," in *Proceedings of the 2013 Intelligent Vehicles Symposium (IV)*, pp. 829–834, Gold Coast, Australia, June 2013.
- [51] L. Kong, M. K. Khan, F. Wu, G. Chen, and P. Zeng, "Millimeter-wave wireless communications for iot-cloud supported autonomous vehicles: overview, design, and challenges," *IEEE Communications Magazine*, vol. 55, no. 1, pp. 62–68, 2017.
- [52] U. Farooq, M. Amar, E. Ul Haq, M. Usman Asad, and H. Muhammad Atiq, "Microcontroller based neural network controlled low cost autonomous vehicle," in *Proceedings of the 2010 Second International Conference on Machine Learning and Computing (ICMLC)*, pp. 96–100, Bangalore, India, February 2010.
- [53] J. Choi, V. Va, N. Gonzalez-Prelcic, R. Daniels, C. R. Bhat, and R. W. Heath, "Millimeter-wave vehicular communication to support massive automotive sensing," *IEEE Communications Magazine*, vol. 54, no. 12, pp. 160–167, 2016.
- [54] W.-J. Park, B.-S. Kim, D.-E. Seo, D.-S. Kim, and K.-H. Lee, "Parking space detection using ultrasonic sensor in parking assistance system," in *Proceedings of the 2008 Intelligent Vehicles Symposium*, pp. 1039–1044, Eindhoven, Netherlands, June 2008.
- [55] K. Zikidis, A. Skondras, and C. Tokas, "Low observable principles, stealth aircraft and anti-stealth technologies," *Journal of Computations & Modelling*, vol. 4, no. 1, pp. 129–165, 2014.
- [56] J. Jackson, R. Saborio, S. A. Ghazanfar, D. Gebre-Egziabher, and B. Davis, *Evaluation of Low-Cost, Centimeter-Level Accuracy OEM GNSS Receivers*, Minnesota Department of Transportation, Saint Paul, MI, USA, 2018.
- [57] B. Hofmann-Wellenhof, L. Herbert, and E. Wasle, *GNSS—Global Navigation Satellite Systems: GPS, GLONASS, Galileo, and More*, Springer Science & Business Media, Berlin, Germany, 2007.
- [58] M. L. Psiaki, T. E. Humphreys, and B. Stauffer, "Attackers can spoof navigation signals without our knowledge. Here's how to fight back GPS lies," *IEEE Spectrum*, vol. 53, no. 8, pp. 26–53, 2016.
- [59] D. Margaria, E. Falletti, and T. Acarman, "The need for GNSS position integrity and authentication in its: conceptual and practical limitations in urban contexts," in *Proceedings of the 2014 IEEE Intelligent Vehicles Symposium Proceedings*, pp. 1384–1389, Dearborn, MI, USA, June 2014.
- [60] S. Zhang, J. Chen, F. Lyu, N. Cheng, W. Shi, and X. Shen, "Vehicular communication networks in the automated driving era," *IEEE Communications Magazine*, vol. 56, no. 9, pp. 26–32, 2018.
- [61] National Conference of State Legislatures, *UCI Kdd Cup 1999 Data Data Set*, National Conference of State Legislatures, Washington, DC, USA, 1999.
- [62] R. Molina-Masegosa and J. Gozalvez, "LTE-V for sidelink 5G V2X vehicular communications: a new 5G technology for short-range vehicle-to-everything communications," *IEEE Vehicular Technology Magazine*, vol. 12, no. 4, pp. 30–39, 2017.
- [63] J. B. Kenney, "Dedicated short-range communications (DSRC) standards in the United States," *Proceedings of the IEEE*, vol. 99, no. 7, pp. 1162–1182, 2011.
- [64] L. Chen and C. Englund, "Cooperative ITS—EU standards to accelerate cooperative mobility," in *Proceedings of the 2014 International Conference on Connected Vehicles and Expo (ICCVE)*, pp. 681–686, Vienna, Austria, November 2014.
- [65] Z. Ren and Y. Gao, "Design of electronic toll collection system in expressway based on RFID," in *Proceedings of the 2009 International Conference on Environmental Science and Information Application Technology*, pp. 779–782, Wuhan, China, July 2009.

Research Article

Study on a Right-Turning Intelligent Vehicle Collision Warning and Avoidance Algorithm Based on Monte Carlo Simulation

Chuanliang Shen, Shan Zhang , Zhenhai Gao , Binyu Zhou, Wei Su, and Hongyu Hu

State Key Laboratory of Automotive Simulation and Control, Jilin University, Changchun 130025, China

Correspondence should be addressed to Zhenhai Gao; gaozh@jlu.edu.cn

Received 21 November 2019; Revised 15 May 2020; Accepted 6 July 2020; Published 1 August 2020

Academic Editor: Shan Bao

Copyright © 2020 Chuanliang Shen et al. This is an open access article distributed under the Creative Commons Attribution License, which permits unrestricted use, distribution, and reproduction in any medium, provided the original work is properly cited.

With the development of intelligent vehicle technology, the demand for advanced driver assistant systems kept increasing. To improve the performance of the active safety systems, we focused on right-turning vehicle's collision warning and avoidance. We put forward an algorithm based on Monte Carlo simulation to calculate the collision probability between the right-turning vehicle and another vehicle (or pedestrian) in intersections. We drew collision probability curves which used time-to-collision as the horizontal axis and collision probability as the vertical axis. We established a three-level collision warning system and used software to calculate and simulate the collision probability and warning process. To avoid the collision actively when turning right, a two-stage braking strategy is applied. Taking four right-turning collision conditions as examples, the two-stage braking strategy was applied, analysing and comparing the anteroposterior curve diagram simultaneously to avoid collision actively and reduce collision probability. By comparison, the collision probability 2 s before active collision avoidance was more than 80% and the collision probability may even reach 100% in certain conditions. To improve the active safety performance, the two-stage braking strategy can reduce the collision probability from exceeding 50% to approaching 0% in 2 s and reduce collision probability to less than 5% in 3 s. By changing four initial positions, the collision probability curve calculation algorithm and the two-stage braking strategy are validated and analysed. The results verified the rationality of the collision probability curve calculation algorithm and the two-stage braking strategy.

1. Introduction

With the development of vehicle active safety systems, ADAS can solve traffic safety problems in challenging crashes situations. The current ADAS focuses mainly on turning left, and studying the right-turning process was also important for improving traffic safety. Considering that the driver in mainland China was sitting on the left side, there was a large blind spot in the process of turning right, and the algorithm was designed by taking the right turn as an example. The right-turning condition was special and relatively complex [1] because drivers needed to give attention to pedestrians crossing the road while avoiding vehicles coming from the left side and drivers had a visual blind spot during the right-turning [2]. Therefore, the right-turning condition of an intelligent vehicle was studied and analysed.

In intersections, the intelligent vehicle's turning condition was a complex traffic scene which possesses a high accident rate [3, 4]. There are increasing numbers of collisions between right-turning vehicles and pedestrians (or other vehicles) [5, 6]. Therefore, it was necessary to reduce the collision probability by technical means. At present, most previous studies focused on the forward collision warning (FCW) system and active collision avoidance [7]; however, there was a lack of research on the collisions caused by right-turning vehicles. Some researchers estimated the motion state of vehicles and pedestrians [8, 9]. By establishing a probability model, Hashimoto et al. predicted and identified a pedestrian's crossing decision in advance [10]; however, this research lacked the calculation of collision probability for a vehicle on a right-turning course. In right-turning collision-related research, Sitao et al. put forward an intersection optimization design to reduce the collision

probability between right-turning vehicles and pedestrians [11], but it cannot cover all possible right-turning collisions in intersections. Zhao et al. have conducted research in intelligent vehicles active collision avoidance related fields [12]. Choi and Zhao et al. adopted the autonomous emergency braking (AEB) system to avoid collisions [13, 14]. However, these studies were not combined with the intelligent vehicle's right-turning condition. In this paper, Monte Carlo simulation was used to establish a random simulation algorithm which simulates the right-turning intelligent vehicle's collision probability.

The current research is summarized as follows:

- (1) At present, most previous studies focused on the forward collision warning (FCW) system and autonomous emergency braking (AEB) system; however, there was a lack of research on the collisions caused by right-turning vehicles.
- (2) The current research focused on pedestrian intention prediction and identification, without considering the right-turn condition. The existing research on the right turn was not comprehensive enough, and the research should be extended to the vehicle and pedestrian protection during the right turn.
- (3) At present, AEB early warning and active intervention were mature, but there was relatively little research on early warning of traffic conflicts during the right-turn process. Current research lacked the calculation of collision probability for a vehicle on a right-turning course. The early warning mechanism should be introduced into the field of right-turn collision warning.

In order to calculate the collision probability accurately, extensively covering all possible collisions during right-turning, and actively avoiding a collision, the system described in this paper not only calculated the collision probability and designed the three-level collision warning system (CWS) but also actively avoided the collision to reduce the collision probability.

According to the algorithm based on Monte Carlo simulation to calculate the collision probability, we have improved the performance of the active safety systems, which contributed to right-turning vehicle's collision warning and avoidance. We established a three-level collision warning system and used software to calculate and simulate the collision probability and warning process. To avoid the collision actively when turning right, a two-stage braking strategy was applied. Therefore, we calculated the probability of collision, through the warning level and active intervention to improve the safety of the right-turning process and reduce the accident rate.

2. Establishing the Collision Safety Model and Warning Mechanism

2.1. Collision Safety Model Based on Time-to-Collision. Our study analysed the right-turning condition and predicted four different collision modes during the right-turning process. The CWS was designed for each collision

scenario, and the two-stage braking strategy was designed for each scenario to actively and simultaneously avoid collisions. Finally, by changing four initial positions, the collision probability curve calculation algorithm and the two-stage braking strategy were validated and analysed. This control scheme's technical roadmap is shown in Figure 1.

The collision warning and avoidance algorithm's main process was as follows:

- (1) The information gathering process needs to collect the vehicle's velocity information and classify it into four modes. The four modes were as follows: a collision between a vehicle which turned right into the lane and another vehicle which merged into the same lane from the left side (scenario 1); a collision between a right-turning vehicle merging into the lane and pedestrians crossing the road in the same lane (scenario 2); a collision between the pedestrians crossing the road ahead and a right-turning vehicle (scenario 3); and a collision between a right-turning vehicle merging into the lane and another vehicle existing in the lane (scenario 4). The four modes are shown in Figure 2.
- (2) We calculated the collision probability for these four modes and used the vehicle's and pedestrian's safety profile as the collision's criteria. We generated random variables for velocity and turning radius and simulated the collision probability curve using a collision probability calculation algorithm based on Monte Carlo simulation. We accumulated collision probability and plotted the collision probability curve on the three-level warning figure.
- (3) We output the warning level through the three-level warning region and performed the two-stage braking strategy in the specific scenario.

In our study, we adopted the collision safety model based on time-to-collision (TTC) [1]. The driver's danger perception caused a delay, and the braking system also caused a delay.

The total delay was as follows: the time in which driver included stimulation (D_1), identification and decision time (D_2), time to control action (D_3), and braking system delay time (d).

To ensure safety, it was necessary to ensure the safety time threshold (D_s) greater than the sum of delay (D_{sum}), so the CWS needed to take actions before D_{sum} , as expressed by the following equations:

$$D_{sum} = D_1 + D_2 + D_3 + d, \quad (1)$$

$$D_s > D_{sum}. \quad (2)$$

D_{sum} was generally within 3 s [15]; therefore, D_s should be greater than 3 s. To reach reliable intelligent vehicle safety during right-turning conditions, the collision warning and avoidance algorithm was designed for a TTC of 5 s.

2.2. Establishment of Collision Warning Mechanism. The three warning levels for right-turning collisions of intelligent vehicles [16, 17] were defined as follows:

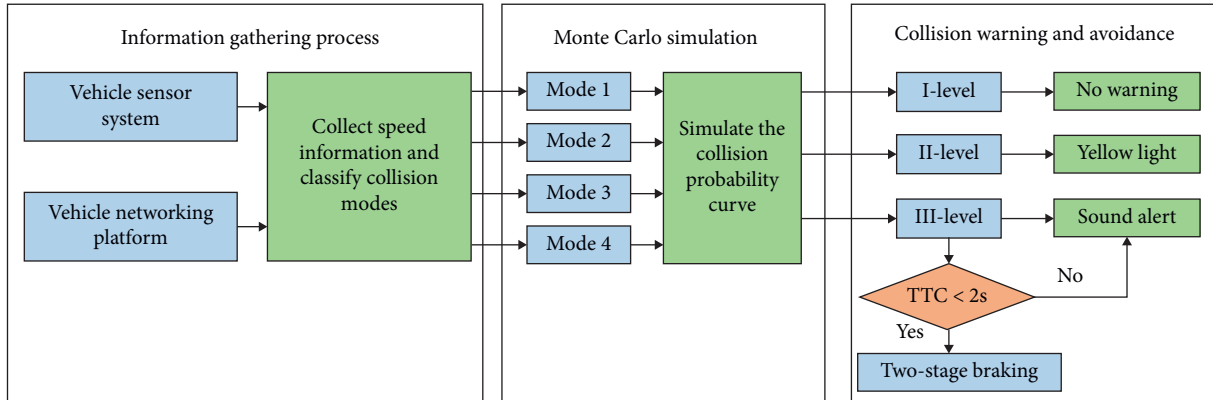


FIGURE 1: The control scheme's roadmap.

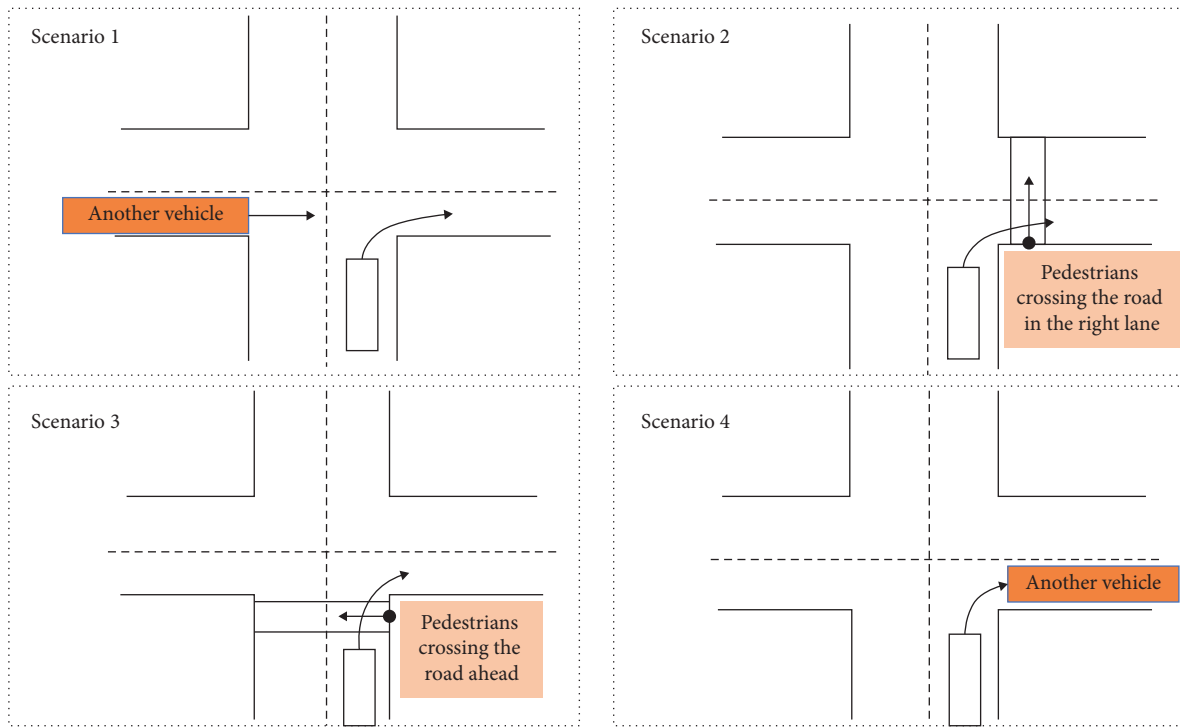


FIGURE 2: Schematic diagrams of the four modes.

I-level: it is low collision probability; vehicle's right-turning process was safe, so the warning system did not warn the driver.

II-level: the intelligent vehicle had a certain collision probability; the warning system reminded the driver by displaying a yellow light in the dashboard.

III-level: a collision could happen immediately, and the warning system reminded the driver to take action. If the TTC was within 2 s, the intelligent vehicle would perform the two-stage braking strategy to actively avoid the collision.

Many researchers believed that a collision between the vehicle and other vehicles or between the vehicle and pedestrians should have different collision warning figures, collision

warning icons should be different according to the crashing objects, and their systems generated different collision warning figures based on different collision objects [18, 19]. We used a conservative warning figure as the only collision warning figure, which can simultaneously simplify the collision warning mechanism and ensure security. The specific areas of the CWS are shown in Table 1 and drawn, as shown in Figure 3. During the simulations, the area where the collision probability curve was located is the warning level.

2.3. Geometric Modelling of Vehicle's and Pedestrian's Safety Profiles. The vehicle's right-turning process was regarded as a rigid body motion, and the vehicle's centre (O_1) was placed on its geometric centre. The length of the right-turning

TABLE 1: Division of three-level collision warning regions.

Three-level warning mechanism	TTC $\in (0,2)$	TTC $\in (2,5)$
I-level region (I-region)	$\{PC \mid 0 \leq PC \leq -0.1 \text{ TTC} + 0.5\}$	$\{PC \mid 0 \leq PC \leq \text{TTC}/30 + 7/30\}$
II-level region (II-region)	$\{PC \mid -0.1 \text{ TTC} + 0.5 \leq PC \leq 0.5\}$	$\{PC \mid \text{TTC}/30 + 7/30 \leq PC \leq 0.1 \text{ TTC} + 0.3\}$
III-level region (III-region)	$\{PC \mid 0.5 \leq PC \leq 1\}$	$\{PC \mid 0.1 \text{ TTC} + 0.3 \leq PC \leq 1\}$

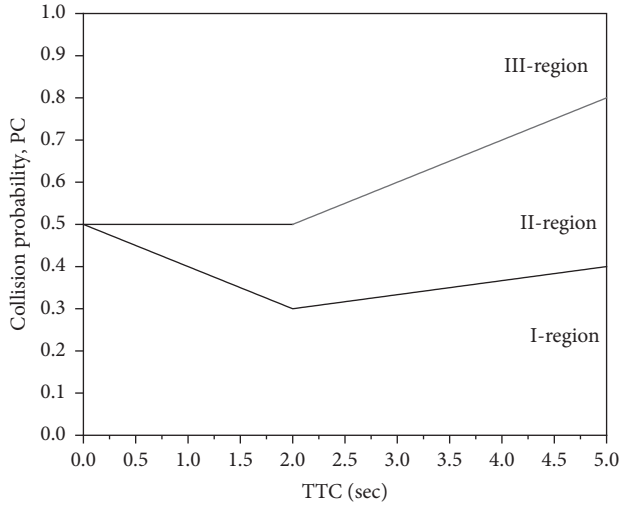


FIGURE 3: Three-level collision warning regions.

vehicle was L_1 and the width W_1 . A second vehicle's length was L_2 , and the width was W_2 . The coordinate system was based on O_1 , and another vehicle's centre was O_2 at coordinates (a, b) . The velocity of the right-turning vehicle is V_1 , and the angle with the X -axis was θ_1 . Another vehicle's velocity was V_2 , and the angle with the X -axis is θ_2 . The vehicle's coordinate system is shown in Figure 4. During the simulation, the second vehicle's or pedestrian's position was unchanging, and reversed speed equal to the speed of the second vehicle or pedestrian was applied to the turning vehicle. If the right-turning vehicle's centre (O_1) crossed into the second vehicle's or pedestrian's safety profiles, a collision occurs.

Many scholars regarded the car as a contour [20, 21]; based on this, the second vehicle's and pedestrian's safety profiles were developed. In this study, we expanded the contour of another vehicle or pedestrian, and the expansion size was the size of the turning vehicle and used this size to establish the vehicle's and pedestrian's safety profiles. If the turning vehicle's centre crossed into the safety profiles, the collision occurred.

When another vehicle collides with the right-turning vehicle, this situation could be used as the safe contour threshold. The vehicle's safety profile was built up as follows.

The front of the vehicle's safety profile was a circle with the front centre S_2 as the centre point and $(L_1 + W_2)/2$ as the radius. The vehicle's rear safety profile was constructed in the same way as the front, and the transition part was a rectangle. The vehicle's safety profile is shown as Figure 5.

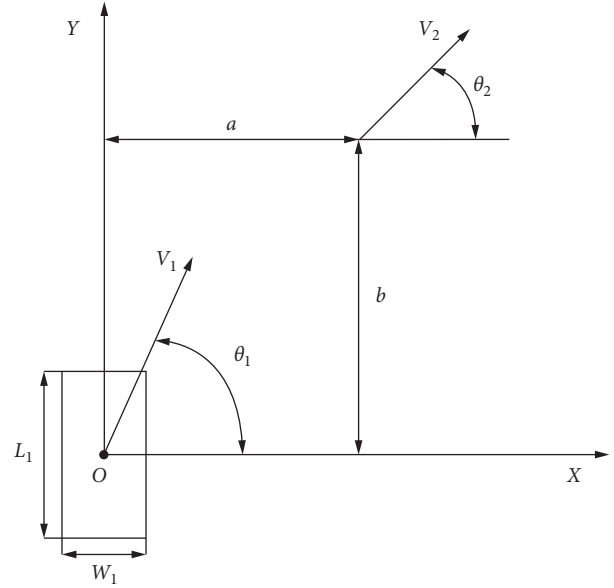


FIGURE 4: Vehicle's coordinate system.

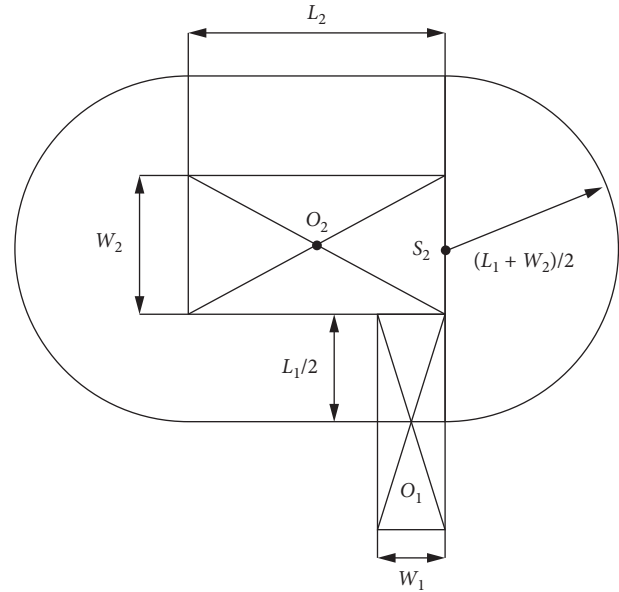


FIGURE 5: Vehicle's safety profile.

In the same way, the pedestrian's safety profile was centred on the pedestrian, and the pedestrian's geometric area was enlarged to determine whether the vehicle's centre (O_1) crossed into the pedestrian safety profile, which was the collision criterion. When the vehicle's front side collided with the pedestrian, this situation was the pedestrian's safety profile threshold. We defined the pedestrian's profile as a circle with a centre O_2 and radius $D/2$, and the pedestrian's safety profile was a circle with centre O_2 and radius $(D + L_1)/2$. The pedestrian's safety profile is shown in Figure 6.

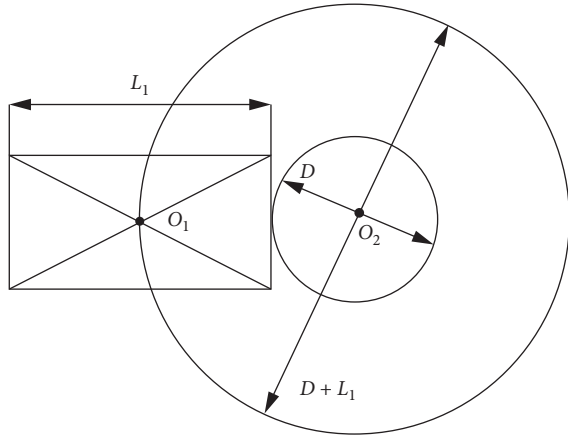


FIGURE 6: Pedestrian's safety profile.

3. Right-Turning Vehicle Collision Probability Calculation Algorithm

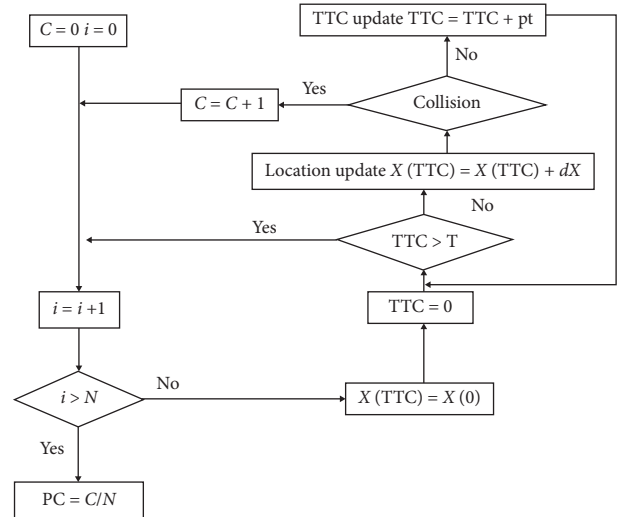
Monte Carlo simulation theory was based on the central limit theorem and the large number theorem [22, 23]. The central limit theorem showed that although the distribution of each random variable M_i was unknown, ΣM_i obeyed a normal distribution and could be converted to a standard normal distribution; therefore, it could be processed using the standard normal distribution properties. We defined $\{M_i\}$ as an independent random variable and part of a sequence of identically distributed random variables, with an expected value of O and variance of k^2 , as shown in

$$\lim_{i \rightarrow \infty} P \left\{ \frac{\sum M_i - io}{\sqrt{i} k} \leq m \right\} = \frac{1}{\sqrt{2 * \pi}} \int_{-\infty}^m e^{-t^2/2} dt = \Phi(m). \quad (3)$$

$\Phi(m)$ represented the value of the standard normal distribution. According to equation (3), the more the samples of random variable M_i were obtained, the closer the distribution was normal, which was the basis of Monte Carlo simulation theory for collision probability.

N random numbers were generated for each random variable V_1 and V_2 and the right-turning radius r . The random variables were assumed to obey the normal distribution with μ as the expected value and σ^2 as the variance [24, 25]. The intelligent vehicle's position was continuously updated as sampling time increases. Sampling time is pt ; each simulation calculated the collision probability within the collision analysis period (T), shown in Figure 7, to calculate whether a collision will occur in T ; according to the vehicle's and pedestrian's safety profiles, PC represented the collision probability. If a collision occurred, the probability is accumulated, and the probability curve is drawn on the three-level warning figure by software.

The calculation process of collision probability for four modes was as follows. First, the right-turning vehicle's angle (θ_1) and coordinate calculation algorithm were introduced. The four modes were slightly different in calculation due to different initial velocity directions and initial positions, but



N : number of random variable samples
 C : number of collisions
 i : number of cycles
 PC : collision probability
 TTC : time-to-collision
 T : collision analysis period
 pt : sampling time
 X : position state variable

FIGURE 7: Flowchart of the collision probability calculation algorithm based on Monte Carlo simulation.

the basic calculation principle was the same. We introduced the calculation process for θ_1 and the right-turning vehicle's coordinates $(x(t), y(t))$. In the i times simulation, the velocity of the right-turning vehicle was $V_1(i)$, turning radius was $r(i)$, and the velocity of the second vehicle was $V_2(i)$. We represented TTC with t , and t represented the simulation time.

The calculation of angle θ_1 was shown in

$$\theta_1 = V_1(i)tr(i)^{-1}. \quad (4)$$

To calculate the position coordinates $(x(t), y(t))$ at the time t using θ_1 , the second vehicle was regarded as stationary and the reverse speed $V_2(i)$ was applied to the right-turning vehicle.

When the condition met the scenario 1, the right-turning vehicle's coordinates $(x(t), y(t))$ were shown in

$$\begin{cases} y(t) = \sin(\theta_1)r(i), \\ x(t) = r(i) - r(i)\cos(\theta_1) - V_2(i)t. \end{cases} \quad (5)$$

When the condition met the scenario 2, the right-turning vehicle's coordinates $(x(t), y(t))$ were shown in

$$\begin{cases} y(t) = \sin(\theta_1)r(i), \\ x(t) = r(i) - r(i)\cos(\theta_1) + V_2(i)t. \end{cases} \quad (6)$$

When the condition met scenario 3, the right-turning vehicle's coordinates $(x(t), y(t))$ were shown:

$$\begin{cases} y(t) = \sin(\theta_1)r(i) - V_2(i)t, \\ x(t) = r(i) - r(i)\cos(\theta_1). \end{cases} \quad (7)$$

When the condition met scenario 4, the right-turning vehicle's coordinates $(x(t), y(t))$ were shown in

$$\begin{aligned} y(t) &= \sin(\theta_1)r(i), \\ x(t) &= r(i) - r(i)\cos(\theta_1) - V_2(i)t. \end{aligned} \quad (8)$$

The second step, in the i times simulation, was to judge if a collision will occur. We needed to judge whether the right-turning vehicle centre O_1 crossed the vehicle's or pedestrian's safety profile. When the condition met the scenario 1 or scenario 4, the safety profile condition of the vehicle was given in equation (9), and the probability was accumulated according to the safety profile condition:

$$\begin{aligned} &\{(x(t) \leq a \pm 0.5L_2) \cap (y(t) \leq b \pm (L_1 + W_2)2^{-1})\} \\ &\cup \{|x(t) - a| - 0.5L_2)^2 + (y(t) - b)^2 \leq (L_1 + W_2)^2 4^{-1}\}. \end{aligned} \quad (9)$$

The collision between the right-turning vehicle and the pedestrians was judged by the pedestrian's safety profile condition, when the condition met the scenario 2 or scenario 3, which was given in the same way as equation (9). The probability was accumulated according to the pedestrian's safety profile condition; the pedestrian's safety profile condition was shown in

$$(x(t) - a)^2 + (y(t) - b)^2 \leq (0.5(L_1 + L_2))^2 2^{-1}. \quad (10)$$

4. Two-Stage Braking Strategy

An intelligent right-turning vehicle collision warning and avoidance algorithm needed a braking strategy to realize active collision avoidance.

We established the two-stage braking strategy. The two-stage braking strategy could select the braking strength independently according to the TTC so that high-efficiency braking could be achieved, and emergency braking could be avoided to prevent the driver from being nervous and misoperating the car. The specific flow of the two-stage braking strategy was as follows:

II-stage braking: if the collision probability reached 50% within 1 s (whether it reached III-level warning within 1 s), we used the II-stage braking with the amount a_{\max} . In the braking process, we considered the braking deceleration (a) approximately linearly increasing with the braking delay (d) and performed a time-domain integral operation on a , so the speed reduction amount could be obtained, thereby obtaining the vehicle speed at each sampling time.

I-stage braking: if the collision probability reached 50% within 1-2 s (whether it reached III-level warning within 1-2 s), we used the I-stage braking with the amount a_{\min} . For the same reason as in the II-stage braking process, we considered the braking deceleration (a) approximately linearly increasing with the braking delay (d) and performed a time-domain integral operation on a . The two-stage braking strategy is shown in Figure 8.

The time-domain integral operation of the acceleration obtained the decrease in velocity, $\Delta V(t)$, during the two-

stage braking process; thereby, we obtained the speed change by time-domain integration of acceleration:

$$\Delta V(t) = \int_0^t a(t)dt. \quad (11)$$

The two-stage braking strategy had two sets of formulas, and equation (12) represented the II-stage braking, which was within 1 s:

$$\Delta V(t) = \int_0^t a(t)dt = \begin{cases} a_{\max} (2d)^{-1}t^2 & (0 < t \leq d), \\ a_{\max} 2^{-1}d + (t - d)a_{\max} & (t > d). \end{cases} \quad (12)$$

Equation (13) represented the I-stage braking, which was within 1-2 s:

$$\Delta V(t) = \int_0^t a(t)dt = \begin{cases} a_{\min} (2d)^{-1}(t - 1)^2 & (0 < t \leq d), \\ a_{\min} 2^{-1}d + (t - 1 - d)a_{\min} & (t > d). \end{cases} \quad (13)$$

Therefore, in each simulation, the right-turning vehicle speed $V_1(i)$ was obtained, and then, the updated speed $V_1^*(i)$ was obtained, which was shown in

$$V_1^*(i) = V_1(i) - \int_0^t a(t)dt. \quad (14)$$

The position coordinates (x_t, y_t) of the vehicle were updated at time t , and the updated coordinates (x_t^*, y_t^*) were shown in

$$\begin{cases} y^*(t) = \sin\left\{\left(V_1(i) - \int_0^t a(t)dt\right) \cdot r(i)^{-1}\right\}r(i), \\ x^*(t) = r(i) - r(i)\cos\left\{\left(V_1(i) - \int_0^t a(t)dt\right) \cdot r(i)^{-1}\right\} - V_2(i)t. \end{cases} \quad (15)$$

5. Simulation Results and Comparative Analysis

5.1. Simulation Results of Each of the Four Modes

Scenario 1: the driver was sitting on the left side and needed to view the right, and it was not convenient to observe the movement of the vehicle in the left side, so it was easy to collide with another vehicle. The parameters in this scenario were defined as follows: $pt = 0.01$ s, $T = 5$ s, $L1 = 8$ m, $W1 = 2$ m, $L2 = 8$ m, and $W2 = 2$ m; the second vehicle's coordinates were $(-9, 12)$. V_1, V_2 , and R consist of 10,000 normally distributed random numbers; $V_1 \sim N(12, 1)$, $V_2 \sim N(15, 1)$, and $R \sim N(20, 1)$. We used the two-stage braking strategy; the specific parameters were as follows: $a_{\max} = 6$ m/s², $a_{\min} = 3$ m/s², and $d = 0.3$ s. The collision probability curve (A curve) and the collision probability curve (B curve) after two-stage braking are shown in Figure 9.

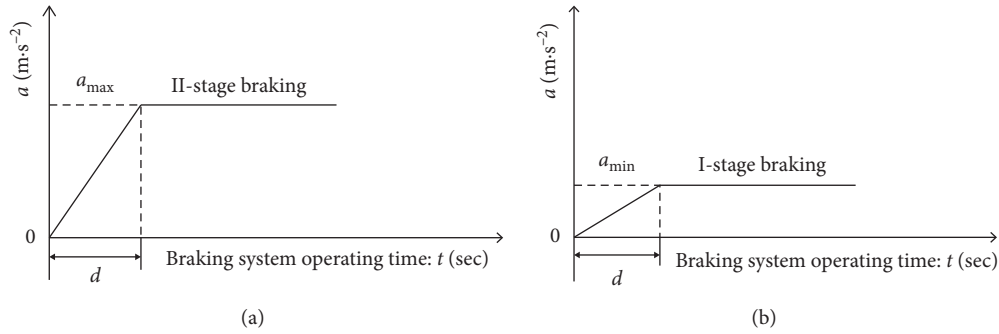


FIGURE 8: The two-stage braking strategy.

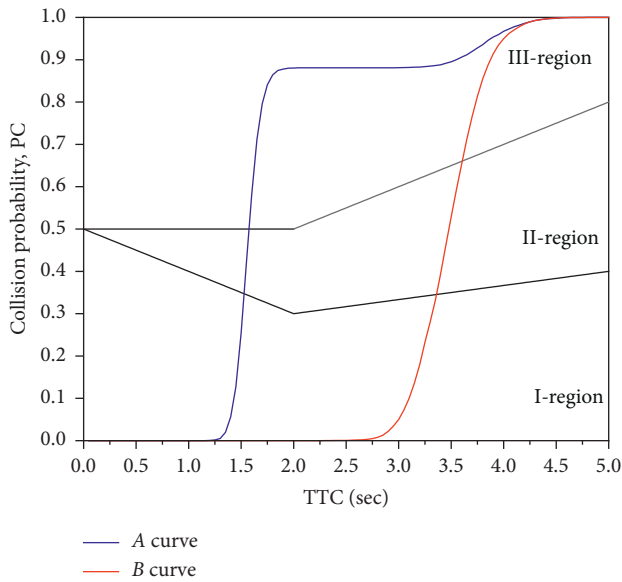


FIGURE 9: Scenario 1: collision probability curve (A curve) and collision probability curve (B curve) after two-stage braking.

Scenario 2: when the vehicle turned right into the lane, it was difficult to find pedestrians who were crossing the road in the lane, so it was easy to cause serious traffic accidents. The parameters in this scenario were defined as follows: $pt = 0.01$ s, $T = 5$ s, $L_1 = 8$ m, $W_1 = 2$ m, and $D = 1.5$ m; the pedestrian's coordinates were (8, 12). V_1 , V_2 , and R consist of 10,000 normally distributed random numbers, $V_1 \sim N(14, 1)$, $V_2 \sim N(1, 2)$, and $R \sim N(20, 1)$; V_2 represented the velocity of the pedestrian in this case. We used the two-stage braking strategy; the specific parameters were as follows: $a_{max} = 6$ m/s², $a_{min} = 3$ m/s², and $d = 0.3$ s. The collision probability curve (A curve) and the collision probability curve (B curve) after two-stage braking are shown in Figure 10.

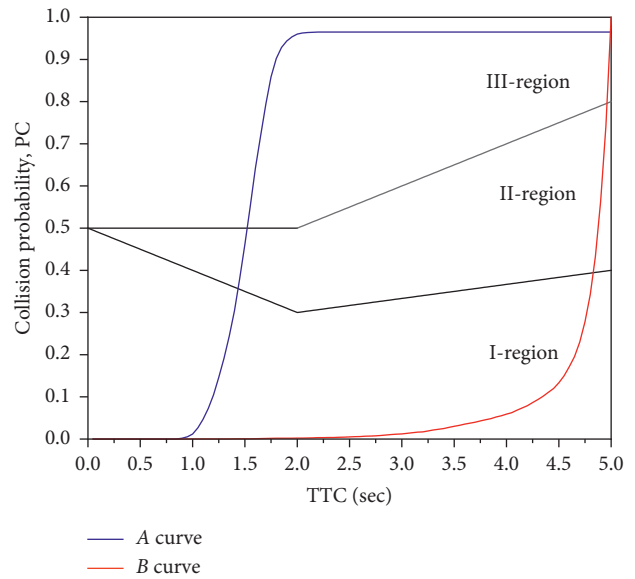


FIGURE 10: Scenario 2: collision probability curve (A curve) and collision probability curve (B curve) after two-stage braking.

Scenario 3: because the driver had blind spots in vision, it is possible for the right-turning vehicle to collide with pedestrians crossing the road. The parameters in this scenario were defined as follows: $pt = 0.01$ s, $T = 5$ s, $L_1 = 8$ m, $W_1 = 2$ m, and $D = 1.5$ m; the pedestrian's coordinates were (3, 9). V_1 , V_2 , and R consist of 10,000 normally distributed random numbers, $V_1 \sim N(10, 1)$, $V_2 \sim N(1, 0.7)$, $R \sim N(20, 1)$; V_2 represented the velocity of the pedestrian in this case. We used the two-stage braking strategy; the specific parameters were as follows: $a_{max} = 6$ m/s², $a_{min} = 3$ m/s², and $d = 0.3$ s. The collision probability curve (A curve) and the collision probability curve (B curve) after two-stage braking are shown in Figure 11.

5.2. Simulation Results Analysis of Four Modes. Through the simulation results from the four modes, by comparing the collision probability curve (A curve) and the collision probability curve (B curve) after two-stage braking, the two-stage braking strategy could reduce the collision probability that was more than 50% within 2 s to nearly 0%. The two-stage braking

strategy shifted the collision probability curve (A curve) to the right so that most of the curve falls in the I-level region. Before the two-stage braking, most of the curve fell in the II-level and III-level regions. Finally, the simulation results showed that the intelligent right-turning vehicle collision probability calculation algorithm could calculate collision probability and the two-

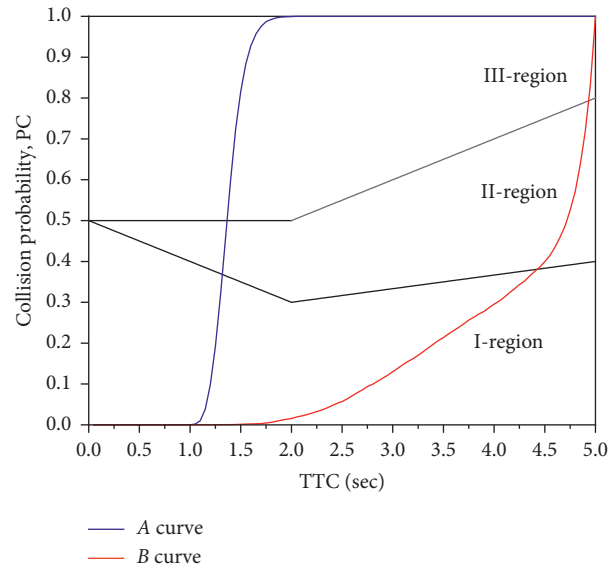


FIGURE 11: Scenario 3: collision probability curve (A curve) and collision probability curve (B curve) after two-stage braking.

Scenario 4: the parameters in this scenario were defined as follows: $pt = 0.01$ s, $T = 5$ s, $L1 = 8$ m, $W1 = 2$ m, $L2 = 8$ m, and $W2 = 2$ m; the second vehicle's coordinates were (9, 12). V_1 , V_2 , and R consist of 10000 normal distribution random numbers, $V_1 \sim N(12, 1)$, $V_2 \sim N(3, 1)$, and $R \sim N(20, 1)$. We used the two-stage braking strategy; the specific parameters were as follows: $a_{\max} = 6$ m/s², $a_{\min} = 3$ m/s², and $d = 0.3$ s. The collision probability curve (A curve) and the collision probability curve (B curve) after two-stage braking are shown in Figure 12.

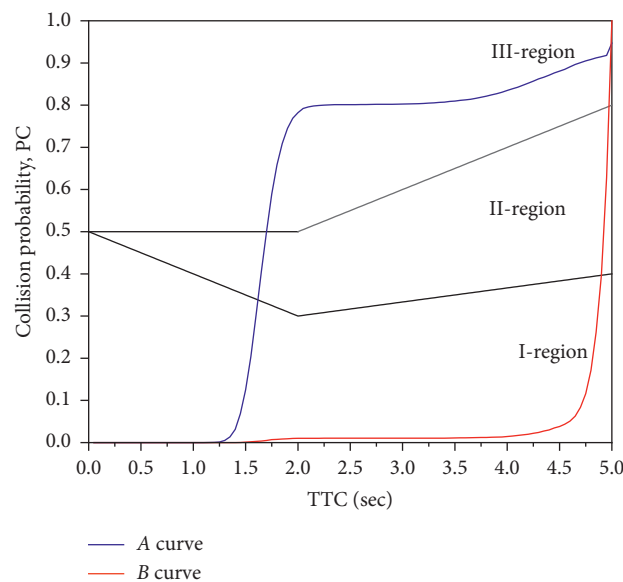


FIGURE 12: Scenario 4: collision probability curve (A curve) and collision probability curve (B curve) after two-stage braking.

stage braking algorithm significantly reduced the collision probability which can improve safety.

5.3. Comparative Analysis. To verify the rationality of the collision probability curve calculation algorithm, we compared and analysed the collision probability curves generated using three different initial positions. Taking scenario 1 as an example and leaving the size of the two vehicles unchanged, we designed three different initial positions and

changed the initial coordinates of the second vehicle, as shown in Table 2.

The collision probability curves (A curve) for the three different initial positions are shown in Figure 13.

From Figure 13, we can conclude that the collision probability was increasing from position 1 to position 3 within the period from 1 to 4.5 s, and the closer the distance between the two vehicles was, the higher the collision probability is. Therefore, the calculation algorithm of the collision probability curve (A curve) can be verified.

TABLE 2: Parameters of three different initial positions (A curve simulation process).

Initial positions	a (m)	b (m)	V_1 (m/s)	V_2 (m/s)	R (m)	pt (s)	T (s)
Position 1'	9	12	$V_1 \sim N(12, 1)$	$V_2 \sim N(15, 1)$	$R \sim N(20, 1)$	0.01	5
Position 2	8	11	$V_1 \sim N(12, 1)$	$V_2 \sim N(15, 1)$	$R \sim N(20, 1)$	0.01	5
Position 3	7	10	$V_1 \sim N(12, 1)$	$V_2 \sim N(15, 1)$	$R \sim N(20, 1)$	0.01	5

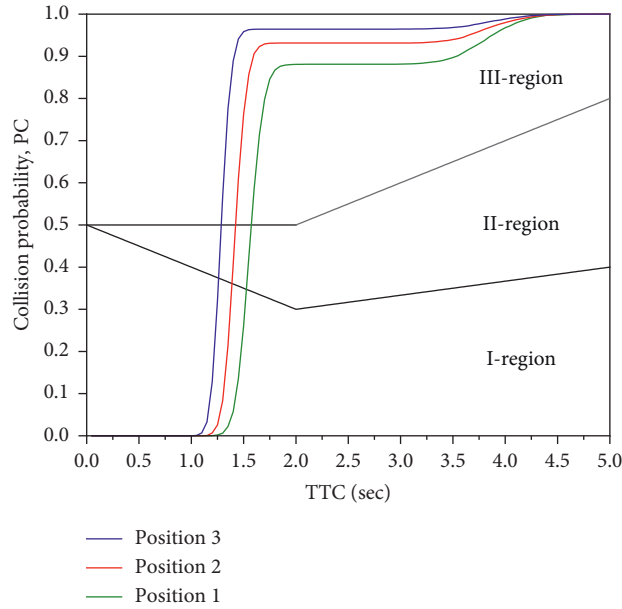


FIGURE 13: Collision probability curves (A curve) for the three different initial positions.

TABLE 3: Parameters of three different initial positions (B curve simulation process).

Initial positions	a (m)	b (m)	V_1 (m/s)	V_2 (m/s)	R (m)	pt (s)	T (s)	a_{max} (m/s ²)	a_{min} (m/s ²)	d (s)
Position 1'	9	12	$V_1 \sim N(12, 1)$	$V_2 \sim N(15, 1)$	$R \sim N(20, 1)$	0.01	5	6	3	0.3
Position 2	8	11	$V_1 \sim N(12, 1)$	$V_2 \sim N(15, 1)$	$R \sim N(20, 1)$	0.01	5	6	3	0.3
Position 3	7	10	$V_1 \sim N(12, 1)$	$V_2 \sim N(15, 1)$	$R \sim N(20, 1)$	0.01	5	6	3	0.3

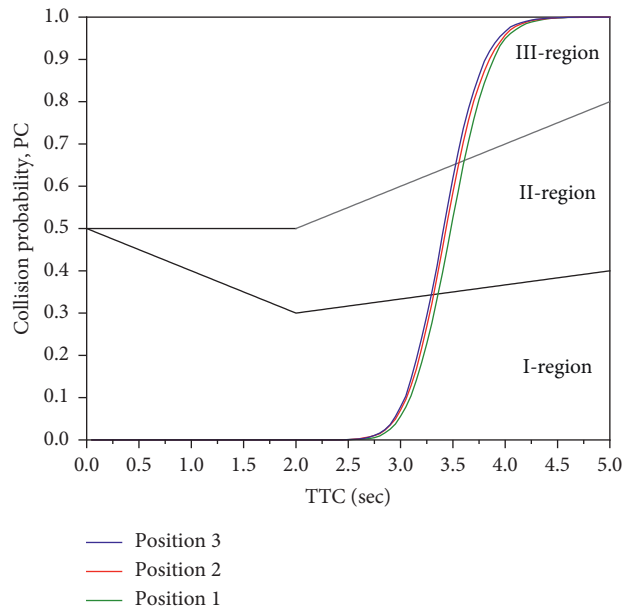


FIGURE 14: Collision probability curve (B curve) after two-stage braking in three different initial positions.

For the same reason, to verify the rationality of the two-stage braking strategy, we compared and analysed the collision probability curves after two-stage braking generated using three different initial positions. Taking scenario 1 as an example and leaving the size of two vehicles unchanged, we designed three different initial positions and changed the initial coordinates of the second vehicle, as shown in Table 3.

The collision probability curve (*B* curve) after two-stage braking using three different initial positions is shown in Figure 14.

From Figure 14, we can conclude that the collision probability was increasing from position 1 to position 3 within the period from 2.5 to 4.5 s, and the closer the distance between the two vehicles is, the higher the collision probability is. Therefore, the two-stage braking strategy can be verified.

6. Conclusion

- (1) Compared with the safety distance model, the safety model based on TTC can more intuitively reflect the degree of danger. The two-stage braking strategy can lower the warning level. Aiming to reduce an intelligent right-turning vehicle's collision probability, we established a three-level warning mechanism and drew the warning figure. Based on Monte Carlo stochastic simulation, we established the collision probability calculation algorithm for an intelligent right-turning vehicle at an intersection and plotted the collision probability curve on the warning figure. The area where the probability curve was located outputs the warning level.
- (2) The two-stage braking strategy was established to actively avoid a collision if the collision probability reaches 50% within 2 s. We analysed four modes for a right-turning vehicle and simulated the collision probability curve (*A* curve) and the collision probability curve (*B* curve) after two-stage braking. Finally, we changed the initial position for comparative analysis and verification.
- (3) The simulation results from the four modes showed that the collision probability reached 80% in the 2 s before active collision avoidance, and the collision probability of some modes could reach 100%. The two-stage braking strategy reduced the collision probability to nearly 0% in 2 s, and the collision probability was reduced to less than 5% in 3 s, which improves safety significantly.
- (4) The collision probability curve calculation algorithm and the two-stage braking strategy were verified and analysed. By comparing three different initial positions, the comparison results showed that the collision probability curve calculation algorithm and the two-stage braking strategy were reasonable.
- (5) We used the Monte Carlo method to calculate the collision probability; collision warning and avoidance were carried out to reduce the collision probability of a right-turning vehicle. Our research laid the foundation for future experiments, and we will carry out experimental analysis better in future.

Through future experiments, we can perfect the collision warning and avoidance algorithm.

Data Availability

All data generated or analysed during this study were included in this article. All data and models used during the study appear in the submitted article. Part data were calculated from the algorithm and the code.

Conflicts of Interest

The authors declare that there are no conflicts of interest.

Acknowledgments

This project was supported by the National Natural Science Foundation of China (Grant nos. 51875237, 51675224, and 51675224).

Supplementary Materials

The supplemental files are the program file compression package. (*Supplementary Materials*)

References

- [1] B. Yu, Y. Chen, R. Wang, and Y. Dong, "Safety reliability evaluation when vehicles turn right from urban major roads onto minor ones based on drivers visual perception," *Accident Analysis & Prevention*, vol. 95, pp. 487–494, 2016.
- [2] G. E. Ru-hai and H. Zhi-fu, "Research on collision warning of the right blind area for large vehicles," *Journal of Chongqing University of Technology (Natural Science)*, vol. 30, no. 10, pp. 1–10, 2016.
- [3] A. Tageldin, T. Sayed, and K. Ismail, "Evaluating the safety and operational impacts of left-turn bay extension at signalized intersections using automated video analysis," *Accident Analysis & Prevention*, vol. 120, pp. 13–27, 2018.
- [4] H. Yoshitake and M. Shino, "Risk assessment based on driving behavior for preventing collisions with pedestrians when making across-traffic turns at intersections," *IATSS Research*, vol. 42, no. 4, pp. 240–247, 2018.
- [5] H. Iasmin, A. Kojima, and H. Kubota, "Safety effectiveness of pavement design treatment at intersections: left turning vehicles and pedestrians on crosswalks," *IATSS Research*, vol. 40, no. 1, pp. 47–55, 2016.
- [6] Y. Ni, M. Wang, J. Sun, and K. Li, "Evaluation of pedestrian safety at intersections: a theoretical framework based on pedestrian-vehicle interaction patterns," *Accident Analysis & Prevention*, vol. 96, pp. 118–129, 2016.
- [7] J. B. Cicchino, "Effectiveness of forward collision warning and autonomous emergency braking systems in reducing front-to-rear crash rates," *Accident Analysis & Prevention*, vol. 99, pp. 142–152, 2017.
- [8] A. Bensebaa and S. Larabi, "Direction estimation of moving pedestrian groups for intelligent vehicles," *The Visual Computer*, vol. 34, no. 6–8, pp. 1109–1118, 2018.
- [9] F. Sun, X. Huang, J. Rudolph, and K. Lolenko, "Vehicle state estimation for anti-lock control with nonlinear observer," *Control Engineering Practice*, vol. 43, pp. 69–84, 2015.
- [10] Y. Hashimoto, G. Yanlei, L. T. Hsu, and K. Shunsuke, "A Probabilistic model for the estimation of pedestrian crossing

- behavior at signalized intersections,” in *Proceedings of the Intelligent Transportation Systems (ITSC), 2015 IEEE 18th International Conference*, IEEE, Las Palmas, Spain, pp. 1520–1526, September 2015.
- [11] H. Sitao, X. Qiaojun, X. Huihui, and X. Gang, “Safety impact analysis of large vehicles right-turn on pedestrians and non-motorized vehicle at signalized intersection,” in *Proceedings of the World Automation Congress (WAC)*, IEEE, Washington, DC, USA, pp. 1–4, June 2012.
- [12] Z. Zhao, L. Zhou, Q. Zhu, Y. Luo, and K. Li, “A review of essential technologies for collision avoidance assistance systems,” *Advances in Mechanical Engineering*, vol. 9, no. 10, p. 1687814017725246, 2017.
- [13] C. Choi and Y. Kang, “Simultaneous braking and steering control method based on nonlinear model predictive control for emergency driving support,” *International Journal of Control, Automation and Systems*, vol. 15, no. 1, pp. 345–353, 2017.
- [14] J. Zhao, “Distance control algorithm for automobile automatic obstacle avoidance and cruise system,” *Computer Modeling in Engineering & Sciences*, vol. 116, no. 1, pp. 69–88, 2018.
- [15] Li Lin, X. Zhu, and Z. Ma, “Driver brake reaction time under real traffic risk scenarios,” *Automotive Engineering*, vol. 36, no. 10, pp. 1225–1229, 2014.
- [16] A. Steinfeld, D. Duggins, J. Gowdy et al., “Development of the side component of the transit integrated collision warning system,” in *Proceedings of the the 7th International IEEE Conference*, IEEE, Washington, DC, USA, pp. 343–348, October 2004.
- [17] R. Aufrère, J. Gowdy, C. Mertz, C. Thorpe, C.-C. Wang, and T. Yata, “Perception for collision avoidance and autonomous driving,” *Mechatronics*, vol. 13, no. 10, pp. 1149–1161, 2003.
- [18] D. Duggins, S. McNeil, C. Mertz, C. Thorpe, and T. Yata, “Side collision warning systems for transit buses: functional goals,” in *Proceedings of the the 79th Annual Transportation Research Board*, Washington, DC, USA, January 2001.
- [19] S. McNeil, D. Duggins, C. Mertz, A. Suppé, and C. Thorpe, “A performance specification for transit bus side collision warning system,” in *Proceedings of the the 9th World Congress on Intelligent Transport Systems*, Chicago, IL, USA, October 2002.
- [20] C. Wang, Z. Li, Y. Chen, and G. Dai, “Research on lane-changing models considering restricted space,” *Journal of Highway and Transportation Research and Development*, vol. 29, no. 1, pp. 121–127, 2012.
- [21] R. Zhang, F. You, X. Chu, L. Guo, H. E. Zhao-cheng, and R. Wang, “Lane change merging control method for unmanned vehicle under V2V cooperative environment,” *China Journal of Highway and Transport*, vol. 31, no. 4, pp. 180–191, 2018.
- [22] M. B. Alaya and A. Kebaier, “Central limit theorem for the multilevel Monte Carlo Euler method,” *The Annals of Applied Probability*, vol. 25, no. 1, pp. 211–234, 2015.
- [23] G. Ökten, B. Tuffin, and V. Burago, “A central limit theorem and improved error bounds for a hybrid-Monte Carlo sequence with applications in computational finance,” *Journal of Complexity*, vol. 22, no. 4, pp. 435–458, 2006.
- [24] K. T. Waldeer, *A Vehicular Traffic Flow Model Based on a Stochastic Acceleration Process*, 2004.
- [25] S. Chandra and A. K. Bharti, “Speed distribution curves for pedestrians during walking and crossing,” *Procedia - Social and Behavioral Sciences*, vol. 104, pp. 660–667, 2013.

Research Article

In Search of the Consequence Severity of Traffic Conflict

Ruoxi Jiang, Shunying Zhu , Pan Wang, QiuCheng Chen, He Zou, and Shiping Kuang

School of Transportation, Wuhan University of Technology, Wuhan, Hubei 430063, China

Correspondence should be addressed to Shunying Zhu; zhusy2001@163.com

Received 16 November 2019; Revised 17 February 2020; Accepted 21 February 2020; Published 13 July 2020

Guest Editor: Zeyang Cheng

Copyright © 2020 Ruoxi Jiang et al. This is an open access article distributed under the Creative Commons Attribution License, which permits unrestricted use, distribution, and reproduction in any medium, provided the original work is properly cited.

Currently, many studies on the severity of traffic conflicts only considered the possibility of potential collisions but ignored the consequences severity of potential collisions. Aiming toward this defect, this study establishes a potential collision (serious conflict) consequences severity model on the basis of vehicle collision theory. Regional vehicles trajectory data and historical traffic accident data were obtained. The field data were brought into the conflict consequences severity model to calculate the conflict severity rate of each section under different TTC thresholds. For comparison, the traditional conflict rate of each section under different TTC thresholds that considered only the number of conflicts was also calculated. Results showed that the relationship between conflict severity rate and influencing factors was somehow different. The conflict severity rate seemed to have a higher correlation with accident rate and accident severity rate than conflict rate did. The TTC threshold value also affected the correlation between conflicts and accidents, with high and low TTC threshold indicating a lower correlation. The results showed that conflict severity rate that considered each single conflict consequence severity was a little better than the traditional conflict rate that considered only the numbers of conflicts in reflecting real risks as a new conflict evaluation indicator. The severity of traffic conflicts should consider two dimensions: the possibility and consequence of potential collisions. Based on this, we propose a new traffic safety evaluation method that takes into account the severity of the consequences of the conflict. More data and prediction models are needed to conduct more realistic and complex research in the future to ensure reliability of this new method.

1. Introduction

A common method for studying traffic safety is based on historical traffic accidents data. This method is logically rational and reliable, but it has some limitations: (a) Traffic accidents are random and accidental. If accident data are insufficient and do not meet statistical requirements, then the influencing factors on traffic accidents cannot be analyzed. Thus, drawing useful conclusions on traffic safety evaluation and improvement will be difficult [1–3]. (b) Accidents or serious traffic conflicts that do not cause serious consequences are often unrecorded. For example, Hauer and Hakkert [4] found that six percent of minor accidents are unrecorded. However, these minor accidents often contain substantial information. (c) The analysis of accident data can only be conducted after the occurrence of an accident. Aiming toward these shortcomings, some scholars proposed the concept of traffic conflict in the 1960s–70s [5, 6] and

developed the traffic conflict technique (TCT) [7]. With the TCT, substantial data can be observed before accidents occur. The technique has some statistical advantages, such as large sample size, short cycle, and small region [8]. The traffic conflict analysis method is also deemed as one of the promising research directions in the field of traffic safety [9].

At present, the traffic conflict measurement indicators that determine the severity of conflicts can be classified as spatial/temporal proximity (including distance, velocity, and time) and evasive action indicators. Time indicators, which combine the distance and velocity, are thus widely used. The most commonly used time indicators include TTC (time to collision) [10] and PET (postencroachment time) [11]. However, most of these indicators can only measure one aspect of conflict severity, that is, the possibility/proximity severity of traffic conflict to a collision, and they do not consider the consequence/outcome severity of potential collisions caused by conflicts [12]. The original Swedish TCT

only defined the severity of conflict as the possibility of an accident and did not consider casualties and property losses [13]. Low TTC/PET values represent a short time to collide and high possibility from conflict to collision. The same TTC/PET values represent the same possibility of collision. Nevertheless, a minor accident caused by small vehicles is obviously different from a serious accident leading to casualties caused by trucks even if their TTC/PET are same; thus the consequence severity of potential collisions should be considered.

Few studies have explored the consequence severity of traffic conflicts. Dutch Traffic Conflict Technique (DOC-TOR), subjective scoring with video recording, is used to evaluate severity. But the consistency and accuracy need to be improved. Evans [14] and Gabauer [15] found that a close relationship exists between the velocity difference and the severity of accident consequences. Therefore, many early studies used velocity difference as an indicator to describe the severity of conflict consequences. However, some works confirmed that the severity of accident consequences is also related to vehicle quality, collision angle, and other factors. Considering only the velocity difference is not enough [16]. As a result, many scholars began to comprehensively consider the physical motion parameters of vehicle (e.g., velocity and acceleration) in their calculation. For example, Bagdadi [17] considers the quality, velocity, and acceleration of vehicles. The theoretical research was valuable, but it needs accurate and continuous data on speed, acceleration, vehicle type, conflict type, collision angle, and vehicle quality before and after collision. Thus, existing studies lacked the support of actual data.

The severity of traffic conflicts should include two dimensions: the possibility of conflict to develop to collision and the severity of potential conflict consequences. However, the latter is neglected sometimes. In the study, theoretical and empirical studies are carried out to address the above problems. The paper comprises three parts. In the first part, a conflict consequence severity model is established. In the second part, data collection method and processing procedure are introduced. In the third part, conflict consequence severity model is verified to determine whether it is better than the traditional model which only considers the possibility of collisions by studying their correlation with historical accident data.

2. Potential Collision Consequences Severity Model

As mentioned above, the severity of traffic conflict includes the possibility and consequence of potential collisions. Distribution in terms of nearness to collisions [7] and pyramid hierarchy [18] shows that serious conflicts are closely related to collisions. Therefore, this paper assumes that, after a serious conflict occurs, no evasive action will be taken, and a conflict will certainly develop to a collision. After a vehicle collision, some kinetic energy is converted into destructive energy for vehicle deformation, which is used to reflect the severity of potential collision consequences in traffic conflicts. Apparently, the greater kinetic

energy is lost, the more serious collision consequences will be and the higher severity of the conflicts consequences will be.

Vehicles collide not only with other vehicles but also with road facilities, such as guardrails and central reservations. Therefore, in the study, collision contains two categories: potential collision under vehicle-vehicle conflict and potential collision under vehicle-road facility conflict. The process is as follows.

2.1. Potential Collision in Vehicle-Vehicle Conflict

2.1.1. Basic Principles and Hypotheses

- (1) Traffic conflict is defined as follows: When two users are close to each other within a certain time and space, a risk of collision exists if they do not change their motion. The difference between collisions and conflicts lies only in whether the driver has taken successful evasion action after conflicts happen. The evasion actions that drivers take are different in postconflict situations and are simplified. The worst effects are considered in the paper, that is, assuming that drivers do not take any evasion action after each serious conflict.
- (2) The conflict in the model is the serious conflict. The indicator for measuring conflict severity (collision possibility) in this study is TTC, which is defined as "the time required for two vehicles to collide if they continue at their present speeds on the same path" [10].
- (3) Vehicle collision is a process of momentum exchange. At the same time, the internal force caused by vehicle collision (acting force and reacting force produced by the collision) is considerably greater than the external force (such as friction force); thus, it can be treated approximately by the law of conservation of momentum.
- (4) Vehicle collision is also a process of energy exchange. During the process of vehicle collision, the light, heat, and sound energy produced by the collision are neglected. To simplify the analysis, this study assumes that a portion of the mechanical energy is converted to the deformation energy of the vehicle before and after the collision. In this study, deformation energy is defined as the destructive energy hidden in each traffic conflict.
- (5) Avoidance measures are not taken into account, and vehicle braking is not considered from the beginning of a serious traffic conflict to collision. Thus, only existing rolling resistance, which is extremely low, is neglected. As the time between the conflict and the collision is short usually, collision speed is similar to serious conflict speed.
- (6) The time from serious conflict to collision is extremely short, and avoidance measures are considered; thus, collision angle can be deemed approximate to the angle when serious conflict occurs.

- (7) Vehicles are defined as rigid bodies with mass in this study. Before and after collision, their mass, centroid position, wheelbase, moment of inertia, and other parameters do not change [19].
- (8) Vehicle height is not considered in vehicle collision, and no phenomenon in which a small vehicle goes under a truck or a truck goes on top of a small vehicle occurs. Vehicle collision only occurs in a plane space, that is, a two-dimensional collision model.
- (9) In this study, the object of data collection is a highway where no head-on collision occurs. Only rear-end and cross collisions are assumed. At the same time, a vehicle is simplified to a point with mass (centroid point) without considering its shape. The centroids of two vehicles are assumed to be in a straight line that coincides with the direction of the collision as the collision occurs. No change in angular momentum occurs.

2.1.2. Phase from Conflict to Collision. The period from conflict to collision is roughly divided into four phases. In the first phase, serious conflict happens between two vehicles. The speed of the vehicle ahead and that of the vehicle behind in one conflict are V_a and V_b , respectively. The angle is α ; as only rear-end conflict and cross conflict are considered, α is -90° to 90° . In the second phase, two vehicles are about to collide, and their deformation is about to begin. At the initial stage, the speeds of two vehicles are V_a and V_b (in hypothesis (5), they are approximately equal to the vehicle speed in serious conflict), and the angle is α (in hypothesis (6), it is approximately equal to the angle in serious conflict). In the third phase, two vehicles collide. The speed of the vehicle behind decreases, and the speed of the vehicle ahead increases. Moreover, the speeds of the two cars are the same V_i at a certain moment. During the period from the second phase to the current phase, a portion of the mechanical energy is converted into deformation energy. In the fourth phase, the speed of the vehicle behind continues to decrease to V'_a and the speed of the vehicle ahead continues to increase to V'_b . However, the two vehicles separate, and the deformation is over. The deformation starts during the period from the second to the third phase, which is the main goal of our research, as shown in Figure 1.

2.1.3. Computational Process. The current work is aimed at the period from the second phase to the fourth phase. During this period, the velocity change caused by collision causes some kinetic energy to be converted into deformation energy. The conversion satisfies the law of conservation of energy. For convenience, the velocity is converted to the X - and Y -axes. The details are as follows:

$$\frac{1}{2}M_a \cdot V_{aX}^2 = \frac{1}{2}M_a \cdot V_{iX}^2 + \frac{1}{2}M_b \cdot V_{iX}^2 + E_X, \quad (1)$$

$$\frac{1}{2}M_a \cdot V_{aY}^2 + \frac{1}{2}M_b \cdot V_b^2 = \frac{1}{2}M_a \cdot V_{iY}^2 + \frac{1}{2}M_b \cdot V_{iY}^2 + E_Y. \quad (2)$$

At the same time, the conversion also satisfies the law of conservation of momentum:

$$M_a \cdot V_{aX} = M_a \cdot V_{iX} + M_b \cdot V_{iX}, \quad (3)$$

$$M_a \cdot V_{aY} + M_b \cdot V_b = M_a \cdot V_{iY} + M_b \cdot V_{iY}, \quad (4)$$

where V_{aX} , V_{aY} , and V_b , respectively, represent the velocities of the vehicle behind (in the X - and Y -axes) and the vehicle ahead after a serious conflict, V_{iX} and V_{iY} , respectively, denote the velocities in the X - and Y -axes at an instant after the collision when the velocity is the same, M_a and M_b , respectively, represent the masses of the vehicles ahead and behind, and E_X and E_Y , respectively, denote the destructive energy (deformation energy) hidden in a traffic conflict in the X - and Y -axes.

The following can be obtained on the basis of Formulas (3) and (4):

$$V_{iX} = \frac{M_a \cdot V_{aX}}{M_a + M_b}, \quad (5)$$

$$V_{iY} = \frac{M_a \cdot V_{aY} + M_b \cdot V_b}{M_a + M_b}. \quad (6)$$

Substitute (5) and (6) into (1) and (2) to calculate

$$E_X = \frac{1}{2} \cdot \frac{M_a \cdot M_b}{M_a + M_b} \cdot V_{aX}^2, \quad (7)$$

$$E_Y = \frac{1}{2} \cdot \frac{M_a \cdot M_b}{M_a + M_b} \cdot [(V_{aX} - V_b)^2]. \quad (8)$$

According to the trigonometric relationship,

$$V_{aX} = V_a \sin \alpha, \quad V_{aY} = V_a \cos \alpha. \quad (9)$$

They are substituted into (7) and (8) to obtain

$$E_X = \frac{1}{2} \cdot \frac{M_a \cdot M_b}{M_a + M_b} \cdot [(V_a \sin \alpha)^2], \quad (10)$$

$$E_Y = \frac{1}{2} \cdot \frac{M_a \cdot M_b}{M_a + M_b} \cdot [(V_a \cos \alpha - V_b)^2]. \quad (11)$$

Finally,

$$E = E_X + E_Y = \frac{1}{2} \cdot \frac{M_a \cdot M_b}{M_a + M_b} \cdot [(V_a \sin \alpha)^2 + (V_a \cos \alpha - V_b)^2]. \quad (12)$$

2.2. Potential Collision in Vehicle-Road Facility Conflict

2.2.1. Basic Principles and Hypotheses

- (1) Vehicle-road facility conflict is defined as follows: When a vehicle and a road facility, such as a central reservations and guardrail, are close to each other within a certain time and space, a risk of collision exists if the vehicle does not change its motion state. The difference between accidents and conflicts lies only in whether the driver has taken successful evasion action after the conflict. Similarly, it is also

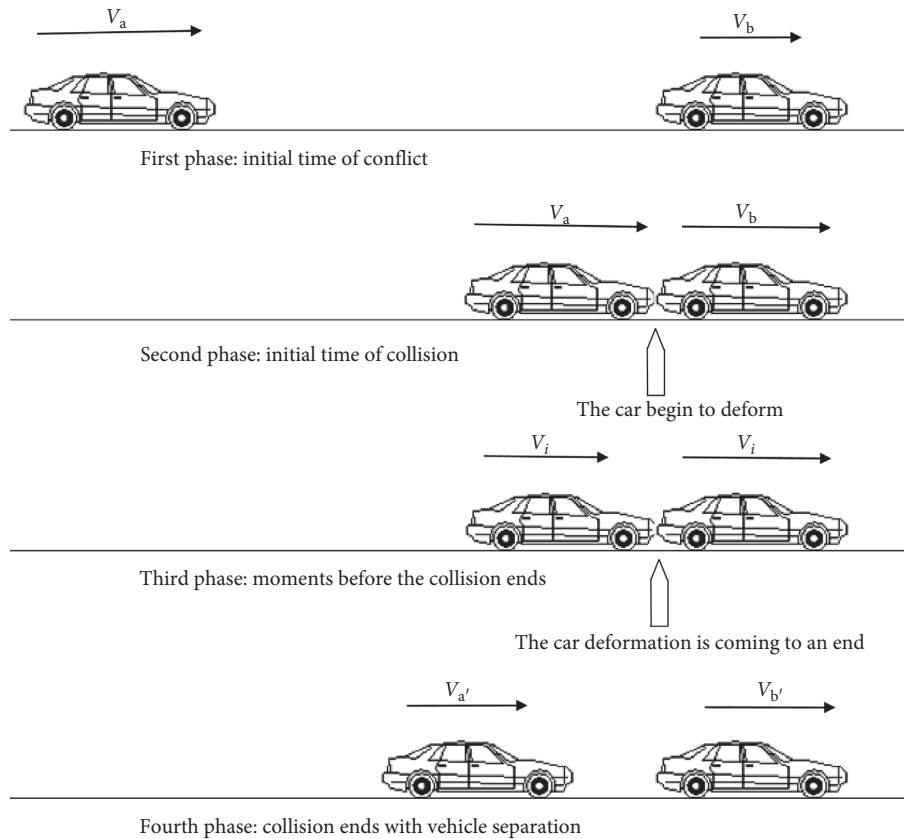


FIGURE 1: Schematic diagram of speed changing during vehicle collision.

simplified. The worst effects are considered here, that is, assuming that the drivers do not take any evasion action after each serious conflict.

- (2) When different types of vehicles collide with facilities, differences in velocity and energy after collisions are observed. The calculation is simplified by dividing collision into two categories: collision of trucks and facilities and collision of small or medium vehicles and facilities. The speed of small and medium vehicles is assumed to decrease to 0 after collision with facilities. By contrast, the speed of trucks is assumed to halve, but the driving direction is unchanged after collision with facilities; chain collision of the opposite lane is not considered here.
- (3) Other hypotheses are basically the same as those for vehicle-vehicle conflict.

2.2.2. Phase from Conflict to Collision

- (1) Collision of small and medium vehicles and road facilities. The period from conflict to collision of small and medium vehicles and facilities is roughly divided into four phases. In the first phase, serious conflict occurs between vehicles and facilities. The instant speed of the vehicles is V_a , and the collision angle is α . In the second phase, the small and medium vehicles collide with the facilities, and the

deformation of the vehicles is about to begin. At the initial stage of collision, the speed is V_a , and the angle is α (the initial collision velocity and angle are assumed to be approximate to the vehicle speed and angle in serious conflict, respectively). In the third phase, the vehicles collide with the facilities, and the speed of the small and medium vehicles decreases to 0; moreover, some of the mechanical energy is converted into deformation energy. In the fourth phase, small and medium vehicles may rebound, but the deformation is over. The deformation starts during the period from the second phase to the third phase, which is the main goal of our research, as shown in Figure 2.

- (2) Collision between trucks and road facilities. The period from conflict to collision between trucks and facilities is roughly divided into four phases. In the first phase, serious conflict occurs between vehicles and facilities. The instant speed of the vehicle is V_a , and the collision angle is α . In the second phase, the trucks collide with the facilities, and the deformation of the vehicles is about to begin. At the initial stage of collision, the speed is V_a , and the angle is α (the initial collision velocity and angle are assumed to be approximate to the vehicle speed and angle in serious conflict, respectively). In the third phase, the vehicles collide with the facilities, and some of the mechanical

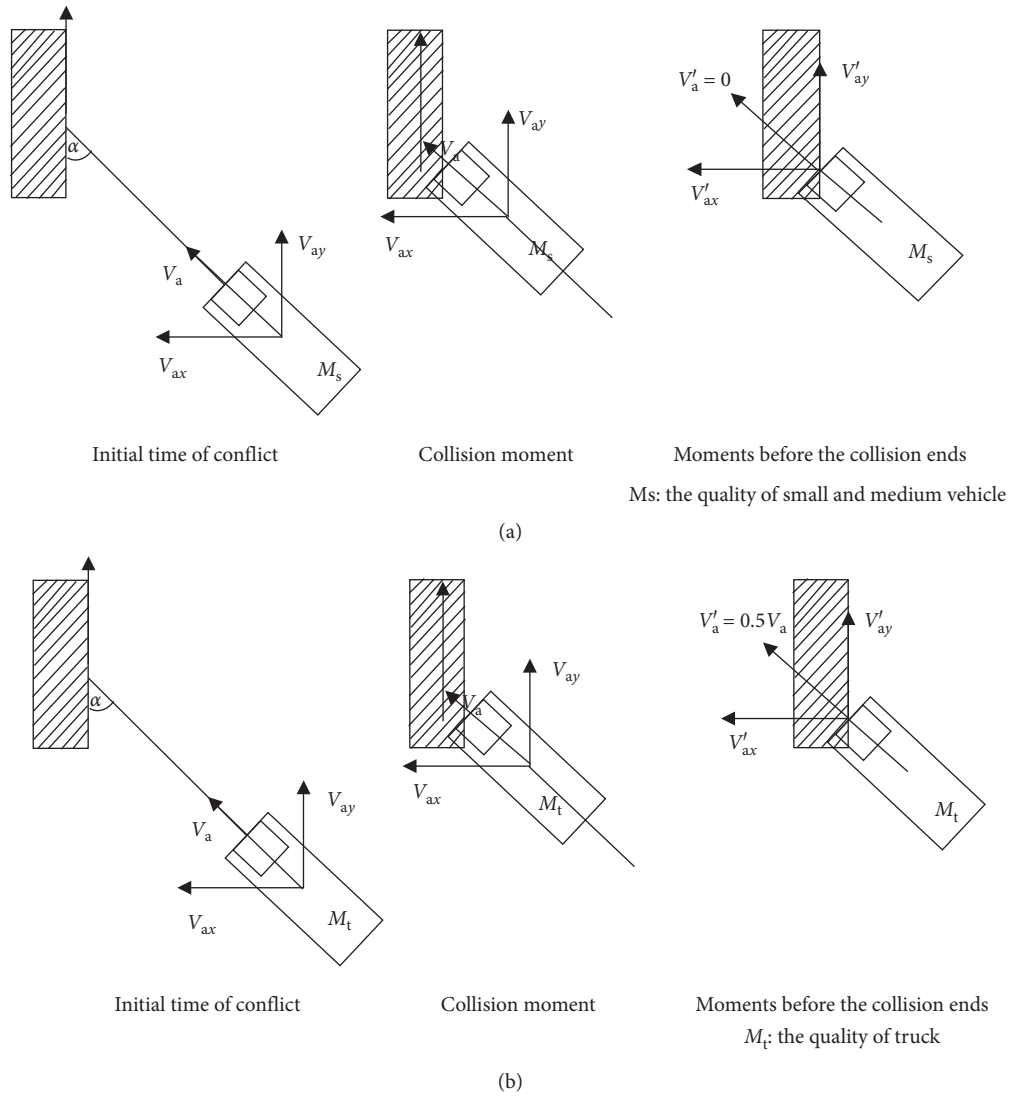


FIGURE 2: Schematic diagram of collision between vehicle and road facility (two categories).

energy is converted into deformation energy. The speed decreases to V'_a ($V'_a = 0.5V_a$). In the fourth phase, the trucks break free from the facilities to run continuously, but the deformation is over. The deformation starts during the period from the second phase to the third phase, which is the main goal of our research, as shown in Figure 2.

2.2.3. *Computational Process.* The research covers the period from the second to the third phase. During this period, the velocity change due to collision causes some kinetic energy to be converted into deformation energy. The conversion satisfies the law of conservation of energy. For convenience, velocity is converted into the X- and Y-axes. The details are shown as follows:

- (1) Collision between small and medium vehicles and facilities

$$\frac{1}{2}M_s V_{ax}^2 = E_X, \tag{13}$$

$$\frac{1}{2}M_s V_{ay}^2 = E_Y, \tag{14}$$

where V_{ax} and V_{ay} , respectively, represent the components of the velocities of small and medium vehicles in the X- and Y-axes before collision, M_s represents the mass of small and medium vehicles, and E_X and E_Y , respectively, denote the destructive energy (deformation energy) hidden in a traffic conflict (X-axis and Y-axis).

According to the trigonometric relation,

$$V_{ax} = V_a \sin \alpha \quad V_{ay} = V_a \cos \alpha. \tag{15}$$

Finally,

$$E = E_X + E_Y = \frac{1}{2}M_s V_a^2. \tag{16}$$

(2) Collision between trucks and facilities

$$\frac{1}{2}M_t V_{aX}^2 = E_X + \frac{1}{2}M_t V_{aX}'^2, \quad (17)$$

$$\frac{1}{2}M_t V_{aY}^2 = E_Y + \frac{1}{2}M_t V_{aY}'^2, \quad (18)$$

where V_{aX} and V_{aY} , respectively, represent the components of the velocities of trucks in the X - and Y -axes before collision, M_t refers to the mass of trucks, and E_X and E_Y , respectively, represent the destructive energy hidden in traffic collision in the X - and Y -axes.

According to the trigonometric relation,

$$V_{aX} = V_a \sin \alpha, \quad V_{aY} = V_a \cos \alpha. \quad (19)$$

Finally,

$$E = E_X + E_Y = \frac{3}{8}M_t V_a^2. \quad (20)$$

3. Data Collection Method and Processing

Comprising regional high-precision videos and historical traffic accident data, the data used in this work were mainly acquired using two methods. (1) Field conflict data were obtained by collecting high-precision videos of continuous vehicles using a UAV (unmanned aerial vehicle) hovering at a high altitude. Follow-ups were dealt with through the video recognition and the traffic conflict identification program. (2) The historical traffic accident data were mainly collected by traffic police and local highway administration bureau. (3) Some other data are processing and assumptions.

3.1. Conflict Data Collection

3.1.1. Location and Time. The video data collection location was the Jinan-Qingdao Highway in Shandong Province, China. The collection period was from August 20, 2017, to September 8, 2017. The collection times were from 9:00 to 10:00 in the morning peak and from 16:00 to 17:00 in the evening peak. At that time, the reconstruction and extension project, that is, the subgrade construction, was in progress. The subgrade was filled and widened on both sides of the road. The original road was kept passing through, but the original guardrails on both sides were dismantled and replaced by temporary guardrails. The road was two-way with four lanes. The width of a lane was 3.75 m, and the speed was limited to 80 km/h. The specific collection location included K43 + 200, K51 + 500, K57 + 580, K58 + 600, K112 + 500, K130 + 500, K131 + 500, K133 + 200, K182 + 000, K186 + 000, K192 + 500, K205 + 000, K255 + 000, K257 + 700, K258 + 260, K266 + 800, K271 + 620, K277 + 500, K278 + 300, and K287 + 000. Data were acquired in each location for 30 min each in the morning and evening peaks.

3.1.2. Device. The PHANTOM 4 PRO UAV from DJI Technology Company was used. The maximum flight altitude of the UAV was 500 m, and the maximum flight time

was 30 min. We prepared 9 batteries; each battery took 8 hours to be fully charged. The maximum video resolution was 4K/60P. The UAV shot the video by hovering statically. The camera was positioned vertically downward, and the flying height was 350–450 m. The lens angle parameters of the UAV were used as bases for calculation. The shooting range was about 600–700 m in length and 300–350 m in width, as shown in Figure 3.

3.1.3. Data Processing. It consists of a video recognition and a traffic conflict identification program (see Figure 4).

(1) Vehicles were identified and tracked via spatiotemporal context visual tracking algorithms based on an own-written program. The real-time continuous trajectory coordinates (X/Y), vehicle width, vehicle ID of all vehicles in the region, and other data served as the outputs. The identifying and tracking rate of video recognition program was about 90%. Most of the trajectory data errors can be controlled within 1 m, mainly including three major steps.

(a) Image Reading and Calibration

Considering the high airflow changes, the video captured by the UAV has a slight jitter, so the latter picture will gradually deviate from the original picture, and the subsequent picture needs to be matched and calibrated with the first frame based on the first frame.

There are many matching methods, and it is considered to select a partial region to calculate the correlation coefficient and then calculate the overall transformation matrix. Finally, in order to ensure the accuracy of the recognition, feature point matching is selected to calculate the transformation matrix.

Selecting the obvious reference object of the first frame such as road and road marking, establishing the coordinate system according to the horizontal direction and the vertical direction, and performing the rotation according to the affine transformation relationship between the pictures, the subsequent pictures can be successfully matched with the frame by frame.

(b) Vehicle Identification

Vehicle identification system usually includes ROI (Region of Interest) extraction and vehicle detection. First, the sequence image is subjected to ROI extraction, and then the image processing method is used to determine whether the area is a vehicle. If it is determined to be a vehicle, the vehicle can be tracked in a subsequent tracking module. Vehicle detection is a prerequisite for tracking, and accurate ROI extraction and vehicle detection can establish a solid foundation for tracking.

The adjacent frame subtraction algorithm is used to identify the ROI area by considering that the Jiqing Highway has the characteristics of faster vehicle speed, more frequent convergence, and less visibility caused by dust. For the detection line method is simple and efficient, so it is used for vehicle detection.



FIGURE 3: UAV collecting high-precision video.

(c) Vehicle Tracking

Tracking is easier when the vehicle is successfully detected. Most vehicle tracking methods follow a basic principle of using space distance to determine whether a vehicle in an adjacent frame is the same vehicle, thereby completing vehicle tracking in the time domain. Based on the characteristics of Jiqing Highway such as faster speeds, high dust, and low visibility, a tracking method called the spatiotemporal context was chosen. This method obtains the best target position by maximizing the target position likelihood function and learning using the fast Fourier transform. Compared with other mainstream methods, this method is more accurate and reliable, and it is more effective in implementation.

(2) About the identifying and tracking rate of video recognition program

We used to randomly select videos from the locations K57 + 580, K58 + 600, K182 + 000, K255 + 000, and K271 + 620 for a total of about 90 minutes for verification. Through statistical analysis, it was found that the video recognition program identified a total of 3,033 vehicles and continued to track 2,923 vehicles, while a total of 3,308 vehicles were recognized by manual observation. The initial identifying rate was about 92%, and the continuous tracking rate was about 88%.

The specific data are given in Table 1.

(3) About trajectory data recognition accuracy and reliability

As the dividing line (white dotted line) of all highways in China is 6 m long, the distance between the dotted lines is 9 m (see Figure 5). Therefore, the accuracy and reliability of the video recognition program can be judged by this standard.

Six hundred vehicles were randomly selected in part of the videos collected at the locations of K57 + 580, K58 + 600, K182 + 000, K255 + 000, and K271 + 620, and 2 s interval coordinate data of each vehicle in X-axis and Y-axis were randomly recorded. At the same time, the position of each vehicle in the video is manually marked by software called PicPick, which operates by clicking the image/video with a mouse to display and measure coordinates. After comparison, 8% of the trajectory errors are below 0.3 m, 21% of the trajectory errors are below 0.5 m, 44% of the trajectory errors are 0.7 m, and 82% of the trajectory errors are below 1 m. Therefore, most of the trajectory data errors can be controlled within 1 m.

- (4) Instantaneous speed, acceleration, vehicle spacing, vehicle driving angle, and other data in traffic conflict for every seven frames were then obtained according to the further processing of the continuous trajectory coordinate data and TTC-based recognition program. TTC is defined as “the time required for two vehicles to collide if they continue at their present speeds on the same path.” The calculation process is basically similar to the previous literature.

The differences lie in the following:

- (1) Vehicles are simplified to a point with mass (centroid point) without considering its shape
- (2) Considering the conflicts between the vehicle and the road facility, the definition and calculation are given in Figure 6

3.2. Historical Traffic Accident Data. The accident data included the time of accident occurrence (accurate to year, month, date, and hour), location of accident occurrence (station number and orientation), type of vehicle involved in accident (small, medium, or truck), type of accident (rear-end collision, overturning, or collision with central separators/guardrails), weather, level of severity, number of casualties (death or injured), and road financial loss, as shown in Figure 7.

Due to the limitation of UAV power, funding, weather, and accident being accidental, the location and time of conflict data collection cannot completely coincide with the actual historical data location and time. So, on the premise of satisfying the data analysis sample size, we need to reasonably expand the time period and location of historical accident data.

After on-site investigations and serious analysis, the period of accident data collection was from June 2017 to November 2017. This time period had little change compared to the time period of video data collection; possible influence conditions such as traffic volume, traffic composition (proportion of various vehicle type), lateral clearance, and traffic organization changed slightly.

Similarly, to eliminate the influence of conditions, we divided the highway into five sections (JQ-1–JQ-5) according to the actual situation such as traffic organization, traffic volume, traffic composition, and lateral clearance. So the situations in every different section were consistent in general. Each section comprised four video data collection locations (see Table 2).

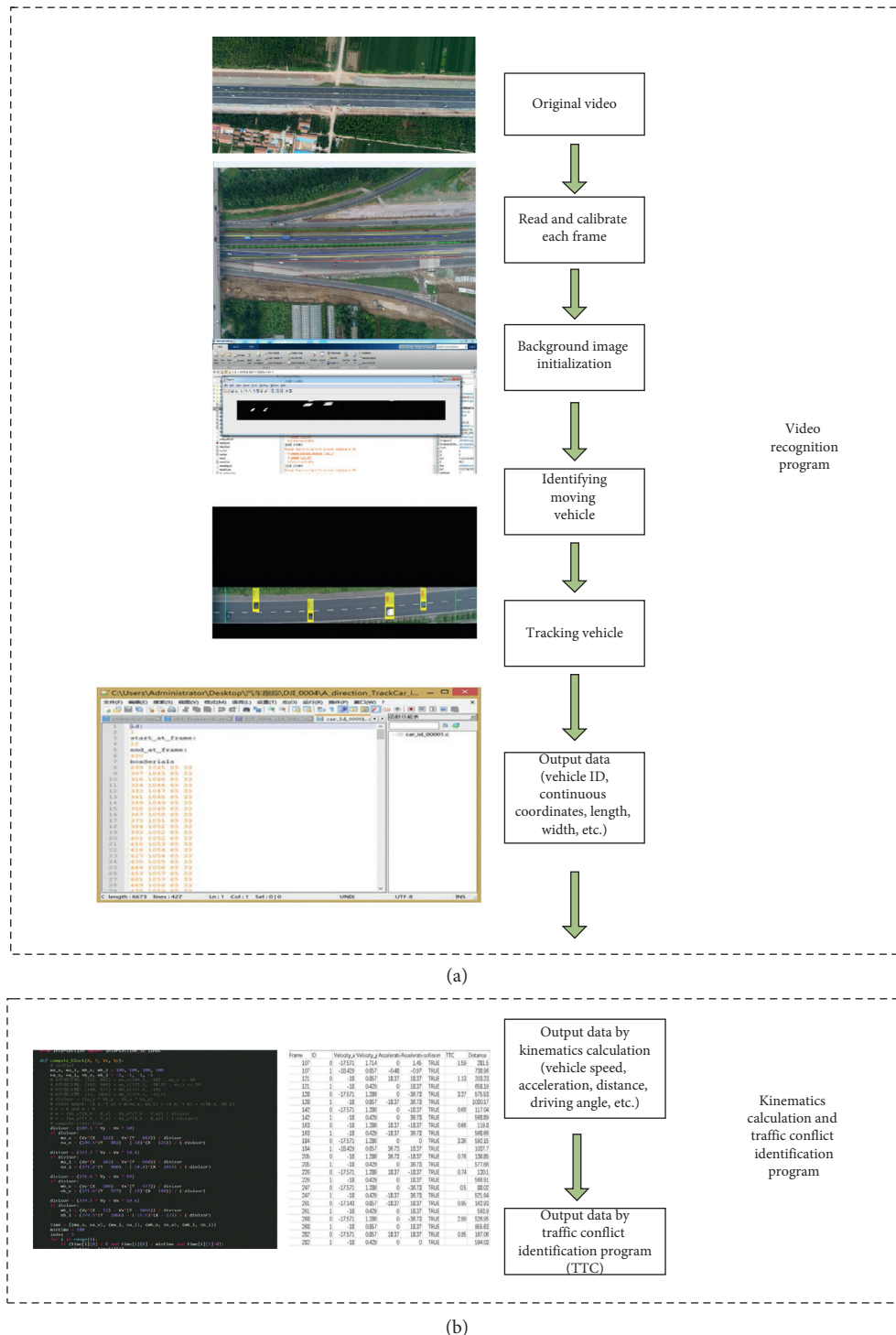


FIGURE 4: Flow-process diagram of video recognition and traffic conflict identification.

3.3. Other Data Processing and Assumptions

3.3.1. *Simplified Processing of TTC Threshold Values.* The conflict in the model in Chapter 2 must be a serious conflict. But no uniform basis for judging serious conflicts exists. As the roads, environments, and methods adopted in studies are different, the threshold values of severe

traffic conflicts adopted by different studies are also different, ranging from 1.0 s to 5.0 s of TTC [13, 20–26]. Therefore, the TTC threshold value of a serious conflict in this study ranged from 1.0 s to 5.0 s, and the step length was 0.5 s. For simplification, the TTC threshold values of vehicle-vehicle and vehicle-road facility conflicts were assumed to be the same.

TABLE 1: Identifying and tracking rate of video recognition program.

Collection locations	Video frames	Video duration (s)	Initial identifying vehicles	Continuous tracking vehicles	Manual observation vehicles	Initial identifying rate (%)	Continuous tracking rate (%)
K57 + 580	35850	1195	452	437	485	93	90
K58 + 600	15600	520	234	225	251	93	90
K182 + 000	33000	1100	738	701	795	93	88
K255 + 000	28880	963	572	558	628	91	89
K271 + 620	53100	1770	1037	1002	1149	90	87
Total	166430	5548	3033	2923	3308	92	88



FIGURE 5: Distance of dividing line of highway in China.

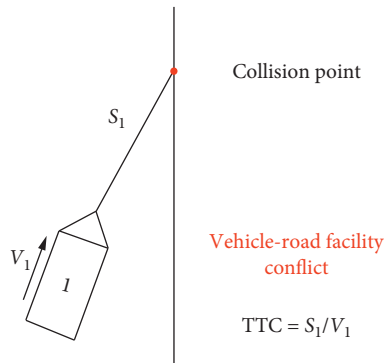


FIGURE 6: Definition and calculation of conflicts between the vehicle and the road facility.

Number	Time of accident occurrence	Location of accident occurrence (stake number/orientation)	Vehicle type of accident	Type of accident	Weather	Level of severity	Number of deaths	Number of injured	Road financial loss (CNY)
1	6/3/2016	Direction from Jinan to Qingdao 105K + 600M	Truck and truck	Raer-end	Foggy	Ordinary	0	0	4020
2	6/3/2016	Direction from Jinan to Qingdao 105K + 700M	Truck and truck	Raer-end	Foggy	Slight	0	0	500
3	6/3/2016	Direction from Jinan to Qingdao 59K + 300M	Truck	Roll-over	Sunny	Ordinary	0	0	3060
4	6/5/2016	Direction from Jinan to Qingdao 92K + 100M	Small car	Roll-over	Sunny	Ordinary	0	0	2250
5	6/6/2016	Direction from Jinan to Qingdao 91K + 500M	Small car	Roll-over	Sunny	Ordinary	0	0	3650
6	6/9/2016	Direction from Jinan to Qingdao 54K + 500M	Truck	Fire	Sunny	Ordinary	0	0	2300
7	6/10/2016	Direction from Jinan to Qingdao 36K + 500M	Small car	Hit the central reservations	Sunny	Slight	0	0	500
8	6/11/2016	Direction from Jinan to Qingdao 102K + 100M	Small car and small car	Raer-end	Sunny	Ordinary	0	0	4800

FIGURE 7: Chart of historical traffic accident data (partial translation display).

TABLE 2: Traffic data of each section.

Section	JQ-1	JQ-2	JQ-3	JQ-4	JQ-5
Station number at the beginning	K36 + 388	K100 + 400	K150 + 480	K214 + 910	K268 + 967
Station number at the end	K100 + 400	K150 + 480	K214 + 910	K268 + 967	K294 + 385
Length (km)	64	50	64	54	25
Percentage of small vehicles	68.9	66.4	63.8	62.5	61.4
Percentage of medium vehicles	9.5	9.7	7.6	8.2	8.5
Percentage of trucks	21.6	23.9	28.6	29.3	30.1
Station numbers of video data collection locations	K43 + 200, K51 + 500, K57 + 580, K58 + 600	K112 + 500, K130 + 500, K131 + 500, K133 + 200	K182 + 000, K186 + 000, K192 + 500, K205 + 000	K255 + 000, K257 + 700, K258 + 260, K266 + 800	K271 + 620, K277 + 500, K278 + 300, K287 + 000

3.3.2. *Assumptions of Vehicle Weight.* Vehicle weight was involved in the measurement model of conflict consequence severity in this study. Obtaining real-time and accurate vehicle weight data by using existing technologies is difficult. Thus, vehicle types in this study were classified as small and medium vehicles and trucks by measuring vehicle length. Vehicle weight was determined according to vehicle type (Table 3).

3.3.3. *Selection and Design of Influencing Factors.* The average traffic volume and truck rate of one-way lane were used as influencing factors in this study.

The experimental scheme was based on the data obtained from every 15 min of video. The actual values of each influence factor were rounded according to step length. For example, if the average traffic volume of the one-way lane was 1135 pcu/h, it was recorded as 1100 pcu/h; if the average traffic volume of the one-way lane was 1278 pcu/h, it was recorded as 1300 pcu/h. According to the actual data, the specific scope was designed as follows (Table 4).

4. Results and Discussion

There are four parts in this chapter: (1) Evaluation indicators of traffic history accident are calculated by historical traffic accident data: accident rate and accident severity rate. (2) Evaluation indicators of traffic conflict are conflict rate and conflict severity rate, where the conflict severity rate is calculated by continuous high-precision vehicle conflict data and is based on the potential collision consequences severity model in Chapter 2. (3) We had analyzed the relationship of conflict rates and conflict severity rates with influencing factors, that is, traffic volume and truck rate. (4) The correlation between conflicts and accidents is also calculated and verifies whether the evaluation indicators that take the consequences of conflict into account are superior to the traditional conflict rate indicators that only consider the number of conflicts; details are given in Figure 8.

4.1. Historical Accident Rate and Accident Severity Rate

- (1) Historical accident rate is calculated according to the following formula:

TABLE 3: Vehicle types.

Vehicle types	Small vehicle	Medium vehicle	Truck
Length (m)	4–6	7–9	10–20
Set weight (t)	1.5	5	30

TABLE 4: Design of influencing factor ranges.

Influence factors	Min.	Max.	Step length
Traffic volume (pcu/h)	300	1500	200
Truck rate (%)*	10	70	10

*Truck rate refers to the proportion of trucks in PCU.

$$A_n = \frac{N}{Q \times L} \quad (21)$$

In Formula (21), A_n refers to the accident rate in each section (JQ1–JQ5) within six months; N refers to the number of traffic accidents (including conflict accidents of two vehicles and one vehicle with facilities); L refers to the length of each section in km; and Q refers to the monthly average daily traffic volume of each section in pcu/d.

- (2) Historical accident severity rate is calculated according to the following formula:

$$A_s = \frac{M}{Q \times L} \quad (22)$$

In Formula (22), A_s refers to the accident severity rate in each section (JQ1–JQ5) within six months, M refers to the sum of direct economic losses in ten thousand yuan (RMB), L refers to the length of each section in km, and Q refers to the monthly average daily traffic volume of each section in pcu/d.

Accident data include the number of casualties and the economic losses in road administration and vehicles. Through normalization, the number of casualties is converted into direct

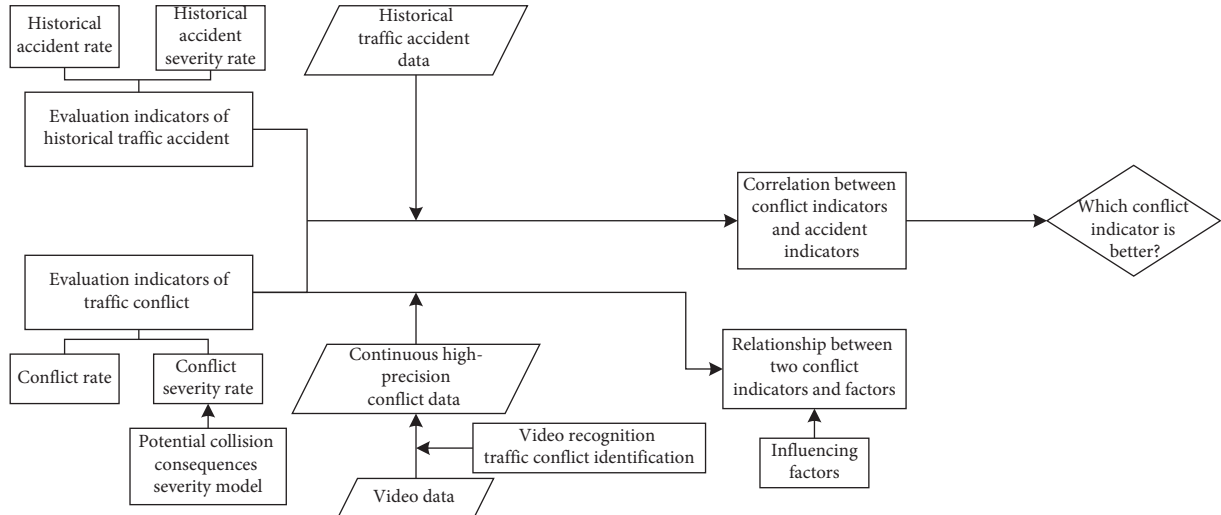


FIGURE 8: Analysis flow diagram.

economic loss. The literature shows that the average age of mortality in road traffic accidents in China is 40 years. On the basis of the retirement age of 60 years, the standard loss incurred in one working day resulting from one death is calculated as 5000. At present, China's per capita working day income is 200 yuan. Therefore, the direct economic loss per death is 1 million yuan. The direct economic loss per injured person is calculated at 30% of that per death, that is, 0.30 million yuan [27].

Therefore,

$$M = M_1 + M_2 + M_3. \quad (23)$$

In Formula (23), M_1 refers to the loss of road administration and vehicles, M_2 refers to the direct economic loss resulting from death, and M_3 refers to the direct economic loss resulting from injuries.

On the basis of formulas (21)–(23), the accident rates and accident severity rates of all sections in June–November 2017 can be calculated (Table 5).

4.2. Traffic Conflict Rate and Conflict Severity Rate

4.2.1. Traffic Conflict Rate. Conflict rate evaluation indicator that considers only the number of conflicts can be calculated according to the following formula:

$$R = \frac{N}{Q \times L}. \quad (24)$$

In Formula (24), R refers to the traffic conflict rate (n/pcu-km), N refers to the number of serious conflicts occurring in a time unit, L refers to the length of the data collection section (km), and Q refers to the traffic volume per hour in the data collection section (pcu/h).

4.2.2. Traffic Conflict Severity Rate. For comparison, traffic conflict severity rate is evaluated with the following formula:

$$s = \frac{\sum_{i=1}^{i=N} E_i}{Q \times L}. \quad (25)$$

TABLE 5: Accident rates and accident severity rates of all sections.

Sections	JQ-1	JQ-2	JQ-3	JQ-4	JQ-5
Accident rate $A_n(10^{-5})$	1.24	1.89	3.87	3.21	3.34
Accident severity rate $A_s(10^{-5})$	1.28	1.25	1.93	1.89	1.76

In Formula (25), s refers to the traffic conflict severity rate (J/pcu-km); N refers to the number of serious conflicts occurring in a time unit; E_i refers to the destructive energy hidden in each time of serious traffic conflict (J), that is, Formulas (12), (16), and (20); L refers to the length of the data collection section (km), and Q refers to the traffic volume per hour in the data collection section (pcu/h).

4.3. Relationship between Conflict Rate/Conflict Severity Rate and Influence Factors

4.3.1. Conflict Rates and Conflict Severity Rates of All Sections under Different TTC Threshold Values. On the basis of the discussion in Chapter 4.2, the average values of the conflict rate and conflict severity rate of each section under different TTC values are obtained. Figure 9 reveals that, with an increase in TTC threshold values, conflict rate and conflict severity rate increase; this effect is in line with the objective situation. If the threshold value is high, serious conflicts that meet the requirements will increase.

4.3.2. Relationship between Conflict Rate/Conflict Severity Rate and Traffic Volume. The relationships of conflict rate and conflict severity rate with traffic volume are established. Specifically, the conflict rate and conflict severity rate are the average values in all sections under different TTC threshold values. ANOVA shows that traffic volume has a significant impact on traffic conflict rate and traffic conflict severity rate ($p = 0 < 0.01$) (F test, where p refers to the probability that the traffic conflict rate is the same as the severity rate under different traffic volumes).

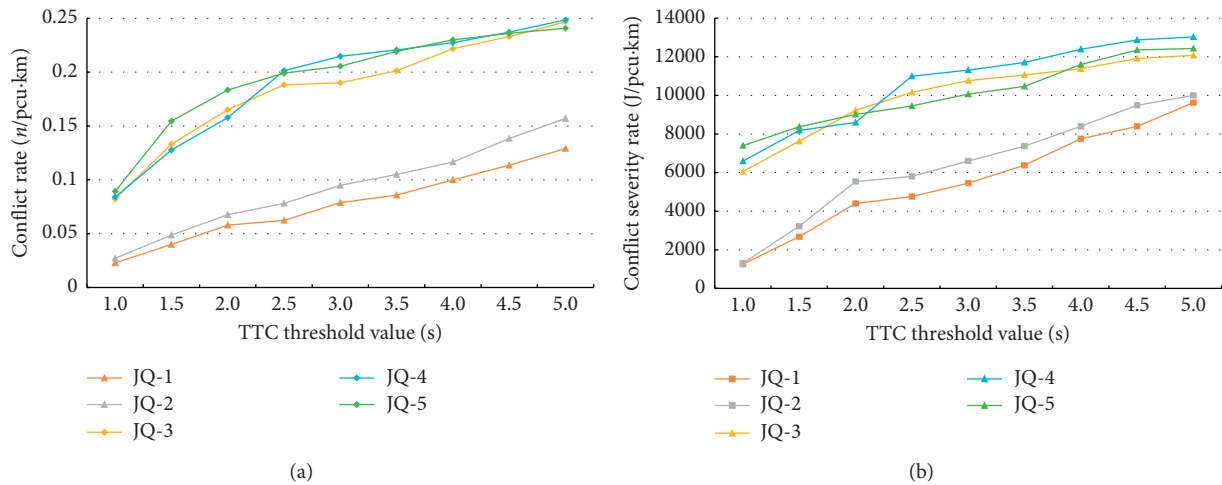


FIGURE 9: Conflict rates and severity rates of all sections under different TTC threshold values.

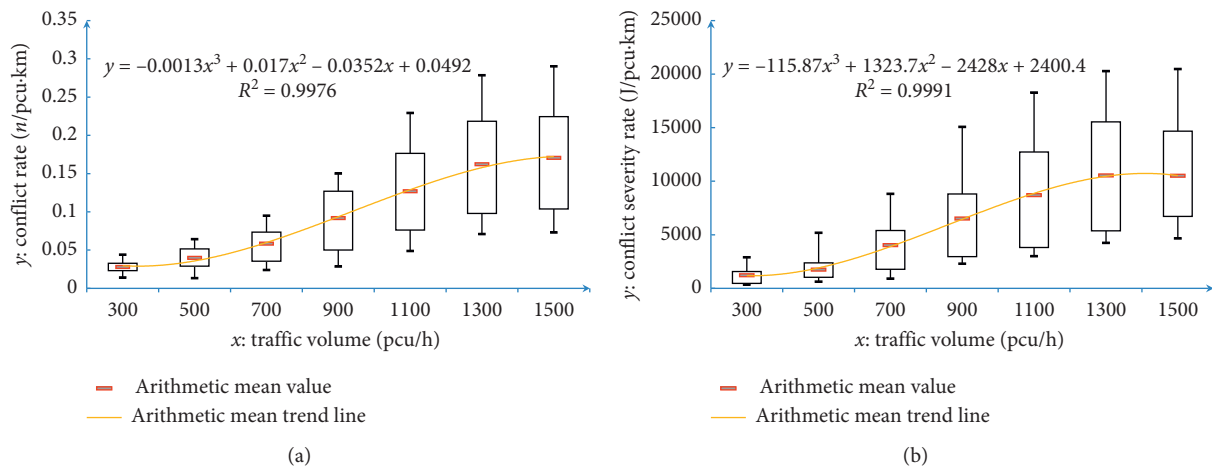


FIGURE 10: Distribution of traffic conflict rates and severity rates under different traffic volumes.

Figure 10 shows the distributions of conflict rates and severity rates under different traffic volumes. Traffic volume is positively correlated with the conflict and severity rate. When traffic volume in a one-way lane is less than 700 pcu/h, the average conflict and severity rates are low. With the increase in traffic volume, the average conflict rate and severity rate increase gradually. Moreover, when traffic volume exceeds 900 pcu/h, the average conflict and severity rates increase rapidly. This relationship is similar to that found in a study on the construction area of the Tomei Expressway in Japan that revealed that 70% of traffic accidents occur in a traffic jam and that the casualty rate caused by accidents in a crowded construction area is over 90%, which is eight to nine times that in noncrowded construction areas [28]. Therefore, a large traffic volume equates to an unsafe construction area. As traffic volume exceeds 1300 pcu/h, differences are observed between conflict rates and severity rates; the conflict rate continues to rise slightly, whereas the conflict severity rate declines slightly. This finding may be due to the saturation of traffic flow and the

decrease of the speed and the severity of a single conflict caused by excessive traffic volume. Therefore, the severity rate drops.

4.3.3. Relationship between Conflict Rate/Conflict Severity Rate and Truck Rate. The relationships of conflict rate and conflict severity rate with truck rate are established. Specifically, the conflict rate and conflict severity rate are the average values in all sections under different TTC threshold values. ANOVA shows that truck rate has a significant impact on traffic conflict rate and traffic conflict severity rate ($p = 0 < 0.01$) (F test, where p refers to the probability that the traffic conflict rate is the same as the severity rate under different truck rates).

The relationship between conflict rate and severity rate with truck rate is established, as shown in Figure 11. Under a low truck rate, the conflict rate is low. With a gradual increase in truck rate, the conflict rate gradually increases as well. Then, it reaches the maximum as the truck rate reaches

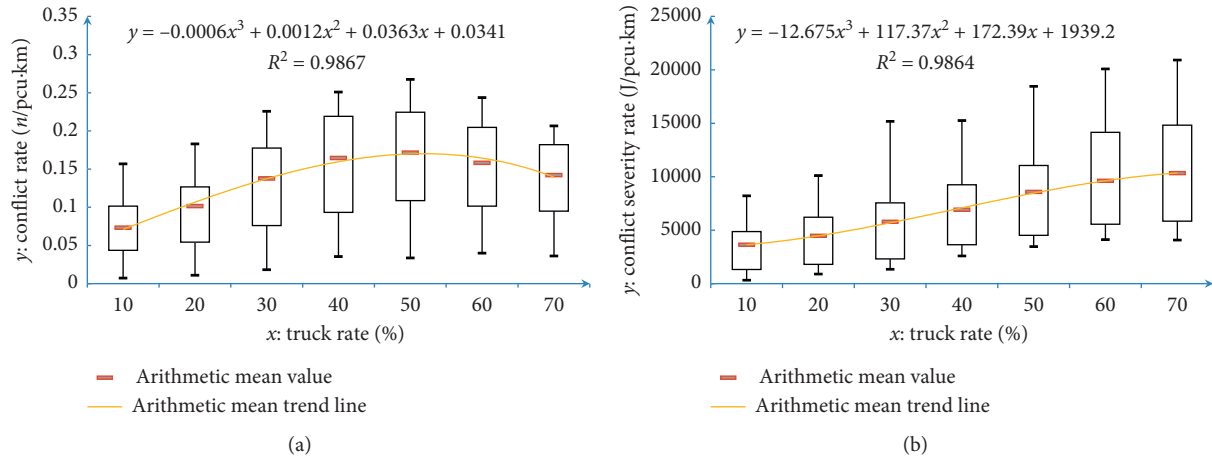


FIGURE 11: Distribution of traffic conflict rates and severity rates under different truck rates.

50%. Afterwards, the conflict rate gradually decreases. This result is similar to the law found by Liang et al. [29]; with an increase in truck rate, the number of conflicts increases first and then decreases, showing a single peak. The reason for this phenomenon is that the inadequate performance of trucks leads to a slower speed than those of other vehicle types, particularly small vehicles. As a result, the emergence of trucks in traffic flow inevitably leads to an increase in the overall speed difference in traffic flow, further causing an increase in conflict. However, when the number of trucks increases, the number of vehicles decreases under the same traffic volume. At the same time, the speed difference decreases gradually with an increase in the number of the same type of vehicles (large truck); thus, the conflict rate decreases gradually after reaching the peak value.

The comparison of conflict rate and severity rate with truck rate in Figure 6 shows that when the truck rate exceeds 50%, the conflict rate decreases, and the conflict severity rate increases, indicating that the severity of consequences caused by truck conflict is great. This finding is consistent with the phenomenon in which trucks easily cause serious accidents in construction areas, as discovered by Pigman and Agent [30].

4.4. Correlation between Conflict Rate/Severity Rate and Accident Rate/Severity Rate. Chapter 4.4 focuses on the correlation between traditional conflict rate and conflict severity rate that consider the consequence severity and accident rate/accident severity rate, respectively. The average values of the conflict rates and conflict severity rates of all sections are obtained. On the basis of the accident rates and accident severity rates of all sections within six months (Table 4), the correlation coefficients are obtained via Pearson correlation analysis.

Figure 12 reveals that conflict severity has higher correlation with either accident rate or accident severity rate than conflict rate does in most cases; in particular, conflict severity rate is most correlated with accident severity rate (purple line); under different TTC threshold values, the correlation is about 0.8–0.85. The correlation between conflict severity rate and

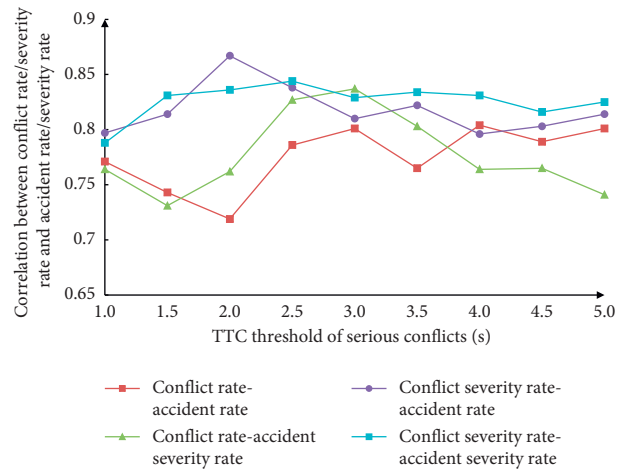


FIGURE 12: Correlation between conflict rate/severity rate and accident rate/severity rate under different TTC threshold values.

accident rate (blue line) is also high. By contrast, the traditional conflict rate has a low correlation (ranging from 0.7 to 0.8) with accident rate and accident severity rate (red and green line) in most cases of different TTC threshold.

As for the TTC threshold values, under low thresholds (1.0s, 1.5s) and high thresholds (more than 3.0s), the correlation values are low. In addition, correlation in the range of 2.0–3.0s is the highest. This result may be due to the low conflict threshold that leads to the strict criteria for detecting conflicts and to neglecting some risks that may lead to accidents. Moreover, a high threshold will allow several low-risk conflicts to be included in the calculation, although many low-risk conflicts do not lead to accidents; thus, the correlation is reduced.

5. Conclusions

This study aims to address the lack of research on the severity of the consequences of potential collisions in traffic conflict and proposes a new method for assessing traffic safety. High-

precision continuous vehicle microdata obtained by UAV tell us real-time conflict risk including traditional possibility/proximity severity of traffic conflict to a collision, and the consequence/outcome severity of potential collisions caused by conflicts as well, which is exactly what we need to improve.

In this paper, a severity model of potential collision consequences in traffic conflicts is proposed on the basis of vehicle collision theory. Serious conflicts among road vehicles develop into collision accidents when no evasion action is taken. After collision, some kinetic energy is converted into destructive energy, leading to vehicle deformation. We use this energy to reflect the potential consequence severity of traffic conflicts. The proposed model includes two categories: potential collision of vehicle-vehicle conflict and collision of vehicles and road facilities (e.g., guardrails).

The accurate videos of vehicles are collected by a UAV. Vehicle speed, acceleration, vehicle spacing, and other microscopic data of each traffic conflict at any time are obtained through further processing with a video recognition and traffic conflict recognition program (output once every seven frames). Traffic accident data were also collected.

On the basis of the conflict consequence severity model proposed in this study, the microscopic data of vehicles in traffic conflicts were substituted to calculate the conflict severity rates in all sections under different TTC threshold values. At the same time, the conflict rates in each section under different TTC threshold values that consider only the number of conflicts were also calculated. The conflict rates and conflict severity rates were linked to traffic volume and truck rate, respectively. The relationship models are found to be different.

Further correlation analysis of accident rate and accident severity rates showed that the conflict severity rate that considers conflict consequence severity has a higher correlation with accident rate and accident severity rate. At the same time, the threshold value of TTC was an important factor that influences correlation. When thresholds were low (1.0 s, 1.5 s) or high (more than 3.0 s), the correlation was low.

In summary, many current studies on the severity of traffic conflicts focused on the possibility of potential collisions, and less studies explored the severity of the consequences of potential collisions. According to vehicle collision theory, the formula for calculating the consequences severity of potential collision is obtained. The correlation verification of data shows that real risk is a little better reflected by conflict severity rate than by traditional conflict rate. The safety evaluation of traffic conflict should be a combination of both possibility and consequence of potential collisions.

The limitations of this study are some adoption of simplification and idealization processes. Real and complex processes should be considered in follow-up studies. Moreover, due to the time, fund, equipment constraints, and other reasons, the conflict data only cover some time periods in 18 days.

In the future, we will make improvements and follow-up studies from the following aspects: (1) Selection of indicators. Due to words limitation, only the most common TTC

was selected as an indicator for identifying conflicts. Each conflict indicator such as TTC, PET, and MaxD has its own advantages and disadvantages. Under different types of conflict/collision (such as crossing, rear end, and lane change), the differences between indicators are more obvious [31, 32]. We should select better indicators to identify conflicts for different types of conflicts later. (2) Expand the amount of data to collect more conflict and accident data, in addition to the in-depth analysis of the correspondence between the types of accidents and the types of conflicts. (3) This paper directly analyzes the correlation between serious conflicts and accidents under considering possibility/consequence severity and finds that the correlation was okay (probably due to the fact that collection locations were not many). Extreme value theory (EVT) sees a good accident prediction model with high prediction accuracy and correlation with field accidents. We may use mathematical methods such as EVT to predict accidents (number and severity) with more data later [31–33].

Data Availability

The data used to support the findings of this study are available from the corresponding author upon request.

Disclosure

The data were collected in Jinan-Qingdao Highway in Shandong Province, China.

Conflicts of Interest

The authors declare that they have no conflicts of interest.

Authors' Contributions

Study conception, design, and major writing were performed by Jiang Ruoxi and Zhu Shunying. Data collection was carried out by Wang Pan, Zou He, and Kuang Shiping. Analysis and interpretation of results were performed by Jiang Ruoxi and Wang Pan. Draft manuscript preparation was done by Jiang Ruoxi. All authors reviewed the results and approved the final version of the manuscript.

Acknowledgments

This work received funding from the National Natural Science Foundation of China (no. 71771183).

References

- [1] Å. Svensson and C. Hydén, "Estimating the severity of safety related behaviour," *Accident Analysis & Prevention*, vol. 38, no. 2, pp. 379–385, 2006.
- [2] A. Tarko, G. Davis, N. Saunier, T. Sayed, and S. Washington, "White paper surrogate measures of safety," 2009.
- [3] A. Laureshyn, Å. Svensson, and C. Hydén, "Evaluation of traffic safety, based on micro-level behavioural data: theoretical framework and first implementation," *Accident Analysis and Prevention*, vol. 42, no. 6, pp. 1637–1646, 2010.

- [4] E. Hauer and A. S. Hakkert, "The extent and implications of incomplete accident reporting," *Transportation Research Record*, no. 1186, pp. 1–10, 1989.
- [5] N. Saunier and T. Sayed, "Automated road safety analysis using video data," *Transportation Research Record: Journal of the Transportation Research Board*, vol. 2019, no. 1, pp. 57–64, 2007.
- [6] S. R. Perkins and J. I. Harris, "Traffic conflict characteristics: accident potential at intersections," *Psychological Reports*, no. 225, pp. 35–43, 1968.
- [7] W. D. Glauz and D. J. Migletz, "Application of traffic conflict analysis at intersections," Transportation Research Board, National Research Council, Washington, DC, USA, 1980.
- [8] F. Hydén and C. Amundsen, "Proceedings of first workshop on traffic conflicts," 1977.
- [9] G. Douglas, T. Sayed, and L. Pu, "Surrogate safety assessment model and validation," Federal Highway Administration, Washington, DC, USA, 2008.
- [10] J. C. Hayward, *Near-miss Determination through Use of a Scale of Danger*, Pennsylvania Transportation and Traffic Safety Center, York, PA, USA, 1972.
- [11] N. Muhrad, "Traffic conflict techniques and other forms of behavioural analysis: application to safety diagnoses," in *Proceedings of the 6th ICTCT Workshop*, Salzburg, Austria, 1993.
- [12] A. Lareshyna, T. D. Ceunynck, C. Karlsson, Å. Svensson, and S. Daniels, "In search of the severity dimension of traffic events: extended Delta-V as a traffic conflict indicators," *Accident Analysis and Prevention*, vol. 98, pp. 46–56, 2017.
- [13] J. Autey, T. Sayed, and M. H. Zaki, "Safety evaluation of right-turn smart channels using automated traffic conflict analysis," *Accident Analysis and Prevention*, vol. 45, no. 1, pp. 120–130, 2012.
- [14] L. Evans, *Traffic Safety and the Driver*, Van Nostrand Reinhold, New York, NY, USA, 1991.
- [15] D. Gabauer, "Correlating delta-V to occupant injury using event data recorders," 2006.
- [16] L. Zheng, K. Ismail, and X. Meng, "Traffic conflict techniques for road safety analysis: open questions and some insights," *Canadian Journal of Civil Engineering*, vol. 41, no. 7, pp. 633–641, 2014.
- [17] O. Bagdadi, "Estimation of the severity of safety critical events," *Accident Analysis and Prevention*, vol. 50, no. 2, pp. 167–174, 2013.
- [18] C. Hyden, *The Development of a Method for Traffic Safety Evaluation: The Swedish Traffic Conflicts Technique*, Bulletin Lund Institute of Technology, Lund, Sweden, 1987.
- [19] T. Zhang, *The Export and Entrance Ramp of Highway Analysis Based on the Conflict-Energy Law*, Dalian Jiaotong University, Dalian, China, 2011.
- [20] R. V. D. Horst, "The demonstration cycle routes at the hague and tilburg: a behavioural study," in *Proceedings of the 54th Annual Meeting of the Institute of Transportation Engineers*, San Francisco, CA, USA, September 1984.
- [21] G. R. Brow, "Traffic conflicts for road user safety studies," *Canadian Journal of Civil Engineering*, vol. 21, no. 1, pp. 1–15, 1994.
- [22] D. Lord, "Analysis of pedestrian conflicts with left-turning traffic," *Transportation Research Record: Journal of the Transportation Research Board*, vol. 1538, no. 1, pp. 61–67, 1996.
- [23] K. Ozbay, H. Yang, B. Bartin, and S. Mudigonda, "Derivation and validation of new simulation-based surrogate safety measure," *Transportation Research Record Journal of the Transportation Research Board*, vol. 2083, no. 1, pp. 105–113, 2008.
- [24] K. Ismail, T. Sayed, N. Saunier, and C. Lim, "Automated analysis of pedestrian-vehicle conflicts using video data," *Transportation Research Record: Journal of the Transportation Research Board*, vol. 2140, no. 1, pp. 44–54, 2009.
- [25] A. Shariat-Mohaymany, A. Tavakoli-Kashani, H. Nosrati, and A. Ranjbari, "Identifying significant predictors of head-on conflicts on two-lane rural roads using inductive loop detectors data," *Journal of Crash Prevention and Injury Control*, vol. 12, no. 6, pp. 636–641, 2011.
- [26] K. El-Basyouny and T. Sayed, "Safety performance functions using traffic conflicts," *Safety Science*, vol. 51, no. 1, pp. 160–164, 2013.
- [27] J. J. Cao, "Calculation model research on equivalent death toll in traffic accidents," *Journal Of Chongqing Jiaotong University (Natural Science)*, vol. 32, no. 1, pp. 91–94, 2013.
- [28] J. Xing, H. Takahashi, and K. Iida, *Analysis of Bottleneck Capacity and Traffic Safety in Japanese Highway Work Zones*, Transportation Research Board, Washington, DC, USA, 2010.
- [29] G. Liang, F. Wang, W. Wang, X. Sun, and W. Wang, "Assessment of freeway work zone safety with improved cellular automata model," *Journal of Traffic and Transportation Engineering (English Edition)*, vol. 1, no. 4, pp. 261–271, 2014.
- [30] J. G. Pigman and K. R. Agent, *Highway Accidents in Construction and Maintenance Work Zones*, Transportation Research Board, Washington, DC, USA, 1990.
- [31] C. Wang, C. Xu, and Y. Dai, "A crash prediction method based on bivariate extreme value theory and video-based vehicle trajectory data," *Accident Analysis and Prevention*, vol. 123, pp. 365–373, 2019.
- [32] L. Zheng, T. Sayed, and M. Essa, "Validating the bivariate extreme value modeling approach for road safety estimation with different traffic conflict indicators," *Accident Analysis and Prevention*, vol. 123, pp. 314–323, 2019.
- [33] C. Wang, C. Xu, J. Xia, Z. Qian, and L. Lu, "A combined use of microscopic traffic simulation and extreme value methods for traffic safety evaluation," *Transportation Research Part C: Emerging Technologies*, vol. 90, pp. 281–291, 2018.

Research Article

Determinants of Bicyclist Injury Severity Resulting from Crashes at Roundabouts, Crossroads, and T-Junctions

Jinxing Shen, Tiantong Wang, Changjiang Zheng , and Miao Yu

College of Civil Engineering and Transportation Engineering, Hohai University, Nanjing 210098, China

Correspondence should be addressed to Changjiang Zheng; zheng@hhu.edu.cn

Received 26 February 2020; Revised 11 May 2020; Accepted 22 May 2020; Published 10 June 2020

Academic Editor: Feng Chen

Copyright © 2020 Jinxing Shen et al. This is an open access article distributed under the Creative Commons Attribution License, which permits unrestricted use, distribution, and reproduction in any medium, provided the original work is properly cited.

This study explores the contributing factors that influence bicyclist injury severity at three types of intersection: roundabouts, crossroads, and T-junctions. Using bicycle-involved crash data in the UK over nine years (from 2009 to 2017), the bicyclist injury severity (with three severity levels: fatal injury, serious injury, and slight injury) was estimated using the generalized ordered logit (GOL) model and partial proportional odds (PPO) model. The marginal effects of each explanatory variable were computed to investigate the impacts on bicyclist injury severity occurring probabilities. A wide range of variables potentially affecting injury severity was considered, including bicyclist characteristics, intersection characteristics, environmental conditions, bicyclist movement and location preceding the crash, and types of collisions. Our findings show that the PPO model outperforms the GOL model for analyzing the factors that affect the bicyclist injury severity at intersections. The factors that affect cycling safety at various intersections show enormous differences. Specifically, nine variables have significant impacts on bicyclist injury severity at those three types of intersections. And there are only two variables, four variables, and eleven variables that have significant impact on bicyclist injury severity at roundabouts, crossroads, and T-junctions, respectively. The findings of this study can help decision makers better understand the spatial heterogeneity of the factors that influence the bicyclist injury severity at various intersections.

1. Introduction

Cycling is often considered as an economical, convenient, healthy, and sustainable transportation mode, especially suitable for short distance travel, which can offer a wide range of environmental and social benefits [1]. Recently, with the implementation of more than 20,000 bike-sharing schemes around the world, cycling has become a conventional travel mode in many cities [2]. With this in mind, the UK government has designed a series of policies over the past decade to promote the use of the bicycle in the daily journey, with the ambition to increase the bicycle trips from 0.8 billion in 2013 to 1.6 billion in 2025 [3]. Although the government has invested extensively to increase bikeability, bicycle travel mode only shares about 2% of all trips made in the UK, which is much lower than the Netherlands, Denmark, and Germany [4]. Among all the possible explanations, the most widely accepted view is that the safety risks perceived by cyclists are the most critical reasons hindering

the increase of cycling share rate [5–10]. Therefore, it is significant to analyze and determine the influencing factors that affect the safety of bicycle trips, and thereby the government can develop the countermeasures accordingly to lower the severity of cycling risk and increase the level of bicycle use.

A series of studies have been conducted to examine the critical factors related to bicycle safety, including the influence of bicyclist and driver demographics, bicycle and vehicle characteristics, road and environmental factors, and other variables. Behnood and Mannering [11] identified the contributing factors of race, gender, age, and whether the bicyclist wears a helmet that can significantly affect the severity of the bicycle crash. The cyclists who are younger, less educated, and ride longer per week were associated with a higher safety risk [12]. Besides, since bicyclists aged over 65 need more time to perceive and respond to external information, they are more prone to be involved in severe bicycle crashes [13]. By analyzing the police-reported data,

Kim et al. [14] implied that inclement weather, darkness without lighting, speeding, and involvement of trucks could significantly increase the probability of fatal bicyclist injury, and the fault of bicyclists is more likely to result in severe crashes than the drivers. Specifically, Eluru et al. [15] asserted that the age of bicyclists, the speed limit strategies of the road, and the locations and the period of crashes occurrence are the critical factors impacting the bicyclist injury severity. Cycling on the curved road segments, rural roads, and high-speed roads could raise the risk of severe injury [16]. Also, intoxicated bicyclists and automobile drivers, vans, SUVs, light-duty trucks, and roads with a grade or a curve are more likely to be involved in severe crashes [17]. Regarding the bicycle lanes, Morrison et al. [18] insisted that setting up exclusive bicycle lanes was a solution to improve the safety of bicyclists, which reduces the crash risk between bicycles and vehicles and raises the perception of cycling safety, thereby attracting more people to use bikes. However, the level of traffic pressure influenced the outcomes of bicycle lanes on cycling safety, and bicycle lanes on the roads with heavy traffic were more prone to involved in bicycle crashes [19]. Furthermore, the configuration of the adjacent intersections, bicycle traffic volume, and traffic control strategies at intersections could influence the effectiveness of bicycle lanes [20]. Besides, Klassen et al. [21] indicated that the essential factors influencing the severity of bicycle crash at intersections and road segments were not the same. Thus, unique treatments were needed to improve cycling safety at these two types of locations.

Several studies have verified that intersections are particularly dangerous areas due to the crossing traffic streams. Bicyclist crashes at intersections could increase the probability of severe injuries and fatalities [22–26]. Moore et al. [27] stated that there were essential differences in some factors that impact the bicyclist injury severity at intersections and non-intersections, and it was necessary to develop separate models to assess the effects of various factors on the bicyclist injury severity, respectively. Wang et al. [28] believed that the implementation of traffic calming methods, improving street lighting, and stop control strategy could enhance the cycling safety at nonsignalized intersections. Moreover, providing warning information to right-turning drivers when they approach the intersections can reduce conflicts between right-turning vehicles and bicycles on bicycle lanes, which can effectively enhance cycling safety at intersections [29]. Wang and Akar [30] concluded that the provision of bicycle boxes, bicycle crossing signs, and crossing markings at intersections could improve cycling safety, and the safety perceptions varied depending on the typologies of bicyclists. To sum up, although increasing researchers are starting to explore bicyclist safety at intersections, to the best of our knowledge, there is few detailed analysis for the difference of factors affecting bicyclist injury severity at various intersections.

Given the above, the objective of this research is to analyze and compare the influences of different intersection features on bicyclist injury severities in crashes. The cycling crash data used in this study are police-reported, occurred at various intersections in the UK, and the statistical period is

nine years from January 1, 2009, to December 31, 2017. Specifically, we primarily focus on studying the factors affecting bicyclist injury severity cycling crashes at roundabouts, crossroads, and T-junctions. The principal reason is that the probability of bicycle crashes occurring at these three intersections were higher than others in the UK, according to bicycle crash data. The remainder of the paper is organized as follows. Section 2 summarizes and describes the methodology applied to analyze bicyclist injury severity as well as the methods for comparing the models. Section 3 presents data on bicycle crashes that occurred at roundabouts, crossroads, and T-junctions. Section 4 discusses the outcomes of the model estimation and marginal effects, and finally, a conclusion is given in Section 5.

2. Methodologies

In police-reported bicycle crashes, the bicyclist severity is generally recorded using ordinal categories, and it is classified as fatal injury, serious injury, and slight injury. The ordered logit model is used to analyze bicycle crashes, which needs to obey the parallel lines or proportional odds (PO) assumption, and the estimated parameters are the same across the cumulative level [31, 32]. However, some variables affecting the bicycle crash levels at various intersections may be different. Following the recent studies such as Marcoux et al. [33], the generalized ordered logit model (GOL), which can relax the PO assumption for all variables, is selected in this study. Actually, in this study, we are not convinced whether we need to relax the PO constraint for all or some specific variables. Rationally, the partial proportional odds model (PPO) is also selected, for which only partial variables can violate the PO assumption. Moreover, using the same bicycle crash data, comparative analysis of the GOL and PPO model is conducted in this study. The brief information about the two models (GOL and PPO) is described as follows.

2.1. Generalized Ordered Logit (GOL) Model. In this paper, bicyclist injuries are studied by three discrete severity levels according to the police-reported bicycle crashes; accordingly, we coded 1 = slight injury, 2 = serious injury, and 3 = fatal injury. And the contribution of driver characteristics, driver behaviors, collision types, infrastructure characteristics, vehicle types, and environmental conditions is assessed by the crash injury severity model. Following the research by Williams [34], we define the bicyclist injury severity function y_i^* based on the latent regression:

$$y_i^* = X_i\beta_j + \varepsilon_i, \quad (1)$$

where j are the categories of bicyclist injury severities, X_i is a $1 \times p$ vector that contains the values of all the explanatory variables to the bicycle crash i , β_j is a vector of regression coefficients, ε_i a residual term following a logistic distribution, and y_i^* is a latent preference variable. The observed counterpart to y_i^* is y_i , and the severity level y_i of crash i is defined as follows:

$$y_i = \begin{cases} 1, & y_i^* \leq \mu_{i,0}, \\ 2, & \mu_{i,0} < y_i^* \leq \mu_{i,1}, \\ 3, & \mu_{i,1} < y_i^*, \end{cases} \quad (2)$$

where $\mu_{i,0}$, $\mu_{i,1}$, and $\mu_{i,2}$ are the boundaries between the bicyclist severity levels for crash i . As the residual term ε_i follows the logistic distribution, the GOL model can be written as

$$P(y_i > j) = g(X_i \beta_j) = \frac{\exp(\alpha_j + X_i \beta_j)}{1 + \exp(\alpha_j + X_i \beta_j)}, \quad (3)$$

where α_j represents a cutoff point for the cumulative logit of category j . From the above, it can be determined that the probabilities that y_i will take on each of the values 1, 2, and 3 are equal to

$$\begin{cases} P(y_i = 1) = 1 - g(X_i \beta_1), \\ P(y_i = 2) = g(X_i \beta_2) - g(X_i \beta_1), \\ P(y_i = 3) = g(X_i \beta_2). \end{cases} \quad (4)$$

2.2. Partial Proportional Odds (PPO) Model. As mentioned above, unlike the GOL model, the PPO model allows some independent variables to violate the PO assumption, and other independent variables can remain constant for each crash injury severity level. Based on equation 3, suppose that there are only m variables that obey the PO assumption, and the GOL model can be written as

$$P(y_i > j) = g(X_{i,m} \beta + X_{i,p-m} \beta_j) = \frac{\exp(\alpha_j + X_{i,m} \beta + X_{i,p-m} \beta_j)}{1 + \exp(\alpha_j + X_{i,m} \beta + X_{i,p-m} \beta_j)}, \quad (5)$$

where $X_{i,m}$ is a vector of m explanatory variables to the bicycle crash i that satisfies the PO assumption, β is a vector of regression coefficients that is the same for all values of j , $X_{i,p-m}$ is a vector of $p - m$ variables to the bicycle crash i that is free to the PO assumption, and β_j is a vector of regression coefficients that is different for various values of j .

By conducting the Brant test for all independent variables, we can determine variables that satisfy the PO assumption. Particularly, when the independent variables pass the Brant test, it can be considered that those variables satisfy the PO assumption; otherwise, those variables need to be relaxed. For a detailed discussion on this, please refer to Williams [34].

2.3. Model Comparison. In this study, we use the same dataset to fit the GOL model and the PPO model and choose the log-likelihood of the full model (LL_f), Akaike Information Criterion (AIC), and Bayesian Information Criterion (BIC) to compare the performance of those two models.

In the previous study, researchers have proven that AIC and BIC are practical evaluation criteria to assess the quality

of different statistical models [35, 36]. By comprehensively considering the penalty term of the number of predictive variables and the log-likelihood value of those two models, AIC and BIC consider not only the effect of model fitting but also the model complexity. The smaller the values of AIC and BIC are, the better the model fit effect is. The AIC and BIC can be calculated as follows:

$$\begin{aligned} \text{AIC} &= 2k - 2LL_f, \\ \text{BIC} &= k \ln(O) - 2LL_f, \end{aligned} \quad (6)$$

where k is the number of parameters estimated in the model and O is the number of observations.

3. Data Description

The data used in this study were obtained from police-reported cycling crashes that occurred at various intersections in the UK during the nine years from January 1, 2009, to December 31, 2017. According to the latest census, the total population of the UK is about 63.2 million, making it one of the most densely populated areas in the world.

The data used in the study were all obtained from the British Government Digital Service (<https://data.gov.uk/dataset/>). In the UK, intersections are grouped into five categories in bicycle crash dataset reported by the police, including roundabouts, crossroads, T-junction, more than four arms but not a roundabout, and others. From 2009 to 2018, there are about 44,804 police-reported bicyclist injuries that occurred at various intersections in the UK (with all incomplete or incorrect data observations removed), and about 95% of which happened at or near roundabouts, intersections, and T-junction intersections, as shown in Table 1.

According to the statistical characteristics of bicycle crash data at various intersections, we primarily analyze bicyclist injury severity at three categories, including T-junction, roundabout, and crossroads. The characteristics defined in the dataset, including bicyclist characteristics, intersection attributes, environmental factors, bicyclist movement and location factors, and crash characteristics, are studied in this research for their effect on bicyclist injury severity.

The final analysis dataset contains 42,532 crashes, and the descriptive statistics of the variables used are shown in Table 2.

4. Results and Discussion

In this study, the GOL model and PPO model are fitted by a user-written program `gologit2` in Stata 15, and the coefficients of the explanatory variables in these two models were estimated by the maximum likelihood estimation. Estimation results of the GOL and PPO models are shown in Tables 3 and 4, respectively. The summaries of indicators for model comparison are given in Table 5. It is worth noting that the variables excluded in the final model are those that are not statistically significant, at least at the 95% level (p value smaller than 0.05).

TABLE 1: The statistics of total bicycle crashes at various intersections (2009–2018).

Intersection categories	T-junction	Roundabout	Crossroads	Others	Summary
Total number	26475	9127	6931	2272	44804
Percentage (%)	59.09	20.37	15.47	5.07	100

TABLE 2: Descriptive statistics of the variables used in the estimations.

Variable	Roundabouts		Crossroads		T-junctions	
	Mean	S.D.	Mean	S.D.	Mean	S.D.
<i>Bicyclist characteristics</i>						
Male (1 if bicyclist is male; 0 others)	0.809	0.394	0.792	0.406	0.803	0.397
Age 1 (1 if bicyclist is younger than 15 years; 0 others)	0.040	0.195	0.09	0.286	0.115	0.319
Age 2 (1 if bicyclist is older than 16 years and is younger than 25 years; 0 others)	0.172	0.377	0.209	0.406	0.197	0.397
Age 3 (1 if bicyclist is older than 26 years and is younger than 35 years; 0 others)	0.234	0.423	0.281	0.449	0.246	0.430
Age 4 (1 if bicyclist is older than 36 years and is younger than 45 years; 0 others)	0.235	0.424	0.207	0.405	0.202	0.401
Age 5 (1 if bicyclist is older than 46 years and is younger than 55 years; 0 others)	0.195	0.396	0.133	0.339	0.150	0.358
Age 6 (1 if bicyclist is older than 55 years; 0 others)	0.125	0.330	0.081	0.272	0.090	0.286
Citizen (1 if bicyclist dwells in the city; 0 others)	0.885	0.319	0.937	0.243	0.906	0.292
Towner (1 if bicyclist dwells in the town; 0 others)	0.055	0.228	0.029	0.167	0.047	0.212
Villager (1 if bicyclist dwells in the rural area; 0 others)	0.060	0.237	0.034	0.182	0.047	0.212
Part-of-work (1 if journey as part of work; 0 others)	0.098	0.297	0.066	0.249	0.069	0.253
To-from-work (1 if commuting to/from work; 0 others)	0.215	0.411	0.176	0.381	0.164	0.370
Taking-pupil-school (1 if taking pupil to/from school; 0 others)	0.014	0.118	0.010	0.100	0.013	0.114
Pupil-school (1 if pupil riding to/from school; 0 others)	0.013	0.114	0.018	0.134	0.026	0.158
Purpose-others (1 if travel purpose is different from the above four models; 0 others)	0.661	0.473	0.730	0.444	0.728	0.445
<i>Intersection characteristics</i>						
Speed-limit (1 if the speed limit at the intersection is less than or equal to 30 km/h; 0 others)	0.791	0.406	0.931	0.253	0.927	0.261
Junction-control (1 if the intersection is nonsignalized controlled; 0 others)	0.953	0.212	0.517	0.500	0.907	0.290
Nonsignal-pedestrian (1 if pedestrian crossing facilities are nonsignalized controlled crosswalks; 0 others)	0.116	0.321	0.111	0.315	0.126	0.332
Signal-pedestrian (1 if there is pedestrian phase at traffic signal junction; 0 others)	0.027	0.161	0.350	0.477	0.073	0.261
Footbridge (1 if there are footbridges or subways; 0 others)	0.013	0.114	0.009	0.095	0.010	0.100
Central-refuge (1 if there are central refuges; 0 others)	0.079	0.270	0.018	0.134	0.015	0.122
None (1 if there are no pedestrian crossing facilities; 0 others)	0.791	0.406	0.931	0.253	0.927	0.261
Road-dry (1 if road surface is dry; 0 others)	0.725	0.446	0.782	0.412	0.79	0.407
Road-wet (1 if road surface is wet; 0 others)	0.257	0.437	0.194	0.395	0.195	0.396
Road-ice (1 if road surface is ice; 0 others)	0.011	0.105	0.014	0.118	0.007	0.084
Road-others (1 if road surface is different from the above three models; 0 others)	0.007	0.084	0.010	0.100	0.008	0.089
Urban-junction (1 if the intersection is located in an urban area; 0 others)	0.781	0.414	0.927	0.261	0.886	0.318
Divider (1 if the roads have dividers; 0 others)	0.167	0.373	0.260	0.438	0.264	0.440
<i>Environmental condition</i>						
Weekend (1 if the crash occurred at the weekend; 0 others)	0.243	0.429	0.256	0.436	0.273	0.445
Morning-peak (1 if the crash occurred at the morning rush hour; 0 others)	0.202	0.401	0.165	0.371	0.190	0.392
Night-peak (1 if the crash occurred at the afternoon rush hour; 0 others)	0.177	0.382	0.205	0.404	0.227	0.418
Nonpeak (1 if the crash occurred at the off-peak hour; 0 others)	0.622	0.485	0.630	0.483	0.583	0.493
Daylight (1 if it was daylight when the crash occurred; 0 others)	0.754	0.430	0.761	0.427	0.850	0.358
Night-light (1 if the crash occurred at night, and there were lights on the road; 0 others)	0.221	0.415	0.219	0.414	0.189	0.391
Night-nonlight (1 if the crash occurred at night, and there were no lights on the road; 0 others)	0.026	0.158	0.020	0.141	0.039	0.192
Weather-fine (1 if it was fine weather when the crash occurred; 0 others)	0.835	0.371	0.849	0.358	0.871	0.335
Weather-raining (1 if it was raining when the crash occurred; 0 others)	0.122	0.327	0.097	0.297	0.100	0.300
Weather-snowing (1 if it was snowing when the crash occurred; 0 others)	0.008	0.089	0.011	0.105	0.012	0.110
Weather-foggy (1 if it was foggy when the crash occurred; 0 others)	0.010	0.100	0.011	0.105	0.009	0.095
Weather-others (1 if it was other weather when the crash occurred; 0 others)	0.025	0.155	0.032	0.176	0.009	0.095
January (1 if the crash occurred in January; 0 others)	0.089	0.285	0.066	0.249	0.071	0.257
February (1 if the crash occurred in February; 0 others)	0.073	0.261	0.063	0.243	0.063	0.243
March (1 if the crash occurred in March; 0 others)	0.072	0.259	0.080	0.272	0.080	0.272
April (1 if the crash occurred in April; 0 others)	0.073	0.261	0.078	0.268	0.075	0.263
May (1 if the crash occurred in May; 0 others)	0.082	0.274	0.09	0.286	0.092	0.290
June (1 if the crash occurred in June; 0 others)	0.080	0.272	0.095	0.293	0.097	0.297

TABLE 2: Continued.

Variable	Roundabouts		Crossroads		T-junctions	
	Mean	S.D.	Mean	S.D.	Mean	S.D.
July (1 if the crash occurred in July; 0 others)	0.092	0.290	0.102	0.303	0.100	0.300
August (1 if the crash occurred in August; 0 others)	0.081	0.272	0.089	0.285	0.085	0.279
September (1 if the crash occurred in September; 0 others)	0.091	0.288	0.091	0.288	0.100	0.300
October (1 if the crash occurred in October; 0 others)	0.099	0.298	0.101	0.302	0.096	0.295
November (1 if the crash occurred in November; 0 others)	0.094	0.292	0.088	0.283	0.085	0.279
December (1 if the crash occurred in December; 0 others)	0.075	0.263	0.057	0.232	0.057	0.232
<i>Bicyclist movement and location preceding the crash</i>						
Parked (1 if the bicycle is in a state of parking; 0 others)	0.007	0.084	0.01	0.100	0.013	0.114
Waiting-go (1 if the bike is waiting to go straight; 0 others)	0.014	0.118	0.018	0.134	0.031	0.173
Slowing (1 if the bicycle is in a state of deceleration; 0 others)	0.013	0.114	0.02	0.141	0.061	0.239
Moving-off (1 if the bicycle is moving off; 0 others)	0.038	0.192	0.036	0.187	0.058	0.235
Lefting (1 if the bike is turning left; 0 others)	0.007	0.084	0.010	0.100	0.010	0.100
Waiting-left (1 if the bike is waiting to turn left; 0 others)	0.008	0.089	0.010	0.100	0.012	0.110
Righting (1 if the bike is turning right; 0 others)	0.124	0.330	0.051	0.219	0.064	0.245
Waiting-right (1 if the bike is waiting to turn right; 0 others)	0.008	0.089	0.025	0.155	0.042	0.200
Lane-left (1 if the bike is changing lane to left; 0 others)	0.009	0.095	0.010	0.100	0.014	0.118
Lane-right (1 if the bike is changing lane to right; 0 others)	0.012	0.110	0.015	0.122	0.017	0.130
Over-offside (1 if the bike is overtaking at offside; 0 others)	0.016	0.126	0.022	0.148	0.031	0.173
Over-nearside (1 if the bike is overtaking at nearside; 0 others)	0.011	0.105	0.030	0.170	0.027	0.161
Ahead-left (1 if the bike is going ahead left; 0 others)	0.013	0.114	0.014	0.118	0.011	0.105
Ahead-right (1 if the bike is going ahead right; 0 others)	0.056	0.230	0.017	0.130	0.026	0.158
Ahead (1 if the bike is going ahead; 0 others)	0.665	0.472	0.715	0.452	0.582	0.493
Mainway (1 if the bike is on mainway; 0 others)	0.954	0.210	0.927	0.261	0.894	0.308
Busway (1 if the bike is on busway; 0 others)	0.019	0.138	0.023	0.148	0.03	0.170
Cycleway (1 if the bike is on cycleway; 0 others)	0.014	0.118	0.030	0.170	0.049	0.217
Pavement (1 if the bike is on pavement; 0 others)	0.007	0.084	0.011	0.105	0.020	0.141
Bike-location-others (1 if the bike is on other location; 0 others)	0.007	0.084	0.009	0.095	0.009	0.095
Approaching-parked (1 if the bike is approaching junction or waiting/parked at junction approach; 0 others)	0.209	0.406	0.278	0.448	0.367	0.482
Leaving-parked (1 if bike is leaving junction or waiting/parked at junction exit; 0 others)	0.156	0.363	0.071	0.257	0.085	0.279
Leaving-main (1 if the bike is leaving main road; 0 others)	0.016	0.126	0.012	0.110	0.018	0.134
Entering-main (1 if the bike is entering main road; 0 others)	0.016	0.126	0.049	0.217	0.054	0.226
Mid (1 if the bike is located in the intersection; 0 others)	0.604	0.489	0.59	0.492	0.476	0.499
<i>Type of collision</i>						
Collision-point-front (1 if the collision point is on the front side of the bicycle; 0 others)	0.346	0.475	0.528	0.499	0.552	0.497
Collision-point-back (1 if the collision point is on the back side of the bike; 0 others)	0.181	0.385	0.086	0.281	0.084	0.277
Collision-point-right (1 if the collision point is on the right side of the bike; 0 others)	0.139	0.346	0.219	0.414	0.185	0.389
Collision-point-left (1 if the collision point is on the left side of the bike; 0 others)	0.301	0.458	0.131	0.338	0.136	0.344
Collision-point-none (1 if there was no collision point; 0 others)	0.034	0.182	0.037	0.190	0.044	0.205
Secondary-collision-on-road (1 if the secondary collision occurred on the road; 0 others)	0.011	0.105	0.026	0.158	0.032	0.176
Secondary-collision-off-road (1 if the secondary collision occurred off the road; 0 others)	0.017	0.130	0.014	0.118	0.007	0.084
Secondary-collision-none (1 if there is no secondary collision occurred; 0 others)	0.972	0.164	0.96	0.195	0.961	0.192

4.1. Comparison of Models. In this study, according to the estimates of the GOL and PPO models, we adopt AIC, BIC, and pseudo R^2 to compare those two models (as shown in Table 5). It can be concluded that the AIC and BIC values of the PPO model are smaller than those of the GOL model. These two values imply that, given the same dataset, the PPO model produces better fitting results. Besides, a similar implication can be derived from the pseudo R^2 because the value of the PPO model is larger than that of the GLO model. In summary, the PPO model outperforms the GOL model for fitting the data of bicycle crashes that occurred at various intersections. We mainly adopt the PPO model to analyze the bicycle crash data.

It should be noted that the sign of the estimated coefficients cannot intuitively interpret the influence of

explanatory variables on the PPO model outcomes. To present meaningful explanations, we calculate the marginal effects of each variable to evaluate the impacts of estimates on the bicyclist injury severity occurring probabilities. Particularly, the marginal effects demonstrate the difference in outcome probability of each level of bicyclist injury severity caused by one unit change in the explanatory variable (as shown in Table 6).

4.2. Bicyclist Characteristics. In Table 3, several factors are found to be statistically significant in influencing severity outcomes in bicyclist-related crashes. Specifically, it is found that male cyclists are more likely to be involved in fatal or serious injuries at crossroads and T-junctions while

TABLE 3: Estimation results of the GOL model.

Variables	Roundabouts		Crossroads		T-junctions	
	Fatal	Serious	Fatal	Serious	Fatal	Serious
<i>Bicyclist characteristics</i>						
Male		0.100 (0.052)*		-0.169 (0.063)**		-0.088 (0.033)**
Age 1		0.804 (0.132)***		0.32 (0.105)**		0.298 (0.053)***
Age 2		0.652 (0.071)***		0.389 (0.084)***		0.38 (0.043)***
Age 3	1.46 (0.585)*	0.461 (0.062)***		0.398 (0.080)***		0.324 (0.041)***
Age 4		0.330 (0.060)***		0.191 (0.082)*		0.154 (0.041)***
Age 6		-0.25 (0.066)***	-1.306 (0.495)**	-0.305 (0.096)**	-1.501 (0.280)*	-0.279 (0.048)***
Villager					-0.675 (0.246)**	-0.111 (0.057)*
Part-of-work		0.202 (0.074)**				0.15 (0.052)**
To-from-work					1.012 (0.370)**	
Pupil-school						0.366 (0.098)***
<i>Intersection characteristics</i>						
Speed-limit		0.331 (0.048)***	0.944 (0.409)*	0.529 (0.097)***	1.239 (0.231)***	0.441 (0.047)***
Junction-control	1.613 (0.437)***		0.967 (0.342)**		0.723 (0.235)**	
Divider	-1.053 (0.402)**				-0.958 (0.394)*	-0.29 (0.076)***
Urban-junction				0.278 (0.099)**	0.45 (0.246)*	0.321 (0.042)***
<i>Environmental condition</i>						
Weather-fine				0.266 (0.125)*		
Weather-raining		0.188 (0.066)**		0.291 (0.146)*		
Night-peak						0.071 (0.032)*
Night-light						-0.122 (0.033)***
Night-nonlight						-0.195 (0.074)**
February					-0.701 (0.266)**	
May				-0.14 (0.084)*		
June		0.19 (0.080)*				
October				-0.142 (0.079)*		
<i>Bicyclist movement and location preceding the crash</i>						
Parked					-1.971 (1.068)*	1.354 (0.600)*
Waiting-go				0.889 (0.277)**		
Righting		-0.234 (0.089)**			-0.494 (0.248)*	-0.113 (0.051)*
Waiting-right				0.764 (0.377)*		0.418 (0.122)**
Ahead-right		-0.446 (0.106)***				-0.24 (0.073)**
Over-nearside	-2.928 (0.907)**				-1.241 (0.404)**	
Lane-left		-0.483 (0.212)*				
Approaching-parked			1.523 (0.606)*			
Leaving-parked					-0.825 (0.256)**	-0.09 (0.046)*
Entering-main			-1.038 (0.400)**	-0.206 (0.110)*	-1.149 (0.281)***	-0.182 (0.057)**
Busway					-1.387 (0.768)*	
Pavement		-0.534 (0.298)*			-1.35 (0.615)*	
<i>Type of collision</i>						
Collision-point-front				0.51 (0.115)***		0.422 (0.055)***
Collision-point-back		0.234 (0.057)***		0.804 (0.144)***		0.652 (0.070)***
Collision-point-right		0.15 (0.063)*		0.576 (0.122)***		0.444 (0.060)***
Collision-point-left				0.416 (0.128)**		0.544 (0.063)***
Secondary-collision-on-road						-0.264 (0.067)***
Secondary-collision-off-road		-0.78 (0.248)**		-0.482 (0.278)*	-1.491 (0.405)***	-0.679 (0.125)***
Constant	4.394 (0.784)	0.957 (0.132)	2.746 (1.325)	-0.04 (0.208)	4.339 (0.542)	0.227 (0.088)
Number of observations		16418		11,623		14491
Log-likelihood at zero, $LL(0)$		-7800.35		-5544.79		-6810.67
Log-likelihood at convergence, $LL(\beta)$		-6817.51		-4823.41		-5932.77
Pseudo R^2		0.1260		0.1301		0.1289
AIC		15684.71		11189.57		13662.38
BIC		16008.36		11557.61		13989.59

Note. Standard errors are in parentheses. Level of significance: * indicates parameter is significant at 0.05, ** indicates parameter is significant at 0.01, and *** indicates parameter is significant at 0.001.

TABLE 4: Estimation results of the PPO model.

Variables	Roundabouts		Crossroads		T-junctions	
	Fatal	Serious	Fatal	Serious	Fatal	Serious
<i>Bicyclist characteristics</i>						
Male	0.111 (0.052)*	0.111 (0.052)*	-0.16 (0.064)*	-0.16 (0.064)*	-0.089 (0.033)**	-0.089 (0.033)**
Age 1	0.706 (0.143)***	0.706 (0.143)***	0.309 (0.111)***	0.309 (0.110)*	0.275 (0.053)***	0.275 (0.053)***
Age 2	0.654 (0.071)***	0.654 (0.071)***		0.396 (0.085)***	0.373 (0.043)***	0.373 (0.043)***
Age 3	0.467 (0.062)***	0.467 (0.062)***	0.405 (0.080)***	0.405 (0.080)***	0.325 (0.041)***	0.325 (0.041)***
Age 4	0.336 (0.060)***	0.336 (0.060)***	0.194 (0.082)**	0.194 (0.082)**	0.156 (0.041)***	0.156 (0.041)***
Age 6	-0.263 (0.066)***	-0.263 (0.066)***	-1.571 (0.354)***	-0.298 (0.097)**	-1.426 (0.178)***	-0.282 (0.048)***
Villager					-0.716 (0.235)**	-0.114 (0.057)*
Part-of-work	0.188 (0.075)*	0.188 (0.075)*			0.146 (0.052)**	0.146 (0.052)**
To-from-Work					0.981 (0.366)**	
Pupil-school					0.366 (0.098)***	0.366 (0.098)***
<i>Intersection characteristics</i>						
Speed-limit	0.284 (0.054)***	0.284 (0.054)***	1.327 (0.340)***	0.537 (0.097)***	1.287 (0.188)***	0.443 (0.047)***
Junction-control	1.492 (0.424)***		0.843 (0.318)***		0.711 (0.232)**	
Divider	-1.095 (0.397)**				-0.296 (0.076)***	-0.296 (0.076)***
Urban-junction	0.115 (0.055)*	0.115 (0.055)*	0.255 (0.110)**	0.255 (0.110)**	0.329 (0.041)***	0.329 (0.041)***
Road-wet	-4.438 (1.873)*	-4.438 (1.873)*				
<i>Environmental condition</i>						
Weather-fine			0.313 (0.131)**	0.313 (0.131)**		
Weather-raining	0.193 (0.067)**	0.193 (0.067)**	0.308 (0.161)**	0.308 (0.161)*		
Weather-foggy			-2.202 (1.064)**			
Night-peak					0.073 (0.032)*	0.073 (0.032)*
Night-light					-0.118 (0.033)***	-0.118 (0.033)***
Night-nonlight					-0.193 (0.074)**	-0.193 (0.074)**
February					-0.641 (0.263)*	
May			-0.192 (0.105)**	-0.192 (0.105)**		
June	0.208 (0.108)*	0.208 (0.108)*				
October			-0.179 (0.101)**	-0.179 (0.101)**		
<i>Bicyclist movement and location preceding the crash</i>						
Parked					-2.288 (1.003)*	1.314 (0.600)*
Waiting-go			0.869 (0.292)***	0.869 (0.292)***	0.801 (0.172)***	0.801 (0.172)***
Righting					-0.115 (0.050)*	-0.115 (0.050)*
Waiting-right			0.733 (0.388)*	0.733 (0.388)**	0.4 (0.122)**	0.4 (0.122)**
Over-nearside	-2.531 (0.759)**		-2.294 (0.466)***		-1.212 (0.393)**	
Ahead-right	-0.38 (0.120)**	-0.38 (0.120)**			-0.216 (0.072)**	-0.216 (0.072)**
Entering-main			-2.57 (1.063)**		-1.179 (0.239)***	-0.233 (0.055)***
Lane-left	-0.441 (0.220)*	-0.441 (0.220)*	-1.034 (0.561)*	-1.034 (0.561)*		
Busway					-1.389 (0.587)**	
Pavement	-0.495 (0.242)*	-0.495 (0.242)*			-1.285 (0.345)***	
<i>Type of collision</i>						
Collision-point-front			-0.511 (0.116)***	-0.511 (0.116)***	-0.446 (0.055)***	-0.446 (0.055)***
Collision-point-back	0.407 (0.117)***	0.407 (0.117)***	0.812 (0.146)***	0.812 (0.146)***		0.656 (0.070)***
Collision-point-right		0.324 (0.119)**		0.575 (0.123)***		0.457 (0.060)***
Collision-point-left				0.414 (0.130)***		0.576 (0.063)***
Secondary-collision-on-road					-0.319 (0.066)***	-0.319 (0.066)***
Secondary-collision-off-road	-0.753 (0.253)**	-0.753 (0.253)**	-0.477 (0.281)*	-0.477 (0.281)*	-1.636 (0.386)***	-0.69 (0.125)***
Constant	4.576 (1.191)	1.042 (1.123)	4.787 (1.613)	-0.849 (1.460)	4.000 (0.301)	0.528 (0.087)
Number of observations		16418		11623		14491
Log-likelihood at zero, $LL(0)$		-7778.23		-5525.77		-6810.30
Log-likelihood at convergence, $LL(\beta)$		-6776.39		-4788.63		-5929.73
Pseudo R^2		0.1288		0.1334		0.1293
AIC		15669.03		11166.97		13627.88
BIC		15869.39		11424.59		13800.70

Note. Standard errors are in parentheses. Level of significance: * indicates parameter is significant at 0.05, ** indicates parameter is significant at 0.01, and *** indicates parameter is significant at 0.001.

having a decreased likelihood of a slight injury, consistent with previous research [11, 14, 15]. The average marginal effects (as shown in Table 5) show that at crossroads and

T-junctions, the male indicator variable increases the probability of serious injuries by 2.37% and 1.24%, respectively. Instead, the variable increases the probability of

TABLE 5: Indicators for model comparison.

Model	Roundabouts			Crossroads			T-junctions		
	AIC	BIC	Pseudo R^2	AIC	BIC	Pseudo R^2	AIC	BIC	Pseudo R^2
GOL	15684.71	16008.36	0.1260	11189.57	11557.61	0.1301	13662.38	13989.59	0.1289
PPO	15669.03	15869.39	0.1288	11166.97	11424.59	0.1334	13627.88	13800.70	0.1293

TABLE 6: Marginal effects for different bicycle crash injury severity levels at different intersections.

Variables	Roundabouts			Crossroads			T-junctions		
	Fatal	Serious	Slight	Fatal	Serious	Slight	Fatal	Serious	Slight
<i>Bicyclist characteristics</i>									
Male	-0.0003	-0.0145	0.0148	0.0007	0.0237	-0.0244	0.0003	0.0124	-0.0127
Age 1	-0.0022	-0.1149	0.1171	-0.0013	-0.0448	0.0461	-0.0009	-0.0384	0.0392
Age 2	-0.0018	-0.0927	0.0945	0.0020	-0.0584	0.0564	-0.0012	-0.0519	0.0531
Age 3	-0.0012	-0.0655	0.0667	-0.0016	-0.0562	0.0578	-0.0010	-0.0453	0.0463
Age 4	-0.0009	-0.0472	0.0481	-0.0008	-0.0269	0.0276	-0.0005	-0.0217	0.0222
Age 6	0.0007	0.0361	-0.0368	0.0060	0.0372	-0.0433	0.0045	0.0356	-0.0402
Villager							0.0023	0.0140	-0.0163
Part-of-work	-0.0005	-0.0288	0.0293				-0.0005	-0.0203	0.0208
To-from-Work							-0.0031	0.0073	-0.0042
Pupil-school							-0.0012	-0.0510	0.0521
<i>Intersection characteristics</i>									
Speed-limit	-0.0008	-0.0405	0.0413	-0.0054	-0.0706	0.0760	-0.0041	-0.0590	0.0631
Junction-control	-0.0040	-0.0121	0.0161	-0.0034	-0.0065	0.0100	-0.0023	-0.0081	0.0103
Divider	0.0030	0.0034	-0.0064				0.0009	0.0412	-0.0422
Urban-junction	-0.0003	-0.0139	0.0142	-0.0011	-0.0394	0.0405	-0.0010	-0.0458	0.0469
Road-wet	0.0115	0.6092	-0.6207						
<i>Environmental condition</i>									
Weather-fine				-0.0010	-0.0369	0.0379			
Weather-raining	-0.0022	-0.1179	0.1201	-0.0011	-0.0398	0.0409			
Weather-foggy				0.0086	-0.0166	0.0080			
Night-peak							-0.0002	-0.0102	0.0104
Night-light							0.0004	0.0165	-0.0169
Night-nonlight							0.0006	0.0269	-0.0275
February							0.0020	-0.0033	0.0013
May				0.0006	0.0199	-0.0204			
June	-0.0005	-0.0270	0.0275						
October				0.0006	0.0203	-0.0208			
<i>Bicyclist movement and location preceding the crash</i>									
Parked							0.0072	-0.1945	0.1872
Waiting-go				-0.0038	-0.1343	0.1381	-0.0025	-0.1116	0.1142
Righting							0.0004	0.0160	-0.0163
Waiting-right				-0.0033	-0.1162	0.1195	-0.0013	-0.0558	0.0570
Over-nearside	0.0065	-0.0094	0.0029	0.0076	-0.0101	0.0025	0.0038	-0.0157	0.0119
Ahead-right	0.0009	0.0455	-0.0463				0.0007	0.0301	-0.0307
Entering-main				0.0054	0.0241	-0.0295	0.0037	0.0295	-0.0332
Lane-left	0.0010	0.0504	-0.0513	0.0036	0.1288	-0.1324			
Busway							0.0044	-0.0059	0.0015
Pavement	0.0014	0.0733	-0.0747				0.0041	0.0151	-0.0192
<i>Type of collision</i>									
Collision-point-front				0.0020	0.0696	-0.0715	0.0014	0.0622	-0.0636
Collision-point-back	-0.0007	-0.0356	0.0363	-0.0032	-0.1140	0.1172	-0.0002	-0.0932	0.0934
Collision-point-right	0.0016	-0.0238	0.0222	0.0012	-0.0832	0.0820	0.0009	-0.0661	0.0651
Collision-point-left				0.0023	-0.0608	0.0585	-0.0018	-0.0803	0.0821
Secondary-collision-on-road							0.0010	0.0445	-0.0455
Secondary-collision-off-road	0.0021	0.1098	-0.1119	0.0019	0.0680	-0.0699	0.0052	0.0931	-0.0983

serious injuries that happened at the roundabout by 1.45%. The primary reason for this phenomenon may be that bicyclists ordinarily consider that traffic conflicts at roundabouts are more severe, and they could be more careful, which results in lower serious accidents [27].

The age of bicyclists is also a statistically significant variable to analyze the injury severity. Particularly, older bicyclists (older than 55 years) are more likely to be involved in the occurrence of serious injury. According to the average marginal effects in Table 6, this variable increases the occurrence probability of serious injury at roundabouts, crossroads, and T-junctions by 3.61%, 3.72%, and 3.56%, respectively. The result can be supported by previous research [11, 13, 14, 27]. The possible reason for this finding is that the older bicyclists are slower and have a longer reaction and perception times than other age groups. For the younger bicyclists (the bicyclist is younger than 15 years), they are always involved in slight injuries. The indicator increases the probability of slight injury at roundabouts, crossroads, and T-junctions by 11.71%, 4.61%, and 3.92%, respectively. Besides, bicyclists who live in rural areas are more likely to be seriously injured in cycling crashes at T-junctions, and the variable increases the occurrence probability of slight injury by 1.4%.

4.3. Intersection Characteristics. Regarding the intersection characteristics, in Table 5, many statistically significant factors influence bicyclist injury severity. Consistent with previous research [15], traffic control strategies enforced at intersections appear to be effective in reducing the possibility of serious and fatal injury. For instance, regarding the speed limit strategy at intersections, the factor decreases the occurrence probability of serious injuries that occurred at roundabouts, crossroads, and T-junctions by 4.05%, 7.06%, and 5.9%, respectively. However, nonsignalized control strategies at intersections decrease serious and fatal injury while increasing the possibility of slight injuries. Such factor increases the occurrence probability of slight injury at roundabouts, crossroads, and T-junctions by 1.61%, 1%, and 1.03%, respectively. At the nonsignalized intersections, bicyclists and drivers might consciously slow down, thus effectively reducing the occurrence of fatal and severe casualties [28]. Similarly, bicyclists are less likely to be involved in fatal or severe crashes that occurred at urban intersections due to integrated traffic control stratagems.

The widely accepted view is that the implication of road facilities (for example, divider facilities between motor and bicycle lanes) can improve the safety of cyclists. However, this study finds that the provision of divider facilities at roundabouts and T-junctions increases the likelihood of fatal and serious injury. The indicator increases the occurrence probability of serious injury at T-junctions by 4.12%. It is mainly due to the fact that divider facilities are more likely to cause a secondary collision when the crash occurred, and the secondary collision will significantly increase the occurrence of fatal or severe casualties. It is worth noting that, consistent with the results in Kim et al. [14], cycling on wet roads was more prone to severe or fatal injury. To be specific,

the indicator increases the occurrence probability of serious injuries that happened at the roundabouts by 60.92%.

4.4. Environmental Conditions. Several environmental conditions related variables are found to affect bicyclist injury severity significantly, as shown in Table 5. Consistent with previous research, bad weather can result in more dangerous cycling [17, 19, 23]. However, the impact of environmental conditions on the probability of cycling crashes that occurred at the various intersections is quite dissimilar. Interestingly, rainy days only affected the possibility of cycling crashes at roundabouts and intersections, and the variable decreases the likelihood of fatal and serious injury while increasing the occurrence probability of slight injury. In particular, on rainy days, more consideration should be paid to cycling safety at roundabouts, since the factor can increase the occurrence probability of slight injury at roundabouts by 12.01%. Besides, foggy days only have a significant impact on cycling safety at crossroads. In particular, it significantly increases the likelihood of serious injury crashes, and the factor can increase the occurrence probability of serious injury by 12.01%.

It is generally considered that lighting conditions are directly related to the visibility of the bicyclist and drivers, which will directly affect the severity of cycling crashes. However, in this study, we find out that lighting conditions only have a significant effect on the likelihood of serious cycling crashes at T-junctions. Opening up the street lights at night reduces the possibility of the slight injury, and the lack of street lights increases the likelihood of serious injury. However, with or without street lights, we need to be more careful when cycling near T-junctions at night [13, 14].

In previous studies, researchers have found that seasons and months have a significant influence on the probability of bicyclist injury severity [27]. Furthermore, in this study, we discover February and June significantly affect bicyclist injury severity only at T-junctions and roundabouts, separately. In particular, in May and October, we need to pay more attention to the possibility of severe cycling crashes at crossroads, and the factors increase the occurrence probability of serious injury by 1.99% and 2.03%, respectively.

4.5. Bicyclist Movement and Location Preceding the Crash. In Table 5, a wide range of movement-related variables shows a statistically significant influence on the outcome of the bicyclist injury severity. Individually, at roundabouts, making a right turn, changing lanes to the left, and overtaking inside the intersections are statistically significant factors related to bicyclist injury severity. As for cross sections, stopped following going straight, stopped following turning right, overtaking inside the intersections, entering the main road from the intersection, and changing lanes to the left are statistically significant factors related to bicyclist injury severity. And the variables, including parked, stopped following going straight, making a right turn, waiting and turn right, overtaking inside the intersections, entering the main road from the intersection, and riding on the wrong road, will affect the severity of the injury that occurred at the T-junctions.

Particularly, consistent with the previous research [11], parked or making a right turn has a significant effect on cycling safety. Interestingly, in this study, these two factors only appear to have statistically significant impact on the bicyclist injury severity at T-junctions, and the factor of parked at T-junctions increases the occurrence probability of slight injury by 18.72% while decreasing the occurrence probability of serious injury by 19.45%. However, changing lanes to the left does not show any significant influence on the likelihood of bicyclist injury severity at T-junctions and shows a considerable effect on severe or fatal cycling crashes at roundabouts and cross sections. Correspondingly, the factor will increase the occurrence probability of serious injury at roundabouts and crossroads by 5.04% and 12.88%, respectively. Moreover, cycling on the pavement can also significantly impact the likelihood of bicyclist injury severity at roundabouts and crossroads, and the factor increases the occurrence probability of serious injury that occurred at these two types of intersections by 7.33% and 1.51%, respectively.

4.6. Type of Collision. As shown in Table 5, the type-of-collision indicators, including the collision point at the front, back, right, and left, and the secondary collisions that occurred in or off the road, could impact the cycling crash injury severity, and the impact is statistically significant. Similar to previous studies [13, 14, 27], this study also found that the severity of cycling crashes at various intersections can be distinctly affected by the collision point. Specifically, the collision point at the front and left merely appears to have statistically significant impact on the bicyclist injury severity at crossroads and T-junctions, mainly since there are few left-turn traffic volumes at roundabouts. The factor of the collision point at the front will increase the occurrence probability of serious injury at crossroads and T-junctions by 6.96% and 6.22%, respectively. In comparison, the factor of the collision point at the left will decrease the occurrence probability of serious injury at crossroads and T-junctions by 6.08% and 8.03%, respectively. Interestingly, in this study, we discover that the factors of the collision point at the back and left will decrease the probability of serious injury while increasing the likelihood of slight injury. Above all, the collision point at the front or back is mainly caused by cycling when going straight. Due to the faster speed of vehicles, serious cycling crash severity is more likely to occur. Besides, since the vehicle speed is always slower while turning at the intersections, the probability of slight injury is more likely to occur at the left and right collision points.

The widely accepted opinion is that the secondary collision is dangerous. However, in this study, we find that the indicator of secondary-collision-on-road only affects the severity of cycling crashes at T-junctions, and the factor increases the occurrence probability of serious injury by 4.45% while decreasing the occurrence probability of slight injury by 4.55%. Also, it should be noted that the indicator of the secondary-collision-off-road significantly increases the likelihood of severe cycling crashes. In Table 6, the factor increases the occurrence probability of serious injury at roundabouts, crossroads, and T-junctions by 10.98%, 6.8%, and 9.31%, respectively.

5. Conclusions

To improve the cycling safety of bicyclists at various intersections, in this study, we apply the GOL model and PPO model to explore the possible factors that may result in the severity of bicycle injuries. Particularly, according to the statistical characteristics of data on bicycle crashes that occurred in the UK from 2009 to 2019, the intersections in this study are divided into three groups, including roundabouts, intersections, and T-shaped intersections. The bicyclist injury severity is divided into three categories: slight injury, serious injury, and fatal injury. A wide range of possible factors affecting bicyclist injury severities, including bicyclist characteristics, intersection characteristics, environmental conditions, bicyclist movement and location preceding the crash, and types of collisions, is considered.

The model estimation results reveal that the PPO model outperforms the GOL model for analyzing the factors that affect the severity of cycling crashes at various intersections. Further, we calculated the marginal effects of the variables in the PPO model to explore the differences of factors that influence the occurrence probability of bicyclist injury severity at various intersections. Regarding the estimation results of the bicyclist injury severity, we find out that there are gigantic differences in the factors that influence the severity of cycling crashes at various intersections. Particularly, we find that nine variables have significant impacts on bicyclist injury severity at those three types of intersections, including male bicyclists, age, speed limit, traffic control strategies at intersections, urban junctions, overtaking inside the intersections, the collision point at the back of the bicycle, the collision point at the right of the bike, and the secondary collision happened on the roadside. Interestingly, there are two variables (cycling in wet road and cycling in June) that only have significant impact on bicyclist injury severity at roundabouts. And four variables (cycling in fine days, cycling in foggy days, cycling in May, and cycling in October) are discovered to only have significant impact on bicyclist injury severity at crossroads. Surprisingly, up to eleven variables are discovered to only have significant impact on bicyclist injury severity at T-junctions, and the variables include the cyclist is a villager, journey purpose is to or from work, pupil is going to or from school alone, cycling in night peak hours, cycling in the night with a light on the road, cycling in the night without a light on the road, cycling in February, parked, turning right, cycling in the busway, and the secondary collision happened on the road.

Moreover, in this study, we also found that the factors affecting the cycling safety of intersections may also appear to have significant impact in different seasons, which means these factors may not be homogeneous with the time change. Due to the limitations of the PPO model, we cannot consider the temporal heterogeneity of various influencing factors in the analysis, and we will continue to focus on such issues in subsequent studies. With the growing importance relating to bicyclist safety, this paper provides some essential initial findings with the dataset from the UK and also provides some guidance for the analysis of cycling crashes from other countries. Anyway, this study can help decision makers

better understand the spatial heterogeneity of the factors that influence the bicyclist injury severity at various intersections. Thus, more specific and efficient measures can be provided to enhance cycling safety at different types of intersections.

Data Availability

The data used in the study were all obtained from the British Government Digital Service (<https://data.gov.uk/dataset/>).

Conflicts of Interest

The authors declare that they have no conflicts of interest.

Acknowledgments

This research was supported by the National Natural Science Foundation of China (51808187), the Natural Science Foundation of Jiangsu Province (BK20170879), the Fundamental Research Funds for the Central Universities (2019B13514), and the Jiangsu Planned Projects for Postdoctoral Research Funds (1701086B).

References

- [1] Q. Cai, J. Lee, N. Eluru, and M. Abdel-Aty, "Macro-level pedestrian and bicycle crash analysis: incorporating spatial spillover effects in dual state count models," *Accident Analysis & Prevention*, vol. 93, pp. 14–22, 2016.
- [2] Y. Ji, X. Ma, M. He, Y. Jin, and Y. Yuan, "Comparison of usage regularity and its determinants between docked and dockless bike-sharing systems: a case study in Nanjing, China," *Journal of Cleaner Production*, vol. 255, pp. 120110–120121, 2020.
- [3] R. Cervero, S. Denman, and Y. Jin, "Network design, built and natural environments, and bicycle commuting: evidence from British cities and towns," *Transport Policy*, vol. 74, pp. 153–164, 2019.
- [4] N. Grudgings, A. Hagen-Zanker, S. Hughes, B. Gatersleben, M. Woodall, and W. Bryans, "Why don't more women cycle? An analysis of female and male commuter cycling mode-share in England and Wales," *Journal of Transport & Health*, vol. 10, pp. 272–283, 2018.
- [5] J. Lee, M. Abdel-Aty, Q. Cai, L. Wang, and H. Huang, "Integrated modeling approach for non-motorized mode trips and fatal crashes in the framework of transportation safety planning," *Transportation Research Record: Journal of the Transportation Research Board*, vol. 2672, no. 32, pp. 49–60, 2018.
- [6] F. Feng, S. Bao, R. C. Hampshire, and M. Delp, "Drivers overtaking bicyclists—an examination using naturalistic driving data," *Accident Analysis & Prevention*, vol. 115, pp. 98–109, 2018.
- [7] R. Aldred, R. Goel, J. Woodcock, and A. Goodman, "Contextualising Safety in numbers: a longitudinal investigation into change in cycling safety in Britain, 1991–2001 and 2001–2011," *Injury Prevention*, vol. 25, no. 3, pp. 236–241, 2019.
- [8] C. Ma, D. Yang, J. Zhou, Z. Feng, and Q. Yuan, "Risk riding behaviors of urban E-bikes: a literature review," *International Journal of Environmental Research and Public Health*, vol. 16, no. 13, pp. 1–18, 2019.
- [9] L. Hou, J. Duan, W. Wang, R. Li, G. Li, and B. Cheng, "Drivers' braking behaviors in different motion patterns of vehicle-bicycle conflicts," *Journal of Advanced Transportation*, vol. 2019, Article ID 4023970, 17 pages, 2019.
- [10] C. Ma, J. Zhou, D. Yang et al., "Research on the relationship between the individual characteristics of electric bike riders and illegal speeding behavior: a questionnaire-based study," *Sustainability*, vol. 12, no. 3, pp. 1–13, 2020.
- [11] A. Behnood and F. Mannering, "Determinants of bicyclist injury severities in bicycle-vehicle crashes: a random parameters approach with heterogeneity in means and variances," *Analytic Methods in Accident Research*, vol. 16, pp. 35–47, 2017.
- [12] X. Wu, W. Xiao, C. Deng, D. C. Schwebel, and G. Hu, "Unsafe riding behaviors of shared-bicycle riders in urban China: a retrospective survey," *Accident Analysis & Prevention*, vol. 131, pp. 1–7, 2019.
- [13] X. Yan, M. Ma, H. Huang, M. Abdel-Aty, and C. Wu, "Motor vehicle-bicycle crashes in Beijing: irregular maneuvers, crash patterns, and injury severity," *Accident Analysis & Prevention*, vol. 43, no. 5, pp. 1751–1758, 2011.
- [14] J.-K. Kim, S. Kim, G. F. Ulfarsson, and L. A. Porrello, "Bicyclist injury severities in bicycle-motor vehicle accidents," *Accident Analysis & Prevention*, vol. 39, no. 2, pp. 238–251, 2007.
- [15] N. Eluru, C. R. Bhat, and D. A. Hensher, "A mixed generalized ordered response model for examining pedestrian and bicyclist injury severity level in traffic crashes," *Accident Analysis & Prevention*, vol. 40, no. 3, pp. 1033–1054, 2008.
- [16] S. Boufous, L. de Rome, T. Senserrick, and R. Ivers, "Risk factors for severe injury in cyclists involved in traffic crashes in Victoria, Australia," *Accident Analysis & Prevention*, vol. 49, pp. 404–409, 2012.
- [17] E. Robartes and T. D. Chen, "The effect of crash characteristics on cyclist injuries: an analysis of Virginia automobile-bicycle crash data," *Accident Analysis & Prevention*, vol. 104, pp. 165–173, 2017.
- [18] C. N. Morrison, J. Thompson, M. C. Kondo, and B. Beck, "On-road bicycle lane types, roadway characteristics, and risks for bicycle crashes," *Accident Analysis & Prevention*, vol. 123, pp. 123–131, 2019.
- [19] C. Chen, J. C. Anderson, H. Wang, Y. Wang, R. Vogt, and S. Hernandez, "How bicycle level of traffic stress correlate with reported cyclist accidents injury severities: a geospatial and mixed logit analysis," *Accident Analysis & Prevention*, vol. 108, pp. 234–244, 2017.
- [20] M. C. Kondo, C. Morrison, E. Guerra, E. J. Kaufman, and D. J. Wiebe, "Where do bike lanes work best? A bayesian spatial model of bicycle lanes and bicycle crashes," *Safety Science*, vol. 103, pp. 225–233, 2018.
- [21] J. Klassen, K. El-Basyouny, and M. T. Islam, "Analyzing the severity of bicycle-motor vehicle collision using spatial mixed logit models: a City of Edmonton case study," *Safety Science*, vol. 62, pp. 295–304, 2014.
- [22] J. Yuan and M. Abdel-Aty, "Approach-level real-time crash risk analysis for signalized intersections," *Accident Analysis & Prevention*, vol. 119, pp. 274–289, 2018.
- [23] Y. Wang and N. L. Nihan, "Estimating the risk of collisions between bicycles and motor vehicles at signalized intersections," *Accident Analysis & Prevention*, vol. 36, no. 3, pp. 313–321, 2004.
- [24] Y. Guo, Z. Li, Y. Wu, and C. Xu, "Exploring unobserved heterogeneity in bicyclists' red-light running behaviors at different crossing facilities," *Accident Analysis & Prevention*, vol. 115, pp. 118–127, 2018.
- [25] Z. Cheng, Z. Zu, and J. Lu, "Traffic crash evolution characteristic analysis and spatiotemporal hotspot identification of

- urban road intersections,” *Sustainability*, vol. 11, no. 1, pp. 1–17, 2019.
- [26] B. Yu, S. Bao, Y. Chen, and Y. Chen, “Using 3D mobile mapping to evaluate intersection design through drivers’ visual perception,” *IEEE Access*, vol. 7, pp. 19222–19231, 2019.
- [27] D. N. Moore, W. H. Schneider, P. T. Savolainen, and M. Farzaneh, “Mixed logit analysis of bicyclist injury severity resulting from motor vehicle crashes at intersection and non-intersection locations,” *Accident Analysis & Prevention*, vol. 43, no. 3, pp. 621–630, 2011.
- [28] C. Wang, L. Lu, and J. Lu, “Statistical analysis of bicyclists’ injury severity at unsignalized intersections,” *Traffic Injury Prevention*, vol. 16, no. 5, pp. 507–512, 2015.
- [29] Y. Wu, M. Abdel-Aty, O. Zheng, Q. Cai, and L. Yue, “Developing a crash warning system for the bike lane area at intersections with connected vehicle technology,” *Transportation Research Record: Journal of the Transportation Research Board*, vol. 2673, no. 4, pp. 47–58, 2019.
- [30] K. Wang and G. Akar, “The perceptions of bicycling intersection safety by four types of bicyclists,” *Transportation Research Part F: Traffic Psychology and Behaviour*, vol. 59, pp. 67–80, 2018.
- [31] Q. Zeng, W. Hao, J. Lee et al., “Investigating the impacts of real-time weather conditions on freeway crash severity: a bayesian spatial analysis,” *International Journal of Environmental Research and Public Health*, vol. 17, no. 8, pp. 1–15, 2020.
- [32] F. Chen, M. Song, and X. Ma, “Investigation on the injury severity of drivers in rear-end collisions between cars using a random parameters bivariate ordered probit model,” *International Journal of Environmental Research and Public Health*, vol. 16, no. 14, pp. 1–12, 2019.
- [33] R. Marcoux, S. Yasmin, N. Eluru, and M. Rahman, “Evaluating temporal variability of exogenous variable impacts over 25 years: an application of scaled generalized ordered logit model for driver injury severity,” *Analytic Methods in Accident Research*, vol. 20, pp. 15–29, 2018.
- [34] R. Williams, “Understanding and interpreting generalized ordered logit models,” *The Journal of Mathematical Sociology*, vol. 40, no. 1, pp. 7–20, 2016.
- [35] F. Chen, S. Chen, and X. Ma, “Analysis of hourly crash likelihood using unbalanced panel data mixed logit model and real-time driving environmental big data,” *Journal of Safety Research*, vol. 65, pp. 153–159, 2018.
- [36] B. Dong, X. Ma, F. Chen, and S. Chen, “Investigating the differences of single-vehicle and multivehicle accident probability using mixed logit model,” *Journal of Advanced Transportation*, vol. 2018, Article ID 2702360, 6 pages, 2018.

Research Article

Traffic Incident Clearance Time Prediction and Influencing Factor Analysis Using Extreme Gradient Boosting Model

Jinjun Tang,¹ Lanlan Zheng,¹ Chunyang Han,¹ Fang Liu ,² and Jianming Cai ¹

¹Smart Transport Key Laboratory of Hunan Province, School of Traffic and Transportation Engineering, Central South University, Changsha 410075, China

²School of Transportation Engineering, Changsha University of Science and Technology, Changsha 410205, China

Correspondence should be addressed to Fang Liu; rcliufang@163.com and Jianming Cai; jmcai@csu.edu.cn

Received 27 January 2020; Accepted 18 May 2020; Published 9 June 2020

Academic Editor: Feng Chen

Copyright © 2020 Jinjun Tang et al. This is an open access article distributed under the Creative Commons Attribution License, which permits unrestricted use, distribution, and reproduction in any medium, provided the original work is properly cited.

Accurate prediction and reliable significant factor analysis of incident clearance time are two main objects of traffic incident management (TIM) system, as it could help to relieve traffic congestion caused by traffic incidents. This study applies the extreme gradient boosting machine algorithm (XGBoost) to predict incident clearance time on freeway and analyze the significant factors of clearance time. The XGBoost integrates the superiority of statistical and machine learning methods, which can flexibly deal with the nonlinear data in high-dimensional space and quantify the relative importance of the explanatory variables. The data collected from the Washington Incident Tracking System in 2011 are used in this research. To investigate the potential philosophy hidden in data, *K*-means is chosen to cluster the data into two clusters. The XGBoost is built for each cluster. Bayesian optimization is used to optimize the parameters of XGBoost, and the MAPE is considered as the predictive indicator to evaluate the prediction performance. A comparative study confirms that the XGBoost outperforms other models. In addition, response time, AADT (annual average daily traffic), incident type, and lane closure type are identified as the significant explanatory variables for clearance time.

1. Introduction

According to Lindley [1], traffic incidents result in about 60% of nonrecurrent traffic congestions. These congestions may cause lots of adverse effects such as reducing the roadway capacity, increasing the likelihood of secondary incidents [2], and unfavorable social and economic phenomenon [3]. When a traffic incident occurred, timely and reliable incident duration prediction plays an important role in the traffic authorities to design strategy for traffic guidance. In terms of Highway Capacity Manual, there are four phases in traffic incident duration [4]: detection time (the time from incident occurrence to detection), response time (the time from incident detection to verification), clearance time (the time from incident verification to clearance), and recovery time (the time from incident clearance to the normal traffic condition). Severe incidents that are not cleared in time may lead to a twice even three times incident duration [5]. Compared to other phases, clearance time is

the most important and time-consuming phase in the time incident process. Thus, the aims of this paper are to effectively predict the clearance time and investigate the significant influencing factors of clearance time.

Over the past few decades, a large number of works have been undertaken to predict the incident duration time. These approaches can be mainly categorized into statistical approaches and machine learning approaches. Statistical methods have their own model assumptions and predefined underlying relationships between dependent and independent variables [6] which provide the explainable ability to statistical methods. The widely used statistical methods are summarized as follows: probabilistic distribution analyses method [7, 8], regression method [9–13], discrete choice method [14], structure equation method [15], hazard-based duration method [16], Cox proportional hazards regression method [17–19], and accelerated failure time method [20–23]. Unlike statistical methods, machine learning methods are based on a more flexible mapping process that

requires no or less prior hypothesis. And flexible mapping allows machine learning methods to handle the nonlinear data in the high-dimensional space, but it cannot explore the potential relationship between dependent variables and independent variables. These widely used machine learning methods are categorized as K -nearest neighborhood method [24–27], support vector machine method [26–28], Bayesian networks method [29–34], artificial neural networks method [2, 35–37], genetic algorithm [37, 38], tree-based method [25, 39–41], and hybrid method [42].

In summary, conventional incident clearance time prediction studies rely on either statistical models with prior assumptions or machine learning models with poor interpretability [43]. To solve the abovementioned issues, we apply the extreme gradient boosting machine (XGBoost) method to predict the clearance time and then investigate the significant influencing factors of traffic incident clearance time. Because the XGBoost inherits both the advantages of statistical models and machine learning models, which can handle the nonlinear high-dimensional data when computing the relative importance among variables.

In this study, the prediction performance of XGBoost is examined by using the data from the Washington Incident Tracking System in 2011. In order to better explore the potential philosophy hidden in the original data, we cluster the original data in terms of their inherent properties. And then XGBoost model is built for each cluster. The framework of the proposed method is detailed in Section 3.5.

The remaining of this research is organized as follows. The data source is described in Section 2. Section 3 presents the K -means algorithm, the XGBoost algorithm, the Bayesian optimization algorithm, evaluation indicator, and the framework of the proposed method. The model results and discussion are outlined in Section 4. The last section is the conclusion.

2. Data Description

Traffic incident data were collected from the Washington Incident Tracking System (WITS), which occurred on the section from Boeing Access Road (Milepost 157) to the Seattle Central Business District (Milepost 165). This segment is not only a high incident-occurrence area but also takes on heavy traffic demand [44]. Therefore, it was chosen as the research object. And the annual average daily traffic (AADT) comes from the Highway Safety Information System (HSIS) database. The historical weather data were obtained from the National Oceanic and Atmospheric Administration (NOAA)'s weather stations in the region. The components of the data are detailed in Table 1. There are 14 discrete explanatory variables and 2 continuous explanatory variables in this dataset. In terms of their properties, they are divided into six categories: incident, temporal, geographical, environment, traffic, and operational. The detailed value sets of variables are presented as the third column in Table 1. In order to equalize the variability of independent variables, both response time and AADT variables are normalized [41, 43–46].

Totally, 2565 incident records were retrieved from the WITS database for the time period from 1 January to 31 December 2011. The mean and standard values of clearance time are, respectively, 13.10 minutes and 14.63 minutes. A big standard value (14.63 min) means that most of the clearance time values are quite different from their average values. That is, the original data should be processed to make the data organized well.

3. Methodology

3.1. K -Means Algorithm. K -means algorithm, developed by MacQueen [47], is one of the widely used methods in the field of dataset clustering. Samples in the dataset with similar characteristics can be clustered into the same class by using K -means [48]. The data we used in this research are expressed as $\{x_i = [x_{i1}, x_{i2}, \dots, x_{im}], y_i\}$, $i = 1, 2, 3, \dots, n$ and n represents the number of incidents, m is the number of explanatory variables, and the y denotes the actual clearance time. The detailed steps of the K -means algorithm are presented as follows:

Step 1: assuming the number of clusters (K clusters) and choosing the cluster centers from the dataset randomly.

Step 2: determining the clusters of other samples by the distance function as

$$x_i \in C_a, \quad \text{if } |x_i - O_a| < |x_i - O_b|. \quad (1)$$

Here, the O_a and O_b are the centers of the cluster a and cluster b , and C_a denotes the cluster a .

Step 3: after all samples have been clustered, the new center of each cluster should be calculated by using the following equation:

$$O_j = \frac{\sum_{i \in C_a} x_i}{N_C}, \quad j = 1, 2, 3, \dots, K, \quad (2)$$

where N_C is the number of the samples in cluster j .

Step 4: repeating step 2 and step 3 until the center of the cluster is within the permission.

Accordingly, we can find that the value of K and the cluster center are important to the clustering performance, as the clustering of K -means is extremely dependent on the selection of initial cluster center and the number of K . To obtain a reasonable K , we use the silhouette coefficient as the evaluation index, which is proposed by Rousseeuw [49] and defined as follows:

$$s(i) = \begin{cases} 1 - \frac{a(i)}{b(i)}, & \text{if } a(i) < b(i), \\ 0, & \text{if } a(i) = b(i), \\ \frac{b(i)}{a(i)} - 1, & \text{if } a(i) > b(i). \end{cases} \quad (3)$$

TABLE 1: Description of explanatory variables for clearance time.

Category	Variable	Value set
	Response time	R+
		0 = others
		1 = disabled
	Incident type	2 = debris
		3 = abandoned vehicle
		4 = collision
		0 = others
Incident	Lane closure type	1 = single lane
		2 = multiple lane
		3 = all travel lane
		4 = total lane
	Injury involved	0 = no; 1 = yes
	Fire involved	0 = no; 1 = yes
	Work zone involved	0 = no; 1 = yes
	Heavy truck involved	0 = no; 1 = yes
	Time of day	0 = daytime; 1 = night (22:00–6:00)
Temporal	Day of week	0 = weekdays; 1 = weekends
		0 = other seasons
	Month of year	1 = summer (Jun, Jul, and Aug)
		2 = winter (Dec, Jan, and Feb)
Geographic	HOV	0 = no; 1 = yes
		0 = others
Environment	Weather	1 = rainy
		2 = snowy
Traffic	Peak hours (6:00–9:00, 15:00–18:00)	0 = no; 1 = yes
	AADT	R+
Operational	Traffic control	0 = no; 1 = yes
	Washington State Patrol (WSP) involved	0 = no; 1 = yes

Here, the $a(i)$ is the average distance between sample i and other samples within the same cluster, and the $b(i)$ is the lowest average distance of sample i to all the remaining samples.

3.2. Extreme Gradient Boosting Machine Algorithm. Chen and Guestrin [50] proposed the extreme gradient boosting machine (XGBoost) algorithm. It is regarded as the advanced application of gradient boosting machine (GBDT) and adopts decision trees as the base learners for achieving classification and regression. Boosting is the integrated approach that can adjust the predicted error of the current model by adding new models to the model [41]. The predicted result of the boosting model is the sum scores of all models. Accordingly, the prediction of XGBoost is the sum scores of K boosted trees and is shown in the following equation:

$$\hat{y}_i = \varnothing(x_i) = \sum_{k=1}^K f_k(x_i), \quad f_k \in F, \quad (4)$$

where x_i is the i^{th} sample, $f_k(x_i)$ is the score of x_i at the i^{th} boosted tree, and F is the space composed of boosted trees. To decrease the fitting error of XGBoost, there is an improvement in regulation compared to GBDT, and it is presented as follows:

$$\text{obj}(\Theta) = \sum_{i=1}^n l(y_i, \hat{y}_i) + \sum_k \Omega(f_k), \quad (5)$$

where y_i and \hat{y}_i are the actual and predicted values of the i^{th} sample, the former item is the loss function, which needs to be a differentiable convex function, and the latter item is the penalty corresponding to the model complexity for avoiding overfitting. The second item of equation (5) can be detailed as follows:

$$\Omega(f) = \gamma T + \frac{1}{2} \lambda \sum_{j=1}^T w_j^2, \quad (6)$$

where both γ and λ are constants, T denotes the sum number of leaves, and w_j is the score of j^{th} leaf. When equation (6) equals zero, the $\text{obj}(\Theta)$ will convert to the conventional formula of GBDT.

According to equations (5) and (6), the training error and the model complexity are the two main sections of XGBoost. When the previous trees have been trained, the current tree can be trained by using additive training method. It means that when the t^{th} boosted tree is trained, the parameters of the previous trees (from the first tree to the $(t-1)^{\text{th}}$ tree) are fixed and their corresponding variables are constant. Taking the t^{th} boosted tree as an example, the loss can be expressed as follows:

$$\text{obj}(\Theta)^t = \sum_{i=1}^n l(y_i, \hat{y}_i^t) + \sum_{t=1}^T \Omega(f_t). \quad (7)$$

There are two formulas in these two items of (7):

$$\hat{y}_i^t = \hat{y}_i^{(t-1)} + f_t(x_i), \quad (8)$$

$$\sum_{t=1}^T \Omega(f_t) = \left(\sum_{k=1}^{T-1} \Omega(f_k) \right) + \Omega(f_t). \quad (9)$$

The first items of equations (8) and (9) are the sum score and sum regulation of former $(t-1)^{\text{th}}$ trees and the second items of them are the score and regulation of the t^{th} boosted tree, \hat{y}_i^t is the predicted value of the t^{th} iteration, and $\sum_{t=1}^T \Omega(f_t)$ is the regulation of t^{th} iteration.

Equations (8) and (9) are substituted into equation (7), and then equation (7) is expanded by using the following Taylor formula:

$$f(x + \Delta x) \approx f(x) + f'(x)\Delta x + \frac{1}{2}f''(x)\Delta x^2. \quad (10)$$

The $\hat{y}_i^{(t-1)}$ is considered as x and the $f_t(x_i)$ is regarded as Δx . Then, equation (7) is transformed as follows:

$$\begin{aligned} \text{obj}(\Theta)^t &= \sum_{i=1}^n l(y_i, \hat{y}_i^{(t-1)} + f_t(x_i)) + \Omega(f_t) + \text{constant} \\ &\approx \sum_{i=1}^n \left[l(y_i, \hat{y}_i^{(t-1)}) + g_i f_t(x_i) + \frac{1}{2} h_i (f_t(x_i))^2 \right] \\ &\quad + \Omega(f_t) + \text{constant} \\ &= \sum_{i=1}^n \left[g_i f_t(x_i) + \frac{1}{2} h_i (f_t(x_i))^2 \right] + \Omega(f_t) + \text{constant}. \end{aligned} \quad (11)$$

As Chen and Guestrin [50] suggested, $f_t(x)$ can also be written as

$$f_t(x) = \omega_{q(x)}, \quad \omega \in R^K, q: R^d \longrightarrow \{1, 2, \dots, d\}, \quad (12)$$

where $q(x)$ is the leaf node of x , the $\omega_{q(x)}$ indicates the weight of $q(x)$ or that can be considered as the predicted value of the t^{th} iteration, and d is the number of leaf nodes. Then, equation (11) can be expressed as follows:

$$\begin{aligned} \text{obj}(\Theta)^t &= \sum_{i=1}^n \left[g_i \omega_{q(x_i)} + \frac{1}{2} h_i (\omega_{q(x_i)})^2 \right] \gamma T \\ &\quad + \frac{1}{2} \lambda \sum_{j=1}^T w_j^2 + \text{constant} \\ &= \sum_{j=1}^T \left[\left(\sum_{i \in I_j} g_i \right) w_j + \frac{1}{2} \left(\sum_{i \in I_j} h_i + \lambda \right) w_j^2 \right] \\ &\quad + \gamma T + \text{constant}, \end{aligned} \quad (13)$$

where g_i and h_i are the first order and second order of gradient statistics. When the $q(x)$ is fixed, the optimal leaf weight and the metric function can be used to measure the quality of the tree structure $q(x)$ can be calculated:

$$w_j^* = \frac{\sum_{i \in I_j} g_i}{\sum_{i \in I_j} h_i + \lambda}, \quad (14)$$

$$\text{obj}(q) = -\frac{1}{2} \sum_{j=1}^T \frac{\left(\sum_{i \in I_j} g_i \right)^2}{\sum_{i \in I_j} h_i + \lambda} + \gamma T.$$

3.3. Bayesian Optimization Algorithm. Bayesian optimization algorithm (BOA), one of the most famous extendible applications of the Bayesian network, is based on the construction of the probabilistic model. This model defines the distribution of objective function from the input data to output data. In this Bayesian optimization process, the global statistical characteristics are obtained from the optimal solutions and modeled by using the Bayesian network [51]. That is why the BOA shows its advantage in machine learning models because these machine learning models need more accurate parameters to flexibly handle nonlinear high-dimensional data [52]. In this study, the BOA is applied to optimize the parameters in the XGBoost with the aim to accurately predict the traffic incident clearance time.

The accomplishment of Bayesian optimization includes two core parts: prior function (PF) and acquisition function (AC), which is also called the utility function [51]. Gaussian process (GP) is generally considered as the PF. And the AC is used to balance the model exploration and exploitation. The framework of Bayesian optimization is presented in Figure 1 and the main steps are described as follows: (1) The data is split into training data and validation data by using the k -fold cross-validation method. Initialization parameters of the target model are defined as $\{\theta_1, \theta_2, \dots, \theta_n\}$. (2) The accuracy of the target model with initial parameters is evaluated by using validation data, and then the accuracy is recorded. The goal of the optimization is to minimize validation accuracy. (3) Gaussian process (GP) is employed to fit the recorded accuracy. (4) The parameters of the target model are updated in terms of the result of GP. Then, the maximum value of AC is used to select the next point, as it achieves the optimization by determining the next point to evaluate. Probability of improvement, expected improvement, and information gain are the three widely used AC [51]. In this study, expected improvement is chosen as the AC. Then, the best validation accuracy is mathematically written as follows:

$$\alpha(\theta, \text{GP}) = \int_{-\infty}^{\infty} \max(L - L^*, \text{GP}) P_{\text{GP}}(L | \theta) dL, \quad (15)$$

where L is the validation accuracy and $P_{\text{GP}}(L | \theta)$ is the probability of L with θ that is executed by using GP.

3.4. Evaluation Indicator. In general, the mean absolute percent error (MAPE) is a commonly used predictive indicator to evaluate the prediction performance of the regressive model. As mentioned above, the data are described as $\{x_i = [x_{i1}, x_{i2}, \dots, x_{im}], y_i\}$, $i = 1, 2, 3, \dots, n$, that can be considered as a matrix with the size of $n * m$. Specifically, n is

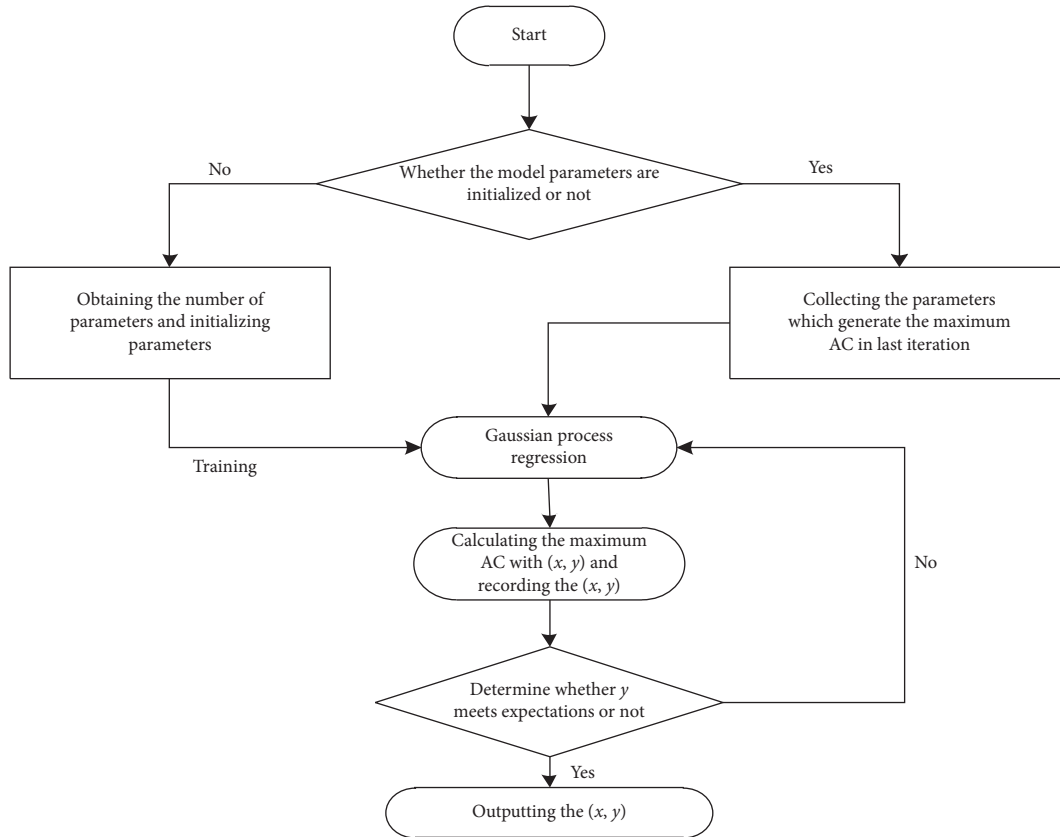


FIGURE 1: Parameter-tuning process of Bayesian optimization.

the number of incidents and y_i represents the actual value of the i^{th} incident. Considering p_i is the predicted value of the i^{th} incident. Then, the MAPE is expressed as follows:

$$\text{MAPE} = \frac{\sum_{i=1}^n |(y_i - p_i)/y_i|}{n} \times 100\%. \quad (16)$$

In terms of this formula, the MAPE is a relative predictive indicator that can measure the prediction performance of the models based on actual values and predicted values.

3.5. Framework of the Proposed Method. As introduced in Section 2, we need a suitable way to handle the original dataset to organize the dataset well for exploring the potential philosophy hidden in data easier. To this end, in this research, we select the K -means algorithm as the method to cluster the original dataset into several categories in which the data are high similarity. Then, the XGBoost model is built for each category to perform prediction. The main steps of the proposed method are introduced as follows:

Step 1: clustering the original data into several categories by using the K -means algorithm. The number of clusters is determined by the optimal silhouette coefficient (the detailed information is introduced in Section 3.1).

Step 2: splitting the clustered data into training data and testing data for each category. Using the training data to construct the XGBoost model.

Step 3: the BOA is used to optimize parameters for each constructed XGBoost model.

Step 4: inputting the testing data into the trained XGBoost, and then the predicted clearance time will be output and recorded.

Step 5: calculating the predictive indicator (MAPE) and the relative importance of explanatory factors

Noting that with the number of traffic incidents increasing, the dataset will be updated continuously, and thus the XGBoost should be retrained.

4. Prediction Result and Discussion

There are two objects of this study: (a) examining the performance of the XGBoost model in predicting clearance time and (b) investigating the significant factors of clearance time. We firstly process the original data, including data clustering, and clustering evaluation. Next, the data are split into training data and testing data with a ratio of 7:3. The XGBoost is trained by using training data, and the testing data are used for model evaluation. Then, comparison research examines the prediction performance of XGBoost. MAPE is chosen as a predictive measure. Finally, the relative importance of all the explanatory variables is calculated, and the significant explanatory variables of incident clearance time are analyzed. Overall, the proposed model is accomplished by coding and executing at Python.

4.1. Data Preprocessing. Before modeling, the original dataset has been processed by means of the K -means algorithm. As described in Section 3.1, the number of clusters (K) is the key parameter of the K -means algorithm. To find the best K , the values of K increasing from 2 to 10 are selected to calculate the corresponding silhouette coefficient, and the results are shown in Table 2. Assuming the iteration stops when the silhouette coefficients for continuous 5 iterations are not improved. The iteration stops when $K=7$, as the silhouette coefficients of continuous 5 iterations are decreasing. In terms of equation (3), a higher silhouette coefficient indicates a better clustering performance. According to Table 2, when $K=2$, the silhouette coefficient reaches the biggest value (0.613), which means K is set as 2 in this study. In this case, the original data are clustered into two clusters in this study. To present each cluster clearly, we draw the scatter plots of the target variable and one of the explanatory variables (which is chosen randomly), shown in Figure 2. The x -axis is clearance time and the y -axis denotes the response time. Figure 2(a) shows the scatter plot of these two variables in the original data, while Figure 2(b) shows the scatter plot of the clustered data. As shown in Figure 2(b), the cluster 1 marked with purple represents relative shorter clearance time, and cluster 2 marked with yellow indicates longer clearance time.

In order to knowledge the characteristic of two clusters clearly, several essential indexes are calculated and presented in Table 3. In total, there are 2246 incidents in cluster 1 and 319 incidents in cluster 2. Regarding cluster 1, the mean, standard, median, and range values of clearance time are 9 minutes, 5.44 minutes, 7.00 minutes, and 22 minutes. In respect to cluster 2, these values, respectively, are 39.25 minutes, 15.25 minutes, 35 minutes, and 75 minutes. Compared median value to mean value within each cluster, we can find that median values are, respectively, bigger than mean values for both two clusters. The result indicates that the distributions of clearance time in two clusters are skewed, instead of normal distribution. Then, we calculate the skew values of two clearance time distributions, and they are 0.92 in cluster 1 and 1.59 in cluster 2. Both of them present right-skewed, which are consistent with previous studies [26, 39, 41]. Distribution figures of clearance time in two clusters are shown in Figures 3(a) and 3(b).

Both Figures 3(a) and 3(b) present long-tail distributions with the range values of 22 and 75. It is difficult to handle the data with such a wide value range [53]. In this case, in order to make the distribution of clearance time closer to the normal distribution, we use data transformation to deal with clearance time data in two clusters. Regarding cluster 1, the skew value of clearance time is 0.92 which is between 0.5 and 1, indicating the median skewed. Therefore, according to the empirical method, we apply the square transformation to handle clearance time in cluster 1. In respect to cluster 2, the skewed value is 1.59 which is larger than 1, leading to a highly skewed. The log transformation is used to convert clearance time in cluster 2. Distributions of transformed clearance time are presented in Figures 3(c) and 3(d). In Figure 3, the blue line is the fitting curve of clustered data and the black line denotes the normal distribution curve

TABLE 2: Corresponding silhouette coefficient of each K .

K	2	3	4	5	6	7
Silhouette coefficient	0.613	0.447	0.422	0.418	0.396	0.352

which is fitted by their calculated mean and standard values. As shown in Figures 3(c) and 3(d), the distributions of transformed data are closer to normal distribution.

4.2. Parameter Optimization. In general, there are three approaches to optimize parameters, including the systematic grid search approach, the random search approach, and the Bayesian optimization approach. The grid search approach works well as it systematically searches the entire search space, but time-consuming. In contrast, the random search approach runs fast while it may miss the best value as it searches randomly in the search space. Bayesian optimization is the process of continuously sampling, calculating, and updating the model. In overall, we apply the Bayesian optimization method to find the optimal parameters in XGBoost. These parameters include max depth of the tree (`max_depth`), the number of trees (`n_estimators`), the learning rate of the tree (`learning_rate`), percent of randomly sampling for trees (`subsample`), sum of minimum leaf node sample weights (`min_child_weight`), and percentage of randomly sampled features (`colsample_bytree`). The increasing of `n_estimators` may improve the accuracy of XGBoost but increase the computing time too. The `max_depth` is used to avoid overfitting. In contrast, the larger `min_child_weight` will result in underfitting. Both `subsample` and `min_child_weight`, respectively, denote the row and column sampling. The meaning of the learning rate is identified to avoid overfitting and increase the robustness of the model [54]. Therefore, all these parameters should be optimal for achieving the best model performance.

The Bayesian optimization is packaged in a module of python, called Hyperopt [55]. The objective function (`f_min`), search space (`space`), optimal algorithm (`algo`), and the maximum numbers of evaluations (`max_evals`) are four main objects of the Hyperopt, which is used to accomplish BOA. In this research, the XGBoost is the `f_min`, tree of Parzen estimator defaults as the `algo`, and the `max_evals` is generally set as 4. Regarding search space, we set `n_estimators` \in [50, 500], `learning_rate` \in [0.05, 0.1], `max_depth` \in [2, 10], `subsample` \in [0.1, 0.9], `colsample_bytree` \in [0.1, 0.9], and `min_child_weight` \in [2, 12]. In addition, we use 5-fold cross-validation during parameter tuning, and the result is shown in Table 4.

Regarding cluster 1, the `n_estimators`, `learning_rate`, `max_depth`, `subsample`, `colsample_bytree`, and `min_child_weight` are, respectively, set as 140, 0.09, 6, 0.5, 0.7, and 3. In respect to cluster 2, the best prediction performance of XGBoost is obtained when the `n_estimators`=100, the `learning_rate`=0.05, the `max_depth`=5, the `subsample`=0.5, the `colsample_bytree`=0.3, and the `min_child_weight`=5. The XGBoost model reaches its best prediction performance when using these optimal parameters. And the MAPE values of optimized XGBoost for two clusters are 0.348 and 0.221, respectively.

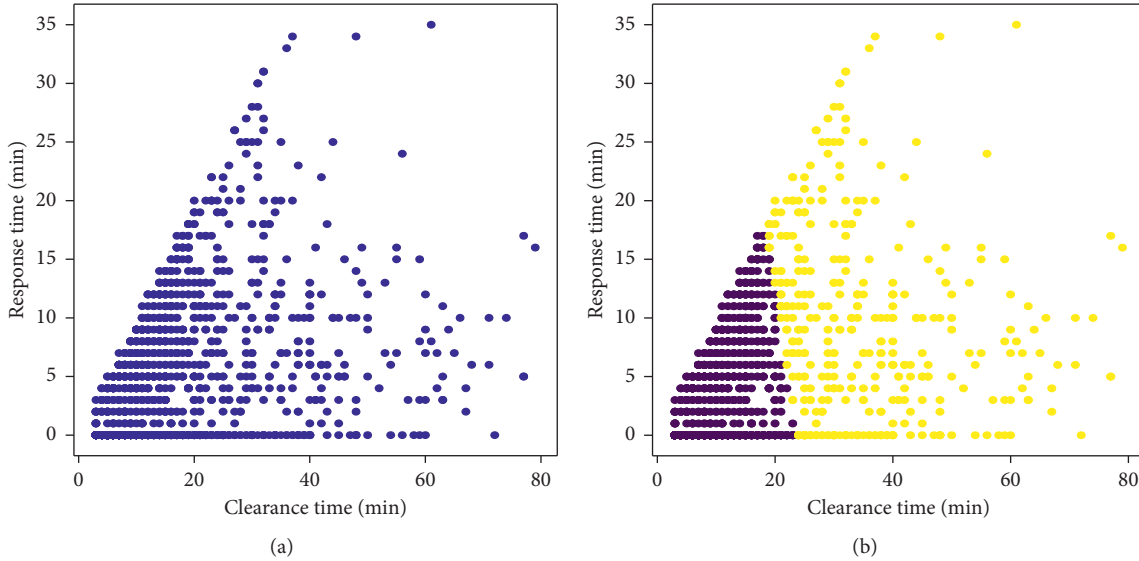


FIGURE 2: Scatter plots of data. (a) Scatter plot of the original dataset. (b) Scatter plot of the clustered dataset.

TABLE 3: Statistical characteristics of clearance time.

Cluster	1	2
Count	2246.00	319.00
Mean	9.00	39.25
Standard	5.44	15.25
Min	3.00	21.00
25%	5.00	29.00
Median	7.00	35.00
75%	12.00	45.00
Max	25.00	96.00
Skew	0.92	1.59
Range	22.00	75.00

4.3. Comparison Analysis. To examine the prediction performance of XGBoost in clearance time prediction, we select several commonly used models including support vector regression (SVR) model, random forest (RF) model, and Adaboost model for comparison. To ensure fair comparison, the testing data and the parameter-tuning method (BOA) of all models are the same. For the SVR model, we select the radial basis function (RBF) as the kernel function. The gamma and penalty C are two key parameters of RBF and are set as 0.1, 64, and 0.15, 32 for two clusters. For the RF model, the number of trees ($n_{estimators}$), the maximum depth of the tree (max_depth), the minimum number of samples of internal node splitting ($min_samples_split$), and the minimum number of leaf nodes ($min_samples_leaf$) are the four key parameters, and they are set as 195, 8, 11, and 23 in the cluster 1 and 100, 13, 18, and 12 in the cluster 2. In regard to the Adaboost model, the same with RF model, $n_{estimators}$, max_depth , and $min_samples_split$ should be identified. In addition, the $learning_rate$ and the maximum features in splitting ($max_features$) also need to be optimized. These parameters of Adaboost in two clusters are set as 470, 6, 25, 0.05, 7 and 425, 9, 30, 0.11. The MAPE for four candidates is shown in Table 5, and the smallest values for two clusters are marked in bold.

As shown in Table 5, for cluster 1, the MAPE values of XGBoost, SVR, RF, and Adaboost are 0.348, 0.363, 0.357, and 0.383. The XGBoost represents the smallest MAPE, showing its superiority in clearance time prediction for cluster 1. As for cluster 2, the MAPE values of XGBoost, SVR, RF, and Adaboost are 0.221, 0.253, 0.228, and 0.231. Compared to other models, the XGBoost represents the smallest MAPE (0.221). It means the XGBoost model outperforms SVR, RF, and Adaboost in both two clusters. This result confirms the superiority of XGBoost in clearance time prediction.

4.4. Importance Evaluation for Explanatory Factors. Different explanatory variables have different effects on the target factor [56, 57]. To investigate the significant factors of clearance time, the relative importance of each explanatory factor is calculated by using the XGBoost with optimal parameters for two clusters. An explanatory factor with higher relative importance means that it generates a stronger effect on clearance time [41]. In this study, we assume that factors with relative importance greater than 8.0% are defined as significant explanatory factors, the relative importance of the general factor is from 2.5% to 8.0%, and the remaining explanatory factors are considered as insignificant factors. In this case, the explanatory factors with its importance are shown in Table 6.

As for cluster 1, AADT (17.70%), incident type (17.30%), response time (15.10%), and lane closure type (8.00%) are categorized into the significant explanatory factors of clearance time as their relative importance is bigger than 8.00%. The general factors of clearance time include six explanatory factors, such as WSP involved (7.60%), month of year (6.10%), traffic control (5.00%), weather (4.70%), day of week (4.60%), and peak hours (3.10%). And the remaining HOV (2.50%), time of day (2.10%), heavy truck involved (1.70%), injury involved (1.70%), and work zone involved

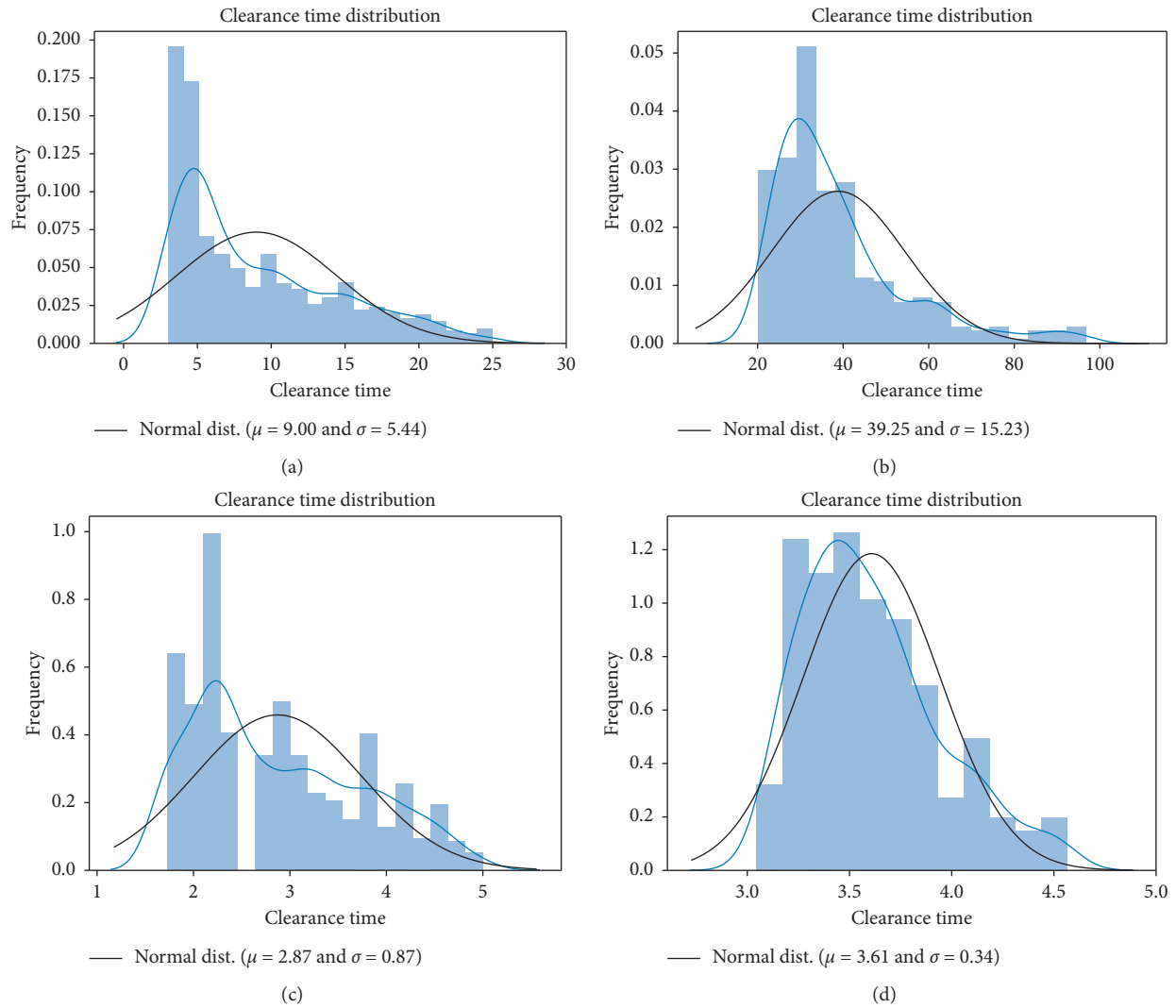


FIGURE 3: Distributions of clearance time. (a) Original clearance time distribution of cluster 1. (b) Original clearance time distribution of cluster 2. (c) Log-transformed clearance time distribution of cluster 1. (d) Square-transformed clearance time distribution of cluster 2.

TABLE 4: The optimal parameters in XGBoost.

Cluster	1	2
$n_estimators$	140	100
$learning_rate$	0.09	0.05
max_depth	6	5
$subsample$	0.5	0.5
$colsample_bytree$	0.7	0.3
min_child_weight	3	5

(0.30%) are regarded as the insignificant explanatory variables in cluster 1. Regarding cluster 2, four explanatory factors are included in significant explanatory factors to clearance time, including AADT (14.00%), incident type (12.8%), response time (22.30%), and lane closure type (8.40%). And fire involved (8.40%), weather (6.10%), month of year (6.10%), traffic control (6.10%), injury involved (5.00%), and HOV (2.80%) are the general explanatory factors. Peak hours (2.20%), heavy truck involved (2.20%),

TABLE 5: Prediction results for different models.

Cluster	XGBoost	SVR	RF	Adaboost
1	0.348	0.363	0.357	0.383
2	0.221	0.253	0.228	0.231

WSP involved (1.70%), day of week (1.10%), time of day (0.60%), and work zone involved (0.20%) are categorized into insignificant explanatory factors to incident clearance time.

That is, for both two clusters, AADT, incident type, response time, and lane closure type are considered as the significant explanatory factors of clearance time. But the same factor may generate varying impacts on clearance time in the different datasets [58]. In detail, the AADT is the greatest contribution to shorter clearance time in cluster 1 and generates the second impacts on longer clearance time in cluster 2 with the relative importance of 17.70% and 14.00%, respectively. Generally speaking, AADT represents

TABLE 6: Relative importance of explanatory factors on clearance time.

Cluster		1		2	
Rank	Variable	Relative importance (%)	Variable	Relative importance (%)	
Significant explanatory factors	1	AADT	17.70	Response time	22.30
	2	Incident type	17.30	AADT	14.00
	3	Response time	15.10	Incident type	12.80
	4	Lane closure type	8.00	Lane closure type	8.40
General explanatory factors	5	WSP involved	7.60	Fire involved	8.40
	6	Month of year	6.10	Weather	6.10
	7	Traffic control	5.00	Month of year	6.10
	8	Weather	4.70	Traffic control	6.10
	9	Day of week	4.60	Injury involved	5.00
	10	Peak hours	3.10	HOV	2.80
Insignificant explanatory variables	11	HOV	2.50	Peak hours	2.20
	12	Fire involved	2.50	Heavy truck involved	2.20
	13	Time of day	2.10	WSP involved	1.70
	14	Heavy truck involved	1.70	Day of week	1.10
	15	Injury involved	1.70	Time of day	0.60
	16	Work zone involved	0.30	Work zone involved	0.20

the characteristic of current traffic [59, 60]. That is, the traffic congestion with a high AADT may make the incident difficult to clear, leading to longer clearance time. As for incident type, it respectively contributes 17.30% and 12.80% to short and long clearance time and ranks the second in cluster 1 and the third in cluster 2. As shown in Table 1, the incident type factor consists of disabled vehicles, debris, abandoned vehicles, collision, and others. These incidents may block normal traffic [61, 62]. In this case, the transportation authorities may make a series of strategies to deal with the problems caused by these incidents [63, 64]. Interestingly, the longer clearance time seems less sensitive to incident type than shorter clearance time. Maybe a long clearing time means a high severity of the crash. With the relative importance of 15.10% and 22.3%, the response time factor is the third contributor for shorter clearance time in cluster 1 and yields the biggest impacts on longer clearance time in cluster 2. The result shows that longer clearance time is more sensitive to response time compared to shorter clearance time, which is consistent with the previous studies [18, 19]. For every minute, the response time increases, and the clearing time will increase by one percent [18, 19]. The lane closure type factor is the fourth contributed factor for both two clusters. It indicates the severity of incidents by restricting vehicles from entering the incident site [41].

5. Conclusions

In this study, XGBoost is applied to predict incident clearance time that occurred on the freeway and investigates the significant factors of clearance time by using the data collected from the Washington Incident Tracking System in 2011. We firstly introduce the original data and the proposed method briefly. The original data are clustered by using the *K*-means algorithm for better exploring the underlying relationship. Then, we built the XGBoost model for each cluster. Each clustered data is divided into 70% training data and 30% testing data. Training data are applied for modeling XGBoost and optimizing parameters on the basis of 5-fold

cross-validation BOA. Testing data are used to measure the prediction performance of XGBoost. And the MAPE is considered as the predictive indicators in this paper. To examine the model performance of XGBoost, support vector regression (SVR), random forest (RF), and Adaboost are chosen to predict the clearance time. The comparing study manifests that the XGBoost outperforms the other three models with the lowest MAPE in both two clusters. To obtain the significant factors of clearance time, we calculate the relative importance of each explanatory factor and then define the quantitative indexes about significant explanatory factors, general explanatory factors, and insignificant explanatory factors. The result is that response time, AADT, incident type, and lane closure type are the significant explanatory factors of clearance time.

It is worth noting that the traffic incident is the time-sequential process [65]. And almost the incident information is acquired from that process [66]. Modeling based on the acquired incident information is the limitation of the proposed method in this study. Because, during the initial stage of the incident, the prediction may not be accurate due to the acquired information is incomplete. For future research, multistage updates of information should be a promising future research direction. In addition, strategies about dealing with the unobserved heterogeneity of dependent variables, especially in traffic incidents filed, may be a hot topic, due to some omitted variables (e.g., driving behavior) that may generate potential impacts on the target variable.

Data Availability

The traffic incident data used to support the findings of this study are available from the corresponding author and first author upon request.

Conflicts of Interest

The authors declare that there are no conflicts of interest regarding the publication of this paper.

Acknowledgments

This research was supported by the National Natural Science Foundation of China (71701215), Innovation-Driven Project of Central South University (no. 2020CX041), Foundation of Central South University (no. 502045002), Science and Innovation Foundation of the Transportation Department in Hunan Province (no. 201725), and Postdoctoral Science Foundation of China (nos. 2018M630914 and 2019T120716).

References

- [1] J. A. Lindley, "Urban freeway congestion: quantification of the problem and effectiveness of potential solutions," *IET Intelligent Transport Systems*, vol. 57, no. 1, pp. 27–32, 1987.
- [2] E. I. Vlahogianni, M. G. Karlaftis, and F. P. Orfanou, "Modeling the effects of weather and traffic on the risk of secondary incidents," *Journal of Intelligent Transportation Systems*, vol. 16, no. 3, pp. 109–117, 2012.
- [3] M. W. Adler, J. V. Ommeren, and P. Rietveld, "Road congestion and incident duration," *Economics of Transportation*, vol. 2, no. 4, pp. 109–118, 2013.
- [4] H. C. Manual, *Highway Capacity Manual*, National Research Council, Washington, DC, USA, 2000.
- [5] S. Madanat and A. Feroze, "Prediction models for incident clearance time for borman expressway," Final Report FHWA/IN/JHRP-96/10, Purdue University, West Lafayette, IN, USA, 1997.
- [6] L.-Y. Chang and H.-W. Wang, "Analysis of traffic injury severity: an application of non-parametric classification tree techniques," *Accident Analysis & Prevention*, vol. 38, no. 5, pp. 1019–1027, 2006.
- [7] T. F. Golob, W. W. Recker, and J. D. Leonard, "An analysis of the severity and incident duration of truck-involved freeway accidents," *Accident Analysis & Prevention*, vol. 19, no. 5, pp. 375–395, 1987.
- [8] G. Giuliano, "Incident characteristics, frequency, and duration on a high volume urban freeway," *Transportation Research Part A: General*, vol. 23, no. 5, pp. 387–396, 1989.
- [9] A. J. Khattak, J. L. Schofer, and M.-H. Wang, "A simple time sequential procedure for predicting freeway incident duration," *IVHS Journal*, vol. 2, no. 2, pp. 113–138, 1995.
- [10] A. Khattak, X. Wang, and H. Zhang, "Incident management integration tool: dynamically predicting incident durations, secondary incident occurrence and incident delays," *IET Intelligent Transport Systems*, vol. 6, no. 2, pp. 204–214, 2012.
- [11] A. J. Khattak, J. Liu, B. Wali, X. Li, and M. Ng, "Modeling traffic incident duration using quantile regression," *Transportation Research Record: Journal of the Transportation Research Board*, vol. 2554, no. 1, pp. 139–148, 2016.
- [12] A. Garib, A. E. Radwan, and H. Al-Deek, "Estimating magnitude and duration of incident delays," *Journal of Transportation Engineering*, vol. 123, no. 6, pp. 459–466, 1997.
- [13] S. Peeta, J. L. Ramos, and S. Gedela, "Providing real-time traffic advisory and route guidance to manage borman incidents on-line using the hoosier helper program. Joint transportation research program," FHWA/IN/JTRP-2000/15, Indiana Department of Transportation and Purdue University, West Lafayette, IN, USA, 2000.
- [14] P. W. Lin, N. Zou, and G. L. Chang, "Integration of a discrete choice model and a rule-based system for estimation of incident duration: a case study in Maryland," in *Proceedings of the CD-ROM of Proceedings of the 83rd TRB Annual Meeting*, Washington, DC, USA, 2004.
- [15] J. Y. Lee, J. H. Chung, and B. Son, "Incident clearance time analysis for Korean freeways using structural equation model," *Proceedings of the Eastern Asia Society for Transportation Studies*, vol. 7, pp. 1850–1863, 2010.
- [16] N. E. Breslow, "Analysis of survival data under the proportional hazards model," *International Statistical Review/Revue Internationale de Statistique*, vol. 43, no. 1, pp. 45–57, 1975.
- [17] D. S. Bennett, "Parametric models, duration dependence, and time-varying data revisited," *American Journal of Political Science*, vol. 43, no. 1, pp. 256–270, 1999.
- [18] J.-T. Lee and J. Fazio, "Influential factors in freeway crash response and clearance times by emergency management services in peak periods," *Traffic Injury Prevention*, vol. 6, no. 4, pp. 331–339, 2005.
- [19] L. Hou, Y. Lao, Y. Wang et al., "Time-varying effects of influential factors on incident clearance time using a non-proportional hazard-based model," *Transportation Research Part A: Policy and Practice*, vol. 63, pp. 2–12, 2014.
- [20] D. Nam and F. Mannering, "An exploratory hazard-based analysis of highway incident duration," *Transportation Research Part A: Policy and Practice*, vol. 34, no. 1, pp. 85–102, 2000.
- [21] A. Stathopoulos and M. G. Karlaftis, "Modeling duration of urban traffic congestion," *Journal of Transportation Engineering*, vol. 128, no. 6, pp. 587–590, 2002.
- [22] A. T. Hojati, L. Ferreira, S. Washington, and P. Charles, "Hazard based models for freeway traffic incident duration," *Accident Analysis & Prevention*, vol. 52, pp. 171–181, 2013.
- [23] R. Li and P. Shang, "Incident duration modeling using flexible parametric hazard-based models," *Computational Intelligence and Neuroscience*, vol. 2014, Article ID 723427, 10 pages, 2014.
- [24] H. J. Kim and H.-K. Choi, "A comparative analysis of incident service time on urban freeways," *IATSS Research*, vol. 25, no. 1, pp. 62–72, 2001.
- [25] K. W. Smith and B. L. Smith, "Forecasting the clearance time of free-way accidents," Technical Report STL-2001-01, Center for Transportation Studies, University of Virginia, Charlottesville, VA, USA, 2014.
- [26] G. Valenti, M. Lelli, and D. Cucina, "A comparative study of models for the incident duration prediction," *European Transport Research Review*, vol. 2, no. 2, pp. 103–111, 2010.
- [27] Y. Wen, S. Y. Chen, Q. Y. Xiong, R. B. Han, and S. Y. Chen, "Traffic incident duration prediction based on K-nearest neighbor," *Applied Mechanics and Materials*, vol. 253–255, pp. 1675–1681, 2012.
- [28] W. W. Wu, S. Y. Chen, and C. J. Zheng, "Traffic incident duration prediction based on support vector regression," in *Proceedings of the ICCTP*, pp. 2412–2421, Nanjing, China, August 2011.
- [29] S. Boyles, D. Fajardo, and S. T. Waller, "A Naive Bayesian classifier for incident duration prediction," in *Proceedings of the TRB 86th Annual Meeting Compendium of Papers CD-ROM*, Washington DC, USA, 2007.
- [30] K. Ozbay and N. Noyan, "Estimation of incident clearance times using Bayesian networks approach," *Accident Analysis & Prevention*, vol. 38, no. 3, pp. 542–555, 2006.
- [31] H. Park, A. Haghani, and X. Zhang, "Interpretation of Bayesian neural networks for predicting the duration of detected incidents," *Journal of Intelligent Transportation Systems*, vol. 20, no. 4, pp. 385–400, 2015.
- [32] C. Chen, G. Zhang, R. Tarefder, J. Ma, H. Wei, and H. Guan, "A multinomial logit model-Bayesian network hybrid approach for driver injury severity analyses in rear-end crashes," *Accident Analysis & Prevention*, vol. 80, pp. 76–88, 2015.

- [33] C. Chen, G. Zhang, Z. Tian, S. M. Bogus, and Y. Yang, "Hierarchical Bayesian random intercept model-based cross-level interaction decomposition for truck driver injury severity investigations," *Accident Analysis & Prevention*, vol. 85, pp. 186–198, 2015.
- [34] F. Zong, X. Chen, J. Tang, P. Yu, and T. Wu, "Analyzing traffic crash severity with combination of information entropy and bayesian network," *IEEE Access*, vol. 7, pp. 63288–63302, 2019.
- [35] E. I. Vlahogianni and M. G. Karlaftis, "Fuzzy-entropy neural network freeway incident duration modeling with single and competing uncertainties," *Computer-Aided Civil and Infrastructure Engineering*, vol. 28, no. 6, pp. 420–433, 2013.
- [36] C.-H. Wei and Y. Lee, "Sequential forecast of incident duration using artificial neural network models," *Accident Analysis & Prevention*, vol. 39, no. 5, pp. 944–954, 2007.
- [37] C. X. Ma, W. Hao, F. Q. Pan, and W. Xiang, "Road screening and distribution route multi-objective robust optimization for hazardous materials based on neural network and genetic algorithm," *PLoS One*, vol. 13, no. 6, Article ID e0198931, 2018.
- [38] Y. Lee and C.-H. Wei, "A computerized feature selection method using genetic algorithms to forecast freeway accident duration times," *Computer-Aided Civil and Infrastructure Engineering*, vol. 25, no. 2, pp. 132–148, 2010.
- [39] C. Zhan, A. Gan, and M. Hadi, "Prediction of lane clearance time of freeway incidents using the M5P tree algorithm," *IEEE Transactions on Intelligent Transportation Systems*, vol. 12, no. 4, pp. 1549–1557, 2011.
- [40] Q. He, Y. Kamarianakis, K. Jintanakul, and L. Wynter, "Incident duration prediction with hybrid tree-based quantile regression," *Complex Networks and Dynamic Systems*, vol. 2, pp. 287–305, 2013.
- [41] X. Ma, C. Ding, S. Luan, Y. Wang, and Y. Wang, "Prioritizing influential factors for freeway incident clearance time prediction using the gradient boosting decision trees method," *IEEE Transactions on Intelligent Transportation Systems*, vol. 18, no. 9, pp. 2303–2310, 2017.
- [42] W. Kim and G.-L. Chang, "Development of a hybrid prediction model for freeway incident duration: a case study in Maryland," *International Journal of Intelligent Transportation Systems Research*, vol. 10, no. 1, pp. 22–33, 2012.
- [43] J. J. Tang, L. L. Zheng, C. Y. Han et al., "Statistical and machine-learning methods for clearance time prediction of road incidents: a methodology review," *Analytic Methods in Accident Research*, vol. 27, Article ID 100123, 2020.
- [44] Y. J. Zou, J. J. Tang, L. T. Wu, K. Henrickson, and Y. H. Wang, "Quantile analysis of freeway incident clearance time," *Proceedings of the Institution of Civil Engineers-Transport*, vol. 170, no. 5, pp. 296–304, 2017.
- [45] Y. J. Zou, X. Z. Zhong, J. J. Tang et al., "A copula-based approach for accommodating the underreporting effect in wildlife-vehicle crash analysis," *Sustainability*, vol. 11, no. 2, pp. 1–13, 2019.
- [46] Y. Zou, X. Ye, K. Henrickson, J. Tang, and Y. Wang, "Jointly analyzing freeway traffic incident clearance and response time using a copula-based approach," *Transportation Research Part C: Emerging Technologies*, vol. 86, pp. 171–182, 2018.
- [47] J. MacQueen, "Some methods for classification and analysis of multivariate observations," *Proceedings of the Fifth Berkeley Symposium on Mathematical Statistics and Probability*, vol. 1, pp. 281–296, 1967.
- [48] Y. Wang, K. Assogba, Y. Liu, X. Ma, M. Xu, and Y. Wang, "Two-echelon location-routing optimization with time windows based on customer clustering," *Expert Systems with Applications*, vol. 104, no. 104, pp. 244–260, 2018.
- [49] P. J. Rousseeuw, "Silhouettes: a graphical aid to the interpretation and validation of cluster analysis," *Journal of Computational and Applied Mathematics*, vol. 20, pp. 53–65, 1987.
- [50] T. Q. Chen and C. Guestrin, "XGBoost: a scalable tree boosting system," in *Proceedings of the 22nd ACM SIGKDD International Conference on Knowledge Discovery and Data Mining*, pp. 785–794, San Francisco, CA, USA, 2016.
- [51] Q. Shang, D. Tan, S. Gao, and L. L. Feng, "A hybrid method for traffic incident duration prediction using BOA-optimized random forest combined with neighborhood components analysis," *Journal of Advanced Transportation*, vol. 2019, Article ID 4202735, 11 pages, 2019.
- [52] E. Brochu, V. M. Cora, and N. D. Freitas, "A tutorial on Bayesian optimization of expensive cost functions, with application to active user modeling and hierarchical reinforcement learning," Technical Report UBC TR-2009-23, Department of Computer Science, University of British Columbia, Vancouver, BC, Canada, 2009.
- [53] S. Wang, R. Li, and M. Guo, "Application of nonparametric regression in predicting traffic incident duration," *Transport*, vol. 33, no. 1, pp. 22–31, 2018.
- [54] J. Tang, J. Liang, C. Han, Z. Li, and H. Huang, "Crash injury severity analysis using a two-layer Stacking framework," *Accident Analysis & Prevention*, vol. 122, pp. 226–238, 2019.
- [55] J. Bergstra, B. Komer, D. Yamins, C. Eliasmith, and D. Cox, "Hyperopt: a Python library for model selection and hyperparameter optimization," *Computational Science & Discovery*, vol. 8, no. 1, Article ID 014008, 2015.
- [56] X. X. Ma, S. R. Chen, and F. Chen, "Correlated random-effects bivariate Poisson lognormal model to study single-vehicle and multivehicle crashes," *Journal of Transportation Engineering-ASCE*, vol. 142, no. 11, 2016.
- [57] Y. Yan, Y. Zhang, X. Yang, J. Hu, J. Tang, and Z. Guo, "Crash prediction based on random effect negative binomial model considering data heterogeneity," *Physica A: Statistical Mechanics and Its Applications*, vol. 547, Article ID 123858, 2020.
- [58] F. Chen, X. X. Ma, S. R. Chen, and L. Yang, "Crash frequency analysis using hurdle models with random effects considering short-term panel data," *International Journal of Environmental Research and Public Health*, vol. 13, no. 11, p. 1043, 2016.
- [59] Y. Wang, K. Assogba, J. Fan, M. Xu, Y. Liu, and H. Wang, "Multi-depot green vehicle routing problem with shared transportation resource: integration of time-dependent speed and piecewise penalty cost," *Journal of Cleaner Production*, vol. 2019, no. 232, pp. 12–29, 2019.
- [60] C. X. Ma, J. B. Zhou, X. C. Xu, F. Q. Pan, and J. Xu, "Fleet scheduling optimization of hazardous materials transportation: a literature review," *Journal of Advanced Transportation*, vol. 2020, Article ID 5070347, 16 pages, 2020.
- [61] C. X. Ma, W. Hao, W. Xiang, and W. Yan, "The impact of aggressive driving behavior on driver injury severity at highway-rail grade crossings accidents," *Journal of Advanced Transportation*, vol. 2018, Article ID 9841498, 10 pages, 2018.
- [62] C. X. Ma, D. Yang, J. B. Zhou, Z. X. Feng, and Q. Yuan, "Risk riding behaviors of urban E-bikes: a literature review," *International Journal of Environmental Research and Public Health*, vol. 16, no. 13, Article ID 2308, 2019.
- [63] Y. Yan, Y. Dai, X. Li, J. Tang, and Z. Guo, "Driving risk assessment using driving behavior data under continuous tunnel environment," *Traffic Injury Prevention*, vol. 20, no. 8, pp. 807–812, 2019.

- [64] C. Ding, X. Ma, Y. Wang, and Y. Wang, "Exploring the influential factors in incident clearance time: disentangling causation from self-selection bias," *Accident Analysis & Prevention*, vol. 85, pp. 58–65, 2015.
- [65] F. L. Mannering and C. R. Bhat, "Analytic methods in accident research: methodological frontier and future directions," *Analytic Methods in Accident Research*, vol. 1, pp. 1–22, 2014.
- [66] Y.-S. Chung, Y.-C. Chiou, and C.-H. Lin, "Simultaneous equation modeling of freeway accident duration and lanes blocked," *Analytic Methods in Accident Research*, vol. 7, pp. 16–28, 2015.

Research Article

A Study on Correlation of Traffic Accident Tendency with Driver Characters Using In-Depth Traffic Accident Data

Lin Hu,^{1,2} Xingqian Bao,¹ Hequan Wu,^{1,2} and Wenguang Wu ^{1,2}

¹School of Automotive and Mechanical Engineering, Changsha University of Science and Technology, Changsha 410114, China

²Hunan Province Key Laboratory of Safety Design and Reliability Technology for Engineering Vehicle, Changsha University of Science and Technology, Changsha 410114, China

Correspondence should be addressed to Wenguang Wu; wuwenguanglq@126.com

Received 24 December 2019; Accepted 27 March 2020; Published 2 June 2020

Academic Editor: Feng Chen

Copyright © 2020 Lin Hu et al. This is an open access article distributed under the Creative Commons Attribution License, which permits unrestricted use, distribution, and reproduction in any medium, provided the original work is properly cited.

Traffic accidents are often related to the driver's driving behavior, which is mainly decided by his or her characters. In order to explore the correlation of traffic accident risk with driver characters, the age, driving experience, and driving style were statistically analyzed based on the China In-Depth Accident Study (CIDAS) database. Taking the number of casualties in the accident as evaluation indicators, the grey cluster analysis was used to classify the drivers into four accident risk ranks: low, medium to low, medium to high, and high. The results show that drivers aged 18–30 years are more likely to induce accidents; drivers with 6–10 years of driving experience have the highest risk to accidents, followed by drivers with 4–5 years of driving experience; and the driving style is also highly correlated with accident risk tendency.

1. Introduction

In China, especially in urban roads, due to mixed traffic flows, the traffic situation is more complicated. Although the accident rate is decreasing year by year, the number of casualties is still high every year [1]. For example, it is reported 0.9 per cent year-on-year decrease for 2018 in China, but there were still 166,906 traffic accidents in cars, which killed 46,161 people and injured 169,046 people. In addition, according to the reports of traffic accidents, nearly 90% of accidents are caused by human factors, and the human becomes one of the most unstable factors in causing traffic safety problems [2]. Traffic accidents are often related to the driver's driving behavior, which is mainly decided by his or her characters, such as the age, driving experience, and driving style. Drivers' willingness to reflect the driving style characteristics is based on their own driving ability, danger, and emergency handling attitude [3, 4]. It is particularly urgent to study the correlation of traffic accident risk tendency with driver characters.

Accident Tendency Theory is one of the ancient and most widely known accident causation theories, which holds

that accidents are indeed related to human personality [5]. In addition, from the statistical point of view, a certain type of driver would show more likely to be accident-prone than other drivers under the same driving environment conditions, which can be called the driver's accident tendency. In other words, accident propensity refers to individuals who have the characteristics of accident-prone among drivers [6].

The Grey System Theory was founded in 1982 by the Chinese scholar Professor Deng Julong. It is a systematic subject with the uncertainty system, which is mainly used to study the "small sample uncertainty problem" and describes the versatile factors that are difficult to describe quantitatively [7, 8]. The generation and development of known information is used to extract valuable information and achieve a correct description of the system's operational behavior, evolutionary rules, and effective monitoring [9]. The problem of traffic accident risk with driver characters is not only complicated but also changes with time and environment. It can be summarized as follows: the system factors are not completely clear, the relationship between factors is not completely clear, the system structure is not fully known, and the principle of the system is not

completely clear, that is to say, the system is an “information incomplete” system. Therefore, the system consisting of people and vehicles is a typical grey system, which is suitable for the grey system theory [10].

Exploring the correlation of traffic accident risk with driver characters, such as the age, driving experience, and driving style, would be an effective way to improve the traffic safety [11]. Based on the statistics of the actual traffic accident cases occurred from 2014 to 2016 in the CIDAS database, this paper analyzes the characters of drivers involved in these accidents, and the grey cluster analysis was used to classify the drivers into four accident risk ranks. This study would provide a theoretical basis for improving the domestic traffic design and standardizing the driving behavior of drivers.

2. Data and Methods

2.1. Data. The China In-Depth Accident Study (CIDAS) project was launched on July 15, 2011, by China Automotive Technology Research Center and several well-known automobile enterprises. It aims to provide basic data support and technical services for the automobile industry through in-depth investigation, analysis, and research on road traffic crashes in China [12].

356 crash cases are selected from the road vehicle accidents of the CIDAS project from 2014 to 2016 based on the following sampling criteria: (1) passenger car involvement, (2) detailed records of driver characters, (3) detailed injury records, (4) clear causation of the accident, and (5) age of the drivers ranging between 18 and 60 years.

2.2. Methods. A grey cluster evaluation model is established to classify the drivers' accident risk rank, and the main steps are as follows:

- (1) Giving the cluster whitening number: select n clustering objects, get m clustering indicators, and construct an $n \times m$ matrix.
- (2) Inputting the cluster whitening number into the computer, entering the grey clustering analysis and evaluation algorithm, including the clustering whitening number to be averaged and dimensionless; determining the grey class where each clustering index value belongs to each clustering object; using the valuation method or interpolation method to obtain the whitening weight function value of each grey class; calibrating the clustering weight grey number matrix; and constructing the clustering matrix.
- (3) Performing grey evaluation based on the result of step (2).

2.2.1. Definition of Grey Cluster Objects and Indicators. The numbers of minor injuries, serious injuries, and deaths in the accident are selected as the evaluation indicators, and

then the evaluation index matrix is constructed according to the following equation:

$$X_{m \times n} = \begin{bmatrix} 9 & 4 & 5 \\ 10 & 4 & 0 \\ 4 & 2 & 0 \\ \vdots & \vdots & \vdots \\ 1 & 0 & 0 \end{bmatrix}, \quad (1)$$

where m represents the number of the evaluation object, $m \in \{1, 2, 3, \dots, 47\}$; n is the evaluation index, $n \in \{1, 2, 3\}$; and $n = 1, 2, 3$ represents the number of minor injuries, serious injuries, and deaths in the accident, respectively. The range method is used to measure the indicators without dimension, shown as equation (2):

$$X_{mn} = \frac{x'_{mn} - x_{\min}}{x_{\max} - x_{\min}}, \quad (2)$$

where x'_{mn} is the elements in the matrix and x_{\min} and x_{\max} are the minimum and the maximum element in the matrix, respectively. The evaluation matrix after dimensionless processing is shown in the following equation:

$$X_{m \times n} = \begin{bmatrix} 0.9 & 0.4 & 0.5 \\ 1.0 & 0.4 & 0 \\ 0.4 & 0.2 & 0 \\ \vdots & \vdots & \vdots \\ 0.1 & 0 & 0 \end{bmatrix}. \quad (3)$$

2.2.2. Determining of Ash and Whitening Values. The driver accident risk rank is classified into four levels: low, medium to low, medium to high, and high. It is represented by the grey class $k = 1, 2, 3,$ and $4,$ respectively, and then the evaluation matrix after dimensionless treatment is used to perform the cumulative frequency analysis [13, 14]. The whitening values of the four levels of the driver's risk tendency are represented by $\lambda_n^1, \lambda_n^2, \lambda_n^3, \lambda_n^4,$ which are the relative values of the cumulative frequencies of the curves of 15%, 40%, 60%, and 85%, respectively. The matrix of λ is described in the following equation:

$$\lambda = (\lambda_n^1, \lambda_n^2, \lambda_n^3, \lambda_n^4) = \begin{bmatrix} 0.1 & 0.1 & 0.3 & 0.4 \\ 0 & 0 & 0.1 & 0.3 \\ 0 & 0 & 0 & 0.2 \end{bmatrix}. \quad (4)$$

2.2.3. Construction of the Grey Class Whitening Weight Function. The segmentation function can be used to construct the whitening weight function of the driver's risk tendency of inducing an accident [15–17]. The symbol f_n^k indicates the whitening weight function of the n th clustering evaluation index, which belongs to subclass K . The whitening weight function of the indicator corresponding to minor injury, severely injury, and death is $f_1^k, f_2^k,$ and $f_3^k,$ respectively. Taking the minor injury indicator f_1^k for

example, the whitening weight function of four levels of risk tendency can be obtained from equations (5) to (8)

$$f_1^1 = \begin{cases} 1, & x \in [0, 0.1], \\ 0, & x \in (0.1, 1], \end{cases} \quad (5)$$

$$f_1^2 = \begin{cases} 0, & x \notin [0.1, 0.3], \\ \frac{0.3 - x}{0.3 - 0.1}, & x \in [0.1, 0.3], \end{cases} \quad (6)$$

$$f_1^3 = \begin{cases} 0, & x \notin [0.1, 0.4], \\ \frac{x - 0.1}{0.3 - 0.1}, & x \in [0.1, 0.3], \\ \frac{0.4 - x}{0.4 - 0.3}, & x \in (0.3, 0.4], \end{cases} \quad (7)$$

$$f_1^4 = \begin{cases} 0, & x \in [0, 0.3], \\ \frac{x - 0.3}{0.4 - 0.3}, & x \in (0.3, 0.4], \\ 1, & x \in (0.4, 1]. \end{cases} \quad (8)$$

Then, the clustering weight will be determined by the following equation:

$$\eta_n^k = \begin{cases} \frac{\lambda_n^k}{\sum_{n=1}^3 \lambda_n^k} \cdot \left(1 - \frac{b}{i}\right), & \lambda_j^k \neq 0, \\ \frac{1}{i}, & \lambda_j^k = 0, \end{cases} \quad (9)$$

where η_n^k and λ_n^k are the clustering weight and whitening value, respectively, of the n th evaluation index in the k th grey category and b is the number of λ_n^k , which is equal to 0, $i = 3$.

According to equation (9), the grey cluster weight matrix of each evaluation index can be obtained for each subclass. Then, the reanalysis of grey clustering will be performed, the grey cluster evaluation value σ_m^k , which means the cluster evaluation value of the m th evaluation object in the k th grey class can be determined by the following equation:

$$\sigma_m^k = \sum_{n=1}^3 f_m^k X_m^n \eta_n^k. \quad (10)$$

The cluster evaluation value sequence of the evaluation object m $\sigma_m^k = (\sigma_m^1, \sigma_m^2, \dots, \sigma_m^k)$ will be used to identify the accident tendency level of m .

3. Results

3.1. Characters of Accident Vehicles Drivers. Traffic accidents are often related to the driver's driving behavior, which is mainly decided by his or her characters, and age, driving experience, and driving style are the main characters related with the handling performance [18–22].

3.1.1. Age. The drivers were divided into four age groups: 18 to 30 years old, 31 to 40 years old, 41 to 50 years old, and 51 to 60 years old. Figure 1 shows the age distribution of the drivers in traffic accident vehicles.

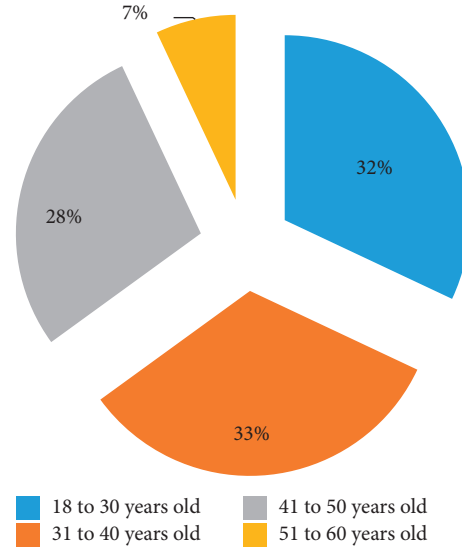


FIGURE 1: Age distribution of the drivers in traffic accident vehicles.

Figure 2 shows the number of casualties caused by different age groups.

Drivers aged 31–40 years account for the maximum number of traffic accidents, while drivers aged 51–60 years have the minimum number of traffic accidents and they also have the lowest casualties. Drivers in the 41–50 age group have the highest number of fatal accidents, followed by drivers in the 51–60 age group. The visual characteristics, response time, speed estimation accuracy, and operation ability of drivers would change with the increase of age to a certain extent [23–25], so age would consequently influence a driver's accident risk tendency.

3.1.2. Driving Experience. Driving experience is an objective evaluation index related with the driver's driving ability [26–29]. In this study, the drivers were divided into six groups based on their driving experience: 3 years and below, 4 to 5 years, 6 to 10 years, 11 to 15 years, 16 to 20 years, and 20 years and above. Figure 3 shows the distribution of driving experience of drivers in accidents.

It can be seen that the drivers in the 6–10-year driving experience group contribute the most number of accidents, followed by the drivers in the 3-year driving experience group, and the drivers with 20 years or more driving experience account for the lowest number of accidents.

3.1.3. Road Types. Figure 4 shows the distribution of the road types where the accident occurred. In this study, four kinds of road types are involved: straight, curved road, intersection, and crossroad. The accidents occurred on the straight road account for the highest proportion (44.45%) in the total accidents, followed by intersections and crossroads. If we consider the integration of data at intersections and crossroads, the number of accidents at intersections is more than half of the total number of accidents, which is consistent with other literatures [30–33].

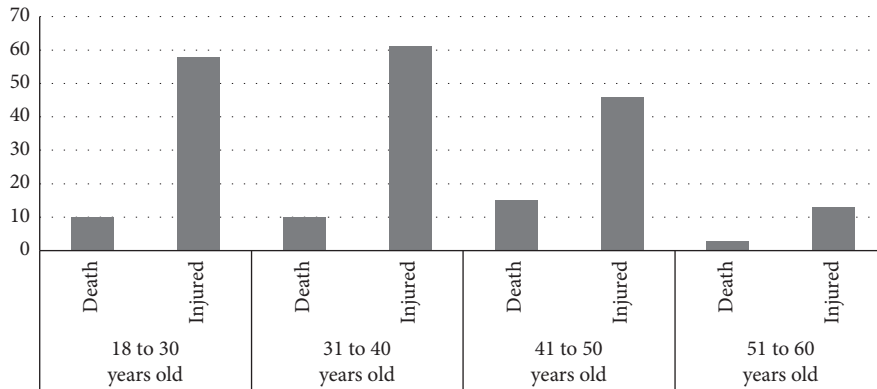


FIGURE 2: Casualties caused by drivers of different ages.

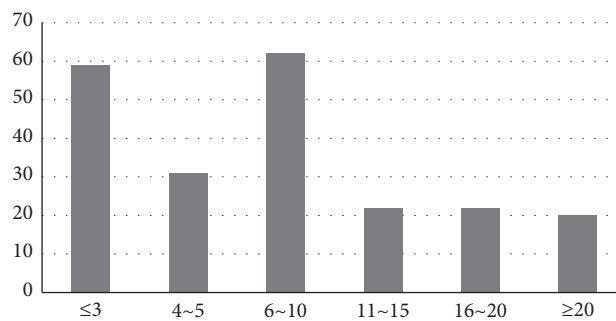


FIGURE 3: Distribution of driving experience of drivers in accidents.

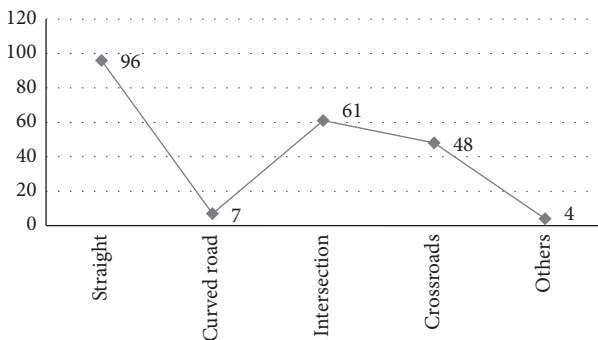


FIGURE 4: Distribution of road types in accidents.

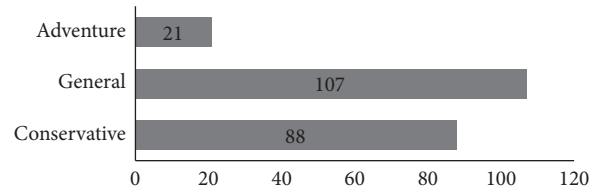


FIGURE 5: Distribution of driving styles of drivers in accidents.

3.1.4. *Driving Style.* Due to the significant deviation of the driver’s gender in data samples, the accident cases involved female driver only accounts for 7.5% of the total sample, and the correlation of the driver’s driving style with accident risk tendency was analyzed without gender-specific.

Figure 5 shows the distribution of driving styles of the accident vehicle drivers, which were recorded for each accident case in the CIDAS database, but the driving styles were declared by the driver himself. In the CIDAS database, the driving styles include three types that are adventure style, conservative style, and general style [34].

It can be seen from Figure 5, the general style and conservative style should be responsible for most accidents, which were not agreed with common recognition that the

adventure style drivers will have higher accident rates [35–38].

3.2. Analysis of Driver’s Accident Risk Tendency

3.2.1. *Grey Cluster Objects and Indicators.* The drivers were divided into 47 classification groups as the object of grey clustering based on their age, driving experience, and driving style. The nonexistent combination and the combination with zero evaluation index were eliminated, as shown in Table 1.

3.2.2. *Assessment Value of Drivers’ Accident Risk Tendency in Various Character Groups.* Table 2 lists the grey clustering assessment value of drivers’ accident risk tendency in various character groups, and the groups with high accident risk tendency are given in italic.

TABLE 1: Grouping of driver characteristics.

Number	Driver characters			Evaluation index		
	Age/year	Driving experience/year	Driving style	Slightly injured	Seriously injured	Death toll
1	18 to 30 years old	≤3	Conservative	9	4	5
2	31 to 40 years old	≤3	Conservative	10	4	0
3	41 to 50 years old	≤3	Conservative	4	2	0

45	51 to 60 years old	11~15	Adventure	0	0	1
46	41 to 50 years old	16~20	Adventure	3	0	0
47	51 to 60 years old	16~20	Adventure	1	0	0

TABLE 2: Grey clustering calculation results of accident tendency of each group with driver characteristics.

Number	Driver characters			Anecdotal tendency
	Age/year	Driving experience/year	Driving style	
1	18 to 30 years old	≤3	Conservative	Medium to high
2	31 to 40 years old	≤3	Conservative	Medium to high
3	41 to 50 years old	≤3	Conservative	Medium to high
4	18 to 30 years old	4~5	Conservative	High
5	31 to 40 years old	4~5	Conservative	Medium to high
6	41 to 50 years old	4~5	Conservative	High
7	18 to 30 years old	6~10	Conservative	Medium to low
8	31 to 40 years old	6~10	Conservative	Medium to low
9	41 to 50 years old	6~10	Conservative	High
10	31 to 40 years old	11~15	Conservative	Medium to high
11	41 to 50 years old	11~15	Conservative	Medium to low
12	51 to 60 years old	11~15	Conservative	Low
13	41 to 50 years old	16~20	Conservative	Low
14	51 to 60 years old	16~20	Conservative	Medium to low
15	41 to 50 years old	≥20	Conservative	Medium to low
16	51 to 60 years old	≥20	Conservative	Low
17	18 to 30 years old	≤3	General	High
18	31 to 40 years old	≤3	General	Medium to high
19	41 to 50 years old	≤3	General	Medium to high
20	18 to 30 years old	4~5	General	High
21	31 to 40 years old	4~5	General	Medium to low
22	41 to 50 years old	4~5	General	Medium to low
23	51 to 60 years old	4~5	General	Medium to low
24	18 to 30 years old	6~10	General	High
25	31 to 40 years old	6~10	General	High
26	41 to 50 years old	6~10	General	High
27	51 to 60 years old	6~10	General	Low
28	18 to 30 years old	11~15	General	Low
29	31 to 40 years old	11~15	General	Medium to high
30	41 to 50 years old	11~15	General	Medium to low
31	31 to 40 years old	16~20	General	Medium to low
32	41 to 50 years old	16~20	General	Medium to high
33	51 to 60 years old	16~20	General	Medium to low
34	31 to 40 years old	≥20	General	Low
35	41 to 50 years old	≥20	General	Medium to low
36	51 to 60 years old	≥20	General	Medium to low
37	18 to 30 years old	≤3	Adventure	High
38	41 to 50 years old	≤3	Adventure	Medium to high
39	18 to 30 years old	4~5	Adventure	Medium to high
40	31 to 40 years old	4~5	Adventure	Medium to low
41	41 to 50 years old	4~5	Adventure	Medium to high
42	18 to 30 years old	6~10	Adventure	Medium to high
43	31 to 40 years old	6~10	Adventure	Medium to low
44	41 to 50 years old	6~10	Adventure	Medium to high
45	51 to 60 years old	11~15	Adventure	High
46	41 to 50 years old	16~20	Adventure	Medium to low
47	51 to 60 years old	16~20	Adventure	Medium to high

4. Discussion and Conclusions

4.1. Age Characteristics of Drivers with High Accident Tendency. The age distribution of drivers with high accident risk tendency is mainly concentrated in the age group of 18 to 30 years old. The main accident causation is the driver's illegal driving behaviors, such as robbing road priority and overtaking, and these accidents usually occurred in rush hours. From the perspective of psychological characteristics, young people have strong aggressive psychology, blind self-confidence, and possible expectation imbalance.

4.2. Driving Experience Characteristics of Drivers with High Accident Tendency. From the perspective of the driving experience, the drivers with 6–10 years of driving experience have the highest risk tendency, followed by the drivers with 4–5 years of driving experience. Drivers who have just started driving for 3 years or less are more cautious in their mental preparation, and drivers with more than 10 years of driving experience can deal with all kinds of unexpected situations with all kinds of skills. While a driver who is not senior but has some proficiency in road traffic rules and driving skills will be more risky when overtaking, violating, and so on and consequently has a higher risk tendency to causing accidents.

4.3. Driving Style Characteristics of Drivers with High Accident Tendency. It can be seen from the results that three driving styles of drivers have similar accident risk tendency, and the general drivers should be responsible for the most accidents, which was not agreed with the common recognition that the adventure style drivers will have higher accident rates. The main reasons for this result are as follows: first, the driving style was declared by drivers themselves, there may be subjective interference in the classification of the driver's driving style, people often misjudge themselves, or they do not consider the change of their driving style during their trip, for example, the irregular driving of other vehicles make them feel anger or confusion; second, the accident rate of three styles of drivers would be a better evaluating indicator to indicate the correlation of the driver's driving style with accident risk tendency.

What we need to point out here is that, in this study, only the numbers of drivers in different age groups, driving style groups, and road types are used in statistical analysis, but in fact, drivers in different age groups would have different exposure of driving. Younger or middle-aged drivers may have more traveling miles than teen or older drivers. The number of causalities per mile may be a better indicator than considering only the number of causalities, and different road types also take up different proportions of all the trips. If the exposure of different types can be considered, the importance of intersections could be better explained. But due to the lack of relevant data in the current database, these parameters cannot be obtained right now. Considering the important statistical significance of these parameters, we will further update the procedure of in-depth accident investigation and record more valuable data.

The above research results show that drivers aged 18–30 years are more likely to induce accidents; drivers with 6–10 years of driving experience have the highest risk to accidents; and the driving style is also highly correlated with accident risk. The research on the characters of drivers with high accident risk tendency is conducive to targeted education and prevention of accidents in the future driving training and management.

Data Availability

The data used to support the findings of this study have been deposited in the figshare repository. The link is <https://figshare.com/s/bd4d605f61a1bf71fba7>.

Conflicts of Interest

The authors declare that there are no conflicts of interest.

Acknowledgments

This work was financially supported by the Hunan Province Natural Science Outstanding Youth Fund (No. 2019JJ20017) and the National Natural Science Foundation of China (No. 51875049/51705035).

References

- [1] Ministry of Public Security, *Annual Report on Road Traffic Accidents of the People's Republic of China*, Traffic Management Bureau of the Ministry of Public Security, Beijing, China, 2015.
- [2] J. W. Niu, X. M. Zhang, Y. P. Sun et al., "Research on driving behavior of drivers taking over autopilot vehicles in dangerous situations," *China Journal of Highway and Transport*, vol. 31, no. 6, pp. 272–280, 2018.
- [3] L. Sun, R. S. Chang, Y. Dong et al., "Impact of driving experience on driver's driving style and traffic violations," *Chinese Journal of Health Psychology*, vol. 22, no. 2, pp. 222–224, 2014.
- [4] S. Li, "Effect of risk behavior attitude on drivers' driving style," *Chinese Journal of Health Psychology*, vol. 24, no. 10, pp. 1458–1460, 2016.
- [5] H. Q. Jin, Y. S. Song, S. L. Zhang et al., "Construction of control model for traffic accident prevention system based on accident orientation theory," *Ergonomics*, vol. 17, no. 1, pp. 73–77, 2011.
- [6] H. Q. Jin, "Driving Suitability," Hefei, Anhui People's Publishing House, Hefei, China, 1995.
- [7] F. Y. Dong, M. D. Xiao, B. Liu et al., "Analysis of the construction method of whitening weight function in grey system teaching," *Journal of North China University of Water Engineering, Natural Science Edition*, vol. 31, no. 3, pp. 97–99, 2010.
- [8] J. B. Hu and X. T. Cao, "Analysis of driver characteristics of road traffic accidents," *China Journal of Highway and Transport*, vol. 22, no. 6, pp. 106–110, 2009.
- [9] Z. D. Zhao, "Application and analysis of grey system theory in automobile engineering," *Journal of Chongqing University of Technology (Natural Science)*, vol. 28, no. 3, pp. 10–16, 2014.
- [10] S. Y. Yan, *Weapon Equipment Ergonomics*, Harbin, pp. 344–359, Harbin Institute of Technology Press, Weihai, China, 2009.

- [11] M. Q. Guan and Q. N. Gong, "Analysis of drivers' incidence tendency of construction vehicles based on grey clustering method," *Highway*, vol. 22, no. 11, pp. 182–187, 2017.
- [12] L. Hu, X. Hu, J. Wan, M. Lin, and J. Huang, "The injury epidemiology of adult riders in vehicle-two-wheeler crashes in China, Ningbo, 2011–2015," *Journal of Safety Research*, vol. 72, pp. 21–28, 2020.
- [13] H. M. Zhou, Y. Sun, and X. J. Xu, "Research on freedom lane change behavior of urban road vehicles based on random utility theory," *Journal of Transportation Research*, vol. 3, no. 2, pp. 9–16, 2017.
- [14] L. Hu, Y. Zhong, W. Hao et al., "Optimal route algorithm considering traffic light and energy consumption," *IEEE Access*, vol. 6, pp. 59695–59704, 2018.
- [15] L. Hu, J. OU, J. Huang, Y. Chen, and D. Cao, "A review of research on traffic conflicts based on intelligent vehicles," *IEEE Access*, vol. 8, pp. 24471–24483, 2020.
- [16] P. Kumar, M. S. Bains, N. Bharadwaj et al., "Impact assessment of driver speed limit compliance behavior on macroscopic traffic characteristics under heterogeneous traffic environment," *Transportation Letters The International Journal of Transportation Research*, vol. 4, no. 3, pp. 1–12, 2018.
- [17] W. Qi, R. Z. Wang, and L. Wang, "Driving risk detection model of deceleration zone in expressway based on generalized regression neural network," *Journal of Advanced Transportation*, vol. 2018, no. 6, Article ID 8014385, 8 pages, 2018.
- [18] L. Hu, S. Y. Fang, and Q. Chen, "Research on parameters influence of automobile-two-wheel vehicle collision accident reconstruction based on orthogonal experiment," *Automotive Engineering*, vol. 38, no. 5, pp. 567–573, 2016.
- [19] L. Hu, X. Hu, Y. Che et al., "Reliable state of charge estimation of battery packs using fuzzy adaptive federated filtering," *Applied Energy*, vol. 262, 2020.
- [20] P. Yong, C. J. Fan, L. Hu et al., "Tunnel driving occupational environment and hearing loss in train drivers in China," *Occupational and Environmental Medicine*, vol. 76, no. 1, pp. 97–104, 2019.
- [21] H. J. Hou, L. S. Jin, Z. W. Guan et al., "The influence of driving style on driving behavior," *China Journal of Highway and Transport*, vol. 31, no. 4, pp. 22–31, 2018.
- [22] Y. L. Zhai, Y. Q. Jin, and H. F. Chen, "Fatigue characteristics of drivers of different ages based on EEG signal analysis," *China Journal of Highway and Transport*, vol. 31, no. 4, pp. 63–81, 2018.
- [23] Z. Zhang, L. Zhang, L. Hu, and C. Huang, "Active cell balancing of lithium-ion battery pack based on average state of charge," *International Journal of Energy Research*, vol. 44, no. 4, pp. 2535–2548, 2020.
- [24] H. Q. Wu, S. J. Kuang, and H. B. Hou, "Research on application of electric vehicle collision based on reliability optimization design method," *International Journal of Computational Methods*, vol. 16, no. 7, pp. 1–15, 2019.
- [25] L. ZhengY. S. Chen et al., "Research on static distance of queuing vehicles at signalized intersection based on computer vision," *Journal of Highway and Transportation Research and Development*, vol. 16, no. 2, pp. 95–100, 2018.
- [26] X. H. Zhao, J. Rong, and Z. Q. Zhang, *Driving Behavior Simulation Experiment Platform and its Application Research*, People's Communications Press, Beijing, China, 2013.
- [27] J. W. Han, Z. Q. Liu, B. Gong et al., "Mechanism analysis of urban road traffic accidents based on bayesian network," *Science and Technology Innovation and Application*, vol. 6, no. 8, pp. 23–24, 2017.
- [28] X. Yue, Y. Ding, H. Hu et al., *Analysis on the Association between Driver's Macroscopic Characteristics and Accident Type of Urban Traffic Accidents*, China Control Conference, Shenyang, China, 2017.
- [29] H. P. Wang and S. Eli, "Fuzzy clustering evaluation of altitude suitability for driving in continuous driving time," *Science Technology and Engineering*, vol. 2, no. 10, pp. 319–324, 2017.
- [30] F. Chen, M. T. Song, and X. X. Ma, "Investigation on the injury severity of drivers in rear-end collisions between cars using a random parameters bivariate ordered probit model," *International Journal of Environmental Research and Public Health*, vol. 16, no. 14, pp. 26–32, 2019.
- [31] F. Chen and S. Chen, "Injury severities of truck drivers in single- and multi-vehicle accidents on rural highways," *Accident Analysis & Prevention*, vol. 43, no. 5, pp. 1677–1688, 2011.
- [32] R. Du, G. Qiu, K. Gao, and L. Hu, "Abnormal road surface recognition based on smartphone acceleration sensor," *Sensors*, vol. 20, no. 2, p. 451, 2020.
- [33] X. Yu, B. Li, T. Zhang, C. Tan, and H. Yan, "Variable weight coefficient optimization of gearshift actuator with direct-driving automated transmission," *IEEE Access*, vol. 8, pp. 4860–4869, 2020.
- [34] K. Gao, S. Huang, F. Han, S. Li, W. Wu, and R. Du, "An integrated algorithm for intersection queue length estimation based on IoT in a mixed traffic scenario," *Applied Sciences*, vol. 10, no. 6, pp. 2078–2088, 2020.
- [35] J. L. Zhang, X. Y. Wang, M. S. Wang et al., "Transition probability and prediction of vehicle driving tendency in three-lane dynamic environment," *Journal of Transportation Systems Engineering*, vol. 17, no. 1, pp. 82–90, 2017.
- [36] Y. Kong, R. S. Chang, T. J. Liu et al., "A comprehensive predictive model of driver's subjective fatigue state and steering wheel angle for accident tendency," *Ergonomics*, vol. 24, no. 2, pp. 40–46, 2018.
- [37] D. Yang, Y. Z. Zhang, Y. Q. Zhang et al., "Comparative study on traffic injuries between Chinese expressways and ordinary highways from 2004 to 2015," *Journal of Third Military Medical University*, vol. 39, no. 6, pp. 589–596, 2017.
- [38] F. Chen, H. R. Peng, X. X. Ma et al., "Examining the safety of trucks under crosswind at bridge-tunnel section: a driving simulator study," *Tunnelling and Underground Space Technology*, vol. 92, p. 103034, 2019.

Research Article

Driving Fatigue Prediction Model considering Schedule and Circadian Rhythm

Qi Zhang ^{1,2}, Chaozhong Wu ^{1,2} and Hui Zhang ^{1,2}

¹Intelligent Transportation Systems Research Center, Wuhan University of Technology, Wuhan, China

²Engineering Research Center of Transportation Safety, Ministry of Education, Wuhan, China

Correspondence should be addressed to Hui Zhang; zhanghuiits@whut.edu.cn

Received 29 December 2019; Accepted 5 February 2020; Published 19 March 2020

Guest Editor: Zeyang Cheng

Copyright © 2020 Qi Zhang et al. This is an open access article distributed under the Creative Commons Attribution License, which permits unrestricted use, distribution, and reproduction in any medium, provided the original work is properly cited.

Driver fatigue level was considered an accumulated result contributed by circadian rhythms, hours of sleep before driving, driving duration, and break time during driving. This article presents an investigation into the regression model between driver fatigue level and the above four time-related variables. With the cooperation of one commercial transportation company, a Naturalistic Driving Study (NDS) was conducted, and NDS data from thirty-four middle-aged drivers were selected for analysis. With regard to the circadian rhythms, commercial drivers operated the vehicle and started driving at around 09:00, 14:00, and 21:00, respectively. Participants' time of sleep before driving is also surveyed, and a range from 4 to 7 hours was selected. The commercial driving route was the same for all participants. After getting the fatigue level of all participants using the Karolinska Sleepiness Scale (KSS), the discrete KSS data were converted into consecutive value, and curve fitting methods were adopted for modeling. In addition, a linear regression model was proposed to represent the relationship between accumulated fatigue level and the four time-related variables. Finally, the prediction model was verified by the driving performance measurement: standard deviation of lateral position. The results demonstrated that fatigue prediction results are significantly relevant to driving performance. In conclusion, the fatigue prediction model proposed in this study could be implemented to predict the risk driving period and the maximum consecutive driving time once the driving schedule is determined, and the fatigue driving behavior could be avoided or alleviated by optimizing the driving and break schedule.

1. Introduction

Driving fatigue is a major safety issue in transportation, which has been identified to be associated with an increased risk of traffic collisions on roads because fatigued drivers tend to be unfocused with reaction time increases and impaired driving performance [1]. Deaths caused by road traffic accidents has risen to 1.35 million in 2018 [2]. Generally, accidents that are directly or indirectly caused by fatigue driving account for 30%–45% [3]. Operating vehicles when drivers are fatigued, they are endangering themselves and others. 31% of highway vehicle drivers admitted to driving while they were unable to keep their eyes open [4]. Approximately, each year 100,000 fatigue driving accidents reported in the United States cause 1,550 deaths and 71,000 injuries [5]. Based on nationwide statistics in Canada, about

20% of drivers nodded off or fallen asleep while driving and kill about 400 Canadians each year [6, 7]. In China, the traffic accident mortality rate caused by fatigue driving is twice that caused by other reasons [8]. With regard to the frequency of fatigue-caused accidents, it accounts for 10%–20% of all road traffic accidents in Europe [9]. To reduce the risk of traffic accidents and prevent fatigued driving [10], most countries have implemented their own hours of driving regulations [11–16]. However, those regulations differ from country to country and mainly include two aspects: the maximum duration on-duty and rest break during driving (Figure 1).

With the aim to detect or predict the fatigue status of drivers, more measurements including contextual, contact, or contactless physiological features; driver behavior; vehicle maneuver; and environment [17, 18], and more complex mathematical algorithms [17, 19, 20] were proposed.

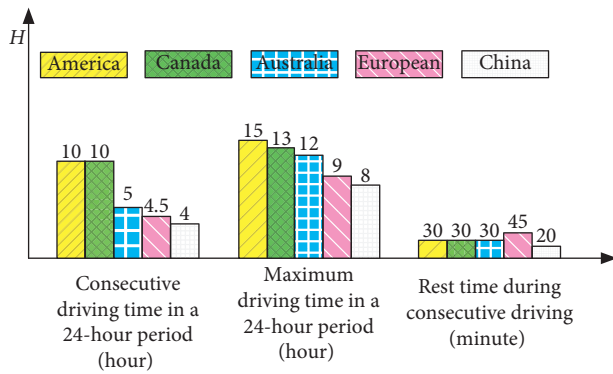


FIGURE 1: National regulation on driving time.

Whether in simulation experiments or field study, devices such as eye trackers and electroencephalograph recorders were equipped to collect data that will be used in algorithms [21–23]. All these studies are processing new algorithms, based on probability or statistics models and specific indicators, driving fatigue detection and prediction models were established through data mining. These studies have demonstrated that driving fatigue is detectable and predictable. However, those algorithms take long terms in driving fatigue data processing and optimal parameters training; even their accuracy of fatigue detection reached 80–90%, not ready to be implemented in real-time fatigue detection and prediction, especially in the case of new samples. This makes such algorithms more suitable for detection rather than for prediction, especially in the field driving environment, and it is difficult to obtain accurate physiological data. And obtained algorithms mostly tend to deal with the subtle driver factors during the driving process, rather than analyzing the fatigue value change throughout a given schedule. So, it is necessary to develop a fatigue prediction model for a whole driving process.

Fatigue is an accumulated result contributed by several factors; generally, fatigue is considered a suboptimal psychophysiological condition caused by sleep, rest, circadian effects, and daily activities [24]; with regard to driving, daily activities specifically refer to driving. Progressive decrement of driving performances proved the negative influence of consecutive driving, which was confirmed closely related to driving fatigue. By analyzing the driving log, Jovanis et al. found that drivers will be fatigued and the accident risk will rise after driving 4 hours without rest or break [25]. After analyzing 1,924 driving events, Lin et al. found the accident risk in the first 4 hours is low. But the risk would increase more than 50% in the following 3 hours, and increased 80–130% during the final hour [26]. Forty drivers were recruited in the field driving experiments, and Ma analyzed their driving records and found that those drivers showed more driving errors and poor driving performance after consecutive driving 3.5 hours [27]. In a 6-hour simulated driving experiment, Jing et al. recorded four drivers' physiological information and found that 235 minutes should be the consecutive driving time threshold [28].

In addition, taking enough sleep and rest during consecutive schedules are the two main effective methods to

relieve fatigue in the field driving environment and simulators. In some driving simulation experiments, the neurocognitive measures of vigilance, reaction time, and driving performance were evidenced to impair after sleep deprivation [29, 30]. Other findings from field experiments also proved that drivers showed more tendencies to be drowsy after experienced sleep deprivation [31, 32]. In a statistical analysis of the hours of sleep for drivers who were involved in a representative sample of crashes, Tefft found that the shorter the drivers slept in the 24 hours before crashing, the more odds the drivers should be culpable for their crashes [33]. Besides the sleep before driving, the rest breaks between driving stages can also help drivers recover from driving fatigue. In the regulation of hours of service (HoS) [34], a term related to rest breaks was firstly included. The rule categorically stated that “Driving is not permitted if more than 8 hours have passed since the end of the driver’s last off-duty or at least 30 minutes since sleeper berth period.” Chen and Xie analyzed 183 crash events and 398 noncrash events and found that the more the rest break was taken, the more the crash odds could be reduced [12]. After 4 hours of consecutive field driving, Yuhua et al. found that it was difficult for electrocardiograph signal return to a normal level unless male and female drivers rested at least 24 and 27 minutes, respectively [35]. The circadian rhythms have been proved to have an impact on drivers’ fatigue; their alertness and performance vary across the day driven by the circadian rhythm [36]. The circadian rhythm also caused a higher proportion of sleep-related accidents to occur, mostly in the early morning and early afternoon, mainly ranging in two periods (02:00–05:00 and 13:00–16:00) [37–42] between the thick black lines in Figure 2.

It could be concluded that the four time-related indicators, time of sleep before driving, rest time, circadian rhythm, and consecutive driving time, all have an influence on driving fatigue. Those algorithms completed in the previous research used the drivers’ parameters or the relevant parameters of the vehicles being driven; not all of the four time-related factors were taken into account, so these algorithms can only perform short-term fatigue detection of prediction. The purpose of this article is to study a newly developed fatigue prediction model; with more than one feature, the model is expected that the precision could be improved and as concise as possible, only considering the four mentioned variables, and could model the fatigue for the whole driving process.

2. Experimental Design and Data Processing

By cooperating with a commercial transportation company, one regular transportation schedule was finally selected, G70 (Han-Shi) Expressway from Wuhan to Xiangyang, China, which is more than 6 h of round-trip travel. Considering the time span of the experiment was more than 6 hours, all of the participants need to meet the following requirements: no sleep disorder, no job on shift or night routines, in good health, not on medication, and no serious disease in nearly five years; more male drivers were selected during this experiment as shown in Figure 3.

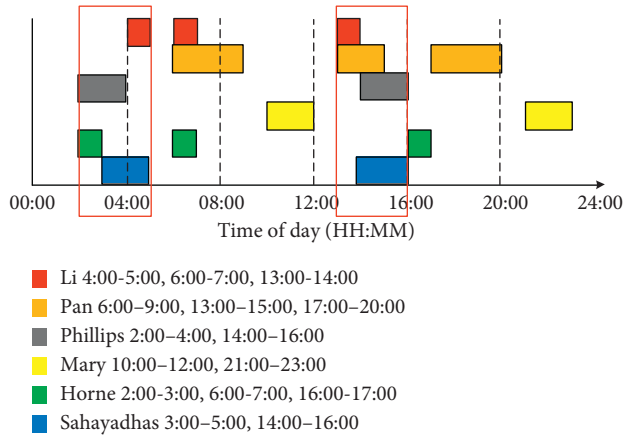


FIGURE 2: Fatigue peak period of the circadian rhythm.

Two weeks before the experiments, one recruitment notice for participant recruiting was issued in the cooperate company, and any driver who was actively licensed and met the appeal requirements can register. All of the participants were also required to abstain from drinking alcohol, tea, and caffeine within 72 hours before the driving schedule, and record their time of sleep within 24 hours before the driving schedule. Finally, a total of 50 participants who were actively licensed and in normal health, especially free from any sleep disorders [43, 44], were recruited from the company; they all signed informed consent agreement prior to their participation and got 500 yuan for his/her contribution, which was almost one time higher than their usual daily salary.

During the schedule, participants could take a break in one service area [1, 8] when they feel extremely fatigued and consider continue driving will lead to high collision risk, and the driver's face and the surrounding environment were recorded by several cameras (Figure 4(a)); a vision-based lane departure warning device Mobileye C2-270 was used to record the lane position data at a sampling rate of 8 Hz (Figure 4(b)), and all of the equipment were installed in one automatic transmission private vehicle (Figure 4(c)).

To obtain data with a large change in the fatigue level, driving schedules started around 09:00, 14:00, 21:00 were selected. However, 16 participants were excluded for various reasons: three drivers failed to complete the schedule, four of them drank alcohol within 24 to 72 hours before their schedules, and nine of them failed to fully cover neither of the two circadian rhythm peak periods. Finally, 34 drivers (middle-aged, mean = 47.8, SD = 5.1, and held the driving license for an average of 18.2 years with a standard deviation of 6.5 years) were selected, and the statistics of their schedules are shown in Figure 5. 24 participants whose schedules started around 09:00 were divided into the morning groups and further divided into three subgroups considering self-reported time of sleep within 24 hours before their schedules (time of sleep was recorded by one wearable device: smart bracelet) [45]. Every five participants whose schedules started around 14:00 or 21:00 were divided into the afternoon group and the night group.

The Karolinska Sleepiness Scale (KSS) [46] was used for evaluating subjective sleepiness because of its validity and

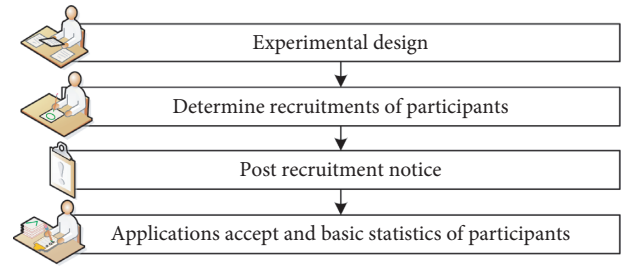


FIGURE 3: Participant selection flow.

reliability, and its scores range from 1 to 9, where 1 indicates extremely alert and 9 indicates extremely sleepy, even falling asleep; the higher the level is, the more fatigued the driver is. The self-reported KSS results of participants were recorded every five minutes by one experiment recorder and used as the subjective fatigue level measurement in this study. After the driver's KSS data were obtained, all KSS data were converted into fatigue value. In this study, the fatigue value is used to substitute the tiredness scores and defined as a nonunit constant, just for data processing and modeling. The fatigue value is transformed from a 9-grade KSS [47] to a 150 unmeasured value considering the actual performance of drivers and the related results in sleep studies [48], the transform process of the conversion between the KSS level and the overall fatigue value and the fatigue value changing data of the four factors are shown in Figure 6.

By analyzing the recorded video of the 34 selected participants, the driver's consecutive driving time, rest time, and the circadian rhythm range during the schedules could be obtained; the real-time fatigue value could be linearly summed to give overall tiredness scores [49], and the basic relationship between the four variables is shown in

$$FI(t) = F_{t_d} + F_{t_s} - F_{t_r} + F_{t_c}, \quad (1)$$

where $FI(t)$ is the total fatigue value in this study, F_{t_d} is the fatigue value caused by consecutive driving, F_{t_s} is the fatigue value after sleep, F_{t_r} is the fatigue value relieved by rest, and F_{t_c} is the fatigue value caused by circadian rhythms.

At first, the KSS levels were transferred to the fatigue value and expanded to 1 Hz by cubic spline interpolation, as shown in Figure 6 (fatigue value). To facilitate the subsequent model establishment, all time-related parameters were counted in seconds. Limited by the experimental conditions, circadian rhythm data were directly cited from exiting chronobiology studies [24, 36]. At the beginning of the experiment, the fatigue value was assumed only caused by circadian rhythm and time of sleep; after removing the fatigue value of the circadian rhythm (F_{t_c}) from the beginning, the remaining fatigue values were considered to be only caused by different times of sleep (F_{t_s}). After removing the fatigue value of circadian rhythm and time of sleep from the total fatigue value, the remaining fatigue values were considered to be caused by driving and rest ($F_{t_d} + F_{t_r}$). Because all of the experiments were carried out in a similar environment, the influence of various factors on driver fatigue, such as traffic flow, weather, and light, was ignored.



FIGURE 4: (a) Driving recorder, (b) mobileye, (c) experimental vehicle.

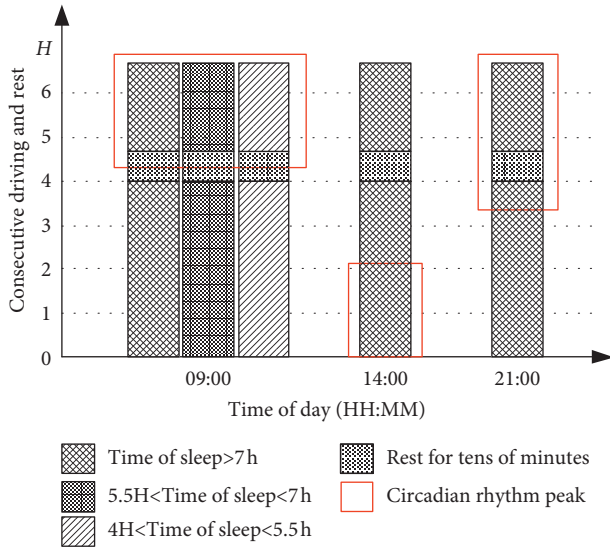


FIGURE 5: Participants' schedule statistics.

Driving performance is another valuable measurement to confirm the drivers' fatigue status; in this study, the standard deviation of lateral position (SDLP) is used as a verification indicator parameter [47, 50, 51]; it reflects the driver's ability to avoid unintentional lane departure or lane crossing. The lane line position was collected by Mobileye at a frequency of 10 Hz, the average of SDLP data in one second was processed into new data after filtering and used as a verification indicator, and the SDLP is computed by

$$SDLP = \sqrt{\frac{\sum_{i=1}^n (d_i - d_{avg})^2}{n}}, \quad (2)$$

where d_i denotes the i^{th} lane position for this horizontal curve segment. The lane position refers to the distance from the center of the vehicle to the right edge of each lane. d_{avg} denotes the average lane position and n denotes the sample size of the lane position.

3. Modeling and Verification

Five participants (three were from the morning group and two were from the other two groups) were randomly selected and used as validation, and their data were not used in the modeling process. In this study, the model validation is

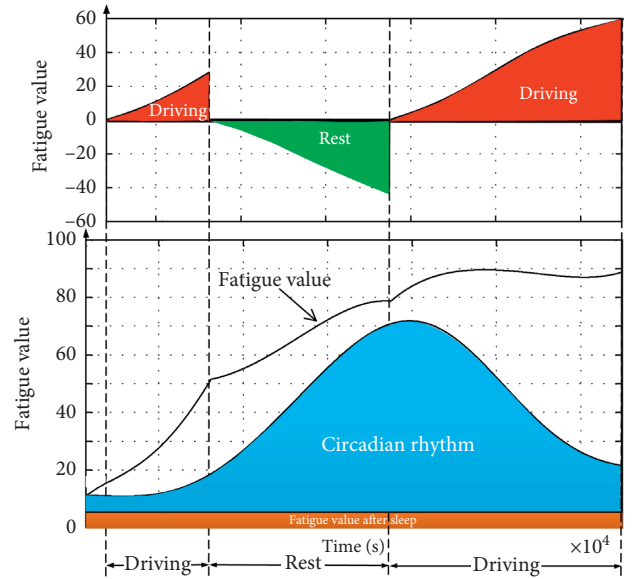


FIGURE 6: Sketch of the fatigue value variation corresponding to each factor.

performed using the root mean squared error (RMSE) and the coefficient of determination (R-square). Although some of the circadian rhythm data are missing, it does not affect its modeling, which has already been mentioned above, and through the above data processing process, the fatigue value data of the four indicators were obtained and their prediction model could be established.

3.1. Modeling of Fatigue Value Contributed by Circadian Rhythm. According to the previous research work, it could be seen that the fatigue value caused by circadian rhythm shows a regular change with the time of the day [36, 49, 51, 52]; in this study, it is assumed to be the same among all participants as an underlying fixed variable. Firstly, the missing circadian rhythm data are interpolated by cubic spline interpolation, and then the effects of circadian rhythm shown in Figure 7 were best fitted with a sum of sin functions shown as

$$F_{t_c} = \sum_{i=1}^8 a_i \sin(b_i t_c + c_i), \quad (3)$$

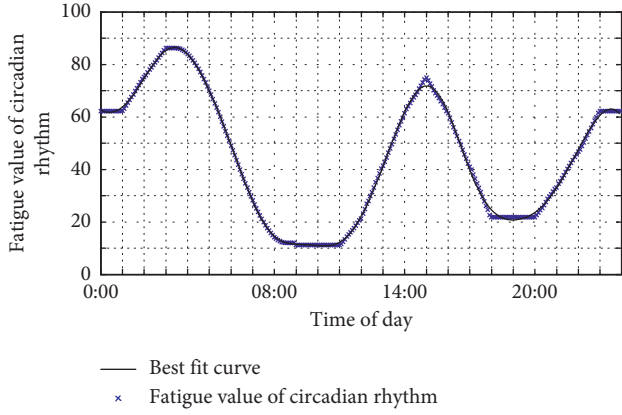


FIGURE 7: Fatigue value changes caused by the circadian rhythm.

where t_c is the time of day, from 0 s to 86400 s; a_i, b_i, c_i ($i = 1, 2, 3, \dots, 8$) are numerical constants and given at the end of this article; and F_{t_c} is the fatigue value caused by circadian rhythm. The SSE, R-square, and RMSE are 146, 0.9991, and 0.7437, respectively.

3.2. Modeling the Fatigue Value Caused by Hours of Sleep.

At the beginning of the experiments, the initial fatigue value of all participants with different times of sleep could be obtained. The fatigue values of different sleeping times could be best fitted with the model as in equation (4), and shown in Figure 8.

$$F_{t_s} = 954.9e^{-0.7211t_s^2}, \quad (4)$$

where t_s is the time of sleep in hours within 24 hours before driving, F_{t_s} is the fatigue value with different times of sleep. The validation parameters are SSE: 180.8, R-square: 0.911, and RMSE: 2.497.

3.3. Modeling of the Fatigue Value Contributed by Consecutive Rest.

In this study, each participant takes rest in the service area. After collecting the fatigue value data before and after the rest, the fatigue value relieving effects of different rest times could be estimated, which could be fitted with the model as in equation (5), and shown in Figure 9.

$$F_{t_r} = \frac{1.216t_r^2 + 1238t_r + 2.417 * 10^5}{t_r + 1.6 * 10^6}, \quad (5)$$

where t_r is the time on rest in seconds, F_{t_r} is the fatigue mitigation value, and the three validation parameters are SSE: 681.0, R-square: 0.8592, RMSE: 4.497.

3.4. Modeling of the Fatigue Value Caused by Consecutive Driving.

This study consists of three sets of experiments: morning group, afternoon group, and night group. In driving stages, different driving times and corresponding changes in the fatigue value are collected and presented in various colors in Figure 10. The analysis of its changing tendency can be obtained as follows:

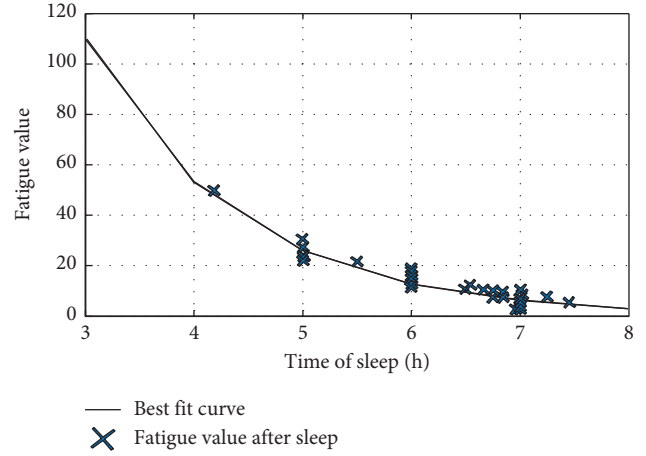


FIGURE 8: Fatigue value changes caused by time of sleep.

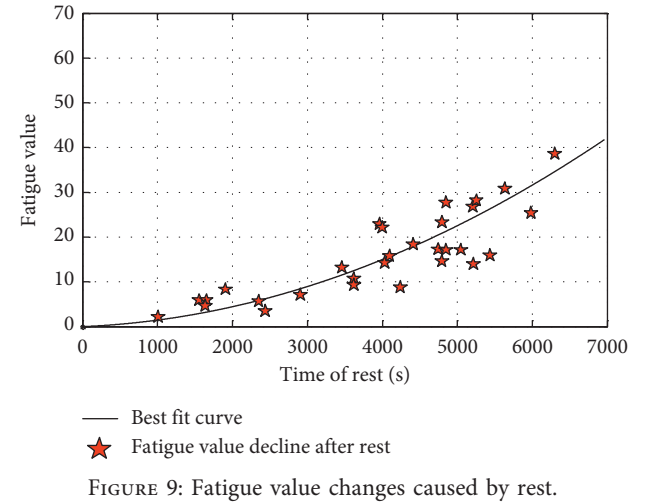


FIGURE 9: Fatigue value changes caused by rest.

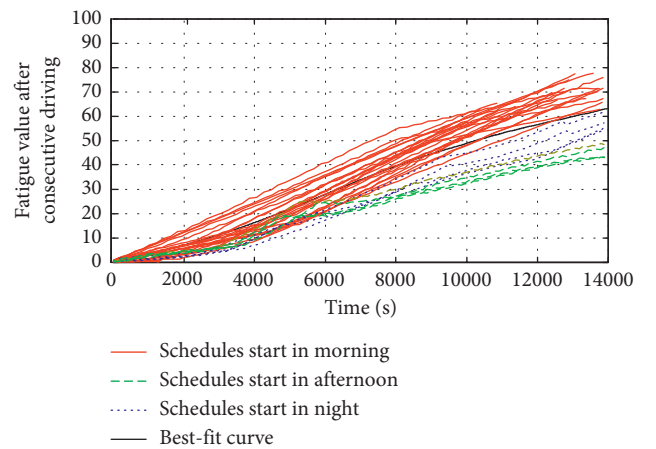


FIGURE 10: Fatigue value changes after consecutive driving.

$$F_{t_d} = 104.4 \sin(4.539 * 10^{-5} t_d - 0.01652) + 2.922 \sin(5.053 * 10^{-4} t_d - 3.135), \quad (6)$$

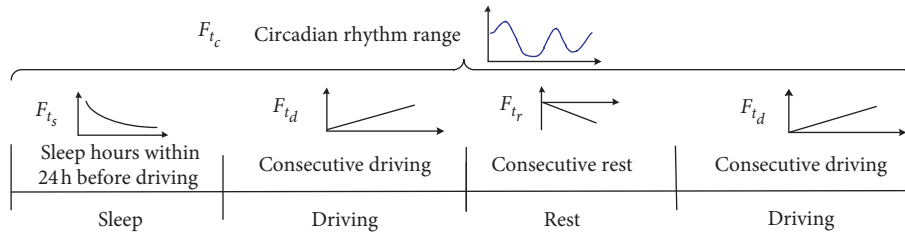


FIGURE 11: Time variable model description.

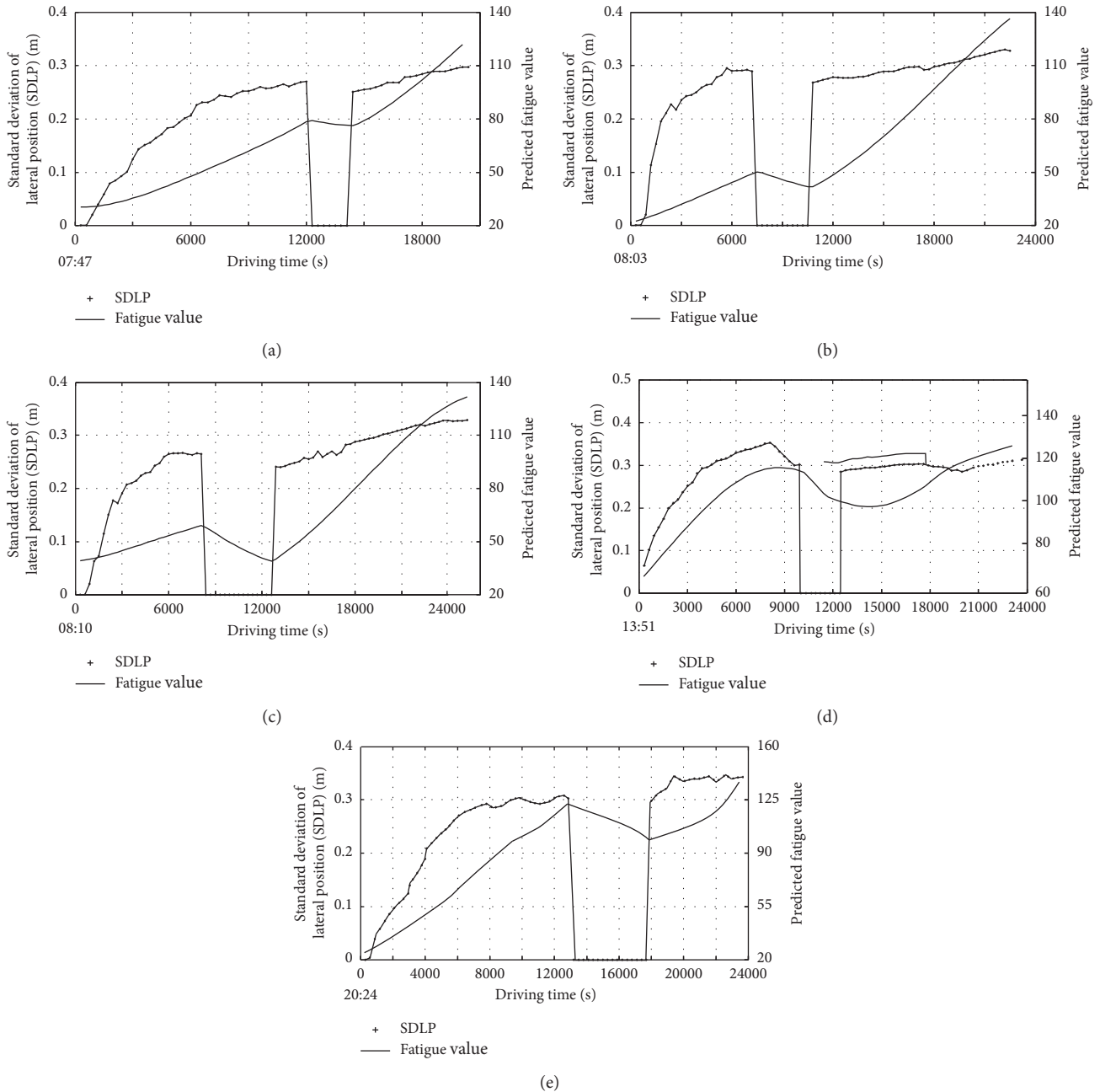


FIGURE 12: Comparison of the SDLP with the fatigue value of the three participants. (a) Subject with 7.4 hours of sleep. (b) Subject with 5.5 hours of sleep. (c) Subject with 3.8 hours of sleep. (d) Subject with 7.7 hours of sleep. (e) Subject with 7.8 hours of sleep.

where t_d are the different driving durations counted in seconds start in the morning, afternoon, and night, respectively, and F_{t_d} are driving fatigue values after consecutive driving. After nearly four hours of driving, it was found that the fatigue value calculated by the model is very close to the actual fatigue value. After the verification of the model, the value of each testing parameter is SSE: 390.4, R-square: 0.9999, and RMSE: 0.221.

3.5. Verification of the Fatigue Value Prediction Model Using SDLP. When drivers start driving, their time of sleep within 24 hours before driving could be collected, the time point when the driver starts driving as well as the whole circadian rhythm range in real time could be identified, and the two fatigue value parts are the basic fatigue value. Additionally, the consecutive driving time and rest time during driving could also be collected in real time. The driving fatigue value at any time point could be calculated using the collected data and established models, as shown in Figure 11.

SDLP data of the five selected participants could also be calculated; after extracting the corresponding time period of the five subjects' schedules, the fatigue value of circadian rhythm during the schedule, and the fatigue value of consecutive driving, rest, and different time of sleep were estimated. The relationship between the two sets of data can be calculated by Spearman's rho using

$$\rho = \frac{\text{cov}(rg_{FI}, rg_{sdlp})}{\sigma_{FI} \sigma_{sdlp}}, \quad (7)$$

where ρ denotes the usual Pearson correlation coefficient but applied to the two ranked sets of data, $\text{cov}(rg_{FI}, rg_{sdlp})$ is the covariance of the two ranked sets of data, and $\sigma_{FI}, \sigma_{sdlp}$ are the standard deviations of the two ranked sets of data.

The Spearman correlation coefficients of the 5 participants are (a): 0.9766, (b): 0.9549, (c): 0.9804, (d): 0.9661, and (e): 0.9035, respectively. Such values indicate that there is a strong correlation between the calculated fatigue value with the model and the SDLP, and the trends of the two sets are also consistent. Because most of the scheduled routes are highways, there were few lanes changing and interacting with other road users, so the change in SDLP could be seen as mainly caused by driver fatigue. For the participants from the morning group (a)–(c), in Figure 12, the trend of SDLP is the most moderate for the one with 7.4 sleep hours. The trends of SDLP of the two participants with 5.5 and 3.8 sleep hours are similar, especially during the period before having a break. In this study, 0.3 was considered as the SDLP threshold [23, 53], and the three participants exceeded the threshold during the later driving stage in their schedules. When 100 was seen as the participants' fatigue value threshold [49, 51, 52], only the SDLP of the participants with 7.4 hours of sleep is less than the threshold. In addition, the shorter the participants' sleep, the more the SDLP exceeds the threshold. For the afternoon group and the night group, the SDLP trends of the two participants are different from each other and the morning group. Compared with other participants, the participants in the afternoon group own the lowest fatigue value, but the

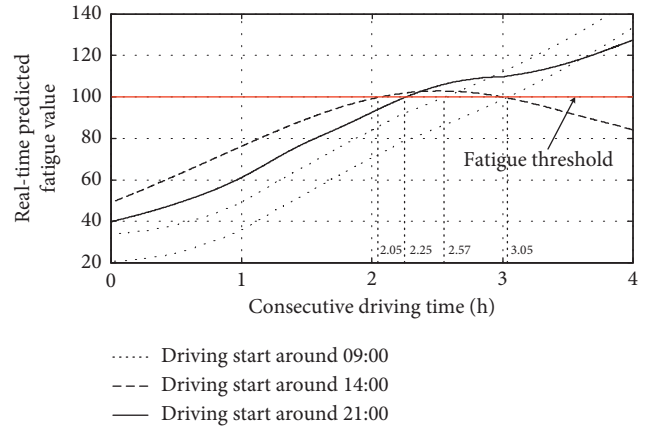


FIGURE 13: Maximum driving time below the fatigue threshold.

SDLP exceeds the threshold at the earliest. However, there is also a turning point at around 8000 s for the two participants for the afternoon group and the night group. When the SDLP of the night participant approaches 0.3 for the first time, its SDLP fluctuates around 0.3. After taking rest in the service area, the SDLP increased significantly.

3.6. Maximum Predicted Consecutive Driving Time. After the model is established and verified, the maximum consecutive driving time of drivers who start driving at different common times could be obtained, as shown in Figure 13. Assuming that the driver starts driving at 09:00, 14:00, and 21:00, respectively, the driving duration before the predicted fatigue value of drivers exceeds the threshold could be calculated. In this study, the threshold was set to 100 by reviewing the physiology-related literature. Because the peak of the circadian rhythm is between 13:00 and 16:00, the fatigue value of the driver who starts driving at 14:00 shows an arched shape. Within the first 2.5 hours of consecutive driving, driving fatigue rises slowly, and then turns to fall. During the whole driving process, driving fatigue reaches the threshold at 2.05 hours for the first time. At the same time, its initial fatigue value is also the highest among the three groups. When the driver starts driving around 09:00, under the influence of low circadian rhythm fatigue value, the initial fatigue value is the lowest among the three kinds; the area between the two dotted lines is the fatigue value changing the range for drivers who have different times of sleep. Before reaching the fatigue threshold, it is almost always the lowest. Finally, the driver will exceed the threshold after 2.57 to 3.05 hours of consecutive driving. Assuming the driver starts driving around 21:00, throughout the whole driving process, its tendency is very familiar to the morning group and their slope is almost the same before the fatigue value threshold, but the fatigue rises more quickly and reaches the threshold after 2.25 hours of consecutive driving.

4. Conclusions and Discussion

Real-time detection of driver fatigue is technically mature, and most of the vehicles have been equipped with different

kinds of relevant equipment to detect whether or not the driver is fatigued. But predicting the driver fatigue degree remains an important research topic. The purpose of this study is intended to predict driver fatigue only using time-related variables, such as consecutive driving time, consecutive rest, time of sleep within 24 hours before driving, and circadian rhythms during driving. Field experiments were conducted to obtain the fatigue-level indicators (KSS) and the driving performance (SDLP). The model in this study was developed from field experiments using an equipped car, which might be more believable than using a driving simulator. The strong correlation between the predicted fatigue value and SDLP collected from the Mobileye demonstrated that the developed method in this study is reliable. A major finding of this study is the establishment of models contributed by circadian rhythm, time of sleep, time of rest, and the detailed modeling of driving duration starting at different times. The analysis results indicated that when drivers reached a higher fatigue level, they would swing around when driving. And driving fatigue affects lane-keeping performance significantly. At the same time, even when the driver is at a low fatigue level, their driving performance will still reduce after driving for a consecutive time. In a word, the results demonstrate that it is possible to predict driver's fatigue degree at a certain moment using the developed driving fatigue prediction model which only considers the four time-related variables. Instead of using KSS to verify the accuracy of the model, the driving performance indicator SDLP was used because the operational indicator standard is more uniform. Even though the KSS has been widely used, for different observers (the observer in this study did not change) and participants, their understanding of fatigue is difficult to maintain in a consistent standard. In our best case, the correlation between the calculated fatigue value and computed SDLP is up to 98%, showing that the model in this study could reflect the drivers' fatigue change trend perfect. The maximum consecutive driving time calculated in this article using the model is really shorter than any existing regulation; even the longest time is only around three hours. It is hard to say whether this is a problem with the model established in the study or the setting of the fatigue value threshold or some urgent improvements in the existing regulations; this will be further studied in future research.

The purpose of this study is to use the time-related variables to predict the time when the driver will be fatigued. In the data analysis process, the authors try to avoid using behavioral, physiological, and vehicle data for modeling. The other variables, including physiological variables (e.g., respiration), behavioral variables (e.g., head position), or vehicle information (e.g., speed), always need to face the problem of statistical frequency when dealing with them. Regardless of the size of the time window used for data processing, a time window is always required when getting an indicator. This results in the inability to perform real-time fatigue prediction. However, this study has several limitations. First, KSS and SDLP used in this study may limit the accuracy of the results. As for driving performance indicators, because of the limited funds and lack of equipment,

only the SDLP was analyzed. In addition, the collection frequency of KSS is a little high (one point every 5 minutes), and this may help drivers keep awake [54]. What is more, in these field experiments, participants need driving on the highway for at least 4 hours, and it may become difficult for drivers to judge their drowsiness [55] after a period of driving. Second, age and gender are the two main important indicators that may affect influent driving performance, but they are not taken into account in this study. Some experimental conditions factors, such as weather and traffic flow, are not considered either. Even though the authors tried their best to ensure that the experiments are conducted in the same conditions, there is still no guarantee that all conditions are the same. Moreover, when drivers restart driving after rest in the service area, the model of driving time needs to be deeply explored. When drivers start driving again, their starting time is close to the starting time of the next set of experiment group. Moreover, for the experiments starting in the afternoon and night, the fatigue accumulated in the daytime before the experiments are only estimated using the hours of sleep, which may be inaccurate, and the fatigue of these drivers should be divided more meticulously in the future work.

Data Availability

The data used in this study are available from the corresponding author on request.

Conflicts of Interest

The authors declare that there are no conflicts of interest regarding the publication of this article.

Acknowledgments

This work was supported by the National Natural Science Foundation of China (61603282, U1764262, 51775396) and the Major Project of Technological Innovation of Hubei Province (2017CFA008).

Supplementary Materials

As shown in Figure 7, the black line is the best fit curve of the fatigue value of circadian rhythm and the curve could be described by equation (3), where F_{t_c} is the fatigue value caused by circadian rhythm; t_c is the time of day, 0 to 86400 seconds from 00:00 every day; and a_i , b_i , c_i ($i=1, 2, 3, \dots, 8$) are numerical constants, and all of the parameters are shown in the below supplementary table. (*Supplementary Materials*)

References

- [1] G. Zhang, K. K. W. Yau, X. Zhang, and Y. Li, "Traffic accidents involving fatigue driving and their extent of casualties," *Accident Analysis & Prevention*, vol. 87, pp. 34–42, 2016.
- [2] World Health Organization, *Global Status Report on Road Safety 2018*, World Health Organization, Geneva, Switzerland, 2018.

- [3] A. W. MacLean, D. R. T. Davies, and K. Thiele, "The hazards and prevention of driving while sleepy," *Sleep Medicine Reviews*, vol. 7, no. 6, pp. 507–521, 2003.
- [4] World Health Organization, *Global Status Report on Road Safety 2013: Supporting a Decade of Action*, World Health Organization, Geneva, Switzerland, 2013.
- [5] National Sleep Foundation, *Drowsy Driving Facts and Stats*, National Sleep Foundation, Washington, DC, USA, 2005, <http://www.drowsydriving.org/about/facts-and-stats/>.
- [6] D. J. Beirness, H. M. Simpson, and K. Desmond, *The Road Safety Monitor 2004: Drowsy Driving*, Traffic Injury Research Foundation, Ottawa, Canada, 2005.
- [7] Canadian Council of Motor Transport, *Canadian Fatigue Related Collisions: Fatality Estimates 2000–2005*, Canadian Council of Motor Transport, Ottawa, Canada, 2010.
- [8] Traffic Management Bureau of the Ministry of Public Security, *China Road Traffic Accidents Annual Statistical Report*, Traffic Management Bureau of the Ministry of Public Security, Wuxi, China, 2017.
- [9] European Union, *European Union Law and Official Journals, Regulation (EC) No 561/2006 of the European Parliament and of the Council of 15 March 2006 on the Harmonisation of Certain Social Legislation Relating to Road Transport and Amending Council Regulations (EEC) No 3821/85 and (EC) No 2135/98 and Repealing Council Regulation (EEC) No 3820/85 (Text with EEA Relevance)*, European Union, Brussels, Belgium, 2006, <https://eur-lex.europa.eu/eli/reg/2006/561/2015-03-02>.
- [10] A. H. Amundsen and F. Sagberg, *Hours of Service Regulations and the Risk of Fatigue- and Sleep-Related Road Accidents: A Literature Review*, Swedish National Road Administration, Oslo, Norway, 2003.
- [11] A. Bernhardt, T. Melo, T. Bousonville, and H. Kopfer, "Scheduling of driver activities with multiple soft time windows considering European regulations on rest periods and breaks," *Schriftenreihe Logistik der Fakultät für Wirtschaftswissenschaften der htw saar No. 12*, Hochschule für Technik und Wirtschaft des Saarlandes, Fakultät für Wirtschaftswissenschaften, Saarbrücken, Germany, 2016.
- [12] C. Chen and Y. Xie, "Modeling the safety impacts of driving hours and rest breaks on truck drivers considering time-dependent covariates," *Journal of Safety Research*, vol. 51, pp. 57–63, 2014.
- [13] Federal Motor Carrier Safety Administration, *Summary of Hours of Service Regulation*, Federal Motor Carrier Safety Administration, Washington, DC, USA, 2006, <http://www.fmcsa.dot.gov/regulations/hours-service/summary-hours-service-regulations>.
- [14] People's Republic of China, *Road Traffic Safety Law of the People's Republic of China*, Beijing, China, 2015, <http://www.bjjtgl.gov.cn/jgj/fl/205308/index.html>.
- [15] L. Wang and Y. Pei, "The impact of continuous driving time and rest time on commercial drivers' driving performance and recovery," *Journal of Safety Research*, vol. 50, pp. 11–15, 2014.
- [16] K. Regal, *60-Day Notice of Proposed Information Collection: Flexible Sleeper Berth Pilot Program*, Federal Motor Carrier Safety Administration, Washington, DC, USA, 2017, <http://carsandracingstuff.com/library/articles/38617.php>.
- [17] G. Yang, Y. Lin, and P. Bhattacharya, "A driver fatigue recognition model based on information fusion and dynamic Bayesian network," *Information Sciences*, vol. 180, no. 10, pp. 1942–1954, 2010.
- [18] T. J. Balkin, W. J. Horrey, R. C. Graeber, C. A. Czeisler, and D. F. Dinges, "The challenges and opportunities of technological approaches to fatigue management," *Accident Analysis & Prevention*, vol. 43, no. 2, pp. 565–572, 2011.
- [19] A. D. McDonald, J. D. Lee, C. Schwarz, and T. L. Brown, "A contextual and temporal algorithm for driver drowsiness detection," *Accident Analysis & Prevention*, vol. 113, pp. 25–37, 2018.
- [20] Q. Ji, P. Lan, and C. Looney, "A probabilistic framework for modeling and real-time monitoring human fatigue," *IEEE Transactions on Systems, Man, and Cybernetics - Part A: Systems and Humans*, vol. 36, no. 5, pp. 862–875, 2006.
- [21] X. Wang and C. Xu, "Driver drowsiness detection based on non-intrusive metrics considering individual specifics," *Accident Analysis & Prevention*, vol. 95, pp. 350–357, 2016.
- [22] J. Chen, H. Wang, and C. Hua, "Assessment of driver drowsiness using electroencephalogram signals based on multiple functional brain networks," *International Journal of Psychophysiology*, vol. 133, pp. 120–130, 2018.
- [23] H. Zhang, C. Wu, X. Yan, and T. Z. Qiu, "The effect of fatigue driving on car following behavior," *Transportation Research Part F: Traffic Psychology and Behaviour*, vol. 43, pp. 80–89, 2016.
- [24] N. Goel, M. Basner, H. Rao, and D. F. Dinges, "Circadian rhythms, sleep deprivation, and human performance," *Progress in Molecular Biology and Translational Science*, vol. 119, pp. 155–190, 2013.
- [25] P. P. Jovanis, K.-F. Wu, and C. Chen, "Effects of hours of service and driving patterns on motor carrier crashes," *Transportation Research Record: Journal of the Transportation Research Board*, vol. 2281, no. 1, pp. 119–127, 2012.
- [26] T. D. Lin, P. P. Jovanis, and C. Z. Yang, "Time of day models of motor carrier accident risk," *Transportation Research Record*, vol. 1467, p. 1, 1994.
- [27] Y. P. Yan-li Ma, "Influences of consecutive driving time on test indicators of driving characteristics," *China Journal of Highway and Transport*, vol. 22, no. 1, pp. 84–88, 2009.
- [28] T. Jing, S. Xinghao, J. Lijuan, S. Qichong, and P. Changxu, "Experimental study of fatigue characteristics of bus drivers under the condition of consecutive driving," *Journal of Transportation Safety & Security*, vol. 3, pp. 87–92, 2013.
- [29] M. L. Jackson, R. J. Croft, G. A. Kennedy, K. Owens, and M. E. Howard, "Cognitive components of simulated driving performance: sleep loss effects and predictors," *Accident Analysis & Prevention*, vol. 50, pp. 438–444, 2013.
- [30] E. Demirdöğen Çetinoğlu, A. Görek Dilektaşlı, N. Ateş Demir et al., "The relationship between driving simulation performance and obstructive sleep apnoea risk, daytime sleepiness, obesity and road traffic accident history of commercial drivers in Turkey," *Sleep Breath*, vol. 19, no. 3, pp. 865–872, 2015.
- [31] S.-W. Lim, J.-W. Paik, H.-J. Lee, L. Kim, and K.-S. Oh, "S49.C sleep deprivation and traffic accident involved professional truck drivers in Korea," *Sleep Medicine*, vol. 8, p. S46, 2007.
- [32] P. Thiffault and J. Bergeron, "Fatigue and individual differences in monotonous simulated driving," *Personality and Individual Differences*, vol. 34, no. 1, pp. 159–176, 2003.
- [33] B. C. Tefft, "Acute sleep deprivation and culpable motor vehicle crash involvement," *Sleep*, vol. 41, no. 10, pp. 1–11, 2018.
- [34] Federal Motor Carrier Safety Administration, "Federal Register," Vol. 76, No. 248, <http://www.gpo.gov/fdsys/pkg/FR-2011-12-27/pdf/2011-32696.pdf>.
- [35] W. Yuhua, Q. I. Chunhua, Z. H. U. Shoulin, X. I. E. Songfang, and Z. Ting, *Study on Driving Fatigue Recovery Time Based on ECG Analysis*, 2017.

- [36] J. D. Minkel and D. F. Dinges, *Circadian Rhythms in Sleepiness, Alertness, and Performance*, Elsevier Inc., Amsterdam, Netherlands, 5th edition, 2010.
- [37] W. J. LI Ping-fan, D.-H. Wang, and L. I. U. Dong-bo, "Analysis on Driving Fatigue before and after Lunch based on Indices of Physiology and Psychology," *Journal of Chang'an University: Natural Science*, vol. 4, pp. 81–86, 2011.
- [38] T. Pan, *Research on Driver's Traffic Quality Obstacle and Solution*, Zhejiang University, Hangzhou, China, 2007.
- [39] R. O. Phillips, "A review of definitions of fatigue - and a step towards a whole definition," *Transportation Research Part F: Traffic Psychology and Behaviour*, vol. 29, pp. 48–56, 2015.
- [40] M. Chipman and Y. L. Jin, "Drowsy drivers: the effect of light and circadian rhythm on crash occurrence," *Safety Science*, vol. 47, no. 10, pp. 1364–1370, 2009.
- [41] J. A. Horne and L. A. Reyner, "Sleep related vehicle accidents," *BMJ*, vol. 310, no. 6979, pp. 565–567, 1995.
- [42] A. Sahayadhas, K. Sundaraj, and M. Murugappan, "Drowsiness detection during different times of day using multiple features," *Australasian Physical & Engineering Sciences in Medicine*, vol. 36, no. 2, pp. 243–250, 2013.
- [43] M. M. de Tlio, F. V. Narciso, S. Tufik et al., "Sleep disorders as a cause of motor vehicle collisions," *International Journal of Preventive Medicine*, vol. 4, no. 3, pp. 246–257, 2013.
- [44] J. C. Stutts, J. W. Wilkins, J. Scott Osberg, and B. V. Vaughn, "Driver risk factors for sleep-related crashes," *Accident Analysis & Prevention*, vol. 35, no. 3, pp. 321–331, 2003.
- [45] M. Pylkknen, M. Sihvola, H. K. Hyvrinen, S. Puttonen, C. Hublin, and M. Sallinen, "Sleepiness, sleep, and use of sleepiness countermeasures in shift-working long-haul truck drivers," *Accident Analysis & Prevention*, vol. 80, pp. 201–210, 2015.
- [46] K. Kaida, M. Takahashi, T. Åkerstedt et al., "Validation of the Karolinska sleepiness scale against performance and EEG variables," *Clinical Neurophysiology*, vol. 117, no. 7, pp. 1574–1581, 2006.
- [47] X. Chuan, W. Xuesong, C. Xiaohong, and Z. Hui, "Driver drowsiness level analysis and predication based on decision tree," *Journal of Tongji University (Natural Science)*, vol. 43, no. 1, pp. 75–81, 2015.
- [48] Y. Thanaboriboon, P. Iamtrakul, S. Srivivat, N. Kotchabhakdi, and M. Leechawengwongs, "S49.D effect of fatigue and sleep deprivation on driving performance: an experimental study in Thailand," *Sleep Medicine*, vol. 8, pp. S46–S47, 2007.
- [49] A. Koh, G. R. Jones, J. W. Spencer, and I. Thomas, "Chromatic analysis of signals from a driver fatigue monitoring unit," *Measurement Science and Technology*, vol. 18, no. 3, pp. 747–754, 2007.
- [50] H. Zhang, C. Wu, Z. Huang, X. Yan, and T. Z. Qiu, "Sensitivity of lane position and steering angle measurements to driver fatigue," *Transportation Research Record: Journal of the Transportation Research Board*, vol. 2585, no. 1, pp. 67–76, 2016.
- [51] P.-H. Ting, J.-R. Hwang, J.-L. Doong, and M.-C. Jeng, "Driver fatigue and highway driving: a simulator study," *Physiology & Behavior*, vol. 94, no. 3, pp. 448–453, 2008.
- [52] D. McEachron, *Chronobioengineering: Introduction to Biological Rhythms with Applications*, Vol. 1, Morgan & Claypool, San Rafael, CA, USA, 2012.
- [53] M. Gastaldi, R. Rossi, and G. Gecchele, "Effects of driver task-related fatigue on driving performance," *Procedia - Social and Behavioral Sciences*, vol. 111, pp. 955–964, 2014.
- [54] C. Jacob de Naurois, C. Bourdin, A. Stratulat, E. Diaz, and J.-L. Vercher, "Detection and prediction of driver drowsiness using artificial neural network models," *Accident Analysis & Prevention*, vol. 126, pp. 95–104, 2019.
- [55] F. Friedrichs and B. Yang, "Drowsiness monitoring by steering and lane data based features under real driving conditions," in *Proceedings of the 18th European Signal Processing Conference*, pp. 209–213, Aalborg, Denmark, August 2010.

Research Article

Optimizing the Junction-Tree-Based Reinforcement Learning Algorithm for Network-Wide Signal Coordination

Yi Zhao , Jianxiao Ma, Linghong Shen, and Yong Qian

College of Automobile and Traffic Engineering, Nanjing Forestry University, Nanjing 210037, China

Correspondence should be addressed to Yi Zhao; zhaoyi207@126.com

Received 31 October 2019; Revised 1 January 2020; Accepted 24 January 2020; Published 21 February 2020

Guest Editor: Zeyang Cheng

Copyright © 2020 Yi Zhao et al. This is an open access article distributed under the Creative Commons Attribution License, which permits unrestricted use, distribution, and reproduction in any medium, provided the original work is properly cited.

This study develops three measures to optimize the junction-tree-based reinforcement learning (RL) algorithm, which will be used for network-wide signal coordination. The first measure is to optimize the frequency of running the junction-tree algorithm (JTA) and the intersection status division. The second one is to optimize the JTA information transmission mode. The third one is to optimize the operation of a single intersection. A test network and three test groups are built to analyze the optimization effect. Group 1 is the control group, group 2 adopts the optimizations for the basic parameters and the information transmission mode, and group 3 adopts optimizations for the operation of a single intersection. Environments with different congestion levels are also tested. Results show that optimizations of the basic parameters and the information transmission mode can improve the system efficiency and the flexibility of the green light, and optimizing the operation of a single intersection can improve the efficiency of both the system and the individual intersection. By applying the proposed optimizations to the existing JTA-based RL algorithm, network-wide signal coordination can perform better.

1. Introduction

Signal control system is an important method of improving the operation of urban traffic. With the development of people's understanding on traffic and technology, urban traffic signal control systems have undergone three stages: single-point, linear coordinated, and regional coordinated. Traffic signal coordination is considered to be more effective in alleviating traffic congestion than single-point and linear coordinated.

1.1. Review of the Literature on Signal Coordination.

Signal coordination has been studied extensively over the past 30 years. The first developed signal coordination control systems include SCOOT [1], SCATS [2], PROLYN [3], OPAC [4], RHODES [5], UTOPIA [6], CRONOS [7], and TUC [8]. Although the signal coordination control can achieve better effects than the single-point signal control and the inductive signal control, there are also many restrictions on the signal coordination control, such as difficulty in

parameter calibration, computational complexity, and poor adaptability and stability.

Considering these restrictions and the fact that the dynamic characteristics of the traffic environment also provide the need for interactive environment-based learning from the environment, machine learning algorithms are proposed to be used in signal coordination control research. Among the machine learning algorithms, the reinforcement learning (RL) algorithm is the most widely used in the field of traffic signal control.

Liang et al. [9] proposed a deep reinforcement learning model to control the traffic light cycle. Aslani et al. [10] introduced the actor-critic method to solve the problem of the trade-off between exploration of the traffic environment and exploitation of the knowledge already obtained. Aslani et al. [11] developed adaptive traffic signal controllers based on continuous residual reinforcement learning to improve their stability. Jeon et al. [12] suggested a novel artificial intelligence that only uses video images of an intersection; the image-based RL model outperformed both the actual operation of fixed signals and a fully actuated operation. Aziz

et al. [13] applied R-Markov Average Reward Technique-based reinforcement learning algorithm for vehicular signal control problem leveraging information sharing among signal controllers in the connected vehicle environment. Darmoul et al. [14] suggested a Immune Network Algorithm-based Multiagent System to control a network of signalized intersections, which is able to handle different traffic scenarios.

Graph theory models can reduce the computational complexity of RL, especially when joint action of multiagents needs to be calculated. But not much research has been done in this area. Some work has included developments in the max-plus algorithm and junction-tree algorithm (JTA); these have been applied to signal coordination control research at the road network level.

Medina and Beenekohal [15] applied the max-plus algorithm as a coordinating strategy in the network-wide signal control problem. However, the max-plus algorithm has two key limitations. Firstly, it is only applicable to tree-structured networks and cannot guarantee the convergence to an optimal solution for general cyclic networks. Secondly, this algorithm only provides a brief loopy propagation that refers to inexact messages received at a node. Thus, it only provides an approximate inference of the exact message being passed. Zhu et al. [16] first proposed the JTA instead of the max-plus algorithm to obtain the best joint action for traffic signals and to realize network-wide signal coordination. JTA was first proposed by Jensen et al. [17]. The advantage of JTA is that it is computationally efficient and can handle looped or acyclic road networks and accurately infer the best joint scheme.

1.2. Motivations and Contributions of this Study. Zhu et al. [16] demonstrated that the test network can perform better under the JTA compared to an adaptive or single-agent RL-based control. Although the network system improved, some intersections still experienced poor operations. Zhu et al. [16] also noted that it is necessary to assess the variance of performance metrics at the intersection level, and modified schemes should be developed to optimize the system to ensure desired level of performance at local intersections.

To summarize, the research goals are as follows:

- (1) To optimize the basic parameters of the JTA algorithm so that the signal coordination control scheme is consistent with actual requirements
- (2) To evaluate the impact of existing algorithms on local intersection operations
- (3) To propose optimization measures for local intersections to improve the practical application value of the algorithm

2. Introducing the Junction-Tree-Based RL Algorithm

2.1. Reinforcement Learning (RL) and Its Application in Signal Control. The basic RL model is shown in Figure 1. It

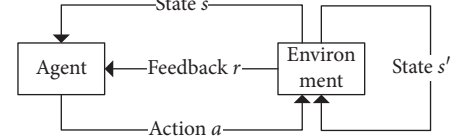


FIGURE 1: The basic reinforcement learning model.

contains an environment, agents, learners, and strategies. The agent obtains the state “s” from the environment and selects action “a” according to the state. The action “a” interacts with the environment, which then returns to a new state “s’” and sends a certain feedback “r” to the agent. After repeated interactions, the agent can learn an optimal strategy for the situations presented.

In the application of RL to traffic signal control, the road network is the environment and the signal control machine is the agent. During the decision period, the signal control machine takes an action to activate a signal phase, and the state of the environment changes accordingly. The goal of the algorithm is to obtain the optimal strategy that can achieve the maximum return. The optimal strategy is to map the activation phase and state of the traffic. The feedback can include average delay and the number of stops. Its value can be extracted directly from the environment.

2.2. Junction-Tree Algorithm and Application in Signal Control. The key idea of the JTA is to find a way to decompose the global computation of joint probability into a set of related local computations. The JTA is introduced to reveal the important connections between global and local probabilistic reasoning using graph theory.

The essence of the JTA is information transmission. The forward transmission is the transfer from the root node to the leaf node, while the reverse transmission is from the leaf node to the root node. The process of information transfer can be expressed by equations (1)–(4).

Forward transmission from v to s :

$$(\psi'_v, \phi'_s) = \arg \max_{v/s} \psi_v. \quad (1)$$

Forward transmission from s to w :

$$\psi'_w = \frac{\phi'_s}{\phi_s} \psi_w. \quad (2)$$

Reverse transmission from w to s :

$$(\psi''_w, \phi''_s) = \arg \max_{w/s} \psi'_w. \quad (3)$$

Reverse transmission from s to v :

$$\psi''_v = \frac{\phi''_s}{\phi'_s} \psi'_v. \quad (4)$$

In the equations above, v is the root node; w is the leaf node; s is the separation node; ψ_v , ψ_w , and ϕ_s denote potential functions of v , w , and s ; ψ'_v , ϕ'_s , and ψ'_w denote

potential functions after forward transmission; and ψ_v'' , ϕ_s'' , and ψ_w'' denote potential functions after reverse transmission.

JTA and RL have the same objective function in terms of calculating the maximum posteriori probability. They both decompose the whole network optimization problem into local subproblems, and both use their Markov attributes to do so. In the probability model, the probability of a node depends on the adjacent nodes. In the coordinated traffic signal control, the phase selection of the intersection depends on the phase of the adjacent intersection. Therefore, JTA is selected to solve a coordinated traffic signal control problem. JTA has great advantages in dealing with coordinated traffic signal control problems because it is the fastest and most accurate inference algorithm.

2.3. The Junction-Tree-Based RL Algorithm. The control flow of the JTA-based RL algorithm method is shown in Figure 2. In the applied method, the RL is the core algorithm of signal control, and the JTA is used to find the signal control scheme with the highest rate of return. Existing research verifies that the applied method is better than the timing signal control, the independent Q learning signal control, and the maximum queue length priority signal control under different traffic intensities.

It should be noted that the RL algorithm can learn the Q value under specific traffic demand and signal control scheme for one or two adjacent intersections. But, the RL algorithm cannot learn the Q value for the whole network with too many intersections because of the large scale of knowledge to be learned. JTA is adopted to achieve the best signal control scheme so that the Q value for the whole network is the best one. In the proposed algorithm, there is no cycle time and split. If the frequency of running JTA is 1 s, then the algorithm can only decide which phase is green light for each intersection in the next 1 s.

3. Optimizing the Junction-Tree-Based RL Algorithm

3.1. Optimizing Basic Parameters

3.1.1. Frequency of Running the JTA. As the JTA determines the phase-switch at intersections, the lower frequency running it, the longer a given phase duration will be. To adjust the signal control scheme according to feedback in time, the frequency to run the JTA should not be lower than the headway of queuing vehicles passing the parking line.

Both Shao et al. [18] and Zhao et al. [19] have verified that the headway is less than 2 s when the queue length is longer than 10 vehicles. However, in existing research on JTA, the frequency is 5 s which cannot meet actual control requirements. In order to improve the sensitivity of the signal control scheme, and considering the minimum step size of the signal control scheme, 1 s is employed in this study.

3.1.2. Intersection Status Division. The JTA-based RL algorithm selects the phase scheme with the highest return according to the state of the road network. Phase schemes

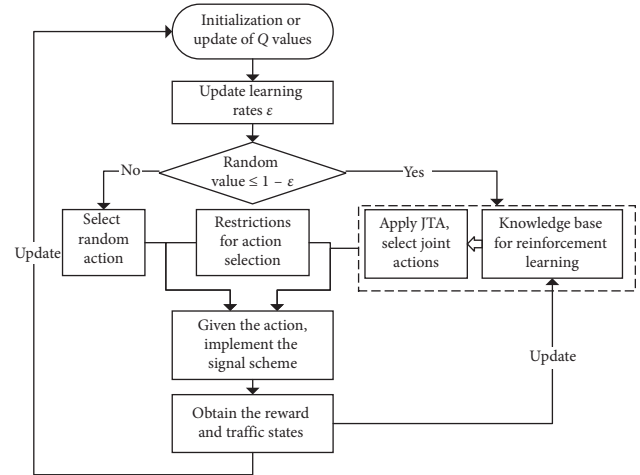


FIGURE 2: The control flow of the JTA-based RL algorithm method.

are determined by the number of intersections and the phases of a single intersection, which are relatively fixed. Therefore, the accuracy of the applied method for signal control is determined by the state of the road network. However, the large number of intersections available when signal coordination control is performed provides a status division that is too detailed and may lead to a long learning time. Existing studies treat the saturation as the evaluation index of intersection entrance, and saturations of all phases are summed and divided into three levels. That is, each intersection contains three states, and the state of two adjacent intersections is divided into nine. In general, this state division is rough and makes the signal control scheme less sensitive to the traffic state of the road network.

Considering that the state will be defined as an eight-dimensional vector in the program of the applied method, the saturation of each intersection entrance is divided into three levels, and then each intersection is divided into 81 states. In future applications, the status of the intersection can be divided in more detail based on specific requirements.

3.2. Analysis of the JTA Information Transmission Mode. The JTA uses the continuity function while calculating the maximum posteriori probability, which should not be directly applied to the information transmission in traffic signal coordination control. Therefore, a new information transmission mode that will be applied in signal coordination control is defined. The new transmission mode, taking four intersections as the example, is shown as follows.

Suppose that all four intersections have only two phases, A and B; phase A is for north-south traffic, and phase B is for east-west traffic. The virtual road network can be transferred into a junction tree using moralization and triangulation, see Figure 3. Intersections 1–3 form a root node; intersections 2–4 form a leaf node, and intersections 2 and 3 form a separation node. The key parameter Q is the value of two adjacent intersections and is shown in Table 1.

The target function of JTA is $\arg \max(Q_{12} + Q_{13} + Q_{24} + Q_{34})$.

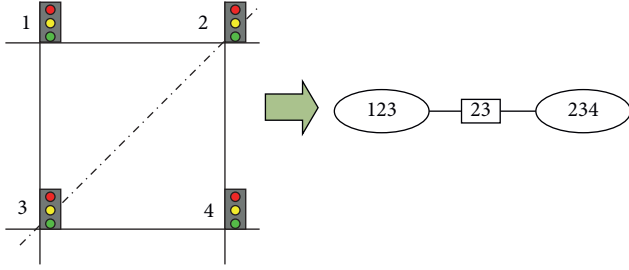


FIGURE 3: Virtual road networks and the corresponding junction tree.

3.2.1. Initialization: Define the Potential Function of all Nodes. The potential functions of the root and leaf nodes are the sum of the Q values of three intersections that form the node. The potential function of the separation node is the phase combination of two intersections that form the node; the initial value is null.

The potential function of the root node is $\psi_{123} = Q_{123} = Q_{12} + Q_{13}$

The potential function of the separation node is $\phi_{23} = \text{Null}$

The potential function of the leaf node is $\psi_{234} = Q_{234} = Q_{24} + Q_{34}$

3.2.2. Forward Transmission from the Root Node to the Separation Node. The transmission function is $(\psi'_{123}, \phi'_{23}) = \arg \max \psi_{123} = \arg \max (Q_{12} + Q_{13})$.

After transmission, ψ_{123} should achieve the max value ψ'_{123} under all possible potential functions ϕ_{23} and also achieve the best phase combination ϕ'_{23} . The transmission result is shown in Table 2.

3.2.3. Forward Transmission from the Separation Node to the Leaf Node. The transmission function is $\psi'_{234} = \phi'_{23} \psi_{234} = \phi'_{23} (Q_{24} + Q_{34})$.

After transmission, the potential function of leaf node ψ_{234} changes to ψ'_{234} .

3.2.4. Reverse Transmission from the Leaf Node to the Separation Node. The transmission function is $\arg \max (Q_{24} + Q_{34})$, $(\psi''_{234}, \phi''_{23}) = \arg \max \psi'_{234} = \arg \max \phi'_{23} (Q_{24} + Q_{34})$.

After transmission, ψ'_{234} should achieve the max value ψ''_{234} under all possible potential functions ϕ_{23} and the best phase combination ϕ''_{23} . The transmission result is shown in Table 3.

By combining ϕ''_{23} and $\arg \max (Q_{24} + Q_{34})$, it is easy to understand that $\phi''_{23} (Q_{24} + Q_{34})$ achieves the maximum value only when ϕ''_{23} selects combination 4. In other words, $\phi''_{23} (Q_{24} + Q_{34})$ can achieve the maximum value only when intersections 2, 3, and 4 are all in phase B; at the same time, ψ''_{234} must be 13.

3.2.5. Reverse Transmission from the Separation Node to the Root Node. The transmission function is $\psi''_{123} = \phi''_{23} \psi'_{123}$.

After transmission, ψ'_{123} changes to ψ''_{123} based on ϕ''_{23} . At this time, ψ''_{123} is 16, and intersection 1 is in phase B. The

result of applying JTA is obtained after the above information transmission occurs, that is, after the joint action of the four intersections becomes (B, B, B, B), which will result in the joint tree achieving its highest potential function.

3.3. Optimizations for Single Intersection's Operation. Network-wide signal coordination control both pursues the system optimization and the requirements of the individual intersection. For example, the queue length of a single intersection entrance should not be too long when the network has a low average queue length. The JTA-based RL algorithm considers system optimization to be the goal; however, this tends to cause the queue lengths of some entrance lanes to be too long.

To improve the performance of single intersections, optimization should be studied.

3.3.1. Information Transmission Rule-Based Optimization.

In the JTA-based RL algorithm, the root and leaf nodes determine the direction of information transmission along the junction tree. Existing study, Zhu et al. [16], simply assigns the endpoints of the junction tree as the root and leaf nodes, without considering the signal control requirements. Analyses of the JTA information transmission modes show that the intersection's phase is determined in the reverse transmission process. For these reasons, it is proposed that the phase of the intersection with poor operation should be determined first. Therefore, the worst running node should be taken as the leaf node while all endpoints of the junction tree are taken as root nodes. The information transmission rule before and after optimizations is shown in Figure 4.

3.3.2. Differentiated Return-Based Optimization.

System Q value of the JTA-based RL algorithm is determined by the Q values of every two adjacent intersections. For example, A and B are adjacent intersections, and entrances of two connecting sections between A and B are saturated with a and b , and then the Q value of A and B can be expressed as $Q(A, B) = a + b$. When $a = 0.1$, $b = 0.8$, then $Q(A, B) = 0.9$; when $a = b = 0.45$, then $Q(A, B) = 0.9$. Saturations of 0.1, 0.45, and 0.8 indicate different service levels, but there is no difference in calculating $Q(A, B)$; thus, the differences cannot be learned in signal timing. Therefore, the differentiated return-based optimization method is proposed to optimize the definition of Q values.

If the saturation q is taken as the evaluation index and varies from 0 to 1, q should be divided into n levels, and the return of the k^{th} level should be 2^k ($k \in [1, n]$). When the saturations of the adjacent intersections A and B are q_1 and q_2 , q_1 belongs to level k_1 , and q_2 belongs to level k_2 . Therefore, the Q value of the adjacent intersections is expressed as follows:

$$Q(A, B) = q_1 * 2^{k_1} + q_2 * 2^{k_2}, \quad (5)$$

TABLE 1: The given Q-value matrix of the virtual road network.

Phase combination	Intersection and phase		Q_{12}	Intersection and phase		Q_{13}	Intersection and phase		Q_{34}	Intersection and phase		Q_{24}
	1	2		1	3		3	4		2	4	
Combination 1	A	A	4	A	A	8	A	A	7	A	A	8
Combination 2	A	B	5	A	B	7	A	B	6	A	B	9
Combination 3	B	A	3	B	A	5	B	A	4	B	A	5
Combination 4	B	B	7	B	B	9	B	B	6	B	B	7

TABLE 2: ψ'_{123} under possible combinations and corresponding ϕ'_{23} .

Phase combination	Intersection and phase		$\max(Q_{12} + Q_{13})$	Intersection and phase
	2	3		
Combination 1	A	A	12	A
Combination 2	A	B	12	B
Combination 3	B	A	13	A
Combination 4	B	B	16	B

where $Q(A, B)$ is the Q value of adjacent intersections A and B, q_1 and q_2 are the saturations of adjacent intersections A and B, and k_1 and k_2 are the levels of q_1 and q_2 .

4. Test Case Study

4.1. Network Description. This study used VISSIM5.4 to build a virtual road network and test the validity of optimizations on the JTA-based RL algorithm. Details about the modules in VISSIM (e.g., car-following, lane-changing, traffic light control) can be found in the VISSIM manual. The JTA-based RL algorithm is coded in VB.net and interacts with VISSIM through the component object model (COM) interface.

A virtual road network same to the one in Zhu et al.'s study [16] was built. Under the same test environment, the results of this study should be more convincing. The network uses a structure with six horizontal and three vertical roads. The number of lanes is randomly set. There are 18 intersections in the network, and each entrance has an independent left turn lane, as shown in Figure 5. Also, the given network is transformed into a junction tree, as shown in Figure 6.

The length of the road section in the test network is set randomly, and channelization schemes of 18 intersections are also not uniform. All 18 intersections in the test network are coordinated intersections. Four phases are considered: (a) E-W + W-E bound through and right turn, (b) N-S + S-N bound through and right turns, (c) dual left from E-S + W-N bound, and (d) dual left from S-W + N-E bound.

The performance of the JTA-based RL algorithm is tested at three levels of congestion: low, medium, and high. The traffic demand is input into the network through the 18 link origins in Figure 5. The congestion levels are reflected in the ranges of the demand inputs, which are 500 vph to 600 vph, 600 vph to 800 vph, and 900 vph to 1200 vph, respectively.

4.2. Test Group Settings. In the test case, queue length w_{ij} is adopted to build the return and objective functions. The

TABLE 3: Combination forms for $\arg \max(Q_{24} + Q_{34})$.

Phase combination	Intersection and phase		$\max(Q_{24} + Q_{34})$	Intersection and phase
	2	3		
Combination 1	A	A	15	A or B
Combination 2	A	B	15	B
Combination 3	B	A	13	B
Combination 4	B	B	13	B

objective function is created to achieve the shortest queue length for the system. The return function is as follows:

$$f_r^{ij}(t) = \frac{q_{ij}^t}{J_{ij}} \times \frac{1}{l_{ij}}, \quad (6)$$

where $f_r^{ij}(t)$ is the return of intersection i in phase j and time t , q_{ij}^t is the traffic volume of the key entrance of intersection i in phase j and time t , J_{ij} is the density of the key entrance when it is congested, and l_{ij} is the lane length available for queueing of intersection i in phase j .

Three test groups are set to test the effectiveness of optimization methods. The details of the settings are as follows:

Group 1: existing research of Zhu et al. [16] applying JTA in signal coordination

- (1) Frequency of running JTA: 5 s
- (2) Intersection status division: each intersection contains three states, and the state of the two adjacent intersections is divided into nine parts
- (3) JTA information transmission mode: the mode introduced in Section 2.2
- (4) Root and leaf node: $V(1, 2, 4)$ is the root node, and $V(14, 16, 17)$ and $V(15, 17, 18)$ are the leaf nodes
- (5) Q value: calculated without regard to the differentiated returns

Group 2: optimizations of basic parameters and information transmission modes

- (1) Frequency of running JTA: 1 s
- (2) Intersection status division: the saturation of each intersection entrance is divided into three levels, and each intersection is divided into 81 states
- (3) JTA information transmission mode: the mode introduced in Section 3.2
- (4) Root and leaf node: same as group 1
- (5) Q value calculated same as group 1

Group 3: optimizations on the information transmission rule and the return

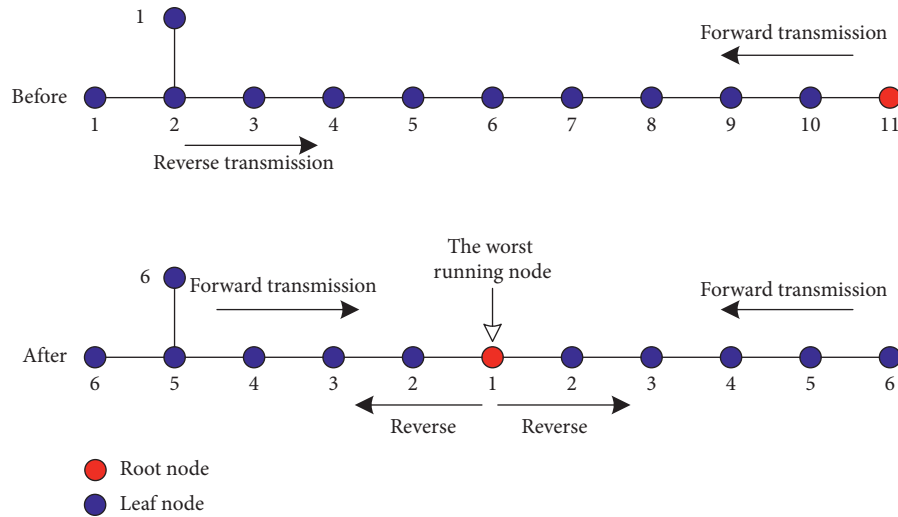


FIGURE 4: Optimization of the JTA information transmission rule.

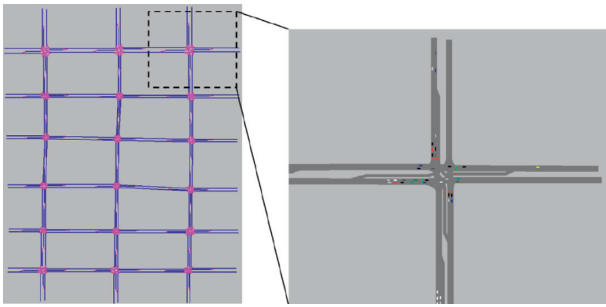


FIGURE 5: Center line representation of the network and a zoomed-in view of one intersection.

- (1) Frequency of running JTA: same as group 2
- (2) Intersection status division: same as group 2
- (3) JTA information transmission mode: same as group 2
- (4) Root and leaf node: the worst running node is taken as the leaf node while all endpoints of the junction tree are taken as root nodes
- (5) Q value-differentiated returns are calculated and applied

In addition to the above settings, the training time of group 1 is 5 h, while that of groups 2 and 3 is 10 h. After training, the three groups are applied in signal coordination; each group contains 10 simulation runs (each with a different random seed), and each simulation lasts 1 h.

The differentiated-return-based optimization method adopted in group 3 is necessary to classify the queue length w_{ij} . This is divided into three levels in this study: the first level is $[0, 0.4)$, the second is $[0.4, 0.7)$, and the third is $[0.7, 1]$. The return of each level is 2, 4, and 8, respectively.

4.3. Test Result Analysis. By comparing the test results of three groups, several conclusions can be drawn as follows.

4.3.1. The Green Light of Each Phase Is More Flexible. Taking intersection 8 as an example, 50 randomly selected continuous phases under medium congestion levels are extracted, and the corresponding green light durations are shown in Figure 7. As the frequency of calling the JTA in group 1 is 5 s, the green time of all phases is a multiple of 5, while the green time in group 2 is not subject to this constraint. The green time in group 2 can be adjusted according to the length of the queue. It can be concluded that optimization of the basic parameters can increase the flexibility of the green light duration, which in turn makes the green light more reasonable.

4.3.2. The Efficiency of Signal Coordination Is Improved. The queue length of the system and the intersection at different congestion levels are shown in Table 4. The queue length of the intersection is the longest queue length of all the entrance lanes while the phase is being switched. The average queue length of the system is the average queue length of all 18 intersections. As the traffic demand is input into the network via link origins, the outermost intersections of the network are directly affected by the traffic input, which may then also affect the evaluation result. Considering the above reasons, only intersections 5, 8, 11, and 14 are selected and analyzed.

In terms of the queue length of the system, the table shows that the length of group 2 is shorter than group 1 by over 10%. It can be concluded that optimizations of basic parameters and the JTA information transmission mode can improve the efficiency of signal coordination. The lengths of group 2 and group 3 are not significantly different, which means that optimizing the operation of a single intersection has little effect on the system operation.

4.3.3. Problems after Parameter Optimization and the Information Transmission Mode Are Still Significant. Optimization methods improve system operation, but the operations of some intersections are still poor. Table 4 shows

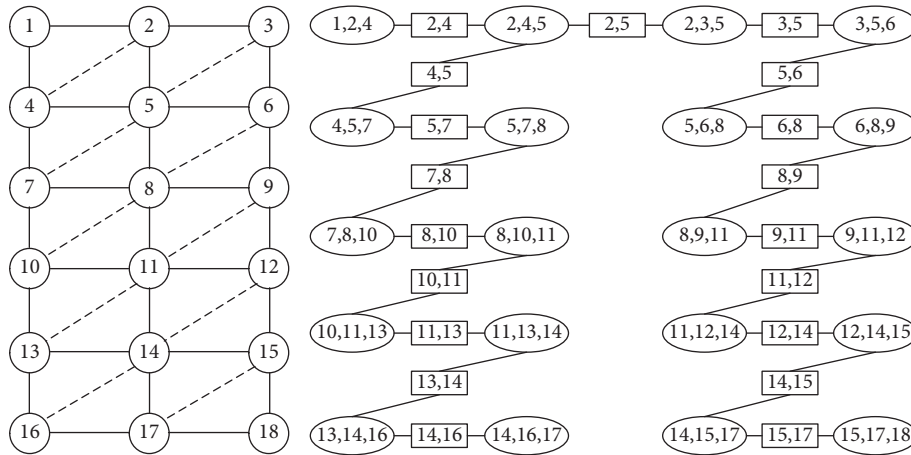


FIGURE 6: Triangulation and junction-tree construction of the test network.

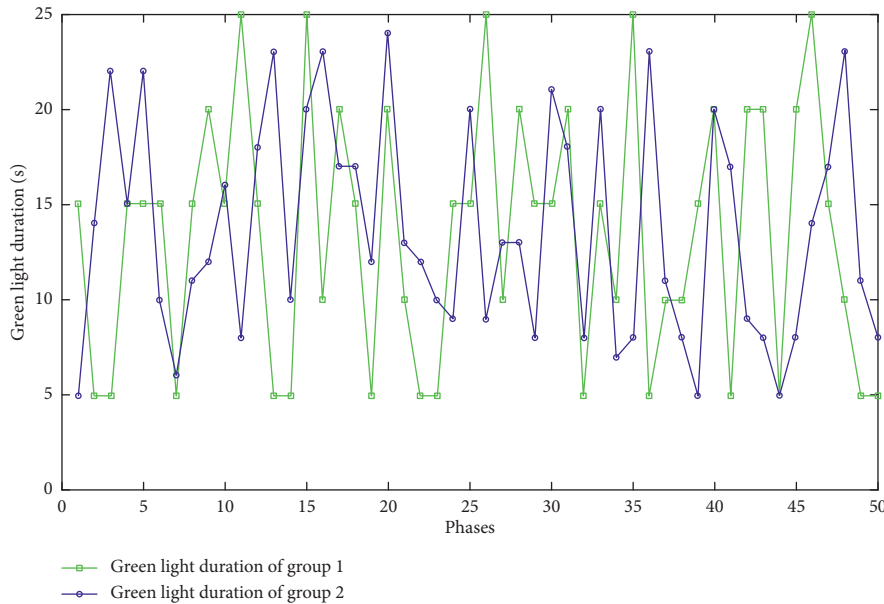


FIGURE 7: The green light duration of intersection 8 in groups 1 and 2.

that the average queue length of some intersections in group 2 is longer than that in group 1; for example, intersection 5 under a low congestion level and intersection 8 under a high congestion level. Queue lengths of 50 randomly selected continuous phases of these two intersections are also shown in Figures 8 and 9. The two figures show intersections with large fluctuations in queue length, such as intersection 5 under low congestion level with a maximum queue length of 0.55 and a minimum queue length of 0.16.

In other words, after optimizing basic parameters and the information transmission mode, the operation of a single intersection still needed to be improved.

4.3.4. Optimizations for Operating Single Intersections Can Reduce the Maximum Queue Length of the System. The maximum queue length of the system under low and

high congestion levels is counted at intervals of 10 s and shown in Figures 10 and 11. It is obvious that the queue length of group 3 is the lowest. In other words, the maximum queue length of the system is reduced after the optimizations for the operation of a single intersection were adopted.

4.3.5. Optimizations for the Operation of a Single Intersection Can Reduce the Fluctuation of the Queue Length at the Intersection. After applying a differentiated return-based optimization, group 3 should be more sensitive towards returns than groups 1 and 2. The queue length of intersection 5 under low congestion levels in different groups can be taken as an example. The variations in the queue lengths are shown in Figure 12. The queue length in group 1 varies from 0.18 to 0.53, group 2 varies from 0.17 to 0.55, and group 3 varies from 0.32 to 0.44. The fluctuation of queue length shows that the

TABLE 4: Queue length-based improvement analysis of optimization methods.

Congestion level	Test group	Average queue length of the system	Average queue length of the intersection			
			Intersection 5	Intersection 8	Intersection 11	Intersection 14
Low	Group 1	0.36	0.35	0.32	0.43	0.37
	Group 2	0.32	0.38	0.30	0.32	0.31
	Group 3	0.33	0.36	0.31	0.35	0.29
Medium	Group 1	0.51	0.50	0.47	0.45	0.53
	Group 2	0.43	0.40	0.42	0.44	0.48
	Group 3	0.44	0.41	0.45	0.42	0.46
High	Group 1	0.83	0.84	0.82	0.76	0.81
	Group 2	0.71	0.73	0.87	0.70	0.69
	Group 3	0.71	0.75	0.81	0.72	0.71

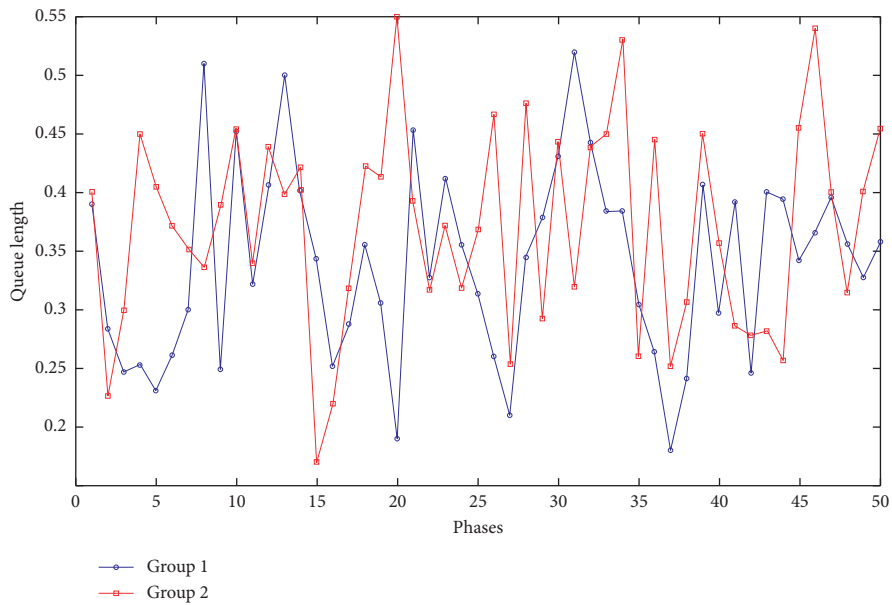


FIGURE 8: Variations in queue length at intersection 5 under low congestion levels.

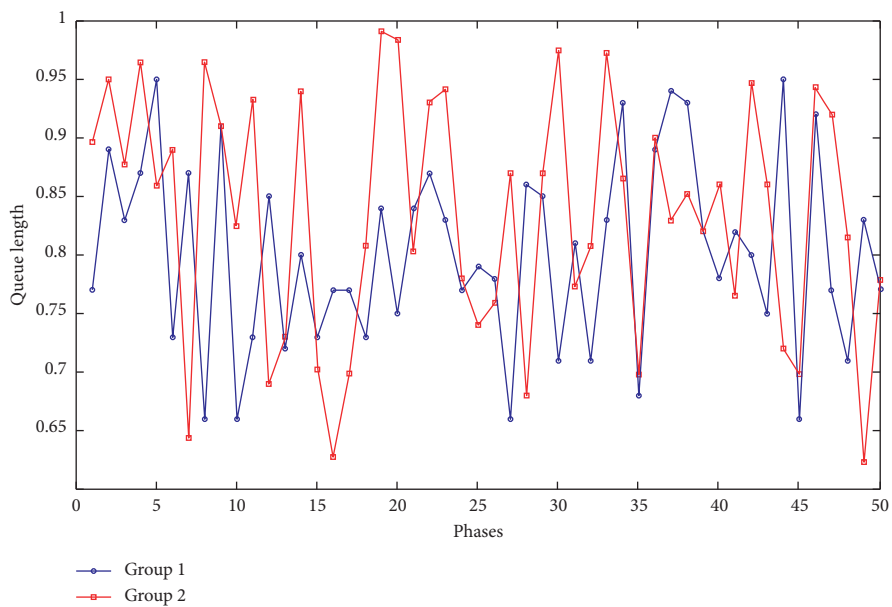


FIGURE 9: Variations in queue length at intersection 8 under high congestion levels.

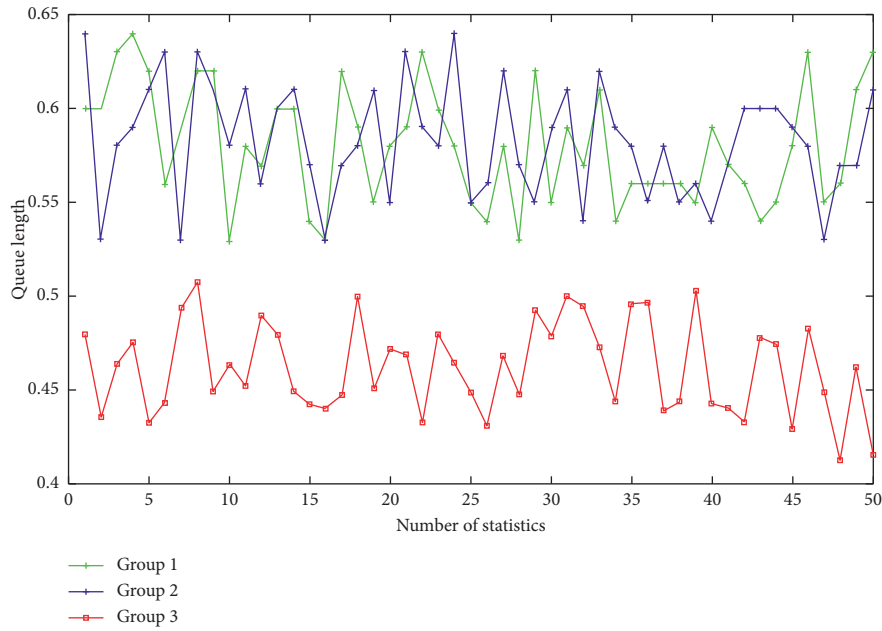


FIGURE 10: The maximum queue length of the system under a low congestion level.

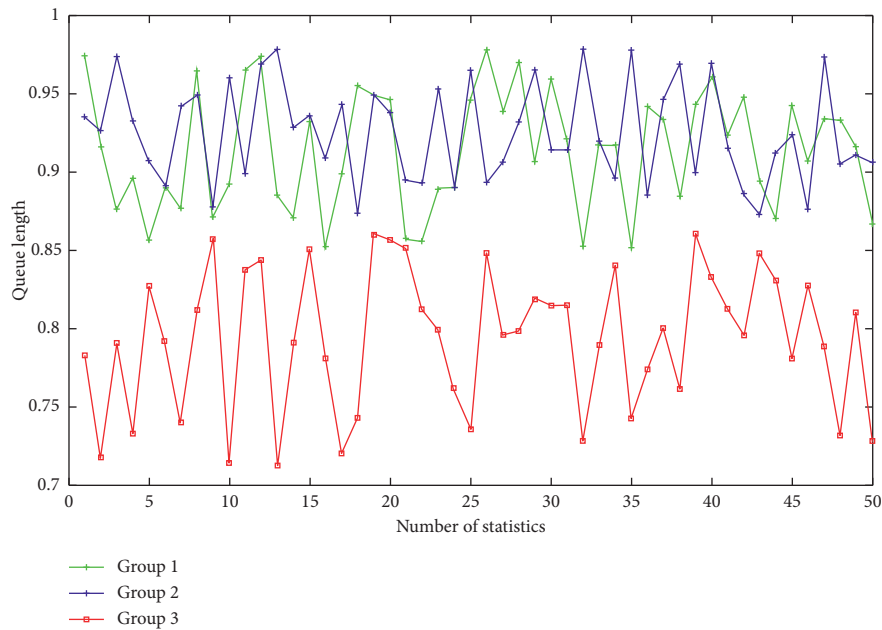


FIGURE 11: The maximum queue length of the system under a high congestion level.

intersections in group 3 have better operations, which benefit from a differentiated return-based optimization.

5. Discussion and Conclusion

The study proposed three optimization methods for the JTA-based RL algorithm which can be used for network-wide signal coordination. Three test groups were built to analyze the optimization effect.

Group 1 used the existing algorithm applying JTA in signal coordination; this group was taken as the control group

Group 2 applied optimizations on basic parameters and the information transmission mode relative to group 1

Group 3 applied optimizations on the transmission rule and the return relative to group 2

Detailed grouping and improvement effects are shown in Table 5.

Table 5 shows that the optimizations proposed in this paper play a good role in improving the operation of the JTA-based RL algorithm used for network-wide signal coordination. Optimizations of basic parameters and

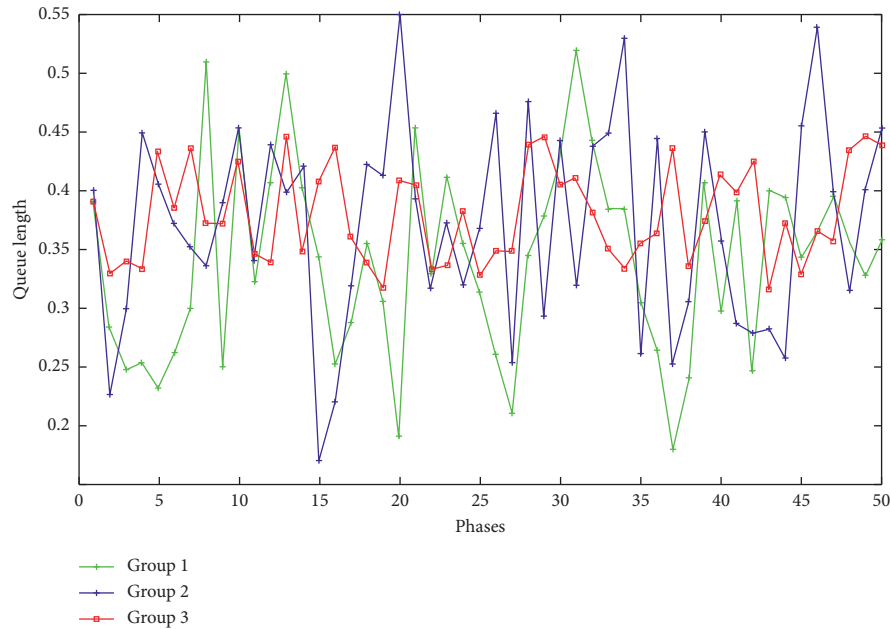


FIGURE 12: Fluctuations in queue length at intersection 5 under differentiated returns and a low congestion level.

TABLE 5: Summary of improvement effect on the JTA-based RL algorithm.

Grouping	Features	Improvement
Group 1	Existing algorithm	The control group
Group 2	Optimizations of basic parameters and the information transmission mode	(i) The green light of each phase was more flexible (ii) The system efficiency of signal coordination improved (iii) The operations of some intersections were still poor which need to be improved
Group 3	Optimizations of the information transmission rule and the return	(i) The maximum queue length of the system was reduced (ii) The fluctuation of the queue length at the intersection was optimized

information transmission modes can improve the system efficiency and the flexibility of green lights. Optimizations of the information transmission rule and the return can improve the efficiency of both the system and of the single intersection. It can be concluded that better operational results can be achieved in network-wide signal coordination by applying the proposed optimizations to existing JTA-based RL algorithms.

However, the results reported here are based on a hypothetical network. Results from real-world implementation should be studied in future research. This would make our conclusions stronger. What is more, each intersection is divided into only 81 states; the possibility of more detailed states division should be studied.

Data Availability

The data used to support the findings of this study are available from the corresponding author upon request.

Conflicts of Interest

The authors declare that they have no conflicts of interest.

Acknowledgments

This work was sponsored by the Natural Science Research Project of Colleges and Universities in Jiangsu Province (19KJB580012).

References

- [1] P. B. Hunt, D. I. Robertson, R. D. Rrtherton, and M. C. Royle, "The SCOOT on-line traffic signal optimization technique," *Traffic Engineering & Control*, vol. 4, no. 23, pp. 190–192, 1982.
- [2] P. R. Lowrie, "The Sydney coordinated adaptive traffic system—principles, methodology, algorithms," in *Proceedings of the International Conference on Road Traffic Signaling*, pp. 67–70, London, UK, April 1982.
- [3] J. J. Henry, J. L. Farges, and J. Tuffal, "The PROLYN real time traffic algorithm," in *Control in Transportation Systems*, pp. 305–310, Pergamon Press, Oxford, UK, 1984.
- [4] N. H. Gartner, "OPAC: a demand-responsive strategy for traffic signal control," *Transportation Research Record*, vol. 906, pp. 75–81, 1983.
- [5] P. Mirchandani and L. Head, "A real-time traffic signal control system: architecture, algorithms, and analysis," *Transportation Research Part C: Emerging Technologies*, vol. 9, no. 6, pp. 415–432, 2001.

- [6] V. Mauro and D. Taranto, "Utopia," in *Proceedings of the Sixth IFAC/IFIP/IFORS Symposium on Control, Computers, Communications on Transportation*, pp. 245–252, Oxford, UK, August 1990.
- [7] F. Boillot, S. Midenet, and J.-C. Pierrelée, "The real-time urban traffic control system CRONOS: algorithm and experiments," *Transportation Research Part C: Emerging Technologies*, vol. 14, no. 1, pp. 18–38, 2006.
- [8] C. Diakaki, M. Papageorgiou, and K. Aboudolas, "A multi-variable regulator approach to traffic-responsive network-wide signal control," *Control Engineering Practice*, vol. 10, no. 2, pp. 183–195, 2002.
- [9] X. Liang, X. Du, G. Wang, and Z. Han, "A deep reinforcement learning network for traffic light cycle control," *IEEE Transactions on Vehicular Technology*, vol. 68, no. 2, pp. 1243–1253, 2019.
- [10] M. Aslani, M. S. Mesgari, S. Seipel, and M. Wiering, "Developing adaptive traffic signal control by actor-critic and direct exploration methods," *Proceedings of the Institution of Civil Engineers—Transport*, vol. 172, no. 5, pp. 289–298, 2019.
- [11] M. Aslani, S. Seipel, and M. Wiering, "Continuous residual reinforcement learning for traffic signal control optimization," *Canadian Journal of Civil Engineering*, vol. 45, no. 8, pp. 690–702, 2018.
- [12] H. Jeon, J. Lee, and K. Sohn, "Artificial intelligence for traffic signal control based solely on video images," *Journal of Intelligent Transportation Systems*, vol. 22, no. 5, pp. 433–445, 2017.
- [13] H. M. A. Aziz, F. Zhu, and S. V. Ukkusuri, "Learning-based traffic signal control algorithms with neighborhood information sharing: an application for sustainable mobility," *Journal of Intelligent Transportation Systems*, vol. 22, no. 1, pp. 40–52, 2017.
- [14] S. Darmoul, S. Elkosantini, A. Louati, and L. Ben Said, "Multi-agent immune networks to control interrupted flow at signalized intersections," *Transportation Research Part C: Emerging Technologies*, vol. 82, pp. 290–313, 2017.
- [15] J. C. Medina and R. F. Beenekohal, "Traffic signal control using reinforcement learning and the max-plus algorithm as a coordinating strategy," in *Proceedings of the 2012 15th International IEEE Conference on Intelligent Transportation Systems*, pp. 596–601, Alaska, USA, September 2012.
- [16] F. Zhu, H. M. A. Aziz, X. Qian, and S. V. Ukkusuri, "A junction-tree based learning algorithm to optimize network wide traffic control: a coordinated multi-agent framework," *Transportation Research Part C: Emerging Technologies*, vol. 58, pp. 487–501, 2015.
- [17] F. V. Jensen, S. L. Lauritzen, and K. G. Olesen, "Bayesian updating in causal probabilistic networks by local computations," *Computational Statistics Quarterly*, vol. 916, no. 4, pp. 269–282, 1990.
- [18] C. Q. Shao, X. H. Du, and G. Q. Li, "Queuing vehicle headway statistic analysis at signalized intersection," *Journal of Highway and Transportation Research and Development*, vol. 4, no. 20, pp. 76–79, 2003.
- [19] Y. Zhao, Y. Ma, J. Lu, Y. Zong, and Q. Wan, "Variability of green time to discharge a specified number of queued vehicles at a signalized intersection," *Mathematical Problems in Engineering*, vol. 2017, Article ID 3723575, 8 pages, 2017.

Research Article

Understanding Electric Bikers' Red-Light Running Behavior: Predictive Utility of Theory of Planned Behavior vs Prototype Willingness Model

Tianpei Tang ^{1,2,3}, Hua Wang ³, Xizhao Zhou,¹ and Hao Gong⁴

¹Business School, University of Shanghai for Science and Technology, Shanghai 200093, China

²School of Transportation and Civil Engineering, Nantong University, Nantong 226019, China

³Department of Civil and Environmental Engineering, National University of Singapore, Singapore 117576

⁴Landmark (Shanghai) Vision Technology Co., Ltd., Shanghai 200233, China

Correspondence should be addressed to Hua Wang; hwang191901@gmail.com

Received 14 December 2019; Accepted 18 January 2020; Published 17 February 2020

Guest Editor: Feng Chen

Copyright © 2020 Tianpei Tang et al. This is an open access article distributed under the Creative Commons Attribution License, which permits unrestricted use, distribution, and reproduction in any medium, provided the original work is properly cited.

To date, electric bikers' (e-bikers') red-light running (RLR) behavior is often viewed as one of the main contributors to e-bike-related accidents, especially for traffic scenarios with high e-bike ridership. In this paper, we aim to understand e-bikers' RLR behavior based on structural equation modeling. Specifically, the predictive utility of the theory of planned behavior (TPB), prototype willingness model (PWM), and their combined form, TPB-PWM model, is used to analyze e-bikers' RLR behavior, and a comparison analysis is made. The analyses of the three modeling approaches are based on the survey data collected from two online questionnaires, where more than 1,035 participant-completed questionnaires are received. The main findings in this paper are as follows: (i) Both PWM and TPB-PWM models could work better in characterizing e-bikers' RLR behavior than the TPB model. The former two models explain more than 80% (81.3% and 81.4%, respectively) of the variance in e-bikers' RLR behavior, which is remarkably higher than that of the TPB model (only 74.3%). (ii) It is also revealed that RLR willingness contributes more on influencing the RLR behavior than RLR intention, which implies that such behavior is dominated by social reactive decision-making rather than the reasoned one. (iii) Among the examined psychological factors, attitude, perceived behavioral control, past behavior, prototype perceptions (favorability and similarity), RLR intention, and RLR willingness were the crucial predictors of e-bikers' RLR behavior. Our findings also support designing of more effective behavior-change interventions to better target e-bikers' RLR behavior by considering the influence of the identified psychological factors.

1. Introduction

In recent decades, as a green, cost-effective, and easy-to-carry transport means, electric bikes (e-bikes) have been adopted and promoted in an increasing number of countries such as Switzerland, Norway, the Netherlands, and China [1–4]. However, the use of e-bikes has been causing increasing e-bike-involved traffic accidents [1, 5, 6]. For example, in China, around 56,200 traffic accidents were caused by e-bikers, resulting in 8,431 fatalities, 63,400 injuries, and direct property losses of 111 million-yuan (equivalent to 16.42 million dollars based on the 2017 average closing exchange rate) between 2013 and 2017 [7]. According to the

statistics of accidents related to two-wheeled vehicles (e.g., e-bikes, regular bicycles, and e-scooters) in typical Chinese cities (including Beijing, Changchun, Ningbo, Foshan, and Weihai), e-bike-involved accidents accounted for 34.8% of the total accidents from July 2011 to June 2016; of the e-bike-involved accidents, the proportions of minor injuries, serious injuries, and fatalities to e-bikers were 70.0%, 12.6%, and 10.6%, respectively [8]. Some studies reported that the speed and weight of e-bikes were both higher than those of regular bicycles, thereby leading to more injuries and fatalities [9]. In addition, previous findings showed that traffic violating behaviors, especially red-light running (RLR) behavior at signalized intersections, partially contributed to e-bikers-related

accidents and fatalities [10–16]. Thus, studies on e-bikers' RLR behavior are needed, especially for countries with high e-bike ownership and e-bike-involved accidents.

Previous studies mainly focused on the influence of the demographics and traffic environment on e-bikers' RLR behavior. Moreover, in the studies of psychological factors associated with violating behavior, e-biker-related studies are less than the pedestrian-related and driver-related studies. A recent study has employed a social cognitive theory, the theory of planned behavior (TPB), to recognize the psychological determinants of e-bikers' intention to violate a red light [17]. Nevertheless, some evidence presented that the utility of the TPB framework is insufficient in predicting the unconscious risk-taking behaviors [18–20], while the prototype willingness model (PWM) might be a superior social cognitive theory in predicting such behaviors than the TPB framework [21]. Herein, the main goal of our work is to investigate the predictive utility of TPB, PWM, and their combined form, TPB-PWM, in e-bikers' RLR behavior and explore the psychological mechanism behind this behavior.

1.1. E-Bikers' RLR Behavior. So far, most existing evidence has revolved around the red-light infringement behavior of cyclists. Specifically, investigations have been performed on the influence of demographics [11–15], psychological factors [11–13], and other risk behaviors (e.g., unhelmeted riding, carrying passengers, using a phone, and listening to music) [14, 16, 22, 23] on cyclists' RLR behavior. However, due to the differences in weight, speed, and acceleration of e-bikes and regular bicycles, there are some discrepancies in the riders' psychology. Some studies discovered that e-bikers have a stronger intention to violate a red light than regular cyclists [13, 24–28]. Among these studies, Yang et al. [27] proposed that the prominent contributors to RLR behavior of cyclists and e-bikers were individual features (i.e., gender and rider type), psychological factors (i.e., conformity tendency), and traffic factors (i.e., waiting position and traffic volume). Investigations have also been performed on the impact of infrastructure conditions on the RLR behavior of cyclists and e-bikers, such as sunshades [26], carriageway, and intersection types [28]. However, apart from the above studies, much less literature has been published specifically on e-bikers' RLR behavior. Recent research conducted by Yang et al. [17] identified the psychological factors (i.e., attitude, perceived behavioral control, moral norm, and self-identify) which significantly influenced the e-bikers' RLR intention based on the TPB framework. However, their study focused on e-bikers' RLR intention, but not on their behavior. Also, it is relatively undesirable to employ the extended TPB framework they proposed to predict e-bikers' RLR intention. Thus, other more efficient models were applied to obtain an in-depth investigation of e-bikers' RLR intention and behavior in our study.

1.2. Theoretical Framework

1.2.1. TPB Framework. TPB has been the most prevalent framework used to identify the social cognitive constructs

that influence traffic violations of drivers, pedestrians, and e-bikers. In reviews of drivers' violations, the TPB framework has successfully explained the violation intentions, including high-speeding [29, 30], drink-driving [31–33], mobile phone use while driving [34, 35], and seatbelt nonuse [36, 37]. In terms of pedestrians' violations, the TPB framework has been employed to understand various pedestrian behavior intentions, such as walking while intoxicated [38], red-light infringement [39, 40], and distracted crossing [41]. In addition to drivers' and pedestrians' violations, Yang et al. [17] also determined the utility of the TPB framework in explaining e-bikers' RLR intention.

As mentioned above, TPB has been supported as a framework for explaining various traffic violations. Nevertheless, it is still unclear whether these behaviors are totally decided by volition. Sheeran et al. [18] pointed out that the TPB framework ignores the spontaneous or heuristic processes, and its hypothesis that a particular behavior is reasoned and premeditated could not match real situations. Also, some studies indicated that the utility of the TPB framework is insufficient in predicting the unconscious risk-taking behaviors [19, 20]. For example, even though e-bikers have a negative attitude towards e-bikers' RLR behavior, they might also have the willingness to violate a red light when there is a traversable space-time gap in the motor vehicle traffic flows.

In this investigation, an extension of the TPB framework (Figure 1) was applied. According to Ajzen's studies [42, 43], RLR intention (RI) reflects an e-biker's readiness to violate a red light. Attitude (AT) refers to an e-biker's positive/favorable or negative/unfavorable perception of RLR behavior. Subjective norm (SN) represents an e-biker's perceived view of whether social referents (e.g., family members and friends) approve or disapprove of RLR behavior. Perceived behavioral control (PBC) reflects an e-biker's perceived view of their ability to violate a red light. In light of previous studies, past behavior was also incorporated into the original TPB framework [29, 44, 45]. Past behavior (PB) represents an e-biker's violating behavior or illegal riding habits in the past and can indicate his/her habit strength [43, 44]. A range of previous research studies has discussed the explanatory power of the extension of the TPB framework with the addition of past behavior, suggesting that past behavior emerged as a key contributor to behavioral intentions and behaviors in particular correlation with perceived behavioral control [19, 29, 43, 44]. In the present model framework, attitude, subjective norm, perceived behavioral control, and past behavior have direct effects on RLR intention and indirect effects on RLR behavior via RLR intention. Also, perceived behavioral control directly influences RLR intention and behavior while indirectly influences RLR intention and behavior through past behavior.

1.2.2. PWM Framework. In fact, e-bikers' crossing behavior is a spontaneous risk-taking behavior that generally requires reactive decisions on how to act in response to changing traffic environmental demands (e.g., traffic signals, traffic volume, and other e-bikers' crossing behaviors) at signalized

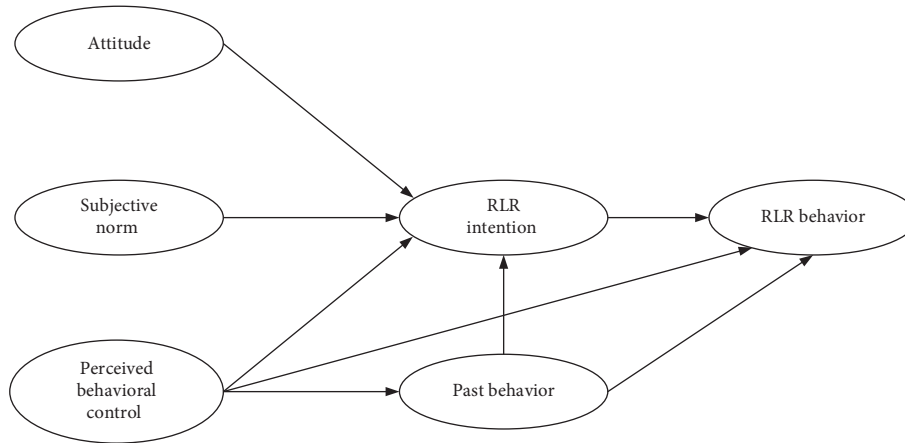


FIGURE 1: An extension of the TPB framework.

intersections. Thus, other decision-making models might be considered in governing RLR behavior. The PWM framework, which focuses on both social reactive decision-making and reasoned one, might contribute to a better understanding of RLR behavior than TPB framework, which is concentrated on reasoned decision-making only. The PWM framework has been successfully applied in examinations of drivers' and pedestrians' violations, such as drink-driving [46], high-speeding [47, 48], texting while driving [48], and pedestrians' violations [21]. As far as we are concerned, no previous research studies have employed the PWM framework in the study on e-bikers' violations. In this work, the PWM framework was adapted from the study of Gibbons et al. [49] (Figure 2). Among the PWM-based variables, prototype perceptions refer to the images of e-bikers (e.g., age and gender) who engage in RLR behavior, consisting of prototype similarity (PS) and prototype favorability (PF) [21, 49]. RLR willingness (RW) denotes the e-biker's willingness to violate a red light when such an opportunity is provided [21, 49]. In the reasoned decision-making pathway, attitude, subjective norm, and past behavior exert direct effects on RLR intention and indirect effects on RLR behavior via RLR intention, while past behavior directly influences RLR behavior. In the social reactive decision-making pathway, attitude, subjective norm, prototype similarity, prototype favorability, and past behavior have direct effects on RLR willingness, and RLR willingness directly affects RLR intention and behavior.

1.2.3. Integrating TPB and PWM Frameworks. A few studies have applied the integrative model which incorporates TPB and PWM frameworks (hereafter, referred to as "TPB-PWM") to investigate a particular behavior in other domains, such as health-protective/risk behavior [50] and organ donation communication [51]. In recent research, Demir et al. [21] compared the utility of TPB, PWM, and TPB-PWM frameworks in explaining the pedestrians' violations, among which PWM and TPB-PWM frameworks had a better predictive power than TPB framework. In light of the original PWM proposed by Gibbons et al. [49], the past behavior was also a crucial predictor and could improve

the PWM's performance. However, the past behavior was not included in Demir et al.'s [21] study, which might have negatively influenced the representativeness of the analysis results. Thus, past behavior was incorporated into three decision-making frameworks in this work. The TPB-PWM framework in this study refers to an extended PWM with the addition of perceived behavioral control, which has a direct effect on RLR intention and behavior (Figure 3).

1.3. Paper Position and Contribution. Little empirical evidence has been reported to support the utility of TPB and PWM frameworks in understanding e-bikers' RLR behavior. In this study, we compared the utility of TPB, PWM, and TPB-PWM frameworks in understanding such behavior, by using the TPB framework as a baseline comparator. This study aimed to test our hypothesis of e-bikers' RLR behavior as being more social reactive (using the PWM/TPB-PWM framework) rather than rational (using the TPB framework). Another aim of this work was to investigate the social cognitive determinants that influence e-bikers' RLR behavior.

2. Methods

2.1. Procedures. An experiment was designed using self-reported questionnaires. In the survey, participants who often used e-bikes (on average at least once a day) were asked to answer a wide range of questions related to each variable of the proposed model frameworks in a hypothetical situation. The situation assumed was described as follows: "You are riding an e-bike to work/school or somewhere on time. When you reach a signalized intersection, the traffic light turns red. In this situation, please answer the following questions."

Before the formal survey in this study, we performed a pilot survey among a small total number of 50 participants using online questionnaires. The purpose of this pilot survey was to ensure that the questionnaire items were easy to understand. Also, the pilot survey was helpful to evaluate the completion time of the survey. Cronbach's α correlation analysis and principal component analysis (PCA) were

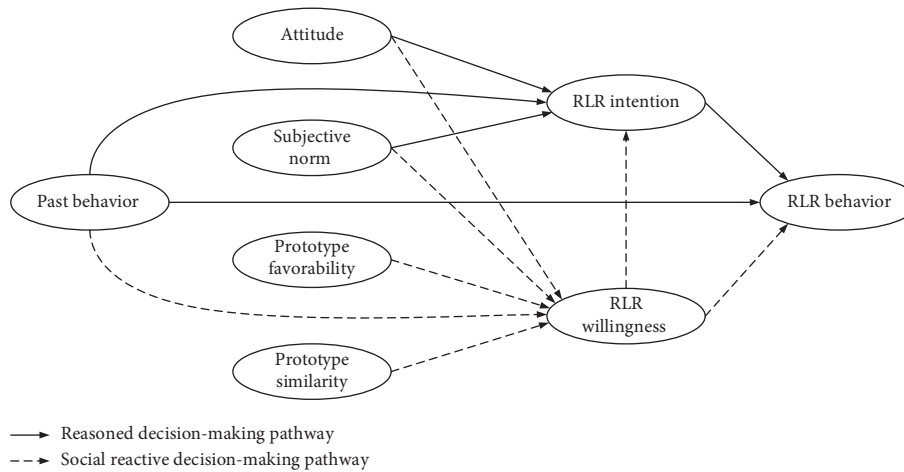


FIGURE 2: PWM framework.

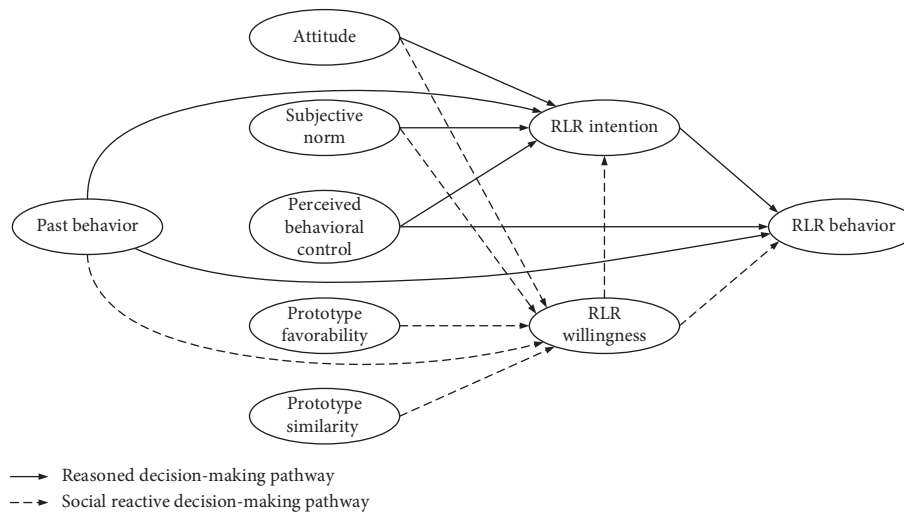


FIGURE 3: TPB-PWM framework.

employed to examine the reliability and validity of the items, and those items that did not pass the examinations were removed. The finalized questionnaire was designed based on the participants' feedback and the test results.

The formal survey was carried out in Shanghai, China, from May to July 2018. The participants were recruited from universities, communities, shopping malls, and office districts. They were required to complete two online questionnaires distributed by an online survey platform (<http://www.wjx.cn>) one month apart. To be specific, the participants were required to complete the first (Time 1) questionnaire, including all items of variables, except for RLR behavior (Table 1). One month later, the participants should complete the second (Time 2) questionnaire to measure the subsequent RLR behavior. Finally, the participants were rewarded with an amount of about \$1 for completing the survey.

2.2. Participants. In this survey, a total number of 1,147 participants completed the Time 1 and Time 2 questionnaires. After excluding 112 invalid questionnaires (e.g.,

inconsistent scoring logic, unusually short completion time, and abnormal score), we obtained a complete and valid sample of $N = 1,035$ participants. The mean age of the final sample of participants was 34.6 ($SD = 9.92$), 68.0% of which were female ($N = 704$); 89.2% used e-bikes at least twice a day on average ($N = 923$), and 74.3% had more than two years of e-bike riding experience ($N = 769$).

2.3. Measures. A 29-item questionnaire was designed to obtain data of participants for this work. The TPB-based items for each variable (i.e., attitude, subjective norm, perceived behavioral control, and RLR intention) and PWM-based items for each variable (i.e., past behavior, prototype perceptions, and RLR willingness) are presented in Table 1. Each item was measured using a 7-point response format. For the variables, we adopted the confirmatory factors analysis (CFA) and Cronbach's α correlation analysis to examine the validity and internal consistency of the items, thereby evaluating the reliability of the survey data. CFA was conducted by PCA. PCA identified that the value of

TABLE 1: Summary of items and internal consistency.

Variable	No.	Item	Reference	PCA (%)	Cronbach's α	
Attitude	AT1	For me, running against a red light in this situation would be ...	Bad to good Foolish to wise Dangerous to safe Unnecessary to necessary	Ajzen [43]; Elliott et al. [47]	72.5	0.873
	AT2					
	AT3					
	AT4					
Subjective norm	SN1	People who are important to me disapprove of my red-light running in this situation. (Strongly disagree to strongly agree)	Demir et al. [21]; Ajzen [43]	73.7	0.821	
	SN2	People who are important to me bother with my red-light running in this situation. (Strongly disagree to strongly agree)				
	SN3	People who are important to me tolerate my red-light running in this situation. (Strongly disagree to strongly agree)*				
Perceived behavioral control	PBC1	I believe that I have the ability to run against a red light in this situation. (Strongly disagree to strongly agree)	Evans and Norman [39]	80.8	0.881	
	PBC2	For me, it is easy to run against a red light in this situation. (Strongly disagree to strongly agree)				
	PBC3	I have control over whether to violate a red light in this situation. (Strongly disagree to strongly agree)				
Past behavior	PB1	How often have you committed the red-light running as an e-biker during the last 12 months? (Never to frequently)	Forward [29]; Potard et al. [45]	87.4	0.928	
	PB2	How often have you ridden faster than the legal speed limit during the last 12 months? (Never to frequently)				
	PB3	How often have you committed the violating crossing as a pedestrian during the last 12 months? (Never to frequently)				
Prototype perceptions	PS1	Prototype similarity	How similar/different are you to/from the person your age and gender that regularly violates a red light? (Very different to very similar)	Elliott et al. [47]	87.7	0.930
	PS2		I am comparable to the typical person my age and gender that regularly violates a red light. (Strongly disagree to strongly agree)			
	PS3		Do you resemble the typical person your age and gender that regularly violates a red light? (Definitely no to definitely yes)			
	PF1	Prototype favorability	How do you think about the typical person your age and gender who regularly violate a red light?			
	PF2		Dynamic Cool			
	PF3		Childish*			
RLR intention	RI1	In such a situation, how likely is it that you will run against a red light? (Extremely unlikely to extremely likely)	Zhou et al. [40]; Ajzen [43]	82.2	0.928	
	RI2	In a similar situation in the future, do you intend to run against a red light? (Definitely do not to definitely do)				
	RI3	In a similar situation in the future, what is the degree that you will avoid running against a red light? (Very weak to very strong)*				
	RI4	In a similar situation in the future, how likely or unlikely is it that you will run against a red light? (Extremely unlikely to extremely likely)				
RLR willingness	RW1	You will wait for the green light to cross in this situation. (Not at all willing to very willing)*	Elliott et al. [47]; Gibbons et al. [49]	86.2	0.920	
	RW2	You will run against a red light when there is a gap in traffic flow. (Not at all willing to very willing)				
	RW3	If other e-bikers around you are running against a red light, what is the degree that you will also run against a red light? (Very weak to very strong)				
RLR behavior	RB1	I have committed the red-light running in the last month. (Strongly disagree to strongly agree)	Elliott et al. [47]	82.3	0.892	
	RB2	How many times have you committed the red-light running over the last month? (None to lots of times)				
	RB3	Overall, how often have you committed the red-light running over the last month? (Never to frequently)				

Note. *Measuring scale is reverse.

Kaiser–Meyer–Olkin (KMO) was 0.973, and each single component accounted for 72.5% to 89.4% of the variance (Table 1), indicating the high validity of the items in the variable. All Cronbach's α coefficients ranged from 0.821 to 0.940, suggesting a high internal consistency (Cronbach's $\alpha > 0.7$) (Table 1). Apart from these items, participants' demographic data (e.g., gender, age, use frequency, and years of riding experience) were also collected.

3. Results

3.1. Descriptive Statistics and Correlations. Table 2 summarizes the descriptive statistics of the variables. The participants reported that they had a negative attitude towards RLR behavior (attitude, mean = 2.79). People who are important to participants (e.g., family members and friends), although subjectively disapprove them to run against a red light, would still tolerate their violating behaviors (subjective norm, mean = 2.52). The participants had moderate control over their ability to violate a red light (perceived behavioral control, mean = 3.86), and they violated traffic rules (e.g., red-light running, high-speeding, and violating crossing) to a moderate extent during the last 12 months (past behavior, mean = 4.24). It is also visible in Table 2 that the participants regarded themselves slightly dissimilar to the prototypical RLR e-bikers (prototype similarity, mean = 3.80) and rated the prototypical RLR e-bikers as moderately negative (prototype favorability, mean = 3.74). Additionally, the participants had a weak intention to violate a red light (RLR intention, mean = 4.06) but a relatively strong willingness to violate a red light whenever an opportunity was provided (RLR willingness, mean = 4.60). Finally, the participants reported that they violated a red light to a moderate extent during one month after completing the Time 1 questionnaire (RLR behavior, mean = 4.20).

Pearson's bivariate correlations were calculated to evaluate the association between each variable (Table 2). The correlations established suggested that all study variables were significantly associated with each other. In particular, RLR intention, RLR willingness, and RLR behavior positively and significantly correlated with attitude, perceived behavioral control, past behavior, prototype similarity, and prototype favorability, while negatively and significantly with subjective norm. RLR behavior was positively and significantly related to RLR intention and willingness. The correlation analysis results support the efficacy of TPB, PWM, and TPB-PWM frameworks in explaining e-bikers' RLR behavior.

3.2. Results of the Structural Equation Modeling. In this section, we have presented the process and results of the path analysis conducted using structural equation modeling in Amos 24. The path models for e-bikers' RLR behavior was evaluated based on TPB, PWM, and TPB-PWM frameworks. Degree-of-fit of the proposed model frameworks was evaluated and modified by multiple indexes, including chi-square divided by degrees of freedom (CMIN/df), root-mean-square error of approximation (RMSEA), goodness-

of-fit index (GFI), normal fit index (NFI), incremental fit index (IFI), comparative fit index (CFI), and Tucker–Lewis index (TLI) [52, 53]. Subsequently, we employed the path analysis to estimate the significance of the direct, indirect, and total effects of the variables in each model and assess the predictive utility of the proposed models. The path analysis results of each model are presented below. The degree-of-fit indexes for three models are summarized in Table 3, while Table 4 displays the direct, indirect, and total effects of the independent variables on RLR intention, willingness, and behavior in three models.

3.2.1. TPB Model. Table 3 showed that the CMIN/df was more than 3 in the initial TPB model, indicating the degree-of-fit of this model to our data was inadequate (CMIN/df = 3.191, RMESA = 0.046, GFI = 0.953, NFI = 0.969, IFI = 0.979, CFI = 0.979, and TLI = 0.975). Based on the suggested modification indices in Amos 24, the initial model path was revised by adding a path from the subjective norm to past behavior. The modified TPB model fitted well to the data (CMIN/df = 2.925, RMESA = 0.043, GFI = 0.958, NFI = 0.972, IFI = 0.981, CFI = 0.981, and TLI = 0.978). The path analysis results revealed that the attitude, subjective norm, and perceived behavioral control were the crucial determiners of RLR intention. RLR behavior was also significantly predicted by RLR intention, perceived behavioral control, and past behavior. The modified TPB model explained 80.4% of the variance of RLR intention and 73.6% of RLR behavior (Figure 4).

3.2.2. PWM Model. The initial PWM model did not obtain a good fit to our data due to the value of more than 3 for the CMIN/df (CMIN/df = 3.246, RMESA = 0.047, GFI = 0.940, NFI = 0.965, IFI = 0.975, CFI = 0.975, TLI = 0.971). Thus, the initial model path was improved based on the suggested modification indices. We removed the path from subjective norm to RLR willingness and added the paths from prototype favorability and similarity to RLR intention, as well as the path from prototype favorability to RLR behavior. The modified PWM model obtained adequate degree-of-fit to the data (CMIN/df = 2.627, RMESA = 0.040, GFI = 0.951, NFI = 0.972, IFI = 0.982, CFI = 0.982, and TLI = 0.979) and explained 76.6%, 77.4%, and 81.3% of the variance of RLR intention, willingness, and behavior, respectively. It is noteworthy that RLR willingness had a greater impact on RLR behavior than RLR intention ($\beta = 0.395$ vs $\beta = 0.173$) (Figure 5).

3.2.3. TPB-PWM Model. As the degree-of-fit of the initial TPB-PWM model to our data was inadequate (CMIN/df = 3.556, RMESA = 0.050, GFI = 0.923, NFI = 0.956, IFI = 0.968, CFI = 0.968, and TLI = 0.963), we applied the same path modifications as those in the modified PWM model. Based on the modification indices, we also omitted the path from perceived behavioral control to RLR behavior. The modified TPB-PWM model fitted well to the data (CMIN/df = 2.438, RMESA = 0.037, GFI = 0.948,

TABLE 2: Means, standard deviations, and bivariate correlations for all study variables.

Variable	1	2	3	4	5	6	7	8	9	Mean	SD
1. Attitude	1.000	-0.460**	0.543**	0.501**	0.528**	0.549**	0.638**	0.630**	0.484**	2.79	1.05
2. Subjective norm		1.000	-0.572**	-0.541**	-0.643**	-0.631**	-0.582**	-0.632**	-0.689**	2.52	1.19
3. Perceived behavioral control			1.000	0.631**	0.701**	0.675**	0.760**	0.622**	0.680**	3.86	1.54
4. Past behavior				1.000	0.607**	0.673**	0.630**	0.742**	0.709**	4.24	1.57
5. Prototype similarity					1.000	0.772**	0.711**	0.685**	0.778**	3.80	1.87
6. Prototype favorability						1.000	0.709**	0.715**	0.739**	3.74	1.73
7. RLR intention							1.000	0.660**	0.688**	4.06	1.49
8. RLR willingness								1.000	0.775**	4.60	1.66
9. RLR behavior									1.000	4.20	1.41

Note. ** $p < 0.01$.

TABLE 3: The degree-of-fit indexes in three models.

Index	TPB model		PWM model		TPB-PWM model	
	Initial	Modified	Initial	Modified	Initial	Modified
CMIN/df	3.191	2.925	3.246	2.627	3.556	2.438
RMESA	0.046	0.043	0.047	0.040	0.050	0.037
GFI	0.953	0.958	0.940	0.951	0.923	0.948
NFI	0.969	0.972	0.965	0.972	0.956	0.970
IFI	0.979	0.981	0.975	0.982	0.968	0.982
CFI	0.979	0.981	0.975	0.982	0.968	0.982
TLI	0.975	0.978	0.971	0.979	0.963	0.979

TABLE 4: Effects of the independent variables on RLR intention, willingness, and behavior in three models.

	RLR intention			RLR willingness			RLR behavior		
	Direct	Indirect	Total	Direct	Indirect	Total	Direct	Indirect	Total
<i>TPB model</i>									
AT	0.291***		0.291***					0.079***	0.079***
SN	-0.114**	-0.027**	-0.141***					-0.158***	-0.158***
PBC	0.527***	0.048**	0.575***				0.254***	0.369***	0.623***
PB	0.094**		0.094**				0.420***	0.025**	0.445***
RI							0.270***		0.270***
<i>PWM model</i>									
AT	0.361***	-0.026	0.335***	0.257***		0.257***		0.160***	0.160***
SN	-0.073*		-0.073*					-0.013*	-0.013*
PB	0.196***	-0.044	0.152***	0.434***		0.434***	0.140**	0.197***	0.337***
PF	0.132*	-0.013*	0.119	0.127*		0.127*	0.285***	0.071***	0.356***
PS	0.364***	-0.021*	0.343***	0.203***		0.203***		0.139***	0.139***
RW	-0.102		-0.102				0.395***	-0.018*	0.377***
RI							0.173***		0.173***
<i>TPB-PWM model</i>									
AT	0.282***	-0.014	0.268***	0.256***		0.256***		0.148***	0.148***
SN	-0.036		-0.036					-0.006	-0.006
PBC	0.428***		0.428***					0.075***	0.075***
PB	0.075	-0.023	0.052	0.432***		0.432***	0.142**	0.179***	0.321***
PF	0.082	-0.007	0.075	0.132*		0.132*	0.283***	0.065***	0.348***
PS	0.191***	-0.011	0.180***	0.199***		0.199***		0.110***	0.110***
RW	-0.054		-0.054				0.393***	-0.009	0.384***
RI							0.175***		0.175***

Note. * $p < 0.05$; ** $p < 0.01$; *** $p < 0.001$.

NFI = 0.970, IFI = 0.982, CFI = 0.982, and TLI = 0.979) and explained a relatively higher percentage of the variance of RLR intention (82.0%), behavior willingness (77.1%), and

RLR behavior (81.4%). We also found that RLR willingness contributed more impact on RLR behavior compared to RLR intention ($\beta = 0.393$ vs $\beta = 0.175$) (Figure 6).

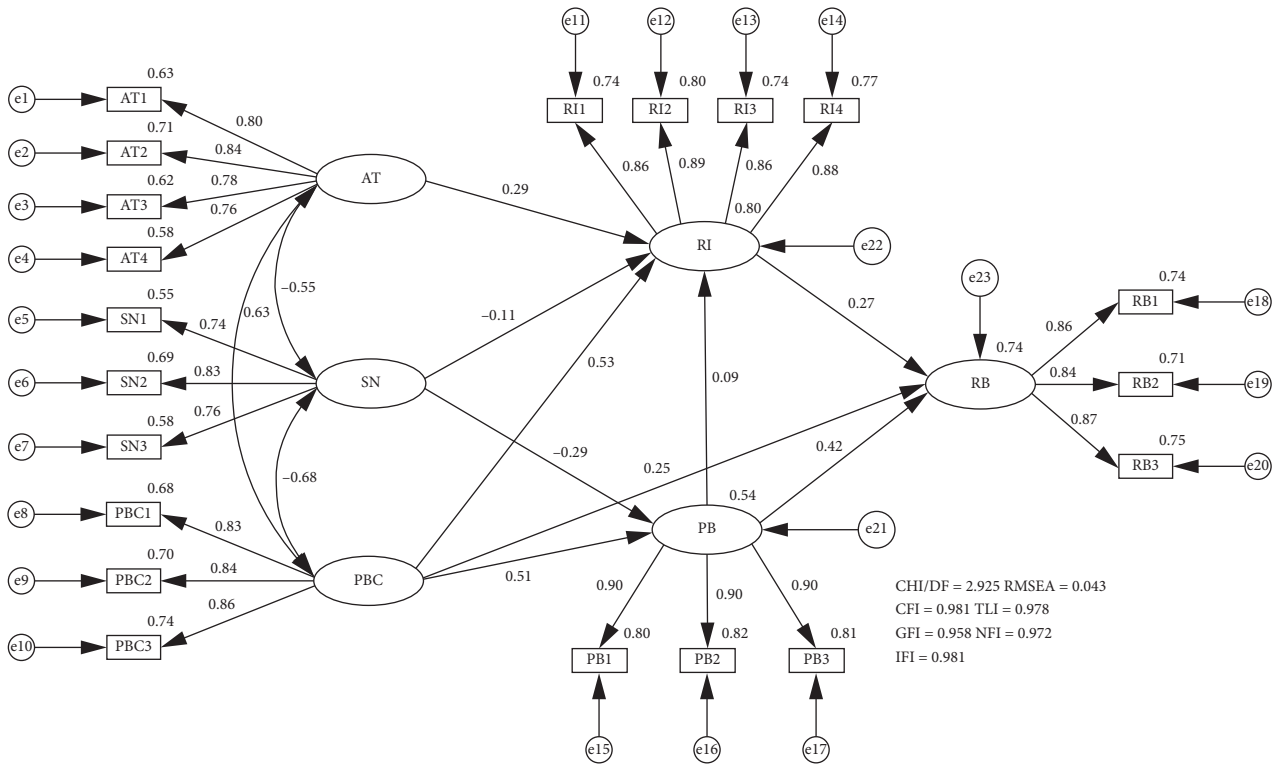


FIGURE 4: The modified TPB model for e-bikers' RLR behavior.

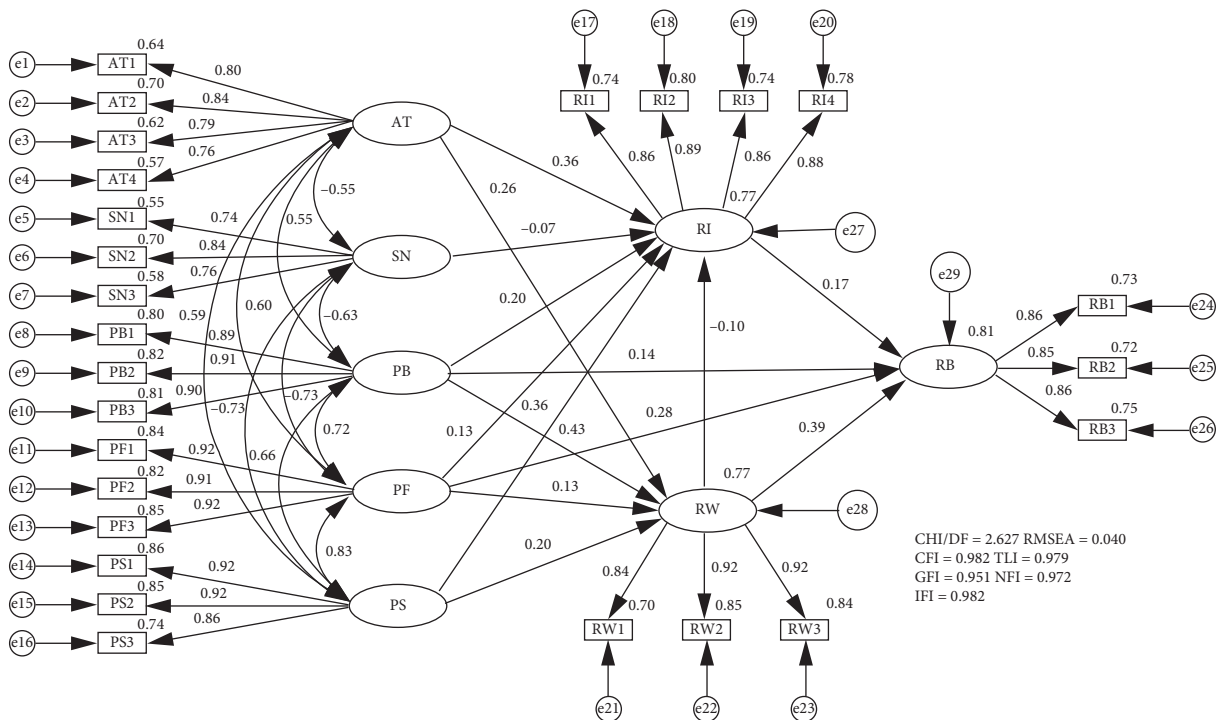


FIGURE 5: The modified PWM model for e-bikers' RLR behavior.

4. Discussion

4.1. Comparison of Predictive Utility. As shown in Tables 3 and 4, the modified TPB, PWM, and TPB-PWM models provided adequate degree-of-fit to the data, but the modified

PWM and TPB-PWM models had a more considerable utility in predicting e-bikers' RLR behavior than the modified TPB model. That is, the PWM and TPB-PWM frameworks provided a more complete account of e-bikers' RLR behavior than the TPB framework.

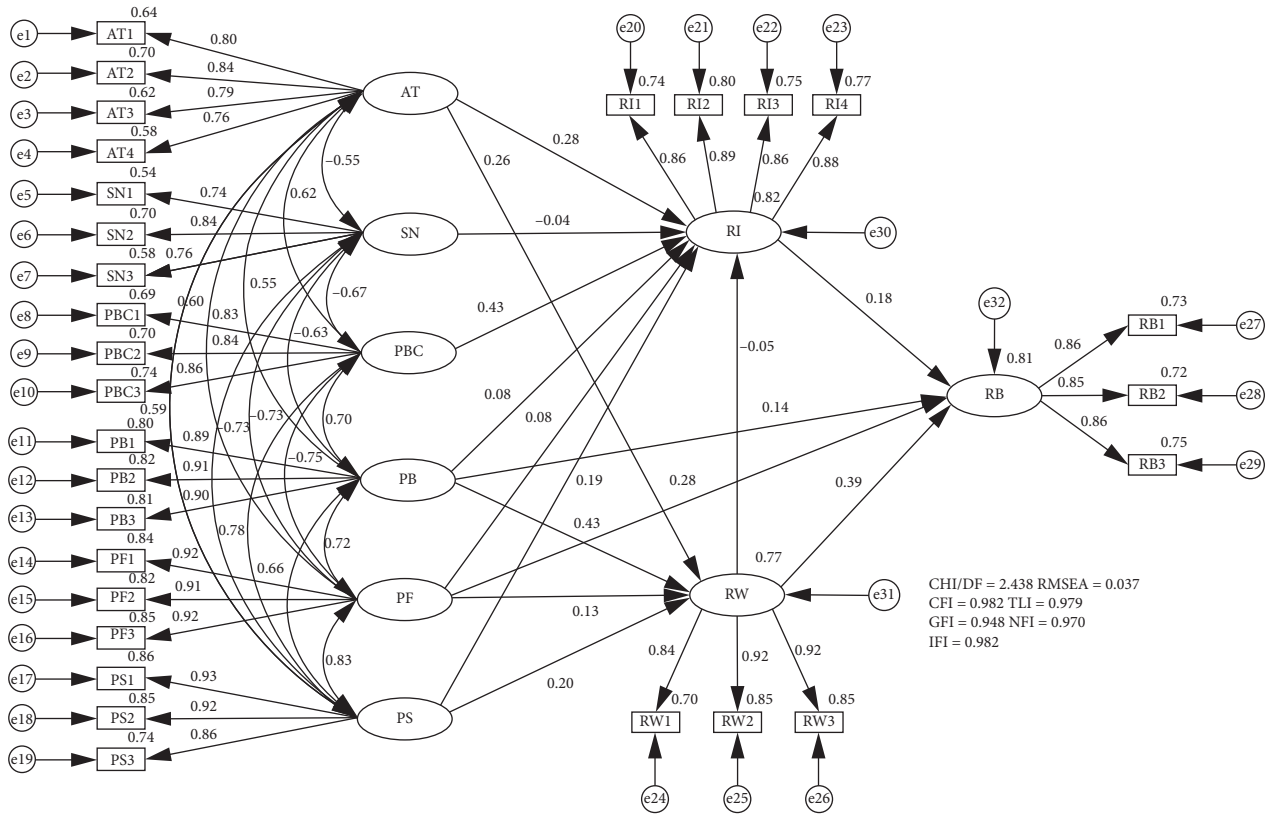


FIGURE 6: The modified TPB-PWM model for e-bikers' RLR behavior.

4.1.1. *Predictive Utility of TPB.* In this study, the extended TPB model with the addition of past behavior explained 80.4% of the variance of RLR intention and 73.6% of RLR behavior. Previous studies obtained similar results, reporting that the TPB framework explained 25%–72.8% of the variance in pedestrians' violation intentions [38–41]. However, these studies focused on predicting pedestrians' behavioral intention but not on their behavior. Demir et al. [21] confirmed the path from intention to behavior for pedestrians' violations. Currently, insufficient evidence exists on the intention-behavior path for e-bikers' violations.

All the variables from the TPB framework had a statistically significant total effect on RLR intention and behavior. Of these variables, perceived behavioral control had the highest total effect (the sum of the direct and indirect effects) on RLR intention, which can be supported across a few studies on pedestrians' violation intention and drink-driving intention [41, 45]. Also, the total effect of perceived behavioral control on e-bikers' RLR behavior was the strongest. In accordance with earlier related findings on pedestrians' violations [21], perceived behavioral control also played an important role in predicting pedestrians' violating behavior. However, in contrast to the results obtained by Demir et al. [21], we established that the subjective norm was statistically significantly associated with RLR intention and behavior. This result was in line with previous research studies which revealed that subjective norm contributed a moderate effect on pedestrians' violation intentions [39, 40, 54]. Among the extended TPB framework, past

behavior as an extended variable contributed a weak effect on RLR intention, which is inconsistent with the related studies on the behavioral intentions of risky riding [30] and drink-driving [31, 45]. However, past behavior was found to be a second-crucial determiner of RLR behavior and added an additional 7.2% to the explained variance for RLR behavior compared to the original TPB model. This result was in good agreement with a previous study on drivers' speeding behavior [55], which reported that the additional past behavior could enhance the explained variance for speeding behavior by an additional 4%. Our findings highlighted the fact that past behavior, with the incorporation into the original TPB framework, improved the predictive power. To some extent, e-bikers' past behavior partially represented their behavioral habits, while the habitual, familiar behavior has been recognized by Ajzen [42] that plays an important role in predicting behavior.

4.1.2. *Predictive Utility of PWM and TPB-PWM.* Compared to the modified TPB framework, the modified PWM and TPB-PWM frameworks explained an additional 7.7% and 7.8% of the variance in RLR behavior. The modified TPB-PWM framework also explained an additional 1.6% of the variance in RLR intention. Interestingly, our findings showed that RLR intention and willingness were crucial predictors of RLR behavior, and the total effect of willingness on RLR behavior was prominently stronger than that of intention. Elliott et al. [47] and Demir et al. [21]

reached similar conclusions for drivers' speeding and pedestrians' violations. They also revealed that behavioral willingness contributed more substantially to violating behavior than behavioral intention. Thus, we concluded that e-bikers might decide on whether to violate a red light through the social reactive pathway rather than the reasoned pathway. This result was also consistent with the conclusions of Gibbons et al. [49], which underlined that the social reactive decision-making was more suitable for predicting risk-taking behavior. Accordingly, as expected, the results revealed that social reactive decision-making is more crucial than reasoned decision-making in determining e-bikers' RLR behavior. This finding is paralleled to the dynamic nature of the riding task, which suggests that social reactive decision-making needs to respond to changing traffic environmental factors.

The model estimation results revealed that the attitude still significantly influenced RLR intention as the TPB model, and furthermore, had a significant total effect on RLR behavior via a mediator variable "RLR willingness." However, the influence of subjective norm on RLR intention and behavior was weakened, and it was no longer a significant variable in the TPB-PWM model. A plausible reason is that the approval of one's family members or friends on RLR behavior has little influence on his/her RLR intention and behavior, which is supported by the results of several investigations on violation intentions of drivers, e-bikers, and pedestrians [17, 21, 29, 32, 40]. For instance, Zhou et al. [40] suggested that the behavior of pedestrian's family members or friends exerts a stronger influence on the pedestrian's intention to violate crossing than their approval of such behavior.

Prototype perceptions (favorability and similarity) played a significant role in predicting RLR intention, willingness, and behavior, except for a special case; that is, the effect of prototype favorability on RLR intention was not significant in the TPB-PWM model, which was caused by the addition of perceived behavioral control. These results revealed that e-bikers who perceived people of their age and gender that regularly violate a red light as favorable and similar had a higher intention/willingness to commit RLR behavior. Although the original PWM framework has no relationship between prototype perceptions and intention, recent studies on pedestrian violations also found that prototype perceptions significantly contributed to intention [47]. More specifically, in the modified PWM model, prototype perceptions had a more significant influence on RLR intention than RLR willingness. Since perceived behavioral control was integrated into the modified TPB-PWM model and significantly influenced RLR intention, prototype perceptions contributed to RLR willingness more considerably.

Perceived behavioral control, as one of the TPB-based variables, still exerted a strong influence on RLR intention, whereas it had a weak effect on RLR behavior since it did not directly affect RLR behavior. In the modified PWM, past behavior was always a crucial predictor of RLR intention, willingness, and behavior, as also established by Gibbons et al. [20, 49]. In the modified TPB-PWM model, although the effect of past behavior on RLR intention was no more significant due to the addition of perceived behavioral control,

past behavior still substantially contributed to RLR willingness and behavior. These findings revealed that e-bikers' perceived ability to violate a red light (perceived behavioral control) was more likely to influence behavioral intention, whereas behavioral habits or experiences (past behavior) had a greater impact on their behavioral willingness. In summary, e-bikers' behavioral habits or experiences substantially influence RLR behavior through social reactive and reasoned pathways. Therefore, bias and deviations in the final results might have been caused in Demir et al.'s [21] study without considering the impact of past behavior.

4.2. Implications of Safety Interventions. The outputs obtained from this study could support the application of safety interventions and thereby further discourage the e-bikers' RLR behavior. The attitude, perceived behavioral control, past behavior, prototype perceptions, RLR intention, and RLR willingness represent particularly good intervention targets since they were the crucial predictors of e-bikers' RLR behavior.

Among these identified psychological factors, the perceived behavioral control was a crucial contributor to e-bikers' RLR intention. This result revealed that if e-bikers perceived the difficulty of violating a red light, they had less intention to commit it. Thus, reducing e-bikers' perceived control might decrease their RLR behavior. For example, radio-frequency identification (RFID) can be integrated into e-bike license plates, combined with traffic cameras, to automatically monitor and capture e-bikes' RLR behavior at signalized intersections. Meanwhile, learning from the management system of drivers' red-light infringement behavior, more stringent penalties (e.g., higher fines and demerit point system) can be employed to limit the e-bikers' RLR behavior. The RLR willingness was especially crucial for RLR behavior. The aforementioned countermeasures would also reduce the opportunity for RLR behavior, thereby weakening the willingness to violate a red light.

Since attitude, prototype perceptions, and past behavior were found to be pronounced predictors of both intention and willingness to engage in RLR behavior, preventative safety interventions are needed to focus on addressing this issue. Therefore, future advertisements and education related to traffic safety could consider creating the images of negative and undesirable e-bikers who violate a red light and enhance the negative and unfavorable perception of the most typical violators. For instance, riding simulation could allow e-bikers to experience traffic crashes or near-crashes as the results of their RLR behavior at signalized intersections, which might make e-bikers directly perceive the negative attributes of RLR behavior. It is expected that identifying violating e-bikers with negative portrayal would reduce e-bikers' RLR behavior. This expectation is supported by the findings of Demir et al. [56], which indicated that identifying speeders with negative portrayal on campus could reduce the incidence of speeding behavior. Also, school-based education can be an important approach to changing or correcting individual attitudes and prototype perceptions, especially correcting younger people's attitudes and prototype

perceptions [40]. In essence, past behavior can indicate individual behavioral habits [42]. Therefore, the proposed advertisements and education, riding simulation, and automated traffic rule enforcement might help e-bikers develop good riding habits. Furthermore, if e-bikers are required to participate in e-bike riding training and pass some riding tests, their illegal riding habits might be corrected.

4.3. Limitations and Future Research. This study employed the social cognitive theories, including the TPB, PWM, and TPB-PWM frameworks, in understanding e-bikers' RLR behavior. Our work extended upon previous studies in e-bikers' RLR behavior which was investigated by using the TPB frameworks. Furthermore, the application of the PWM and TPB-PWM frameworks allowed for an in-depth understanding of the psychological factors influencing e-bikers' RLR behavior. Despite this, our work still had some limitations that need attention and discussion. First, the study sample included e-bikers that were predominantly female and with a large age variance. Previous studies showed that men or young people are more prone to take the risk when driving or riding; also their likelihood to get involved in traffic accidents is greater [11–15, 57, 58]. Hence, the gender and age composition of the study sample might have influenced the results of the proposed model frameworks. More comprehensive studies need to be conducted to elucidate the effects of gender and age differences in the future. Second, the findings of this study might have been affected by the bias inherent in self-report data. Specifically, such bias might have led to an underestimation of past behavior and subsequent RLR behavior due to social desirability and recall bias. Although this work was conducted by the use of voluntary and anonymous questionnaires to reduce social desirability bias, recall bias was still an issue that needed to be addressed. Third, one aim of this study is to predict potential RLR behavior, which requires high accuracy for measuring subsequent RLR behavior, whereas we measured this variable only by self-reports. Therefore, the absence of an objective measurement of subsequent RLR behavior is also a major limitation of this work. In future studies, we can use some objective measurements such as an e-bike data acquisition system to obtain the frequency of subsequent RLR behavior in a given period (one month or more) after completing the Time 1 questionnaire. The fourth limitation is that this study assumes that the use of e-bikes of participants is an equal amount, whereas it varies significantly between participants based on the collected metric of exposure (e.g., use frequency and years of riding experience). As the exposure might be correlated to the psychological variables, the study results would be altered. Therefore, the influence of the exposure factors on the psychological variables and behavior should be considered in future work.

5. Conclusions

The findings of our research suggest that the TPB and PWM are the promising theoretical frameworks for predicting e-bikers' intention or willingness to engage in RLR behavior, as

well as for understanding the effects of psychological variables on RLR behavior. Furthermore, the PWM and TPB-PWM frameworks were found to be superior to the TPB framework in predicting e-bikers' RLR behavior. The present findings validate our hypothesis that e-bikers' RLR behavior is governed by both reasoned and social reactive decision-making, and the influence of the latter is stronger. In the PWM model, attitude, past behavior, and prototype similarity were the crucial predictors of both RLR intention and willingness. Prototype favorability had a relatively weak influence on RLR intention and willingness while exerted a pronounced direct effect on RLR behavior. In the TPB-PWM model, with the addition of perceived behavioral control, the impact of past behavior on RLR intention was reduced by the substantial influence of perceived behavioral control on RLR intention, but past behavior was still a crucial factor in predicting RLR behavior. These results imply the significance of specifically changing the e-bikers' attitude, perceived behavioral control, past behavior, and prototype perceptions towards RLR behavior. Thus, the design of more effective behavior-change interventions is needed, such as advertisements and education, training programs (e.g., riding simulation, riding training, and riding tests), and automated traffic rule enforcement.

Data Availability

The data used to support the findings of this study are available from the corresponding author upon request.

Conflicts of Interest

The authors declare that there are no conflicts of interest regarding the publication of this paper.

Authors' Contributions

T. Tang, H. Wang, and X. Zhou were responsible for study conception and design. H. Gong and H. Wang were involved in data collection. T. Tang, H. Wang, and H. Gong carried out analysis and interpretation of results. T. Tang and X. Zhou prepared the draft manuscript. All authors reviewed the results and approved the final version of the manuscript.

Acknowledgments

This research was supported by the Natural Science Foundation of the Jiangsu Higher Education Institutions of China (no. 19KJB580003), the Science and Technology Project of Nantong City (no. JC2019062), the Science and Technology Project of Jiangsu Province, China (no. BK20190926), the National Natural Science Foundation Council of China (no. 71601142), and the Applied Research Foundation of Social Science of Jiangsu Province (no. 19SYC-110).

References

- [1] S. Papoutsis, L. Martinolli, C. T. Braun, and A. K. Exadaktylos, "E-bike injuries: experience from an urban emergency department—a retrospective study from Switzerland," *Emergency Medicine International*, vol. 2014, p. 5, 2014.

- [2] A. Fyhri, O. Johansson, and T. Bjørnskau, "Gender differences in accident risk with e-bikes-survey data from Norway," *Accident Analysis & Prevention*, vol. 132, Article ID 105248, 2019.
- [3] P. Schepers, K. K. Wolt, and E. Fishman, "The safety of E-bikes in The Netherlands," *International Transport Forum Discussion Papers*, 2018.
- [4] D. Zuev, D. Tyfield, and J. Urry, "Where is the politics? E-bike mobility in urban China and civilizational government," *Environmental Innovation and Societal Transitions*, vol. 30, pp. 19–32, 2019.
- [5] J. P. Schepers, E. Fishman, P. Den Hertog, K. K. Wolt, and A. L. Schwab, "The safety of electrically assisted bicycles compared to classic bicycles," *Accident Analysis & Prevention*, vol. 73, pp. 174–180, 2014.
- [6] T. Weber, G. Scaramuzza, and K.-U. Schmitt, "Evaluation of E-bike accidents in Switzerland," *Accident Analysis & Prevention*, vol. 73, pp. 47–52, 2014.
- [7] Traffic Management Bureau of the Ministry of Public Security, "The people's republic of China road traffic accident annual statistic report," Traffic Management Bureau of the Ministry of Public Security, Wuxi, China, 2018.
- [8] Q. Chen and B. Dai, "Characteristics and casualty analysis of two-wheeler accidents in China, data source: the China in-depth accident study (CIDAS)," *SAE Technical Paper*, vol. 2018, 2018.
- [9] H. P. A. M. Poos, T. L. Lefarth, J. S. Harbers, K. W. Wendt, M. El Mounni, and I. H. F. Reininga, "E-bikers are more often seriously injured in bicycle accidents: results from the Groningen bicycle accident database," *Nederlands Tijdschrift Voor Geneeskunde*, vol. 161, Article ID D1529, 2017.
- [10] F. Chen, M. Song, and X. Ma, "Investigation on the injury severity of drivers in rear-end collisions between cars using a random parameters bivariate ordered probit model," *International Journal of Environmental Research and Public Health*, vol. 16, no. 14, p. 2632, 2019.
- [11] M. Johnson, S. Newstead, J. Charlton, and J. Oxley, "Riding through red lights: the rate, characteristics and risk factors of non-compliant urban commuter cyclists," *Accident Analysis & Prevention*, vol. 43, no. 1, pp. 323–328, 2011.
- [12] M. Johnson, J. Charlton, J. Oxley, and S. Newstead, "Why do cyclists infringe at red lights? An investigation of Australian cyclists' reasons for red light infringement," *Accident Analysis & Prevention*, vol. 50, no. 1, pp. 840–847, 2013.
- [13] C. Wu, L. Yao, and K. Zhang, "The red-light running behavior of electric bike riders and cyclists at urban intersections in China: an observational study," *Accident Analysis & Prevention*, vol. 49, no. 11, pp. 186–192, 2012.
- [14] C.-W. Pai and R.-C. Jou, "Cyclists' red-light running behaviours: an examination of risk-taking, opportunistic, and law-obeying behaviours," *Accident Analysis & Prevention*, vol. 62, pp. 191–198, 2014.
- [15] F. Fraboni, V. Marin Puchades, M. De Angelis, L. Pietrantonio, and G. Prati, "Red-light running behavior of cyclists in Italy: an observational study," *Accident Analysis & Prevention*, vol. 120, pp. 219–232, 2018.
- [16] D. De Waard, F. Westerveld, and B. Lewis-Evans, "More screen operation than calling: the results of observing cyclists' behaviour while using mobile phones," *Accident Analysis & Prevention*, vol. 76, pp. 42–48, 2015.
- [17] H. Yang, X. Liu, F. Su, C. Cherry, Y. Liu, and Y. Li, "Predicting e-bike users' intention to run the red light: an application and extension of the theory of planned behavior," *Transportation Research Part F: Traffic Psychology and Behaviour*, vol. 58, pp. 282–291, 2018.
- [18] P. Sheeran, P. M. Gollwitzer, and J. A. Bargh, "Nonconscious processes and health," *Health Psychology*, vol. 32, no. 5, pp. 460–473, 2013.
- [19] M. Conner and P. Sparks, "The theory of planned behaviour and health behaviours," in *Predicting Health Behaviour: Research and Practice with Social Cognition Models*, M. Conner and P. Norman, Eds., pp. 170–222, Open University Press, Maidenhead, UK, 2nd edition, 2005.
- [20] F. X. Gibbons, A. E. Houlihan, and M. Gerrard, "Reason and reaction: the utility of a dual-focus, dual-processing perspective on promotion and prevention of adolescent health risk behaviour," *British Journal of Health Psychology*, vol. 14, no. 2, pp. 231–248, 2009.
- [21] B. Demir, T. Özkan, and S. Demir, "Pedestrian violations: reasoned or social reactive? Comparing theory of planned behavior and prototype willingness model," *Transportation Research Part F: Traffic Psychology and Behaviour*, vol. 60, pp. 560–572, 2019.
- [22] D. De Waard, P. Schepers, W. Ormel, and K. Brookhuis, "Mobile phone use while cycling: incidence and effects on behaviour and safety," *Ergonomics*, vol. 53, no. 1, pp. 30–42, 2010.
- [23] K. Kircher, C. Ahlstrom, L. Palmqvist, and E. Adell, "Bicyclists' speed adaptation strategies when conducting self-paced vs. system-paced smartphone tasks in traffic," *Transportation Research Part F: Traffic Psychology and Behaviour*, vol. 28, pp. 55, 64–64, 2015.
- [24] X. Yang, M. Huan, B. Si, L. Gao, and H. Guo, "Crossing at a red light: behavior of cyclists at urban intersections," *Discrete Dynamics in Nature and Society*, vol. 2012, Article ID 490810, 12 pages, 2012.
- [25] X. Yang, M. Abdel-Aty, M. Huan, B. Jia, and Y. Peng, "The effects of traffic wardens on the red-light infringement behavior of vulnerable road users," *Transportation Research Part F: Traffic Psychology and Behaviour*, vol. 37, pp. 52–63, 2016.
- [26] Y. Zhang and C. Wu, "The effects of sunshields on red light running behavior of cyclists and electric bike riders," *Accident Analysis & Prevention*, vol. 52, pp. 210–218, 2013.
- [27] X. Yang, M. Huan, M. Abdel-Aty, Y. Peng, and Z. Gao, "A hazard-based duration model for analyzing crossing behavior of cyclists and electric bike riders at signalized intersections," *Accident Analysis & Prevention*, vol. 74, pp. 33–41, 2015.
- [28] K. Schleinitz, T. Petzoldt, S. Kröling, T. Gehlert, and S. Mach, "(E-)cyclists running the red light—the influence of bicycle type and infrastructure characteristics on red light violations," *Accident Analysis & Prevention*, vol. 122, pp. 99–107, 2019.
- [29] S. E. Forward, "The theory of planned behaviour: the role of descriptive norms and past behaviour in the prediction of drivers' intentions to violate," *Transportation Research Part F: Traffic Psychology and Behaviour*, vol. 12, no. 3, pp. 198–207, 2009.
- [30] K. Chorlton, M. Conner, and S. Jamson, "Identifying the psychological determinants of risky riding: an application of an extended theory of planned behaviour," *Accident Analysis & Prevention*, vol. 49, pp. 142–153, 2012.
- [31] D. C. N. Chan, A. M. S. Wu, and E. P. W. Hung, "Invulnerability and the intention to drink and drive: an application of the theory of planned behavior," *Accident Analysis & Prevention*, vol. 42, no. 6, pp. 1549–1555, 2010.
- [32] I. S. Moan and J. Rise, "Predicting intentions not to 'drink and drive' using an extended version of the theory of planned

- behaviour," *Accident Analysis & Prevention*, vol. 43, no. 4, pp. 1378–1384, 2011.
- [33] C. Castanier, T. Deroche, and T. Woodman, "Theory of planned behaviour and road violations: the moderating influence of perceived behavioural control," *Transportation Research Part F: Traffic Psychology and Behaviour*, vol. 18, pp. 148–158, 2013.
- [34] H. E. Nemme and K. M. White, "Texting while driving: psychosocial influences on young people's texting intentions and behaviour," *Accident Analysis & Prevention*, vol. 42, no. 4, pp. 1257–1265, 2010.
- [35] R. Zhou, P.-L. P. Rau, W. Zhang, and D. Zhuang, "Mobile phone use while driving: predicting drivers' answering intentions and compensatory decisions," *Safety Science*, vol. 50, no. 1, pp. 138–149, 2012.
- [36] K. Brijs, S. Daniels, T. Brijs, and G. Wets, "An experimental approach towards the evaluation of a seat belt campaign with an inside view on the psychology behind seat belt use," *Transportation Research Part F: Traffic Psychology and Behaviour*, vol. 14, no. 6, pp. 600–613, 2011.
- [37] K. Okamura, G. Fujita, M. Kihira, R. Kosuge, and T. Mitsui, "Predicting motivational determinants of seatbelt non-use in the front seat: a field study," *Transportation Research Part F: Traffic Psychology and Behaviour*, vol. 15, no. 5, pp. 502–513, 2012.
- [38] B. Gannon, L. Rosta, M. Reeve, M. K. Hyde, and I. Lewis, "Does it matter whether friends, parents, or peers drink walk? Identifying which normative influences predict young pedestrian's decisions to walk while intoxicated," *Transportation Research Part F: Traffic Psychology and Behaviour*, vol. 22, pp. 12–24, 2014.
- [39] D. Evans and P. Norman, "Predicting adolescent pedestrians' road-crossing intentions: an application and extension of the theory of planned behaviour," *Health Education Research*, vol. 18, no. 3, pp. 267–277, 2003.
- [40] H. Zhou, S. B. Romero, and X. Qin, "An extension of the theory of planned behavior to predict pedestrians' violating crossing behavior using structural equation modeling," *Accident Analysis & Prevention*, vol. 95, pp. 4717–424, 2016.
- [41] B. K. Barton, S. M. Kologi, and A. Siron, "Distracted pedestrians in crosswalks: an application of the theory of planned behavior," *Transportation Research Part F: Traffic Psychology and Behaviour*, vol. 37, pp. 129–137, 2016.
- [42] I. Ajzen, "From intentions to actions: a theory of planned behavior," in *Action Control from Cognition to Behavior*, J. Kuhl and J. Beckman, Eds., Springer, Heidelberg, Germany, pp. 11–39, 1985.
- [43] I. Ajzen, "The theory of planned behavior," *Organizational Behavior and Human Decision Processes*, vol. 50, no. 2, pp. 179–211, 1991.
- [44] S. Bamberg, I. Ajzen, and P. Schmidt, "Choice of travel mode in the theory of planned behavior: the roles of past behavior, habit, and reasoned action," *Basic and Applied Social Psychology*, vol. 25, no. 3, pp. 175–187, 2003.
- [45] C. Potard, V. Kubiszewski, G. Camus, R. Courtois, and S. Gaymard, "Driving under the influence of alcohol and perceived invulnerability among young adults: an extension of the theory of planned behavior," *Transportation Research Part F: Traffic Psychology and Behaviour*, vol. 55, pp. 38–46, 2018.
- [46] A. Rivas, C. Abraham, and S. Snook, "Understanding young and older male drivers' willingness to drive while intoxicated: the predictive utility of constructs specified by the theory of planned behaviour and the prototype willingness model," *British Journal of Health Psychology*, vol. 16, no. 2, pp. 445–456, 2011.
- [47] M. A. Elliott, R. McCartan, S. E. Brewster, D. Coyle, L. Emerson, and K. Gibson, "An application of the prototype willingness model to drivers' speeding behaviour," *European Journal of Social Psychology*, vol. 47, no. 6, pp. 735–747, 2017.
- [48] C. Preece, A. Watson, S.-A. Kaye, and J. Fleiter, "Understanding the psychological precursors of young drivers' willingness to speed and text while driving," *Accident Analysis & Prevention*, vol. 117, pp. 196–204, 2018.
- [49] F. X. Gibbons, M. Gerrard, H. Blanton, and D. W. Russell, "Reasoned action and social reaction: willingness and intention as independent predictors of health risk," *Journal of Personality and Social Psychology*, vol. 74, no. 5, pp. 1164–1180, 1998.
- [50] A. Rivas, P. Sheeran, and C. J. Armitage, "Augmenting the theory of planned behaviour with the prototype/willingness model: predictive validity of actor versus abstainer prototypes for adolescents' health-protective and health-risk intentions," *British Journal of Health Psychology*, vol. 11, no. 3, pp. 483–500, 2006.
- [51] M. K. Hyde and K. M. White, "Are organ donation communication decisions reasoned or reactive? A test of the utility of an augmented theory of planned behaviour with the prototype/willingness model," *British Journal of Health Psychology*, vol. 15, no. 2, pp. 435–452, 2010.
- [52] L. T. Hu and P. M. Bentler, "Cutoff criteria for fit indexes in covariance structure analysis: conventional criteria versus new alternatives," *Structural Equation Modeling: A Multidisciplinary Journal*, vol. 6, no. 1, pp. 1–55, 1999.
- [53] B. G. Tabachnick and L. S. Fidell, *Using Multivariate Statistics*, Pearson, Boston, MA, USA, 2013.
- [54] D. Evans and P. Norman, "Understanding pedestrians' road crossing decisions: an application of the theory of planned behaviour," *Health Education Research*, vol. 13, no. 4, pp. 481–489, 1998.
- [55] M. A. Elliott and J. A. Thomson, "The social cognitive determinants of offending drivers' speeding behaviour," *Accident Analysis & Prevention*, vol. 42, no. 6, pp. 1595–1605, 2010.
- [56] S. Demir, B. Demir, and T. Özkan, "When do drivers conform? When do they deviate?" *Transportation Research Part F: Traffic Psychology and Behaviour*, vol. 54, pp. 299–310, 2018.
- [57] R. Zhou, C. Wu, P.-L. Patrick Rau, and W. Zhang, "Young driving learners' intention to use a handheld or hands-free mobile phone when driving," *Transportation Research Part F: Traffic Psychology and Behaviour*, vol. 12, no. 3, pp. 208–217, 2009.
- [58] D. K. Lapsley and P. L. Hill, "Subjective invulnerability, optimism bias and adjustment in emerging adulthood," *Journal of Youth and Adolescence*, vol. 39, no. 8, pp. 847–857, 2010.

Research Article

Developing a New Spatial Unit for Macroscopic Safety Evaluation Based on Traffic Density Homogeneity

Chen Wang , Lin Liu, and Chengcheng Xu 

School of Transportation, Southeast University, Nanjing 210096, China

Correspondence should be addressed to Chengcheng Xu; xuchengcheng@seu.edu.cn

Received 13 November 2019; Accepted 6 December 2019; Published 22 January 2020

Guest Editor: Feng Chen

Copyright © 2020 Chen Wang et al. This is an open access article distributed under the Creative Commons Attribution License, which permits unrestricted use, distribution, and reproduction in any medium, provided the original work is properly cited.

Macrolevel crash modeling has been extensively applied to investigate the safety effects of demographic, socioeconomic, and land use factors, in order to add safety knowledge into traffic planning and policy-making. In recent years, with the increasing attention to regional traffic management and control, the safety effects of macrolevel traffic flow parameters may also be of interest, in order to provide useful safety knowledge for regional traffic operation. In this paper, a new spatial unit was developed using a recursive half-cut partitioning procedure based on a normalized cut (NC) minimization method and traffic density homogeneity. Two Bayesian lognormal models with different conditional autoregressive (CAR) priors were applied to examine the safety effects of traffic flow characteristics at the NC level. It was found that safety effects of traffic flow exist at such macrolevel, indicating the necessity of considering safety for regional traffic control and management. Furthermore, traffic flow effects were also examined for another two spatial units: Traffic Analysis Zone (TAZ) and Census Tract (CT). It was found that ecological fallacy and atomic fallacy could exist without considering traffic flow parameters at those planning-based levels. In general, safety needs to be considered for regional traffic operation and the effects of traffic flow need to be considered for spatial crash modeling at various spatial levels.

1. Introduction

Macroscopic safety evaluation was often conducted, with the purpose of finding factors that could be improved or controlled at the planning stage or during policy-making process. Traditional macroscopic crash models (e.g., Poisson lognormal models) rely on the assumption of independence across observations. However, in recent years, spatial crash models have gained a lot of attention, by adding spatial dependence into macroscopic crash models. Socioeconomic, land use, demographic, and traffic network characteristics were of interest, and they were often aggregated at varying levels of spatial units [1], including Traffic Analysis Zones (TAZ), Census Tracts (CT), census wards, statistical area levels, block groups, counties, and states. In general, spatial crash models have shown their superiority over conventional macroscopic crash models.

However, an important issue of spatial crash models is the choice of a certain level of spatial unit, which is also

called Modifiable Aerial Unit Problem (MAUP). Wang et al. [2] discussed the possible ecological fallacy of spatial aggregation (Davis) that modeling results from spatially aggregated data may not be fully applied to disaggregated data. They also argued the possible atomistic fallacy caused by disaggregated data, which is unable to take “system-wide effects” captured by spatially aggregated data [3, 4]. Abdel-Aty et al. [5] compared spatial crash models based on three different aggregate-level spatial units (i.e., TAZs, CT, and block groups) and found the effects of different spatial units on the significance of model estimates. Xu et al. [6] conducted a sensitive analysis on the effects of different aggregate-level spatial TAZ units. They found that more aggregated TAZs tended to have better model performance but fewer variables. This result was consistent with Wang et al. [2], as spatially aggregated data tend to decrease atomistic fallacy while increase ecological fallacy if not properly aggregated. Gyimah et al. [1] examined the effect of six different aggregate-level spatial units on unobserved

spatial heterogeneity. According to the results, the aggregation level could significantly affect spatial heterogeneity, as well as model performance.

Both Xu et al. [6] and Gyimah et al. [1] pointed out the necessity of defining a new spatial unit from the perspective of macroscopic safety evaluation, instead of using long-term planning-based TAZs. To note, most spatial units like TAZ were not initially defined for safety analysis but for traffic planning purposes. Thus, they are possibly delineated based on the homogeneity of demographic, socioeconomic, or land use factors, regardless of traffic flow characteristics. Traffic flow characteristics were largely found to be associated with crash occurrence and safety in the previous literature. Thus, an aggregate-level spatial unit, like TAZs at any aggregate level, may contain roadways with significantly distinct traffic flow characteristics. As a result, the relationship between traffic flow characteristics and crash occurrence could be weakened or nonsignificant (i.e., an example of ecological fallacy for a spatial unit due to the inhomogeneity in traffic), leading to biased model estimates. To overcome possible ecological fallacy and atomistic fallacy (caused by disaggregated data), Wang et al. [2] claimed the necessity of a better mathematical partitioning scheme based on spatial homogeneity in both demographic and traffic flow characteristics.

There are many different spatial partitioning methods in the literature to define spatial units, such as k -means algorithm, AZP [7], and REDCAP (regionalization with dynamically constrained agglomerative clustering and partitioning) [8]. Some have also been introduced into spatial crash modeling. In order to study the effect of enforcement on road crashes in Greece, Yannis et al. [9] formed spatial units based on spatial homogeneity in traffic characteristics and road safety parameters, with a direct k -means algorithm. Yannis concluded the statistical results might be more reliable if spatial units are more homogeneous. Xu et al. [6] proposed a zoning scheme of aggregating similar TAZs into a spatial unit, based on REDCAP. The homogeneity of crash risk was considered as the clustering criteria. However, although considering spatial homogeneity in various factors, these partitioning methods still rely on predefined spatial units for planning, such as TAZ.

Ji and Geroliminis [10] introduced a graph cut minimization method to divide urban traffic networks into multiple spatial units. With such method, a traffic network was partitioned into spatial units with homogeneous traffic flow characteristics, and macroscopic fundamental diagram (MFD) of each region was successfully identified. Such method is very flexible, by not depending on any sort of predefined spatial unit (e.g., TAZs). Although initially proposed for controlling traffic and improving congestion, the idea of the graph cut minimization method could also be beneficial for macroscopic safety evaluation. As traffic flow characteristics have been shown strong relationships with crash, it is reasonable to believe that a spatial unit aggregating roadway with similar traffic flow characteristics would be more suitable for spatial crash modeling. Based on such method, the underlying relationship between traffic flow and

crash may be better explored. Thus, active regional traffic control and management strategies [11–15] could be expected to improve macroscopic safety, by managing traffic flow in some certain state with lower crash risk.

Thus, in this paper, we will define a new spatial unit for macroscopic safety evaluation, by considering the homogeneity of traffic densities. A graph cut method will be introduced, based on which a spatial partitioning procedure is proposed. Two Bayesian spatial modeling techniques are employed to analyze crash data at the new level, in order to identify possible traffic flow effects on safety. The remainder of the paper is organized as follows. In Section 2, we present the detail of the graph cut minimization method for spatial partitioning as well as spatial modeling techniques. Section 3 gives a brief description of the data. Section 4 summarizes the spatial partition results and modeling results and includes a discussion. The last part concludes the paper and recommends future research directions.

2. Spatial Partitioning

2.1. A Normalized Cut (NC) Minimization Method. In order to divide an area into multiple regions, a normalized cut minimization (NC) method is introduced, considering intersections as nodes and roadways as edges. NC method has been used in the previous literature for spatial partitioning [10].

Suppose the node set V in an undirected graph $G = (V, E)$ where E indicates the set of edges in G . Assume that each edge between two vertices v_i and v_j carries a non-negative weight $w_{ij} = w_{ji} \geq 0$. The weight adjacency matrix of the graph can be defined as $W = (w_{ij})_{i,j=1,\dots,n}$. When $w_{ij} = 0$, it indicates that the two vertices are not connected. The degree of a vertex $v_i \in V$ is defined as $d_i = \sum_{j=1}^n w_{ij}$. The degree matrix D is defined as the diagonal matrix with degree d_1, d_2, \dots, d_n on the diagonal.

Consider edge to be a measure of the similarity between nodes. We want to find a partition of the graph such that edges between different groups have a very low weight, indicating that points in different clusters are dissimilar from each other. Moreover, the edges within a group need to have high weights, implying that points within the same cluster are similar.

For two disjoint subsets A and B ,

$$\text{cut}(A, B) = \sum_{i \in A, j \in B} w_{ij}. \quad (1)$$

In 2000, Shi and Malik proposed a 2-way normalized cut functions: Ncut and Nassoc, which indicate the homogeneity and heterogeneity of two clusters:

$$\begin{aligned} \text{Ncut}(A, B) &= \frac{\text{cut}(A, B)}{\text{cut}(A, V)} + \frac{\text{cut}(A, B)}{\text{cut}(B, V)}, \\ \text{Nassoc}(A, B) &= \frac{\text{cut}(A, A)}{\text{cut}(A, V)} + \frac{\text{cut}(B, B)}{\text{cut}(B, V)}, \end{aligned} \quad (2)$$

$$\text{cut}(A, A) + \text{cut}(A, B) = \text{cut}(A, V),$$

$$\text{Ncut}(A, B) = 2 - \text{Nassoc}(A, B).$$

Thus, the objective can be determined as the minimization of Ncut:

$$\begin{aligned} \min_x \quad & \text{Ncut}(x). \\ \text{s.t.} \quad & x \in V. \end{aligned} \quad (3)$$

Minimizing Ncut value exactly is NP-complete. The discrete solution can be approximated efficiently by solving an eigenvalue system in the real value domain. A common way is to convert the normalized cut into the unnormalized graph Laplacian. Set

$$w(i, j) = \begin{cases} \exp\left(-(d_i - d_j)^2\right), & a_{ij} = 1, \\ 0, & a_{ij} = 0. \end{cases} \quad (4)$$

Then, we have

$$\begin{aligned} \min_x \quad & \text{Ncut}(x) = \min_y \frac{y^T(D - W)y}{y^T D y}, \\ \text{s.t.} \quad & x_i = 1 \text{ if } x_i \in A, \\ & x_i = 1 \text{ if } x_i \in B, \\ & y_i \in \{-1, b\}, \\ & y^T D 1 = 0, \end{aligned} \quad (5)$$

where D is an $N * N$ diagonal matrix with $d_{ii} = \sum_j \omega(i, j)$ on its diagonal. $D - W$ is the Laplacian matrix, known to be positive semidefinite. Based on Rayleigh–Ritz theorem, the solution is to solve the generalized eigenvalue system:

$$(D - W)y = \lambda D y, \quad (6)$$

where λ is the eigenvalue and y is the eigenvector. The second smallest eigenvector is called the Fiedler vector, which is the real-valued solution to normalized cut problem.

2.2. A Recursive Half-Cut Partitioning Procedure. To apply the above method for spatial partitioning, we propose a recursive half-cut procedure:

Step 1: set up a weighted graph $G = (V, E)$ based on the topology of traffic network. Intersections are treated as nodes while roadways are considered as edges.

Step 2: set the weight on the edge connecting two nodes, using a measure of similarity between two notes (i.e., traffic density).

Step 3: solve $(D - W)y = \lambda D y$ for eigenvectors with the smallest eigenvalues.

Step 4: cut the graph into two clusters based on the second smallest eigenvector (i.e., Fiedler vector).

Step 5: decide if the current partition should be further divided.

Step 6: repeat the first five steps until certain criteria were met.

When partitioning a graph with the Fiedler vector, different strategies can be used. There are three general ways: (1) partition the graph with the median value; (2) cut the graph with value 0 (negative versus positive); and (3) cut the graph based on the largest interval between every two elements. In this study, the third approach was utilized.

2.3. Spatial Model Configuration. Crash modeling includes severity modeling [16–18] and crash frequency modeling [19, 20]. Spatial crash modeling belongs to crash frequency modeling, which contains multiple model structures [21–26], including Poisson lognormal model, negative binomial spatial model, Poisson lognormal spatial model, geographic weighted Poisson regression model, and Bayesian spatial varying-coefficient model. Since the purpose of this study is to examine the effect of traffic flow characteristics, two Bayesian lognormal models with different CAR priors were applied, since they have been widely applied in many different research fields such as epidemiology.

A generalized Bayesian lognormal model with CAR prior can be presented as

$$\begin{aligned} Y_i & \sim \text{Poisson}(\lambda_i), \\ \ln(\lambda_i) & = \ln(E) + \beta_0 + \beta_k X_{ik} + \theta_i + \phi_i, \end{aligned} \quad (7)$$

where λ_i is the expected mean of crash occurrence for observation i ; E is the exposure/expectation for observation i ; β_k is the parameter coefficient of k th variable; X_{ik} is the k th variable for i th observation; θ_i is the unstructured error, often assumed as a prior normal distribution; and ϕ_i is the spatial correlation.

For the spatial correlation term ϕ_i , the intrinsic conditional autoregressive prior (CAR prior) can be defined as follows [18]:

$$\phi_i | \phi_{-i}, W, \tau^2 \sim N\left(\frac{\sum_{i \neq j} \phi_j m_{ij}}{\sum_{i \neq j} m_{ij}}, \frac{\tau_c^2}{\sum_{i \neq j} m_{ij}}\right), \quad (8)$$

where m_{ij} denotes the binary entries of proximity matrix (1 represents adjacency while 0 indicates nonadjacency). τ_c is the precision parameter, assumed as a prior gamma distribution. In essence, the conditional expectation ϕ_i is the average of spatial correlations of adjacent areas; conditional variance τ^2 is inversely proportional to the number of adjacent areas.

A Cressie autoregressive prior can be written as follows:

$$\phi_i | \phi_{-i}, W, \tau^2 \sim N\left(\rho \frac{\sum_{i \neq j} \phi_j m_{ij}}{\sum_{i \neq j} m_{ij}} + (1 - \rho) \frac{\sum_{j=1}^n \phi_j}{n}, \frac{\tau_c^2}{\sum_{i \neq j} m_{ij}}\right). \quad (9)$$

Different from IAC priors, the conditional expectation of ϕ_i is modified into the weighted average of the average of adjacency area and the average of the entire area. Weight parameter ρ indicates the intensity of spatial autocorrelation. When $\rho = 0$, it indicates a complete spatial independence, and with the increase of ρ , spatial autocorrelation

increases. When $\rho = 1$, the Cressie model degenerates to an intrinsic CAR model.

Based on a fitted model, the relative risk (RR) of a subregion can be calculated as follows:

$$RR = e^{(\beta_0 + \beta_k X_{ik} + \theta_i + \phi_i)}. \quad (10)$$

3. Data Preparation

Crash data for the central area of Kunshan City (within the Kunshan Middle Ring Road) in 2015 were acquired from the Kunshan Police Department. A total of 5538 crashes were collected. The crash data contain detailed information on drivers, roadways, and vehicles. For each crash record, there is a unique coordinate, which can be further used for locating it on the map. In order to conduct macroscopic crash modeling, spatially aggregated features also need to be collected.

Planning-based data were extracted from the planning department of Kunshan City. More importantly, detailed traffic data are necessary for spatial partition and spatial modeling. Thus, traffic data between 2015.8 and 2015.9 were extracted from microwave detectors with the 30 s interval, including density, speed, and counts. The average traffic density was considered as the measure of traffic homogeneity, used in spatial partitioning. Figure 1 shows the roadway network, the location of microwave detectors, and the land use sketch of the studied area.

As for Bayesian modeling, the total number of crashes was used as the dependent variable. Unlike previous studies, we calculated the expected crash number as exposure. The expected crash number of a spatial unit can be calculated as the total crash number times the proportion of the exposure (daily traffic volume * total population * area size) of the area. The calculation assumed that the expected average risk of each area is comparable. However, it is also reasonable that the relative exposure risk among different areas can largely vary. Many factors could contribute to it, including traffic flow parameters (used as explanatory variables), planning, and land use factors. Four aggregated traffic variables (average flow, average density, average speed, and speed variance) were calculated for each area, which were also used as explanatory variables for spatial modeling. Other explanatory variables include most planning-based aggregated variables, commonly used in the previous literature.

4. Results

4.1. Partitioning Results. The NC partitioning method was applied to partition the graph with 99 nodes (i.e., 99 intersections). Initially, by solving the Laplacian matrix, all eigenvalues were calculated. Based on the similarity of eigenvectors and their spatial adjacency, 8 clusters were determined. However, NC 8 has the area size of 10.98 m², which is much larger than other NCs. In order to obtain all NCs with comparable size, further division efforts were conducted in NC 8, which has 23 intersections within the

area. Based on another two rounds of partitioning on NC 8, 13 NCs were finally delineated, as shown in Figure 2.

The descriptive statistics of planning, roadway, and traffic flow parameters of 13 NCs are summarized in Table 1.

4.2. Model Results. Intrinsic and Cressie Bayesian CAR models were developed to examine the relationship between various variables with crash risk. First, multicollinearity needs to be examined for those variables. VIF tests and stepwise methods were applied to eliminate those variables with high multicollinearity (VIF >10).

Then, for each Bayesian CAR model, 100000 iterations were conducted with 5000 iterations as burn-in period. All three models appeared to reach convergence within the simulation period. Figure 3 gives an illustration of model convergence.

Both intrinsic and Cressie CAR models showed significant traffic flow effects on crash risk. The results were comparable for the two models. Detailed results are shown in Table 2. A region having higher speed variance tends to have higher crash risk. This is reasonable. With higher traffic density, there is a slight increase in crash risk. Previous literature studies suggest controversial findings on the relationship between density and crash risk. Some claimed a positive linear relationship while others suggested a quadratic function. It is reasonable to expect that, at first, the higher density creates more interaction and thus more crashes. While it reaches some certain point, the traffic becomes congested and the speed significantly drops down. In this case, crashes could possibly decrease. Since we only consider an average effect without regarding spatial and temporal heterogeneity, the detailed density effect of each zone needs to be further explored. Average daily traffic volume (ADT) was not found to be significant as the explanatory variable, implying that traffic volume is not significantly connected with average crash risk. Thus, the effect of ADT on crash risk could be considered as the only exposure effect (Figure 4).

As for the effects of planning/roadway factors on crash risk, there are slight differences between the two models. According to intrinsic CAR models, the increase of major/minor arterial density will increase crash risk. This was consistent with the previous literature. There is no significant relationship between local road density and crash risk. It was expected that the increase of local roads would lower crash risk, according to the previous literature. A possible reason could be the inclusion of significant traffic flow variables adjusts the effects of local roads density. In other words, traffic flow variables could be endogenous variables that cannot be ignored. According to the Cressie CAR model, with the increase of industrial land use, crash risk decreases by 2.5%. More school land use and residential land use are associated with higher crash risk. This was reasonable in China. During morning and evening peak hours, parents pick children to increase the disorder of traffic. Thus, it is critical to deal with school land use. Those low-income residential areas are older district. Buildings are too old so that there is enough parking space. Oftentimes, roadways



FIGURE 1: (a) Roadway network and location of microwave detectors and (b) land use sketch of the subject area.

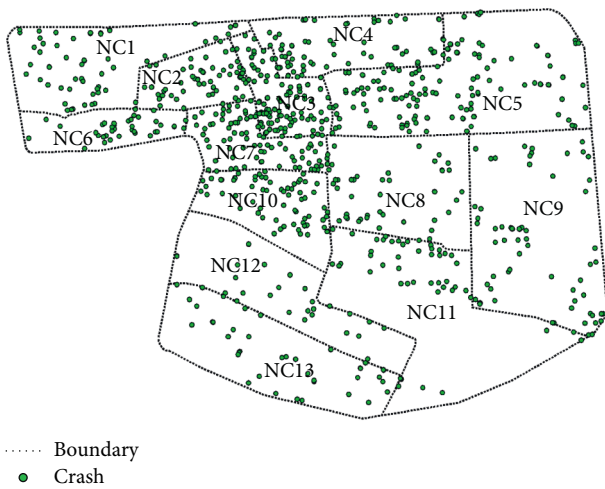


FIGURE 2: Final NC partitioning results.

TABLE 1: Descriptive analysis of 13 NCs.

Roadway characteristics	Min	Max	Mean	SD
Area (km ²)	1.016	4.269	2.329	1.237
Roadway density (km/km ²)	3.181	10.919	6.923	2.423
Major arterials (km/km ²)	0.392	4.805	2.648	1.396
Minor arterials (km/km ²)	0.022	2.386	1.432	0.660
Land use characteristics	Average percentage (%)			
School land use	2.391			
Public land use	5.761			
Commercial land use	11.822			
Industrial land use	9.816			
Low-income residentials	1.015			
High-income residentials	28.265			

were occupied by vehicles. These could be potential safety issues. Thus, certain traffic management could be considered.

The relative risk of each spatial unit was also calculated, based on the two models. In general, two models estimated the similar results. Comparing with crash frequency, it should be noted that spatial models can effectively identify

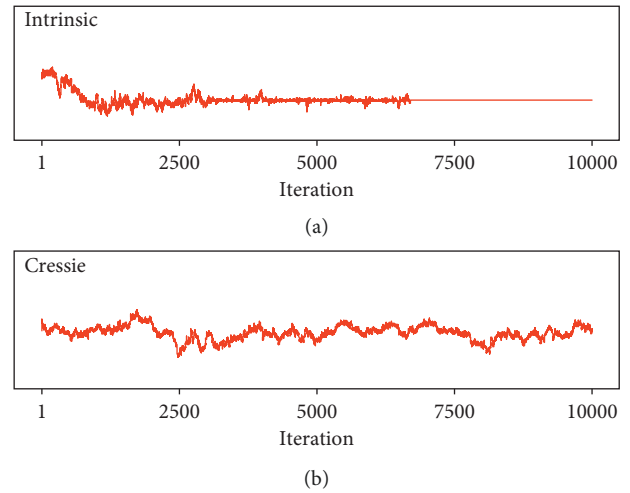


FIGURE 3: Illustration of Bayesian model convergence: intrinsic (a) and Cressie (b).

actual relative risk, by accounting for exposure and spatial autocorrelation.

4.3. Ecological Fallacy and Atomic Fallacy. To further discuss ecological fallacy and atomic fallacy, spatial modeling was also conducted for another two spatial units: TAZ and Census Tract (CT) zone. For each spatial unit, two models were developed, one considering traffic flow parameters (model 2) and another without considering them (model 1). Detailed results can be found in Table 3. Note that both original TAZ and CT were decided by the Kunshan Traffic Planning Department (as shown in Figure 5).

For CT model 2, average daily traffic volume, average speed, business, administrative, and public service land use were found as significant variables. For TAZ model, only land use variables were found as significant, including the public management and public service, business, and residence. Using TAZ as spatial units, there were no significant traffic flow effects on crash risk. However, for CT units, traffic flow effects emerge.

TABLE 2: Two bayesian modeling results of NC spatial units.

Varibale	BYM intrinsic CAR			BYM cressie CAR		
	Mean	s.d.	95% CI	Mean	s.d.	95% CI
Roadway density	-0.136	0.067	(-0.239, -0.012)	-0.081	0.091	(-0.206, 0.096)
Major arterial density	0.089	0.199	(-0.526, 0.309)	0.222	0.252	(-0.158, 0.596)
Minor arterial density	0.121	0.313	(-0.304, 1.012)	-0.601	0.242	(-1.083, -0.193)
School land use	-0.224	0.150	(-0.841, 0.015)	0.047	0.111	(0.034, 0.228)
Public land use	0.032	0.106	(0.121, 0.700)	0.066	0.058	(-0.049, 0.176)
Commercia land use	-0.066	0.033	(-0.099, 0.008)	0.040	0.018	(-0.074, 0.085)
Industrial land use	-0.037	0.019	(-0.064, 0.006)	-0.025	0.025	(-0.067, -0.012)
Low-income residence	0.222	0.194	(-0.257, 0.531)	0.145	0.201	(-0.185, -0.510)
High-income residence	-0.026	0.032	(-0.076, 0.011)	-0.013	0.019	(-0.046, 0.015)
Daily traffic density	0.021	0.010	(0.009, 0.033)	0.014	0.012	(0.007, 0.028)
Average traffic speed	0.013	0.024	(-0.023, 0.052)	0.011	0.020	(-0.017, 0.041)
ADT	0.223	0.141	(-0.019, 0.788)	0.213	0.131	(-0.011, 0.634)
Speed variance	0.082	0.012	(0.053, 0.114)	0.077	0.011	(0.049, 0.103)

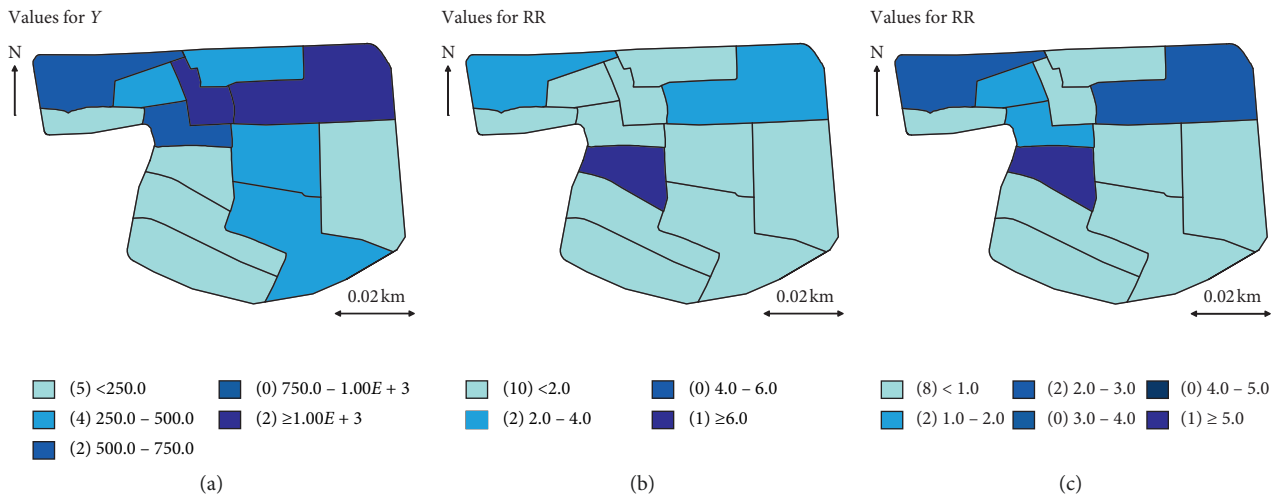


FIGURE 4: Crash count, relative risk of intrinsic and Cressie model estimation. (a) Crash Count. (b) Intrinsic model estimation. (c) Cressie model estimation.

TABLE 3: Bayesian modeling results of CT and TAZ model.

Variables	CT model 2*		CT model 1		TAZ model 2*		TAZ model 1	
	Mean	s.d.	Mean	s.d.	Mean	s.d.	Mean	s.d.
Intercept	-3.034	0.665	-2.993	0.385	-2.603	0.438	-2.702	0.425
<i>Planning parameters</i>								
Minor arterials								
Local roads					-0.001	0.005	-0.001	0.004
Public service land use	0.040	0.017	0.057	0.021	0.025	0.009	0.027	0.010
Commercial land use	0.053	0.016	0.078	0.017	0.046	0.011	0.048	0.010
Residential land use	—	—	0.027	0.009	0.029	0.007	0.031	0.009
<i>Traffic parameters</i>								
Daily traffic density	-0.1264	0.0318			0.02459	0.02557		
Average traffic speed	0.0216	0.0062	—	—	0.00161	0.00535		
ADT	-0.0415	0.0090			-0.0109	0.00674		
Speed variance	0.0432	0.0076			-0.0321	0.00339		

*The modeling efforts of adding traffic flow parameters to the corresponding spatial levels.

It is known that TAZ is delineated by land use, socio-economics, and demographics. From the results, it can be concluded that the major issue of TAZ-based spatial

modeling is the risk of atomic fallacy. In other words, the actual traffic flow effects were not detected based on TAZs. Moreover, in practice, any active interventions or policies



FIGURE 5: (a) TAZ and (b) CT spatial units of the studied area.

cannot be proposed on regional traffic flow control or management to improve traffic safety, as only land use parameters were found as significant.

For the CT-based model, average daily traffic volume (ADT) was found as a significant variable, with a negative sign indicating that higher traffic volume would result in lower crash rates. This finding could be challenged because traffic volume was considered positively associated with crash risk as the crash exposure, per the previous literature studies. In addition, average speed was found to be positively associated with regional crash risk. However, according to Abdel-Aty et al. [27], relatively low-speed area tended to have higher crash risk. Moreover, previous literature largely suggested the insignificance of possible linear relationship between average speed and crash risk [28]. Thus, the significant traffic flow effects from CT appear to be ecological fallacy [29]. As known, CT was also defined based on nontraffic parameters.

5. Conclusion

Crash occurrence was believed and found to be associated with traffic flow characteristics. Macroscopic spatial crash modeling was initially conducted with the purposes of adding safety consideration into long-term traffic planning and policy-making, as spatial units used were mainly defined from the planning perspective. However, it could also be expected to propose some effective control and management strategies to improve not only efficiency but also regional traffic safety. Thus, exploring the possible linkage among traffic flows and crash risk at regional level appears to be necessary. In addition, previous literature argued the major flaw of TAZ-based spatial modeling of both atomic fallacy and ecological fallacy. Thus, conducting macroscopic spatial crash modeling using a better-defined spatial unit is of interest in this paper.

Based on a normalized cut minimization method, we defined a spatial unit for regional safety evaluation. Microwave

data were used to partition the subject area into multiple parts, according to the homogeneity of traffic density. Crash data, planning data, and traffic data were all collected for spatial modeling purpose. In order to account for the spatial dependency among each unit and the potential overfitting issue (caused by the availability of detectors), two Bayesian CAR models were employed.

The results proved the existence of traffic flow effects at macrolevels. Note that this level was often used to study regional traffic control and management strategies. Thus, it indicates the necessity of deeply examining the relationship among traffic flow characteristics (e.g., MFD) and crash risk at regional level, in order to enlighten traffic professionals to propose time-dependent active regional traffic control and management strategies for safety improvement.

Admittedly, the current study still has some limitations. First, most traffic data were collected for arterial roads, where microwave detectors are installed. Only those roads can be used as edges in graph cut minimization. Thus, limited by the sparsity of microwave detectors and the size of the subject area, only 13 NC zones were finally defined. This could possibly cause overfitting issue. Bayesian CAR models were introduced to deal with the issue, and the coefficients were assumed to follow prior normal distributions (similar with L2 regularization). In our future study, we will obtain more detailed traffic data through different ways and expand the study area. Second, spatial and temporal heterogeneities were not considered in this model. Spatial heterogeneity had been discussed in the previous literature. Since this study mainly focuses on defining new spatial unit and comparing it with other units, spatial heterogeneity could be examined in the future, especially for the effect of traffic characteristics. Moreover, since NC is defined based on traffic flow data instead of planning data, temporal heterogeneity can also be discussed in the future. Third, only three simple aggregated traffic parameters were considered in the study. It is interesting to extract other features of traffic flow (e.g.,

macroscopic fundamental diagram (MFD) and examine their possible effects on safety. Last, it appeared that macrolevel traffic flow parameters were not significant at TAZ levels. It deserves a deeper investigation and possible endogenous factors need to be examined in the future.

Data Availability

Crash data are confidential and cannot be shared without permission from the local government in China.

Conflicts of Interest

The authors declare that they have no conflicts of interest.

Acknowledgments

This research has been supported by the National Key R&D Program of China (2018YFE0102700).

References

- [1] R. Gyimah, M. Saberi, and M. Sarvi, "The effect of variations in spatial units on unobserved heterogeneity in macroscopic crash models," *Analytic Methods in Accident Research*, vol. 13, pp. 28–51, 2017.
- [2] C. Wang, M. A. Quddus, T. Ryley, M. Enoch, and L. Davison, "Spatial models in transport: a review and assessment of methodological issues," in *Proceedings of the 91st Annual Meeting of the Transportation Research Board*, Washington, DC, USA, 2012.
- [3] R. B. Noland and M. A. Quddus, "A spatially disaggregate analysis of road casualties in England," *Accident Analysis & Prevention*, vol. 36, no. 6, pp. 973–984, 2004.
- [4] R. Haynes, A. Jones, V. Kennedy, I. Harvey, and T. Jewell, "District variations in road curvature in England and Wales and their association with road-traffic crashes," *Environment and Planning A: Economy and Space*, vol. 39, no. 5, pp. 1222–1237, 2007.
- [5] M. Abdel-Aty, J. Lee, C. Siddiqui, and K. Choi, "Geographical unit based analysis in the context of transportation safety planning," *Transportation Research Part A: Policy and Practice*, vol. 49, pp. 62–75, 2013.
- [6] P. Xu, H. Huang, N. Dong, and S. C. Wong, "Sensitivity analysis in the context of regional safety modeling: identifying and assessing the modifiable areal unit problem," *Accident Analysis & Prevention*, vol. 70, pp. 10–120, 2014.
- [7] D. Martin, "Extending the automated zoning procedure to reconcile incompatible zoning systems," *International Journal of Geographical Information Science*, vol. 17, no. 2, pp. 181–196, 2003.
- [8] D. Guo and H. Wang, "Automatic region building for spatial analysis," *Transactions in GIS*, vol. 15, no. 1, pp. 29–45, 2011.
- [9] G. Yannis, E. Papadimitriou, and C. Antoniou, "Multilevel modelling for the regional effect of enforcement on road accidents," *Accident Analysis & Prevention*, vol. 39, no. 4, pp. 818–825, 2007.
- [10] Y. Ji and N. Geroliminis, "On the spatial partitioning of urban transportation networks," *Transportation Research Part B: Methodological*, vol. 46, no. 10, pp. 1639–1656, 2012.
- [11] A. Kouvelas, M. Saeedmanesh, and N. Geroliminis, "Enhancing model-based feedback perimeter control with data-driven online adaptive optimization," *Transportation Research Part B: Methodological*, vol. 96, pp. 26–45, 2017.
- [12] N. Geroliminis, J. Haddad, and M. Ramezani, "Optimal perimeter control for two urban regions with macroscopic fundamental diagrams: a model predictive approach," *IEEE Transactions on Intelligent Transportation Systems*, vol. 14, no. 1, pp. 348–359, 2013.
- [13] H. Zhao, Q. Chen, W. Shi, T. Gu, and W. Li, "Stability analysis of an improved car-following model accounting for the driver's characteristics and automation," *Physica A: Statistical Mechanics and Its Applications*, vol. 526, Article ID 120990, 2019.
- [14] D. Sun, H. Zhao, H. Yue, M. Zhao, S. Cheng, and W. Han, "ST TD outlier detection," *IET Intelligent Transport Systems*, vol. 11, no. 4, pp. 203–211, 2017.
- [15] H. Zhao, H. Yue, T. Gu, and W. Li, "CPS-based reliability enhancement mechanism for vehicular emergency warning system," *International Journal of Intelligent Transportation Systems Research*, vol. 17, no. 3, pp. 232–241, 2019.
- [16] F. Chen, M. Song, and X. Ma, "Investigation on the injury severity of drivers in rear-end collisions between cars using a random parameters bivariate ordered probit model," *International Journal of Environmental Research and Public Health*, vol. 16, no. 14, p. 2632, 2019.
- [17] F. Chen and S. Chen, "Injury severities of truck drivers in single- and multi-vehicle accidents on rural highways," *Accident Analysis & Prevention*, vol. 43, no. 5, pp. 1677–1688, 2011.
- [18] C. Wang, C. Xu, J. Xia, and Z. Qian, "Modeling faults among E-bike-related fatal crashes in China," *Traffic Injury Prevention*, vol. 18, no. 2, pp. 175–181, 2017.
- [19] C. Wang, C. Xu, J. Xia, Z. Qian, and L. Lu, "A combined use of microscopic traffic simulation and extreme value methods for traffic safety evaluation," *Transportation Research Part C: Emerging Technologies*, vol. 90, pp. 281–291, 2018.
- [20] C. Wang, C. Xu, and Y. Dai, "A crash prediction method based on bivariate extreme value theory and video-based vehicle trajectory data," *Accident Analysis and Prevention*, vol. 123, pp. 365–373, 2019.
- [21] J. Besag, J. York, and A. Molli, "Bayesian image restoration, with two applications in spatial statistics," *Annals of the Institute of Statistical Mathematics*, vol. 43, no. 1, pp. 1–20, 1991.
- [22] W. Cheng, G. S. Gill, R. Dasu, M. Xie, X. Jia, and J. Zhou, "Comparison of Multivariate Poisson lognormal spatial and temporal crash models to identify hot spots of intersections based on crash types," *Accident Analysis & Prevention*, vol. 99, pp. 330–341, 2017.
- [23] H. Huang, B. Song, P. Xu, Q. Zeng, J. Lee, and M. Abdel-Aty, "Macro and micro models for zonal crash prediction with application in hot zones identification," *Journal of Transport Geography*, vol. 54, pp. 248–256, 2016.
- [24] T. Wang, "Incorporating safety into transportation planning for small and medium-sized communities," Master thesis, Iowa State University, Ames, IA, USA, 2011.
- [25] T. Wang, R. R. Souleyrette, and K. Gkritza, "Incorporating safety into transportation planning at smaller agencies," in *Proceedings of the TRB 92nd Annual Meeting*, Washington, DC, USA, January 2013.
- [26] J. Lee, M. Abdel-Aty, and X. Jiang, "Development of zone system for macro-level traffic safety analysis," *Journal of Transport Geography*, vol. 38, pp. 13–21, 2014.
- [27] M. Abdel-Aty and A. Pande, "Identifying crash propensity using specific traffic speed conditions," *Journal of Safety Research*, vol. 36, no. 1, pp. 97–108, 2005.

- [28] P. Marchesini and W. Weijermars, *The Relationship between Road Safety and Congestion on Motorways*, SWOV Publication R-2010-12, Leidschendam, Netherlands, 2010.
- [29] G. A. Davis, "Is the claim that "variance kills" an ecological fallacy?," *Accident Analysis & Prevention*, vol. 34, no. 3, pp. 343–346, 2002.